論文 / 著書情報
Article / Book Information

題目(和文)	スメクチック液晶を形成する主鎖型高分子のモルフォロジーに関する研究
Title(English)	Study on Morphology of Main Chain Polyesters Forming Smectic Liquid Crystals
著者(和文)	戸木田雅利
Author(English)	Masatoshi Tokita
出典(和文)	学位:工学博士, 学位授与機関:東京工業大学, 報告番号:乙第3368号, 授与年月日:1999年12月31日, 学位の種別:論文博士, 審査員:
Citation(English)	Degree:Doctor of Engineering, Conferring organization: Tokyo Institute of Technology, Report number:乙第3368号, Conferred date:1999/12/31, Degree Type:Thesis doctor, Examiner:
学位種別(和文)	博士論文
Type(English)	Doctoral Thesis

Study on Morphology of Main Chain Polyesters Forming Smectic Liquid Crystals

A Dissertation for the Degree
Doctor of Engineering

by

Masatoshi Tokita

Department of Polymer Chemistry
Tokyo Institute of Technology
1999

Study on Morphology of Main Chain Polyesters Forming Smectic Liquid Crystals

Contents

Chapter 1

General Introduction

The introduction of flexible alkylene spacers between the rigid aromatic units as a mesogen in the polymer backbone is a proven method for obtaining thermotropic liquid crystalline phases. The resulting polymers are termed main-chain liquid crystalline polymers (LCPs). The main-chain LCP is a semiflexible linear chain of repetitive units that participates in forming the mesophase structure as in the low-molecular-weight material which can be modeled by rods. The appearance of the mesophase is the consequence of the existence of anisotropic intermolecular interactions associated with the form and with the chemical nature of the molecules. Thus the liquid crystal character of the polymer molecules should also proceed from the rod like conformation of the chain backbone. Such an extended conformation is the consequence of the connectivity of the repeat units.

Thermotropic LCPs form isotropic liquid, LC, and crystal phases in order of decreasing temperature. Thus the LC forms from the isotropic liquid, where the macromolecule possesses a huge number of internal degree of freedom, i.e. rotational isomeric states and changes between the different states which are populated according to the laws of Boltzmann statics. As the large majority of conformations are coil-like, it is said that polymers in the liquid state represent 'random coils'. Moreover they intertwine with each other like as spaghetti that one delays in eating. Thereby, at the transformation from the isotropic liquid to the liquid crystal, these chains have to separate from each other and alter their coiled configuration to a rod-like one. But there must be considerable doubt as to whether a long polymer chain reaches the rod-like configuration from out to

out and forms the liquid crystal thoroughly.

This question arises from the morphology of macromolecular crystals.[1] Cooling a polymer melt below the equilibrium melting point produces structures which are only *in part* crystalline. One observes layer-like crystallites which are separated by disordered amorphous regions, thus setting up a lamellar two-phase structure. The key question of polymer crystal morphology is the fate of the long molecular chain at the surface of the lamellar crystal. Keller first presented evidence for a folded chain lamella.[2] Electron microscopy and electron diffraction on solution grown single crystals of polyethylene clearly proved the necessity for chain folding. The lamellae of about 100 Å thickness had molecular chains of much greater length oriented in the direction of the lamellar thickness. Fischer presented evidence that spherulites of melt-grown polyethylene and nylon are most likely basically lamellar rather than fibrillar.[3] The folded-chain crystal is now regarded as the general morphology for polymers, not only synthetic polymers such as polyethylene and nylon, but also natural polymers such as polypeptide and cellulose. Though extended chain crystals of polyethylene are grown on the crystallization from the melt under hydrostatic pressure above 3.0 kbar,[4] it has revealed that chain extension is a secondary process after initial chain folding.[5] A sufficiently regular, flexible linear macromolecules crystallized from the mobile random state thus always crystallize first in a chain-folded configuration. On the other hand, lower melting points of folded-chain crystals and lamellar thickening on annealing the document that the chain fold is thermodynamically metastable.[6-8] Here the question of the reason behind the prominent existence of the chain folding in polymer crystals becomes of prime importance. The reason is connected with the kinetics of nucleation and crystallization of polymers from mobile random liquid state.[9-15] The rules which control structure formation during crystallization are kinetical criteria rather than equilibrium thermodynamic.

The structure which develops is that with the maximum growth rate rather than that with the lowest free energy.

Let us now turn to the case of the polymer liquid crystal. The existence of chain foldings in the polymer liquid crystal has been suggested by theoretical debates on the polymer chain configuration in the nematic field,[16-21] neutron scattering measurements for the nematic main-chain LCPs,[22-25] and electron microscopy (TEM) and diffraction (ED) for the polymer solid crystallized from the nematic phase.[26-30] The flexible polymer chain tends to maximize entropy, in other words, to takes random-coil configuration. This polymer entropy is antagonistic to orientational order of the LC field. The LC field, distorting to be locally parallel to a random polymer, would develop a large elastic energy; equally a chain stretched out to be parallel to a LC field loses a lot of entropy. Thus, the complexity and subtlety in the main-chain LCPs comes from the interplay between long-range orientational order of the liquid crystal and the polymeric tendency to maximize entropy. de Gennes[16] first pointed out that a semiflexible long chain in the nematic field may recover some part of the entropy lost due to the ordering of the mesogenic units by forming hairpin folding where the chain executes a counter-reversal (180°) with respect to the director. The experimental data for the measurement of the degree of chain configuration are available for small-angle neutron scattering (SANS) for only one homologous nematic polymer, poly(4,4'-dioxy-2,2'-dimethylazoxybenzene alkanedioyl)s.[22-25]

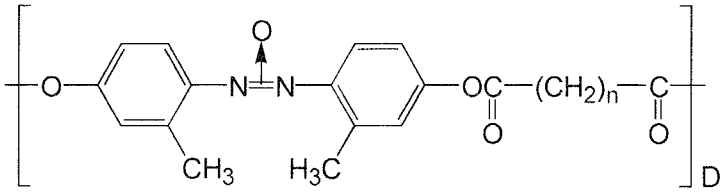

D'Allest et al.[22] showed that in the nematic state these polymers might be considered as coils having the symmetry of flattened rotational ellipsoids with the long principal axis in the direction of the director. Both the radius of

gyration, R_G, in the isotropic state and the radius of gyration parallel to the director, $R_{\parallel}$, in the nematic state increases as the molecular weight in increased. Li et al.[24,25] recently established the existence of one or two hairpin foldings by fitting the scattering data into a model of rigid cylinder. On the other hand, Geil et al.[26-29] found a folded chain lamellar structure for liquid crystalline polymers crystallized from the nematic state with electron microscopy (TEM) and diffraction (ED). The ED studies suggested adjacent reentry, and indicated no change in lateral molecular packing at the crystal-nematic transition. The results were interpreted as suggesting similar folded chain, lamellar morphology in the nematic state. Takahashi and Nagata[30] have studied the morphology of the solid of a smectic crystalline polymer by TEM and small-angle X-ray scattering (SAXS), and found that the stacked lamellar structure is formed.

Let us now look at the morphology of the polymer liquid crystal from a angle in line with that of the polymer crystal. The liquid crystal has a long-range orientational order, which force the polymer chain to take up an extended configuration. Smectic liquid crystals have long-range one-dimensional positional (smectic layer) order for the polymer repeat unit. Some of them have three-dimensional long-range positional order as in a crystal, but differ from a crystal in that molecules rotate along its long axis.[31] They are called 'crystalline' smectic. Though some order of a crystal is lacking in the liquid crystals, the polymer chain takes up an extended configuration in the liquid crystal field as in the continuous crystal lattices. A long polymer chain seems to be hardly achieved to be rod-like configuration perfectly along its entire length in finite time of the liquid crystal formation as seen in polymer crystallization. It is hence likely that the chain folding exists in the polymer liquid crystal as in the polymer crystal and that the liquid crystal formation from the isotropic liquid state takes place partially. If the chain foldings exist, how are they accommodated in the liquid crystalline phase. It is also debatable whether the

polymer crystallizes completely from the liquid crystalline state.

To examine these points in more detail, this thesis treats two types of smectic liquid crystal formed by the main-chain polyesters having the biphenyl moiety as a common mesogen. The first is the smectic phases of poly(alkylene 4,4′-bibenzoate)s:

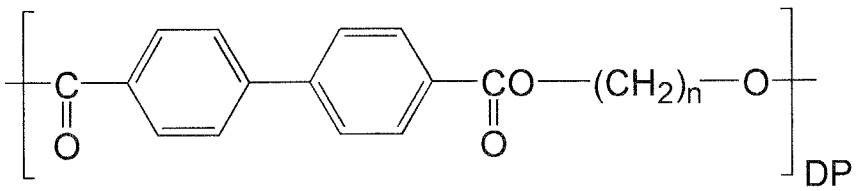

The polymers are designated as BB-*n* (*n*: carbon number of the methylene spacer).[32-41] These BB-*n* polyesters invariably form smectic mesophases when *n* varies from 3 to 9. In BB-*n* with an even *n*, a smectic A (S_A) phase is formed. In contrast, the smectic structure of BB-*n* with an odd *n* was identified as a smectic CA (S_{CA}) phase. The smectic melt of the BB-*n* polyesters shows an unusual orientation that is the chain axis arranges to perpendicular to the direction of shear flow.[32,41] This unusual orientation is interesting because it is explainable if chain folded lamella exists in the smectic melt, i.e. polymer chains are not extended along the entire length, but folded in the smectic phase. The experimental results on the structural characteristics of the smectic liquid crystals of BB-*n* and the unusual orientation of the smectic melt are presented in the *Chapter 2*. To discuss the chain configuration of the main-chain LCP in the smectic A phase, the solid state morphology of BB-*n* polyesters were studied by small-angle X-ray scattering (SAXS) measurements. The results discussed in the *Chapter 3* show that the chain foldings exist at a thermodynamic equilibrium as an entropy effect in the S_A phase. This conclusion is in line with theoretical debates on the polymer chain configuration in the nematic LC field,[16-21] which is reviews also in the Chapter 3.

Then, transition behavior of the liquid crystalline BB-*n* polyesters was examined in detail. It was found that the liquid crystallization proceeds

promptly and completely from the isotropic liquid while the crystallization takes place partly even from the ordered smectic phase. The solid state of the liquid crystal polymer is thus composed of crystal and smectic LC glass. The glass transition as well as other relaxation processes was investigated by the dynamic mechanical analysis method. These results are discussed in the *Chapter 4*.

The results for the low-ordered smectic LC, namely S_A and S_{CA} show completely opposite trends to that found for the polymeric crystals. S_A and S_{CA} have long-range orientational order and smectic layer structure (one-dimensional positional order). The mesogens in a smectic layer are thus spaced in a liquid-like fashion.[31] Some change in the results is expected for a more ordered 'crystalline' smectic. Thereby a smectic H (S_H) LC formed by the following polymer is treated in this thesis.

The polymer is designated as PB-*n* polyesters,[42-46] where *n* of 6 ~ 20 is the

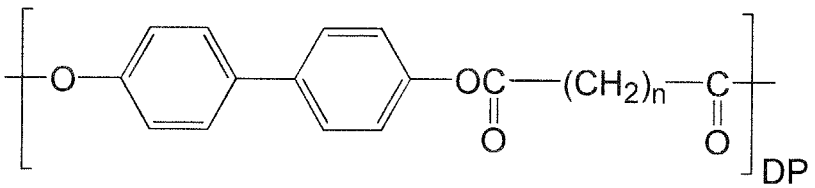

number of methylene units in the spacer moiety. Even-membered PB-*n* polyesters form a S_H phase. The PB-*n* polyesters are characterized in the *Chapter 5* with using high-resolution solid state ^{13}C NMR spectra as well as the DSC and wide-angle X-ray methods. The liquid crystal morphology is discussed in the *Chapter 6* according to the SAXS and transmission electron microscope observations. The overall results indicate that the S_H liquid crystallization takes place imperfectly in a finite period due to the chain folding and that the succeeding annealing causes the alternation of the chain conformation from a folded form to an extended one as observed in the crystallization of conventional polymers. The annealing at a S_H temperature can produce the liquid crystal in which the polymer chain can be assumed to be extended. In the *Chapter 7*, characters of crystallization from the liquid crystals

are examined.

The concluding remarks of this dissertation are summarized in the *Chapter 8*.

References

(1) Wunderlich, B. *Macromolecular Physics*, Academic Press: New York, 1980.

(2) Keller, A. *Phil. Mag.* **1957**, *2*, 1171.

(3) Fischer, E. W. *Z. Naturforsch.* **1957**, *12a*, 753.

(4) Wundelich, B.; Arakawa, T. *J. Polym. Sci. Part A* **1964**, *2*, 3967.

(5) Bassett, D. C., Turner, B. *Phil. Mag.* **1974**, *29*, 925.

(6) Hoffman, J. D.; Weeks, J. J. *J. Chem. Phys.* **1965**, *42*, 4301.

(7) Weeks, J. J. *J. Res. Nat. Bur. Stand.* **1963**, *67A*, 441.

(8) Fisher, E. W., Schmidt, G. F. *Angew. Chem. Internat. Ed.* **1962**, *1*, 488.

(9) Lauritzen, J. I. Jr.; Hoffman, J. D. *J. Chem. Phys.* **1959**, *31*, 1680.

(10) Lauritzen, J. I. Jr.; Hoffman, J. D. *J. Res. Nat. Bur. Stand.* **1960**, *64A*, 73.

(11) Lauritzen, J. I. Jr.; Hoffman, J. D. *J. Res. Nat. Bur. Stand.* **1961**, *65A*, 297.

(12) Price, F. P. *J. Chem. Phys.* **1959**, *31*, 1679.

(13) Price, F. P., *J. Polym. Sci.* **1960**, *42*, 49.

(14) Price, F. P. *J. Chem. Phys.* **1961**, *35*, 1884.

(15) Frank, F. C.; Tosi, M. *Proc. Roy. Soc. (London)* **1961**, A263, 323.

(16) de Gennes, P. G. In *Polymer Liquid Crystals*, A. Cifferri, W. R. Krigbaum, and R. B. Mayer Eds., Academic Press, New York, 1982; p124.

(17) Warner, M.; Gunn, J. M. F.; Baumgartner, A. B. *J. Phys. A* **1986**, *18*, 3007.

(18) Wang, X. J.; Warner, M. *J. Phys. A* **1986**, *19*, 2215.

(19) Warner, M. *Mat. Res. Soc. Proc.* **1989**, *134*, 61.

(20) Williams, D. R. M.; Warner, M. *J. Phys. Fr.* **1990**, *51*, 317.

(21) Williams, D. R. M.; Warner, M. in *Computer Simulation of Polymer*, R. J. Roe Ed.: Prentier-Hall Inc., New Joursey, 1991, p262.

(22) D'Allest, J. F.; Sxiou, P; Blumstein, A.; Blumstein, R. B. *Mol. Cryst. Liq. Cryst* **1993**, *155*, 581.

(23) Arrighi, V.; Higgins, J. S.; Weiss, R. A.; Cimecioglu, A. L. *Macromolecules* **1992**, *25*, 5297.

(24) Li, M. H.; Brulet, A.; Davidson, P.; Keller, P.; Cotton, J. P. *Phys. Rev. Lett.* **1993**, 70, 2293.

(25) Li, M. H.; Brulet, A.; Cotton, J. P.; Davidson, P.; Strazielle, C.; Keller, P. *J. Phys. II (France)* **1994**, *4*, 1843.

(26) Kent, S. L.; Geil, P. H. *J. Macromol. Sci. Phys.* **1992**, *B31*, 413.

(27) Kent. S.; Brennan, J. G.; Geil, P. H. *J. Mater. Sci. Lett.* **1991**, *10*, 1456.

(28) Kent, S. L.; Geil, P. H. *J. Polym. Sci. Polym. Phys.* **1992**, *31*, 1489.

(29) Kent, S. L.; Geil, P. H. *Makromol. Chem. Macromol. Symp.* **1993**, *70/71*, 83.

(30) Takahashi, T.; Nagata, F. *J. Macromol. Sci. Phys.***1989**, *B28*, 34.

(31) Gray, G. W.; Goodby, J. W. *Smectic Liquid Crystal*, Leonard Hill, Glasgow, 1984.

(32) Krigbaum, W. R.; Watanabe, J. *Polymer* **1983**, *24*, 1299.

(33) Watanabe, J.; Hayashi, M. *Macromolecules* **1988**, *21*, 278.

(34) Watanabe, J.; Hayashi, M. *Macromolecules* **1989**, *22*, 4083.

(35) Watanabe, J.; Hayashi, M.; Kinoshita, S.; Niori, T. *Polym. J.* **1992**, *24*, 597.

(36) Watanabe, J.; Kinoshita, S. *J. Phys. II (France)* **1992**, *2*, 1237.

(37) Watanabe, J.; Komura, H.; Niori, T. *Liq. Cryst.* **1993**, *13*, 455.

(38) Watanabe, J.; Hayashi, M.; Morita; A.; Niori, T. *Mol. Cryst. Liq. Cryst.* **1994**, *254*, 221.

(39) Watanabe, J.; Hayashi, M., Morita, A.; Tokita, M. *Macromolecules* **1995**, *28*, 8073.

(40) Watanabe, J.; Hayashi, M.; Tokita, M. *Reactive & Functional Polymers* **1995**, *30*, 191.

(41) Tokita, M.; Osada, K.; Watanabe, J. *Liq. Cryst.* **1998**, *24*, 477.

(42) Krigbaum, W. R.; Watanabe, J.; Ishikawa, T. *Macromolecules* **1983**, *16*, 1271.

(43) Watanabe, J.; Krigbaum, W. R. *Macromolecules* **1984**, *17*, 2288.

(44) Maeda, Y.; Mabuchi, T.; Watanabe, J. *Thermochim. Acta* **1995**, *266*, 189.

(45) Huang, H. W.; Horie, K.; Yamashita, T.; Machida, S.; Sone, M.; Tokita, M.; Watanabe, J.; Maeda, Y. *Macromolecules* **1996**, *29*, 3485.

(46) Huang, H. W.; Horie, K.; Tokita, M.; Watanabe, J., *Polymer* **1999**, *40*, 3013.

Chapter 2

Structure of Smectic Phase of BB-*n* Polyesters and their Unusual Orientation of Molecules under the Flow

ABSTRACT: Even- and odd-membered BB-*n* polyesters (*n* = 3 - 9) form smectic A phase and smectic CA phase, respectively. This odd-even alternation of the smectic structures results from the conformational constraint in which the polymethylene spacer, assuming the more extended conformation, forces the neighbouring mesogens to arrange with the characteristic angular displacement that depends on the odd-even parity of *n*. Thus the polymer chain takes up the extended configuration at least in a local space of the LC field. On the other hand, the fibers drawn from the smectic phases show anomalous molecular orientation where the smectic layers orient parallel to the fiber axis and the polymer chains lie perpendicular to the fiber axis. This anomalous flow orientation suggests strongly that folded chain lamellae formed in the smectic phases.

The biphenyl group is the simplest mesogen with linearity and high symmetry. Its thermal stability is also guaranteed in the temperature range up to 300°C. These characteristics make it easy to analyse the structure and properties of liquid crystals. One of the most typical examples of main-chain liquid crystalline polymers based on the biphenyl mesogen is BB-*n* polyesters,

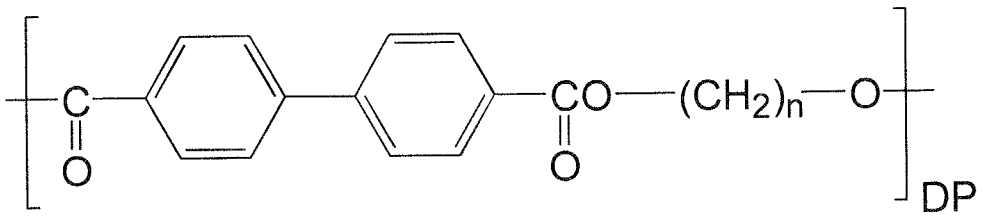

where *n* is the number of methylene units in the spacer.[1-10]

2.1. Odd-Even Effects on Smectic Properties and Structures

BB-*n* polyesters with *n* = 3 - 9 exhibit two transitions in DSC thermograms (see Figure 2.1).[1,2] Thermodynamic data on BB-*n* polyesters based on DSC are given in Figure 2.2. Figure 2.2(a) shows the variation of the transition temperatures with *n*. Here the simple trend is seen that the mesophase temperature region decreases with increasing *n* and finally the mesophase disappears where *n* exceeds 10. The isotropization entropies of liquid crystals are given in Figure 2.2(b). Figure 2.2 indicates the clear odd-even oscillation, with the larger values observed in even-numbered BB-*n* polyesters.

The mesophases observed here can be assigned to the smectic phase from the X-ray observation of the sharp inner layer reflection and the outer broad reflection and also from the microscopic observation of the fan-shaped texture. The spacings of inner reflection, i.e. the smectic layer thicknesses, are plotted against *n* in Figure 2.3. One can observe the odd-even oscillation here also, with a larger spacing in the even-numbered BB-*n* polyesters.

The most striking feature in this system is that the smectic structure appears to differ depending on the odd-even parity of *n*. This was initially

realized from X-ray diffraction observations of oriented fiber specimens.[3] Figure 2.4(a) and (b) show X-ray diffraction patterns of the oriented smectic phases of BB-6 and BB-5, representative of even- and odd-numbered polymers, respectively. In BB-6, as seen in Figure 2.4(a), the layer reflections are located on an equatorial line. This diffraction geometry unambiguously indicates a smectic A (S_A) structure in which the mesogenic groups forming a layer are arranged parallel to the polymer chain and both lie perpendicular to the layers (see Figure 2.4(c) and Figure 2.5(a)).

The BB-5 polyester on the other hand shows a distinct X-ray pattern. The broad outer reflections are split into two portions lying above and below the equator, while the layer reflections appear on a meridional line as in BB-6 (see Figure 2.4(b)).[2,5] In this case therefore, the layered packing structure can be illustrated such that the polymer chains lie perpendicular to the layers as in BB-6 but the mesogenic groups are tilted to the layer normal (see Figure 2.4(d)). The tilt angle is independent of temperature and is estimated around 25° from the splitting angle of the broad reflections. The structure is thus similar to smectic C (S_C) as far as the arrangement of the mesogenic groups within a layer is concerned.

The smectic structure in odd-membered BB-*n* could be uniquely determined from the observation of optical microscopic texture in homeotropic specimens.[5] High birefringence and also various schlieren can be observed. These observations together with the X-ray observations, undoubtedly show that the c-director exists in each layer and its orientation correlation is maintained from the layer to layer. It must be emphasized here that the schlieren texture with a singularity of $s = \pm 1/2$ is observed in this smectic phase. This fact rules out the assignment to a S_C phase[14] and leads to only the smectic structure illustrated in Figure 2.5(b).[6] In this structure, the mesogenic

groups are tilted with respect to the layer normal, but unlike the normal S_C phase, the tilt direction is opposite in adjacent layers. This novel smectic phase was first identified in the present system and called smectic CA (S_{CA}), the s = ± 1/2 disclination of which can be allowed for the c-director orientation as illustrated in Figure 2.6. In Figure 2.6, an edge disclination is coupled with a helical dislocation, that is, one layer is shifted to its neighboring layer after rotation of 180° around a disclination line. The combined effect of edge disclination and helical dislocation is called dispiration,[15] and the present sample allowed its first visual observation.

As a conclusion, the even series of BB-*n* forms a S_A in which both axis of polymer chain and mesogenic group lie perpendicular to the layer (Figure 2.5(a)), while the odd-membered ones form the distinct smectic phase, S_{CA}, in which the polymer chains are perpendicular to the layer but the mesogenic group are tilted to the layer in an alternate fashion (Figure 2.5(b)). In most types of liquid crystals so far observed, uniaxial orientation has been achieved for the long axis of mesogens. In this sense, the S_{CA} phase observed here is quite novel and interesting, since uniaxial ordering cannot be observed for the n-director but only for the c-director.

2.2. Chain Conformation in Smectic Phase

The odd-even appearance of smectic layered structure and the formation of the novel S_{CA} structure are believed to result from a coupling effect of the polymeric and mesogenic properties in which the spatial arrangement of mesogenic groups is strongly related to the conformation of the intervening alkylene spacers.

To account for this effect, conformational analysis of the flexible spacer has been performed within the framework of the rotational isomeric state model,

with evaluation of the angle θ, defined by unit vectors attached to two successive mesogenic groups.[16] The results are shown in Figure 2.7, where the relative numbers of conformers are plotted against θ for BB-6 and BB-5. From this graph we can recognize that the angular distributions in the two ranges 0 - 20° and 90 - 120°. When *n* is odd, the major portion of the angles is located in the region 50 - 90°, and to some extent, orientations are also permitted in the region > 150°. In each system, the conformers with the smaller angular displacement of successive mesogens are in the more extended form. Based on this calculation, we can arrive at the following points which are closely related to the observed characteristics in the smectic layered structures.

1. In the *n*-even series, the parallel orientation of successive mesogenic groups is allowed, conforming more or less to the concept of ordinary uniaxial ordering of the n-director, but in the *n*-odd series, uniaxial orientation of successive mesogenic groups is not allowed (see Figure 2.7).[16]
2. The conformers with the smaller angular displacement in both odd and even systems correspond to the conformers participating in the observed layer structure (compare Figure 2.5 with Figure 2.7).

This explanations the odd-even appearance in the type of smectic phases and at the same time accounts for the specific formation of a S_{CA} phase in the odd series of BB-*n*, leading to the significant conclusion that the structure of the smectic phase strongly promoted by the conformational constraint of a flexible spacer. Further, this conclusion has been supported by comparison of the observed layer thickness with the calculated layer thickness, which corresponds to the distance between the neighboring mesogens in a chain. As seen in Figure 2.3, the absolute value as well as the odd-even oscillation could be perfectly reproduced when the calculation was performed for the confined conformers with the smaller angular displacement.

2.3. Distinct Orientation of Molecules in a Thin S_{CA} Film Stretched from Isotropic melt, Providing Evidence for the Biaxiallity of the S_{CA} Phase

This section mentions distinct molecular orientation in a thin film of S_{CA} phase where the zigzag tilting of mesogenic groups takes place preferentially in a direction perpendicular to the film surface. This is direct evidence for the biaxiallity of the S_{CA} phase.[10]

The polymer used here is BB-$(OEt)_2$ with the following structure,

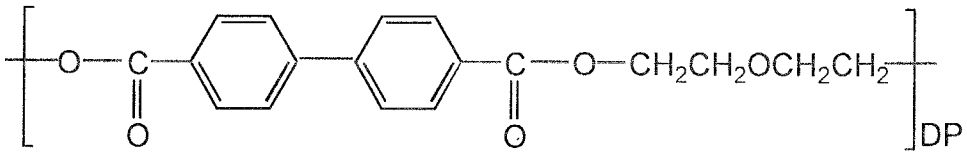

which belongs to the odd homologue of polymers since the number of atoms in the spacer is five. The DSC thermograms BB-$(OEt)_2$ included only a S_{CA} - isotropic transition at 199°C on heating and at 180°C on cooling. No crystallization took place at a normal cooling rate. Oriented film was prepared by stretching the viscous isotropic melt; the rate of stretching was around 1 m s^{-1}. The thickness of the film was around 20 μm. X-ray patterns were taken at a room temperature. Figures 2.8(a) - (c) show the X-ray patterns of film specimens obtained by X-ray irradiation from three characteristic positions. The X-ray patterns exhibit a fairly good orientation of the chain axis and appear different depending on the direction of X-ray irradiation. In the photograph of Figure 2.8(a), where the beam is irradiated parallel to the film surface and perpendicular to the oriented axis (chain axis), the X-ray pattern includes layer reflections on the meridian and broad reflections split above and below the equator. The splitting of the broad reflections can be seen more clearly in curve (a) of Figure 2.9(a) where the intensity distribution $I(\beta)$ was measured as a

function of the azimuthal angle β at a constant diffraction angle of the reflection ($2\theta = 20.5°$). In contrast, when the X-ray beam is irradiated perpendicular to the film surface, the layer reflections are invariably observed on the meridian, but the broad reflections are concentrated on the equator (see Figure 2.8(b) and curve (b) of Figure 2.9(b)). For X-ray irradiation parallel to both the film surface and chain axis, only broad reflections can be observed without any orientation (Figure 2.8(c)). These diffraction profiles dictate the biaxiallity of the S_{CA} phase, in which the zigzag tilting of mesophase groups takes place in a direction perpendicular to the film surface, as illustrated in Figure 2.10(a).

The layer spacing is 16.0 Å and the tilt angle of the repeat unit is around 25°, as estimated from curve (a) of Figure 2.9. There is no difference between the spacings of the broad reflections in the two directions parallel and perpendicular to the tilt direction of the mesogenic groups. This indicates that there is no significant difference between the molecular interactions in these two directions and so the relatively free rotation of biphenyl mesogens takes place around their long axis. This is reasonable since the biaxiallity of the S_{CA} phase is produced by the conformational constraint exerted on the individual chain rather than by intermolecular interaction.

2.4. Unusual Orientation of Molecules in Fibers Drawn from Smectic Melt

During the studies to explore the smectic structural properties characteristic to the main-chain type of polymers by using BB-*n* polyesters,[1-12] it has been found that the smectic phases show the anomalous molecular orientation when the flow deformation is applied. The polymer chains align perpendicular to the flow direction. More recently, the similar orientation behavior of smectic phase has been reported by Alt et al.[13] and by Leland et al.[14]

an orientation behavior is in contrast to that in the nematic phase, in which olymer chains lie parallel to the flow direction. and is surely characteristic polymeric smectic phases. In this section, the study is extended to the behavior on other smectic phases, S_{CA} and S_C phases, and shows that such usual orientation takes place commonly in three types of smectic phases, $_A$, S_C phases. The explanation will be given by the existence of lamellar ure in the smectic phase.

Three representative polyesters, BB-6, BB-5 and BB-4(1-Me), which can the S_A, S_{CA} and S_C respectively, were used in this study. The inherent ities of BB-6, BB-5 and BB-4(1-Me) are 0.49, 0.52 and 0.46 dL g^{-1}, tively, as measured at 30°C by using 0.5 g dL^{-1} solutions in a 60/40 w/w e of phenol and tetrachloroethane.

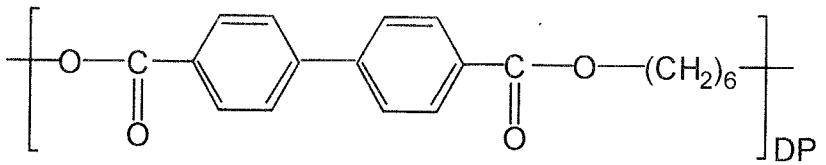

BB-6

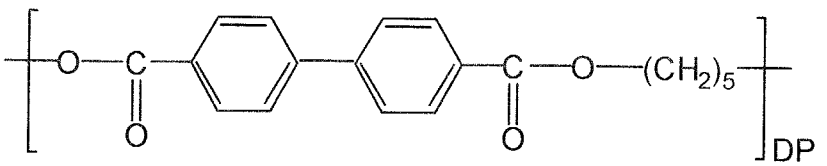

BB-5

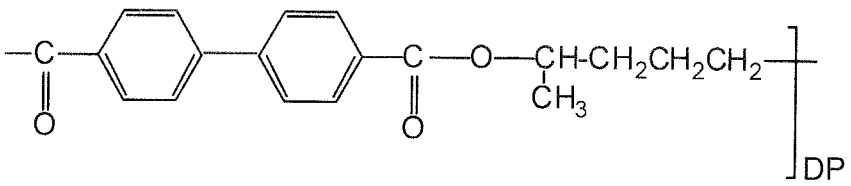

BB-4(1-Me)

-ray diffraction patterns were observed using a Rigaku-Denki RU-200 th Ni- filtered Cu Kα radiation. The stress - strain curves were obtained iiko Instruments TMA 100 with a strain rate of 50 μm min^{-1}.

2.4.1. Fibers Drawn from Isotropic Melt

Figures 2.11a, 2.11b and 2.11c provide X-ray patterns for BB-6, BB-5 and BB-4(1-Me) fibers, respectively, which were taken at a room temperature. Here, the fiber specimens were prepared by drawing the isotropic melt at a rate of about 20 cm sec^{-1}. In BB-6, the crystallization takes place even in as-spun fiber so that its X-ray pattern of Figure 2.11a includes the sharp inner reflections on meridian attributed to the layered structure and several other reflections associated with crystal. In BB-5 and BB-4(1-Me) fibers, the X-ray patterns characteristic to the mesophases are observed even at a room temperature because of a very late crystallization process.[11] In Figure 2.11b for BB-5 fiber, the sharp inner reflection is found on meridian while the broad reflection are split above and below the equator, leading to the S_{CA} structure.[3] In Figure 2.11c for BB-4(1-Me), the inner reflections are split into two positions around meridian and the broad reflections are centered on equator. These characteristic diffraction patterns are attributable to the S_C structure.[5,6] The tilt angle of both axes of mesogens and polymer chain to the layer normal is estimated as 30° from the splitting angle of the layer reflection. The corresponding layer structures in the fibers are illustrated in Figures 2.11d - 2.11f. In all these fibers spun from the isotropic melt, one can find that the polymer chain axis lies parallel to the fiber direction.

2.4.2. Fibers Drawn from Smectic Melt

The fibers can also drawn from the smectic melts if the flow elongation is applied at a relatively low rate of 1 - 2 cm sec^{-1}. The X-ray photographs are shown in Figures 2.12a - 2.12c. In a comparison with the patterns of Figures 2.11a - 2.11c, one can find the several distinct features. For example, the patterns of BB-6 and BB-5 fibers shown in Figures 2.12a and 2.12b are similar

e patterns of Figures 2.11a and 2.11b, respectively, but quite different in ›rientation geometry of reflections with respect to the fiber axis. The layer ctions in the smectic melt-spun fibers appear on the equator, showing that mectic layers lie parallel to the fiber axis, in other words, the polymer chain orients perpendicular to the elongation flow direction. Further, the X-ray rn of Figure 2.12c for the BB-4(1-Me) fiber looks completely different that in Figure 2.11c. The smectic layer reflections are centered on equator :he broad reflections are split on both sides of meridian. These, however, ɔe accounted for by the S_C structure with the layers lying parallel to the axis. From the splitting angle of the outer broad reflections, the tilt angle e S_C can be estimated as around 30° which coincides with that estimated the splitting angle of the layer reflections in Figure 2.12c.[9] In Figures ɨ - 2.12f, the corresponding smectic structures are also illustrated. As d in these figures, it can be safely concluded that an elongation flow of a ·tic melt arranges the smectic layers parallel to the flow direction.

It is noteworthy that the fibers drawn from the smectic melts can be further ʒated even at room temperature. Figure 2.13 shows the stress - strain curve ›ured for BB-5 fiber with a diameter of 0.2 mm. This fiber is composed of the S_{CA} glass as mentioned above; the glass transition temperature ıd 45°C enough higher than room temperature.[11] The stress is proportional e strain at an initial storage of strain until $\varepsilon = 2.5$ %. Apparent modulous mined with the slope is around 0.25 GPa. The Fiber is stretched up to $\varepsilon =$ % with a constant stress of 0.2 MPa and breaks. On unloading at $\varepsilon = 70$ % ·e the fiber breaks, almost all the strain remains as given by the dotted ɜ in Figure 2.13, showing that the strain applied results from the permanent ·mation. The X-ray pattern taken at a strain of 70 % is shown in Figure ɔ. The pattern is not essentially altered from that of unloading fiber shown

in Figure 2.14a, although only a few percent reduction is observed in the layer spacing. This indicates that the elongation process includes neither deformation in the smectic layer nor change in the molecular orientation. Thus, the elongation takes place as if the smectic layers slip to each other so as to lie parallel to the fiber axis.

Actually, such a flow behavior has been observed in the low molecular weight smectic phases where each smectic layer is composed of the molecules[15] (refer to Figure 2.15a). In the polymeric system, however, this mechanism is not acceptable since the mesogenic groups in neighboring layers are linked to each other through a flexible spacer and so each polymer molecule passes through many smectic layers. To explain this orientation, it is postulated that the lamellar type of domains are formed in the smectic field and the flow takes place in the domain boundaries[7] (see Figure 2.15b). Thus, the mechanism given in Figure 2.5b, i.e., the mutual slip of the lamellae, is valid for the anomalous flow behavior. The large permanent deformation without altering the smectic structure is accountable if the chain folded lamellar blocks slip each other under the elongation process.

The unusual orientation of molecules in the fiber drawn from the S_A, S_{CA} and S_C melts of BB-*n* polyesters was observed. In all cases, the smectic layers orient parallel to the fiber axis and the polymer chains lie perpendicular or tilted to the fiber axis. The anomalous flow orientation and the mechanical property of the fiber strongly suggest that chain-folded lamella exists in the smectic phases.

5. Conclusion

Structures of the smectic mesophases of BB-*n* polyesters were ′estigated. In BB-*n* with an even *n*, a S_A phase is formed with both the axis the polymer chain and the biphenyl mesogen lying perpendicular to the ′ers. In contrast, the smectic structure of BB-*n* with an odd *n* was identified a new type of smectic phase, S_{CA}, in which the tilt direction of the mesogenic ɔup is the same in every second layer but opposite between neighbouring ′ers. The biaxiallity of the S_{CA} phase was clarified by X-ray patterns for a n oriented S_{CA} film observed by irradiation from three characteristic positions ative to the film. These smectic structures point out that the polymer chains ɛe most extended configuration at least in a local space of the smectic LC ld. On the other hand, the fibers drawn from the smectic phases show ɔmalous molecular orientation where the smectic layers orient parallel to the er axis and the polymer chains lie perpendicular to the fiber axis. This ɔmalous flow orientation can be explained if chain folded lamellae are ′med in the smectic phases and slip over each other.

References

(1) Watanabe, J.; Hayashi, M. *Macromolecules* **1988**, *21*, 278.

(2) Watanabe, J.; Hayashi, M. *Macromolecules* **1989**, *22*, 4083.

(3) Watanabe, J.; Kinoshita, S. *J. Phys. II (France)* **1992**, *2*, 1237.

(4) Watanabe, J.; Hayashi, M.; Morita, A.; Niori, T. *Mol. Cryst. Liq. Cryst.* **1994**, *254*, 221.

(5) Watanabe, J.; Hayashi, M.; Kinoshita, S; Niori, T. *Polym. J.* **1992**, *24*, 597.

(6) Watanabe, J.; Hayashi, M.; Tokita, M., *Reactive & Functional Polymers* **1996**, *30*, 191.

(7) Tokita, M.; Takahashi, T.; Hayashi, M.; Inomata, K.; Watanabe, J. *Macromolecules* **1996**, *29*, 1345.

(8) Tokita, M.; Osada, K.; Watanabe, J. *Liq. Cryst.* **1997**, *23*, 453.

(9) Watanabe, J.; Hayashi, M.; Niori, T.; Tokita, M.; Nakata, Y. *Prog. Polym. Sci.* **1997**, *22*, 1053.

(10) Tokita, M.; Osada, K.; Watanabe, J. *Liq. Cryst.* **1998**, *24*, 477.

(11) Tokita, M.; Osada, K.; Watanabe, J. *Polym. J.* **1998**, *30*, 589.

(12) Krigbaum, W. R.; Watanabe, J. *Polymer* **1983**, *24*, 1229.

(13) Alt, D. J.; Hudson, S. D.; Garay, R. O.; Fujishiro, K. *Macromolecules* **1995**, *28*, 1575.

(14) Leland, M., Wu, Z., Chhajer, M., Ho, R-M.; Cheng, S. Z. D.; Keller, A.; Kricheldorf, H. R. *Macromolecules* **1997**, *30*, 5249.

(15) Gray, G. W.; Goodby, J. W. *Smectic Liquid Crystals*, Leonard Hill, Glasgow, 1984.

Figure Captions

Figure 2.1. DSC thermograms of BB-5 and BB-6.

Figure 2.2. Variation with carbon number of alkylene spacer (*n*) of (a) transition temperatures (●, crystal-liquid crystal transition; ○, isotropization of liquid crystal) and (b) isotropization entropy of liquid crystal.

Figure 2.3. Variation of smectic layer thickness (○) with *n*. The calculated layer thickness (●) corresponds to the distance between the mesogenic groups averaged over the confined conformers with small angular displacement of successive mesogens (refer to text and Figure 2.7).

Figure 2.4. Oriented X-ray patterns of fibrous smectic phases of (a) BB-6 and (b) BB-5. (c), (d) Packing structures of mesogenic groups within a layer elucidated from X-ray patterns. Here, the oriented fibers were prepared by pulling the isotropic melt and the fiber axis is placed in the vertical direction.

Figure 2.5. Layered structures of smectic phases of (a) BB-6 and (b) BB-5.

Figure 2.6. The c-director orientation around the wedge dispiration with rotational component of π which can be expected for the S_{CA} phase. The translational component gives rise to the step.

Figure 2.7. Distribution of chain conformer calculated for the angle θ defined by two successive mesogens: (a) BB-6; (b) BB-5.

Figure 2.8. X-ray diffraction patterns of the oriented S_{CA} film taken by irradiation from three characteristic positions. (a) Parallel to the film surface and perpendicular to the chain axis; (b) perpendicular to the film surface; (c) parallel to both the film surface and chain axis. In (a) and (b) the chain axis is placed in the vertical direction; in (c) the film surface is parallel to the horizontal direction.

Figure 2.9. Intensity distribution $I(\beta)$ measured as a function of the azimuthal angle β at a diffraction angle of $2\theta = 20.5°$. Curves (a) and (b) are collected from Figure 2.8(a) and 2.8(b), respectively. Here, the equatorial direction corresponds to $\beta = 0°$.

Figure 2.10. (a) Illustration of the biaxial orientation of zigzag molecules in the S_{CA} film where the mesogenic groups are tilted in a direction perpendicular to the film surface. This preferential orientation may be caused by relaxation from the extended arrangement of mesogenic groups on drawing to the stable zigzag arrangement illustrated in (b).

Figure 2.11. X-ray photographs for fibers of (a) BB-6, (b) BB-5 and (c) BB-4(1-Me) drawn from the isotropic melt at a rate of about 1 m sec^{-1}. The fiber axis is in the vertical direction. The molecular arrangements deduced from the X-ray patterns are also illustrated.

Figure 2.12. X-ray photographs for fibers of (a) BB-6, (b) BB-5 and (c) BB-4(1-Me) drawn from the smectic melt at a rate of about 1 cm sec^{-1}. The fiber axis is in the vertical direction. The molecular arrangements deduced from the X-ray patterns are also illustrated.

Figure 2.13. Stress - strain curves of a BB-5 fiber drawn from the S_{CA} melt. Solid curve was observed up to the breaking point and the dotted one is the relaxation curve observed on unloading at the strain of 70 %.

Figure 2.14. Wide-angle X-ray diffraction patterns of BB-5 fiber drawn from the S_{CA} melt taken under various strains of (a) 0 %, (b) 70 %. The fiber axis is in the vertical direction.

Figure 2.15. Schematic comparison of the flow of (a) the low molecular mass smectic phase and (b) polymeric smectic phase. In the polymeric system, chain folded lamellae are formed and slip over each other while in the low molar mass system, smectic layers can slip over each other.

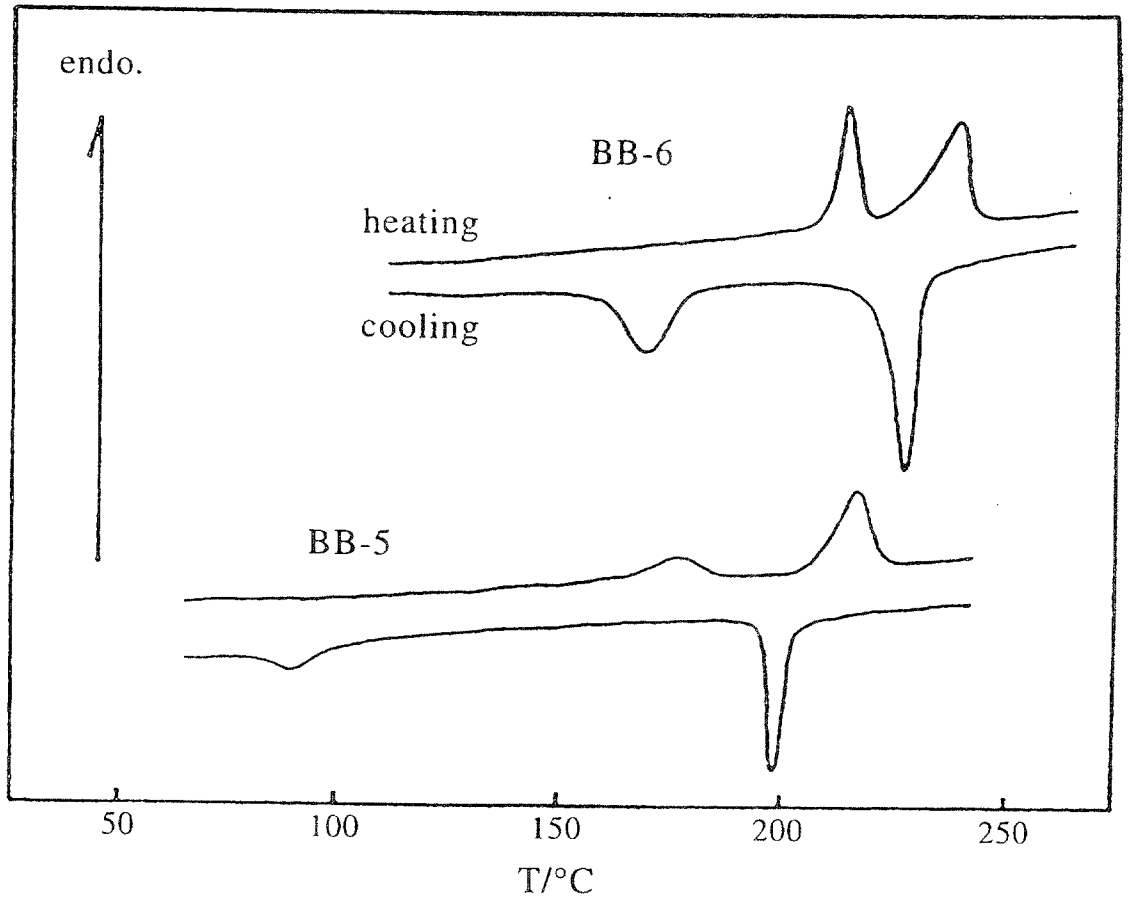

Figure 2.1. DSC thermograms of BB-5 and BB-6.

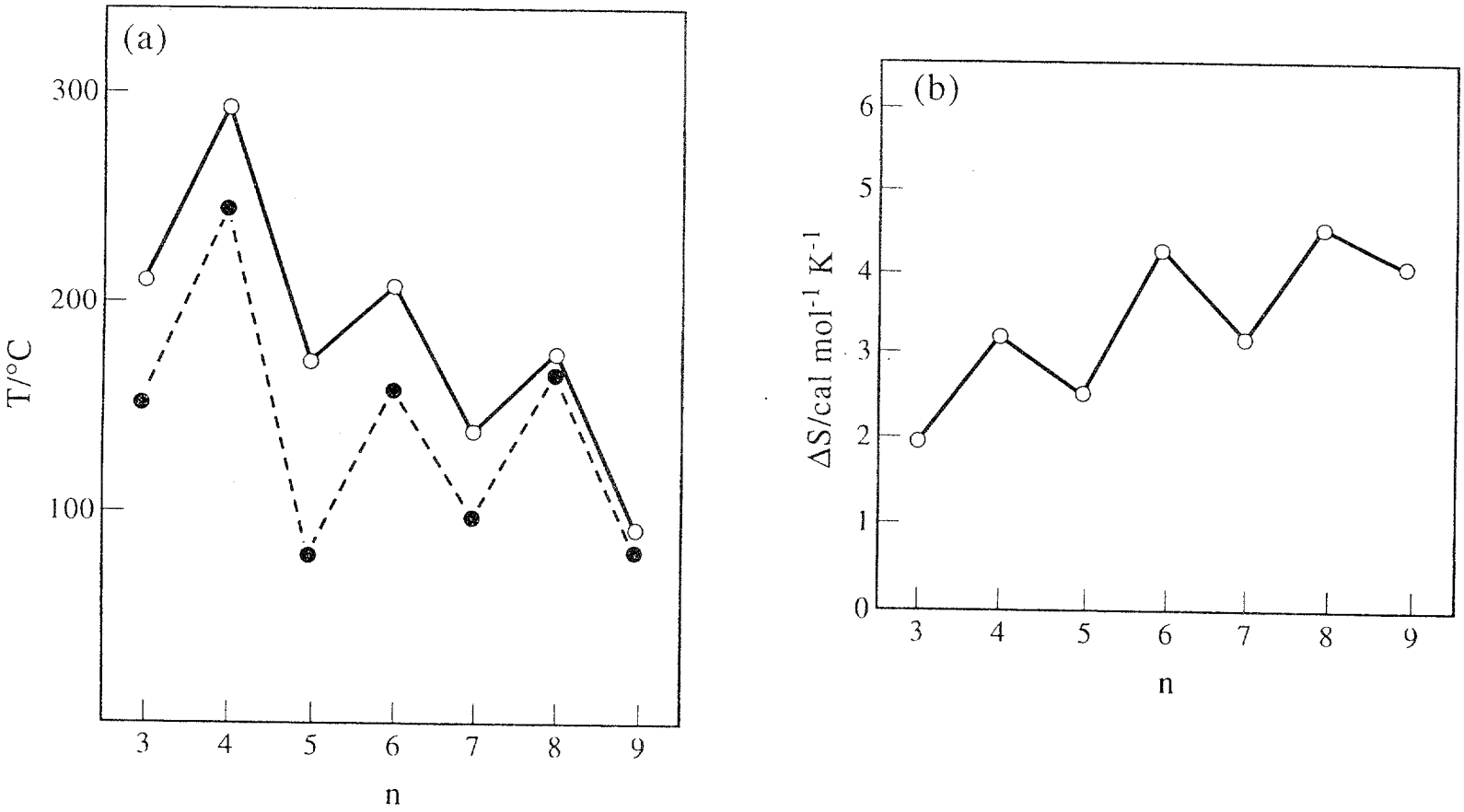

Figure 2.2. Variation with carbon number of alkylene spacer (*n*) of (a) transition temperatures (●, crystal-liquid crystal transition; ○, isotropization of liquid crystal) and (b) isotropization entropy of liquid crystal.

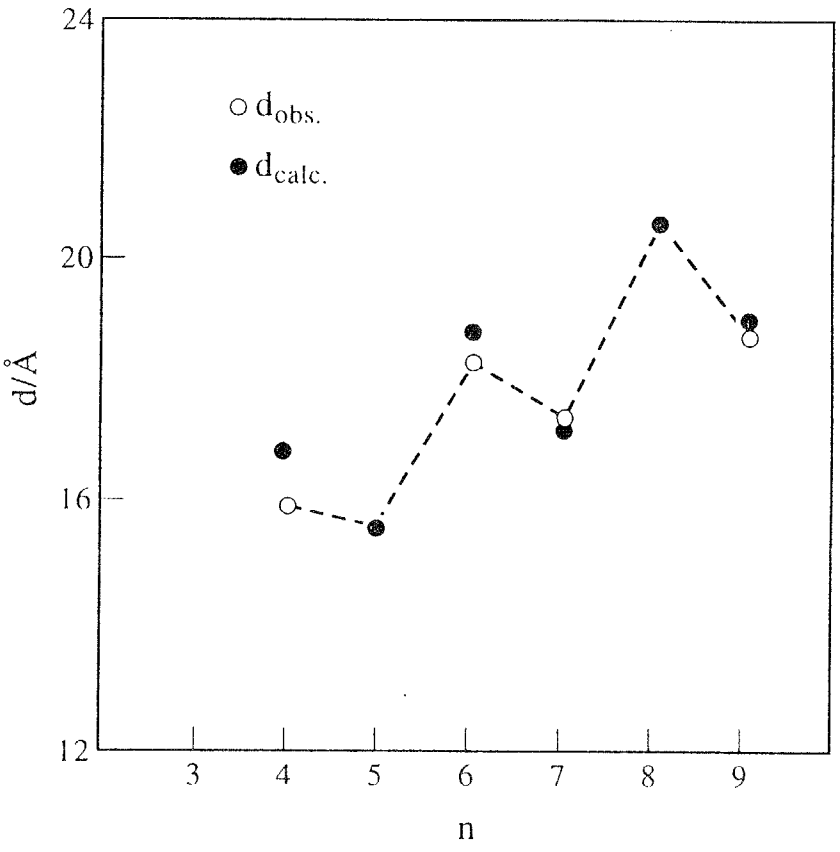

Figure 2.3. Variation of smectic layer thickness (○) with *n*. The calculated layer thickness (●) corresponds to the distance between the mesogenic groups averaged over the confined conformers with small angular displacement of successive mesogens (refer to text and Figure 2.7).

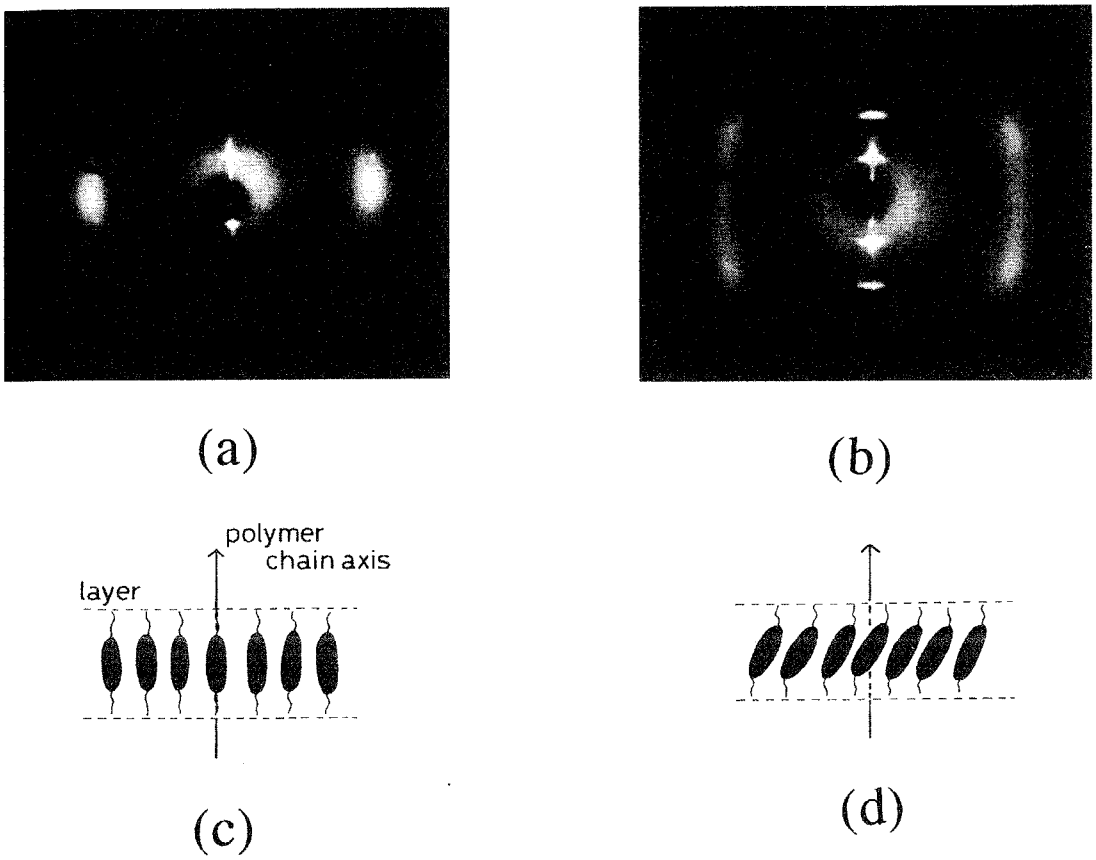

Figure 2.4. Oriented X-ray patterns of fibrous smectic phases of (a) BB-6 and (b) BB-5. (c), (d) Packing structures of mesogenic groups within a layer elucidated from X-ray patterns. Here, the oriented fibers were prepared by pulling the isotropic melt and the fiber axis is placed in the vertical direction.

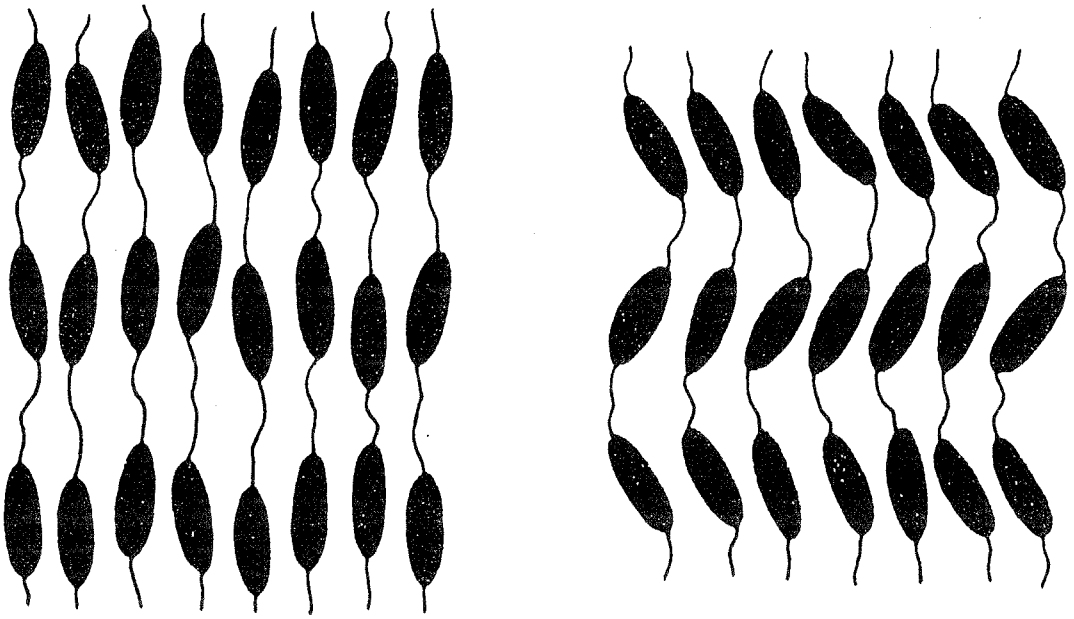

Figure 2.5. Layered structures of smectic phases of (a) BB-6 and (b) BB-5.

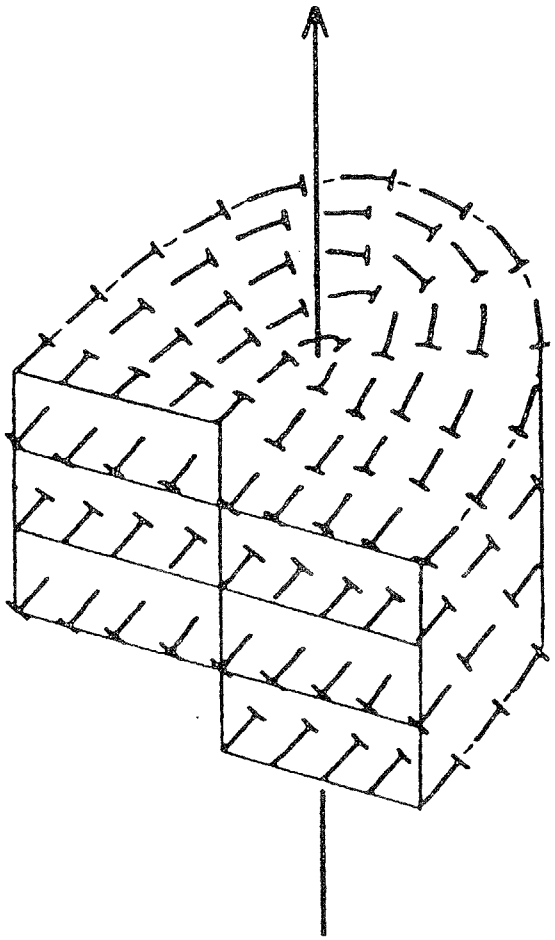

Figure 2.6. The c-director orientation around the wedge dispiration with rotational component of π which can be expected for the S_{CA} phase. The translational component gives rise to the step.

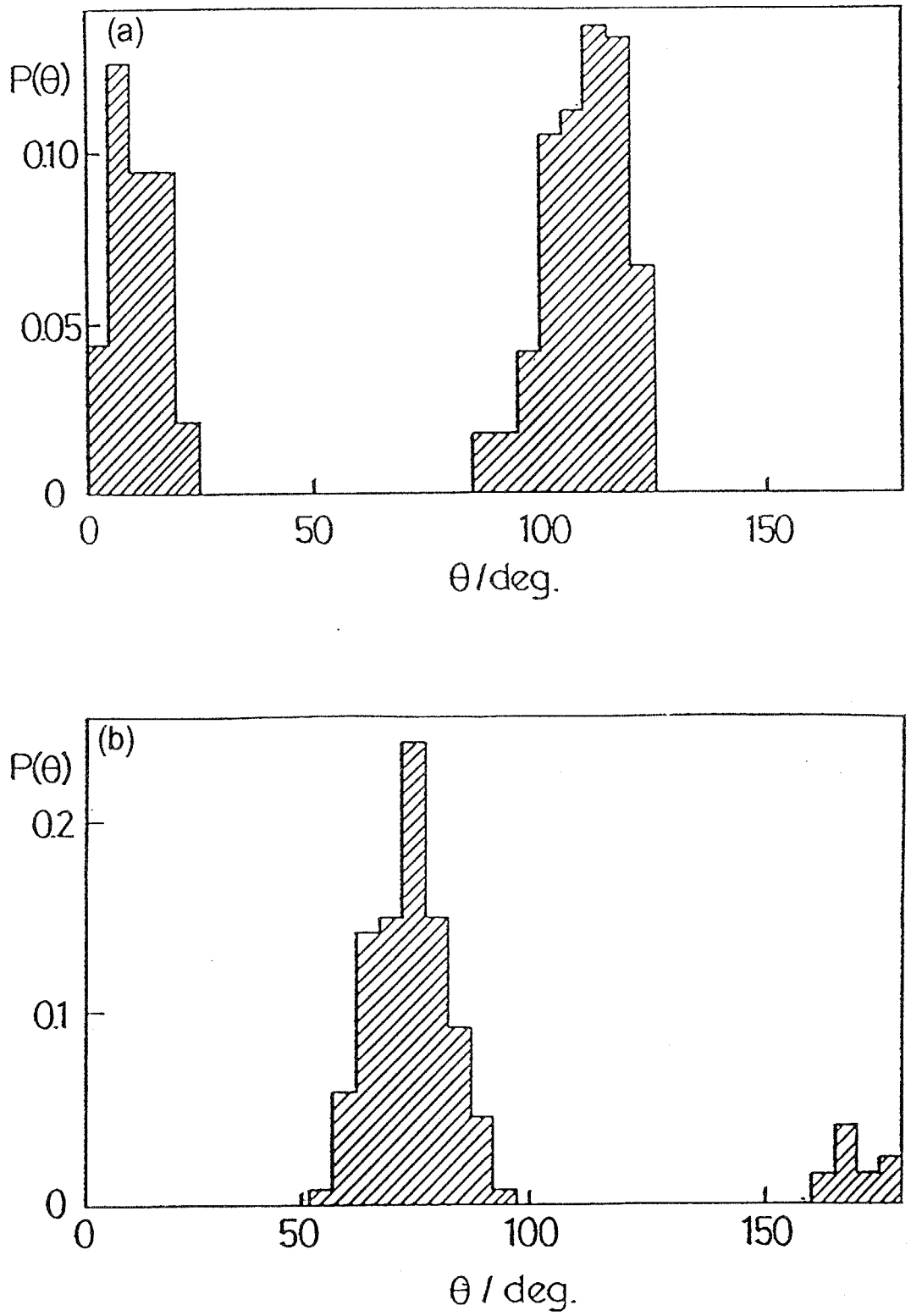

Figure 2.7. Distribution of chain conformer calculated for the angle θ defined by two successive mesogens: (a) BB-6; (b) BB-5.

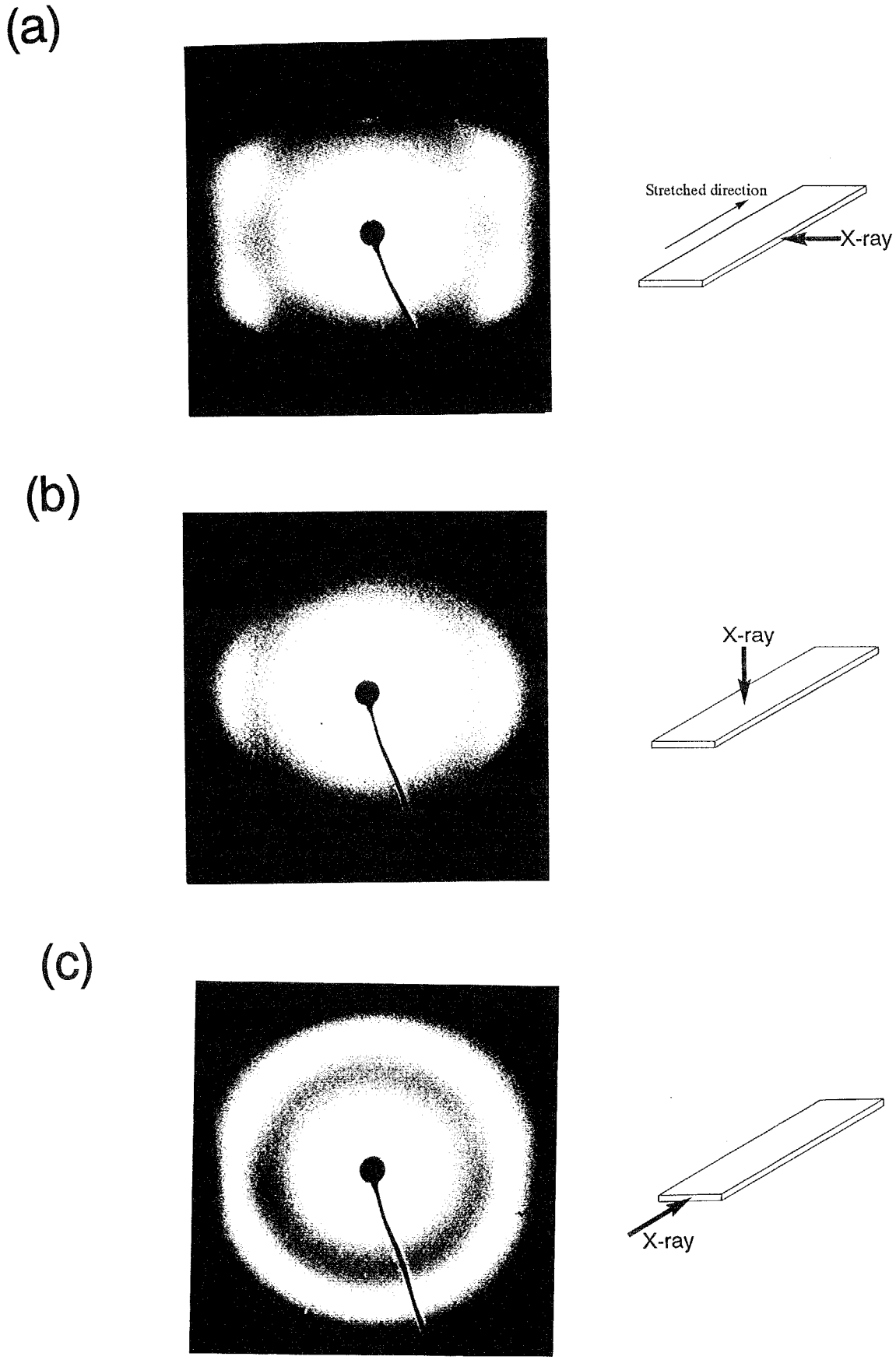

Figure 2.8. X-ray diffraction patterns of the oriented S_{CA} film taken by irradiation from three characteristic positions. (a) Parallel to the film surface and perpendicular to the chain axis; (b) perpendicular to the film surface; (c) parallel to both the film surface and chain axis. In (a) and (b) the chain axis is placed in the vertical direction; in (c) the film surface is parallel to the horizontal direction.

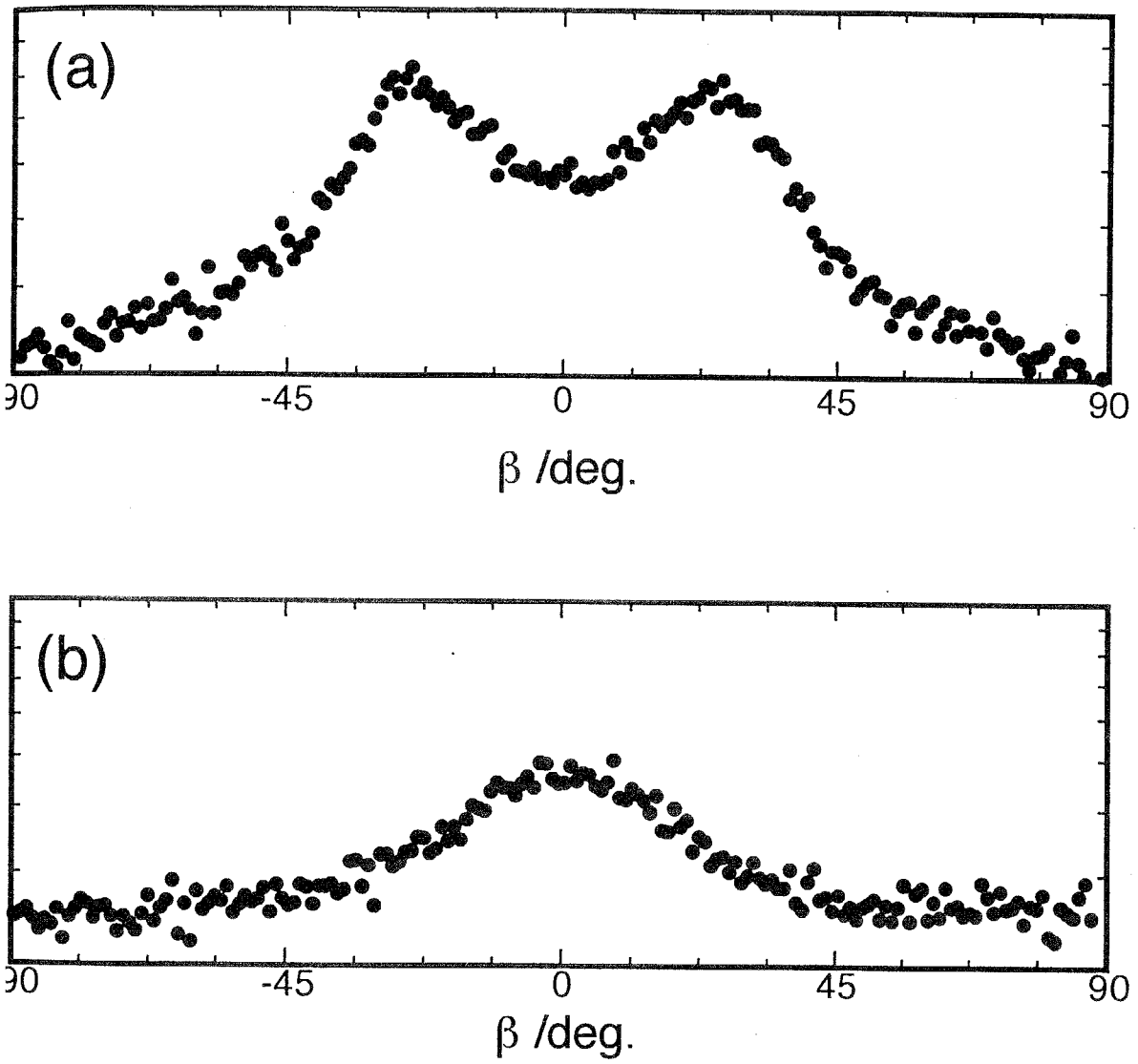

Figure 2.9. Intensity distribution $I(\beta)$ measured as a function of the azimuthal angle β at a diffraction angle of $2\theta = 20.5°$. Curves (a) and (b) are collected from Figure 2.8(a) and 2.8(b), respectively. Here, the equatorial direction corresponds to $\beta = 0°$.

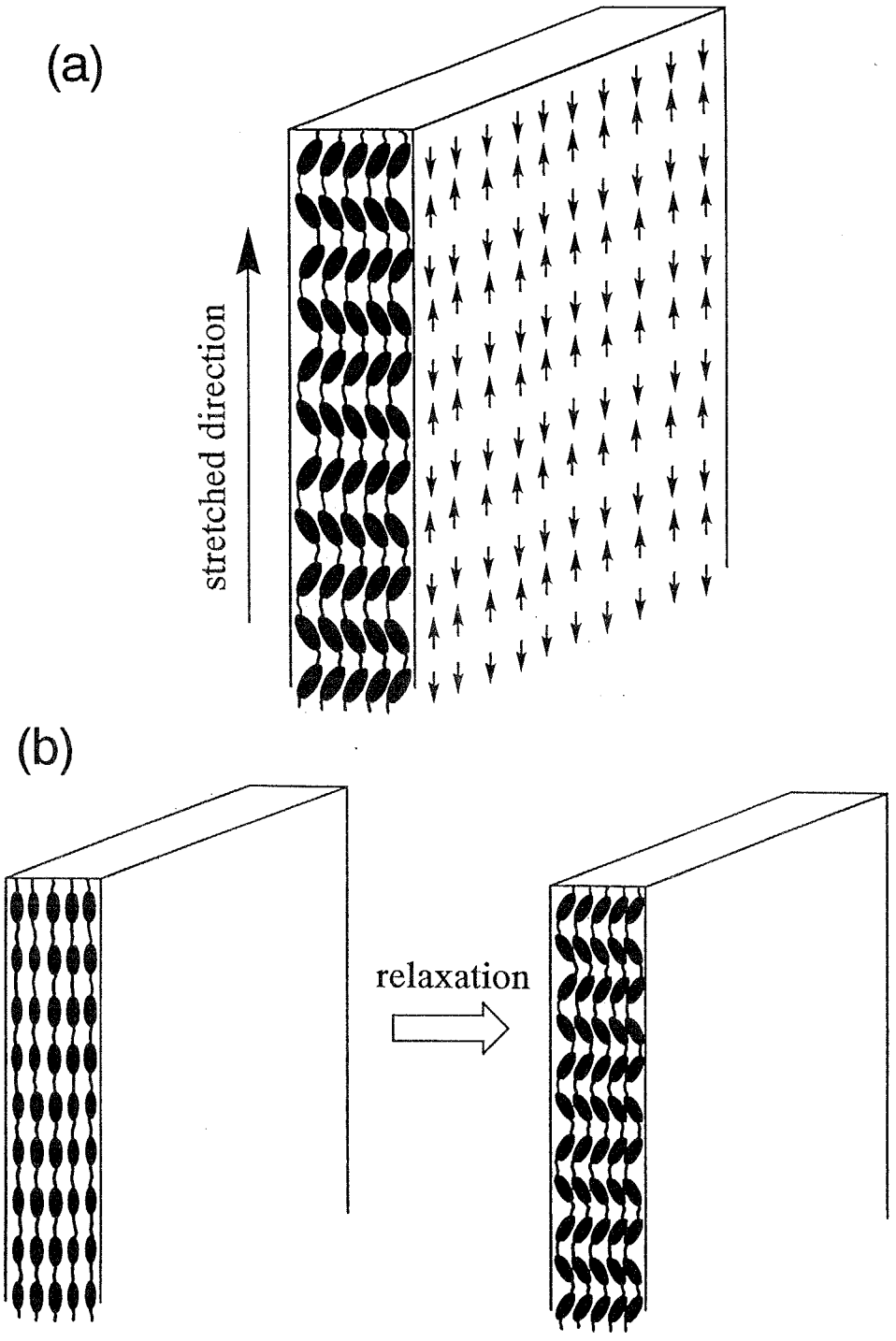

gure 2.10. (a) Illustration of the biaxial orientation of zigzag molecules in ɔ S_{CA} film where the mesogenic groups are tilted in a direction perpendicular the film surface. This preferential orientation may be caused by relaxation ɔm the extended arrangement of mesogenic groups on drawing to the stable ɜzag arrangement illustrated in (b).

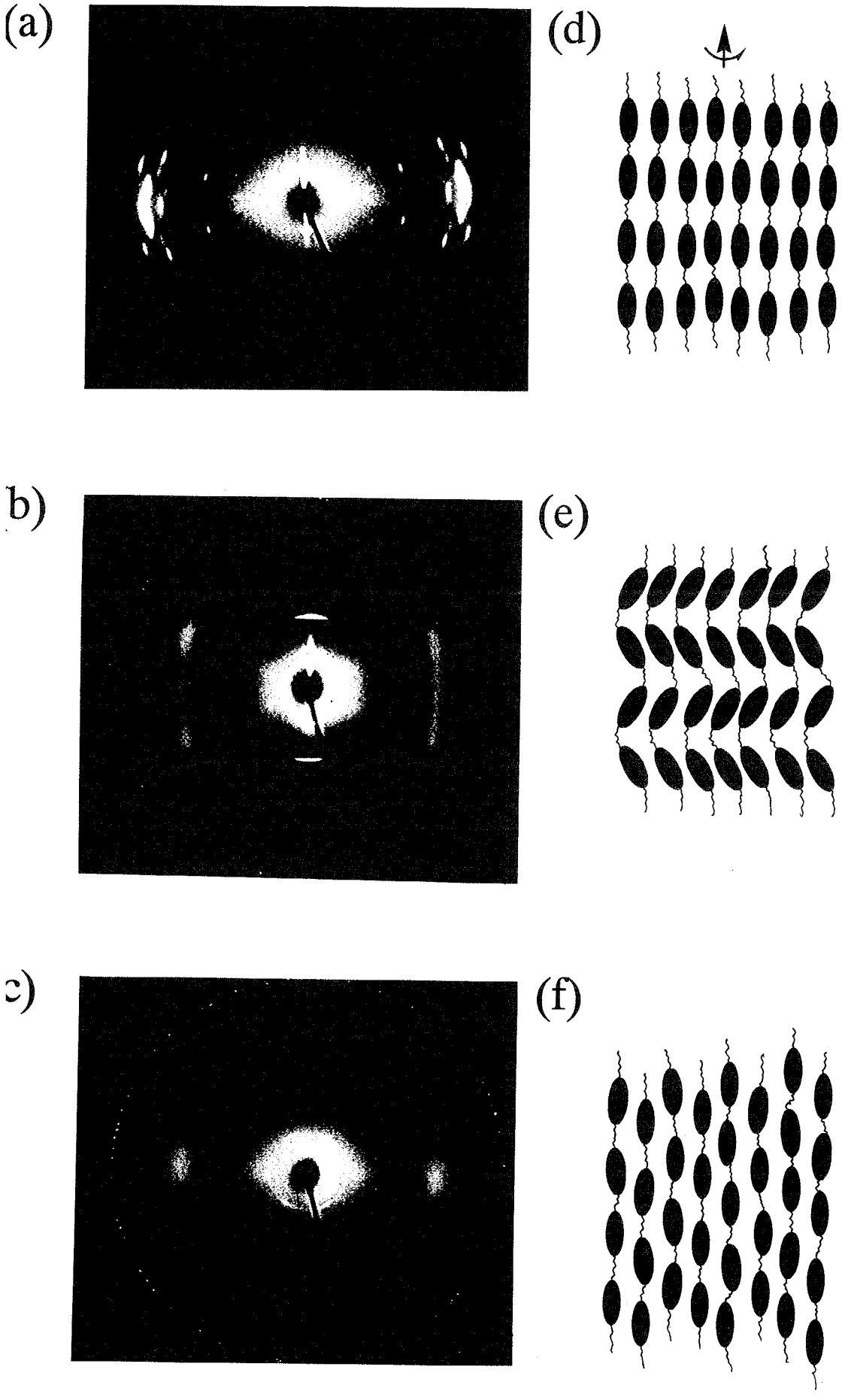

ıre 2.11. X-ray photographs for fibers of (a) BB-6, (b) BB-5 and (c) BB-4(1-Me) drawn from the :opic melt at a rate of about 1 m sec^{-1}. The fiber axis is in the vertical direction. The molecular ngements deduced from the X-ray patterns are also illustrated.

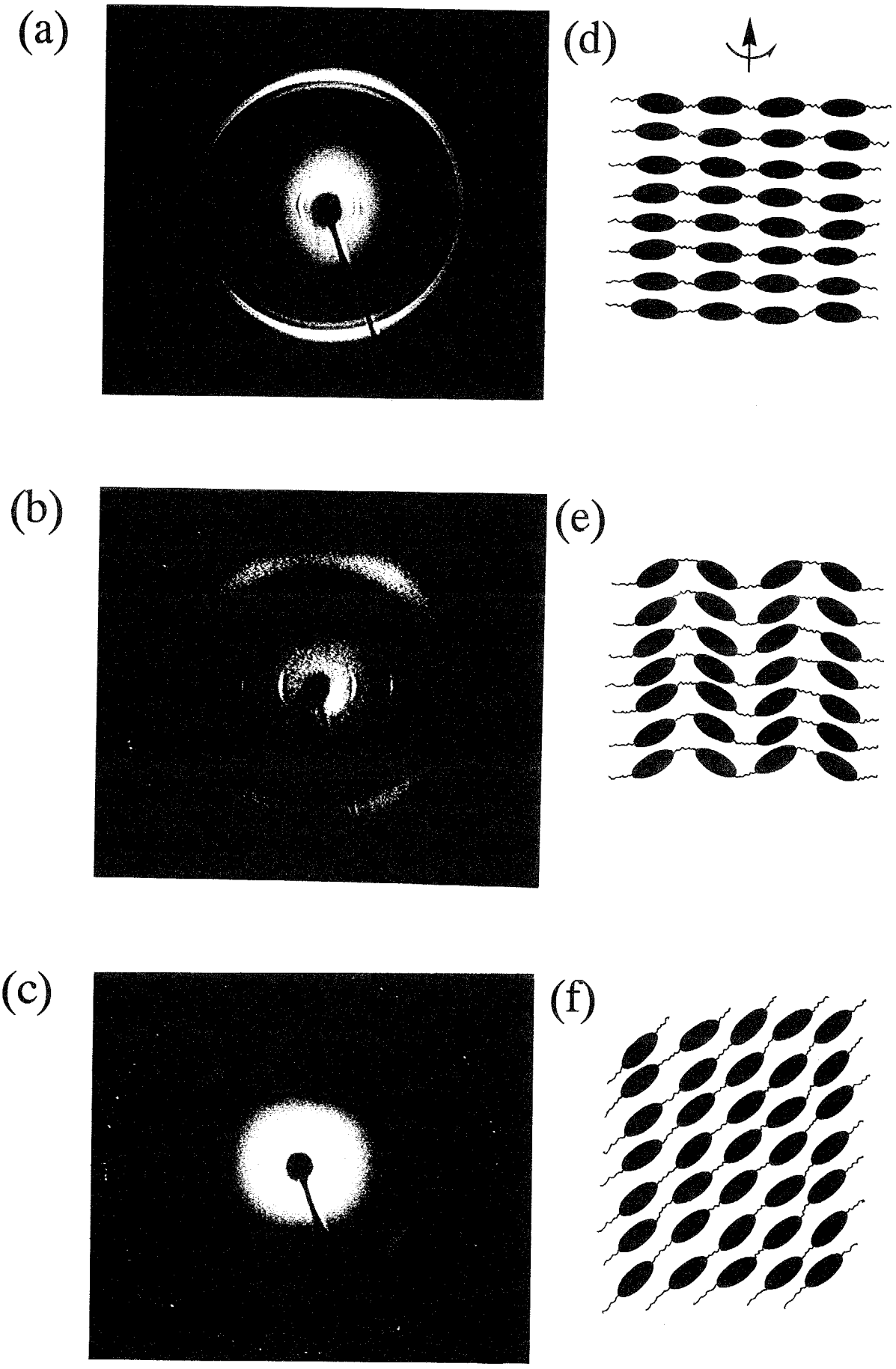

Figure 2.12. X-ray photographs for fibers of (a) BB-6, (b) BB-5 and (c) BB-4(1-Me) drawn from the smectic melt at a rate of about 1 cm sec^{-1}. The fiber axis is in the vertical direction. The molecular arrangements deduced from the X-ray patterns are also illustrated.

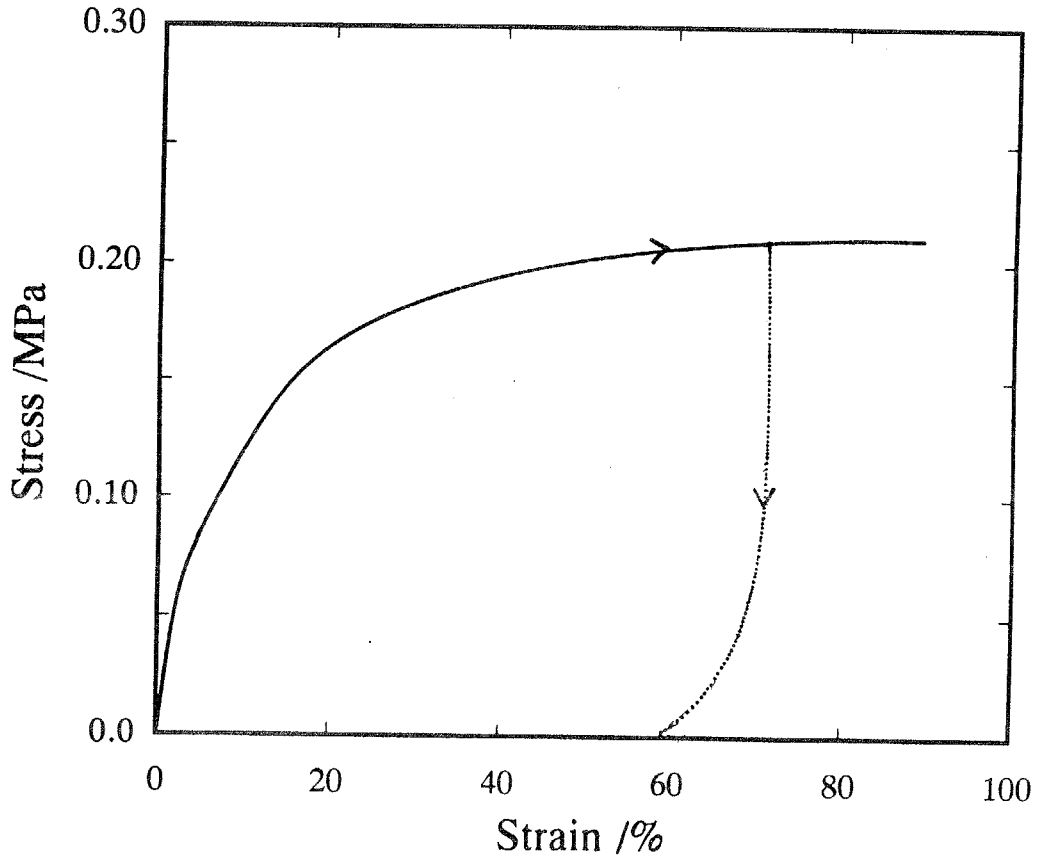

Figure 2.13. Stress - strain curves of a BB-5 fiber drawn from the S_{CA} melt. Solid curve was observed up to the breaking point and the dotted one is the relaxation curve observed on unloading at the strain of 70 %.

(a)

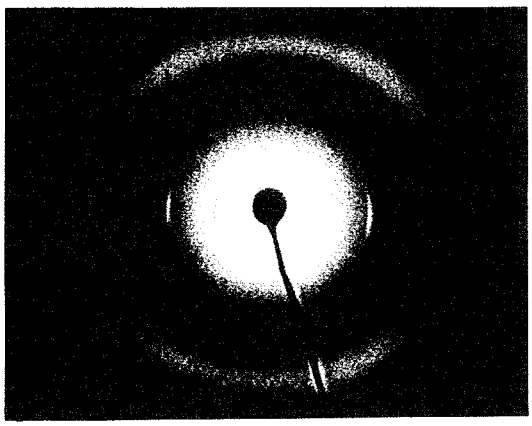

(b)

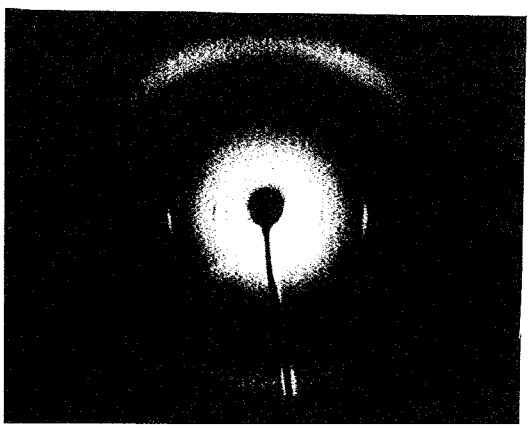

Figure 2.14. Wide-angle X-ray diffraction patterns of BB-5 fiber drawn from the S_{CA} melt taken under various strains of (a) 0 %, (b) 70 %. The fiber axis is in the vertical direction.

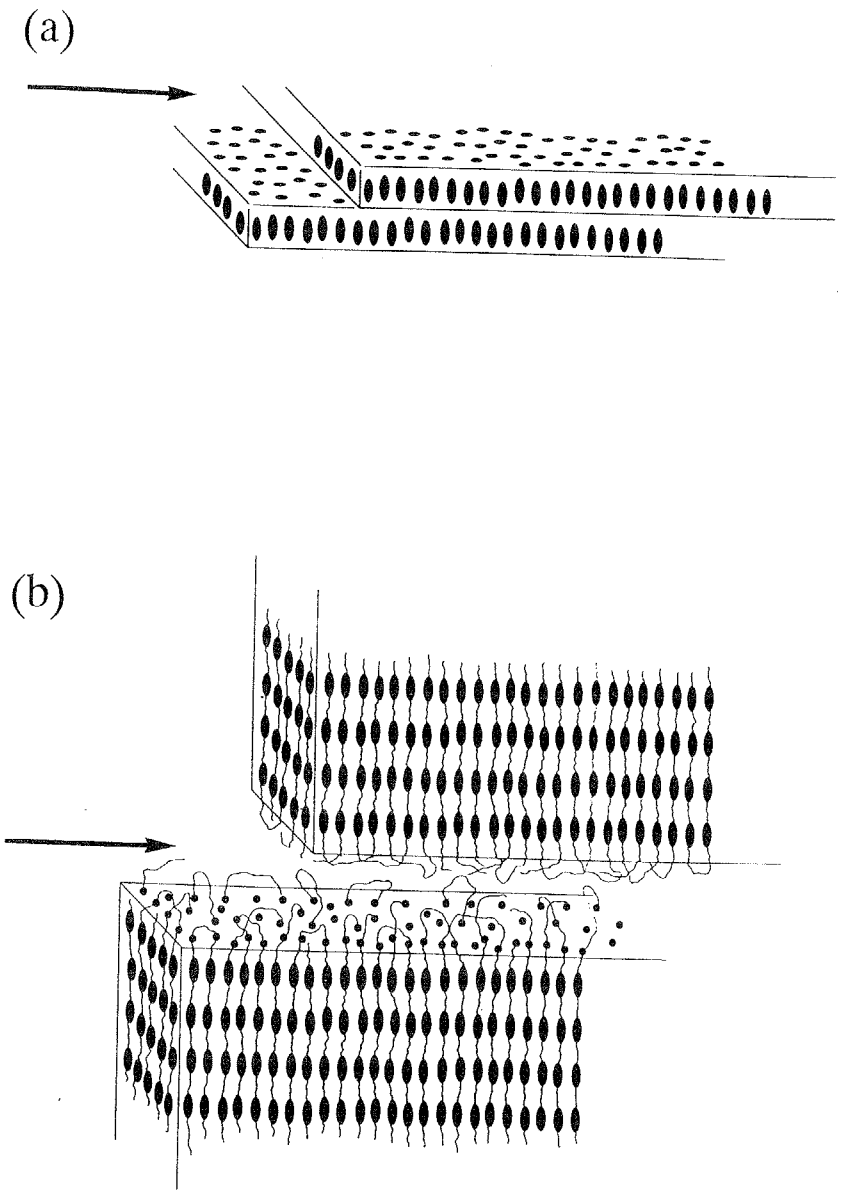

igure 2.15. Schematic comparison of the flow of (a) the low molecular mass mectic phase and (b) polymeric smectic phase. In the polymeric system, chain olded lamellae are formed and slip over each other while in the low molar mass ystem, smectic layers can slip over each other.

Chapter 3

Chain Folding in Smectic A Phase of BB-*n* Polyesters

ISTRACT: The solid state morphology of the main-chain liquid crystal BB-*n* polyesters s studied by the small-angle X-ray scattering (SAXS) method. The BB-*n* Polyester with *n* 6 and 8 forms isotropic, smectic A, and crystal phases in the order of decreasing ıperature; thereby their crystallization taking place from the smectic A phase. The SAXS the crystalline specimens prepared by cooling the isotropic melt at a rate of 10°C min^{-1} ›ws the well-defined reflection maxima which are attributable to the stacked lamellar ıcture. The lamellar spacings are distributed around 250 Å so that an appreciable number chain foldings are included in a chain. The lamellar size is increased by annealing the 'stal like in other crystallizable polymers. In contrast, it is not essentially altered by ıealing the smectic A phase. The results show that the chain folding exist at a ›rmodynamic equilibrium in the smectic A phase. The correlation length between the chain dings is assumed approximately to be 250 Å, which corresponds to 15 times the length of › repeat unit of BB-6. The lamellar spacing increases with a decrease in crystallization nperature. This trend is contrary to that observed in conventional polymers, and is plainable if the chain folding exist at a thermodynamic equilibrium as an entropy effect in › preceding smectic A phase.

3.1. Introduction

The liquid crystalline polymer (LCP) treated in this chapter is the following main-chain LC polyesters designated as BB-*n* [1-6]

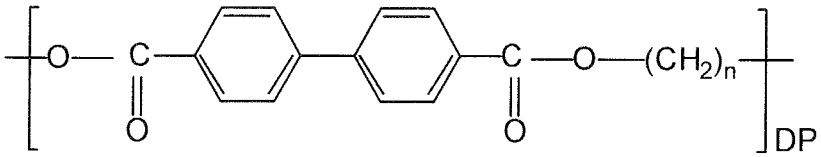

where *n* is the carbon number of the methylene spacer. These BB-*n* polyesters invariably form smectic mesophases when *n* varies from 3 to 9. As BB-*n* with an even *n* forms a S_A phase while that with an odd *n* forms a new type of smectic phase, S_{CA}.[2,3,6] This odd-even alternation of the smectic structures results from the conformational constraint in which the polymethylene spacer, assuming the more extended conformation, forces the neibouring mesogens to arrange with the characteristic angular displacement that depends on the odd-even parity of *n*.[6] Thus, one can picture that the polymer takes up the extended configuration at least in a local space of the smectic LC field. However, it has not been clarified if the polymer chains are extended along the entire length or not.

This important structural aspect of polymer chain configuration in the LC field has been extensively debated theoretically.[7-9] The complexity and subtlety in the main-chain LCPs come from the interplay between long-range orientational order of the liquid crystals and the polymeric tendency to maximize entropy. de Gennes[7] first pointed out that a semiflexible long chain in the nematic phase may recover some part of the entropy lost due to the ordering of the mesogenic units counter-reversal (180°) with respect to the director. The existence of one or two hairpin foldings was recently established by small-angle neutron scattering measurement for poly(4,4′-dioxy-2,2′-dimethyl azoxybenzene alkanedioyl)s in their nematic phases.[10-13] On the other

hand, Takahashi and Nagata[14] have studied the morphology of BB-6 crystals by small angle X-ray and electron microscopic measurements and found that the stacked lamellar structure is formed. This study is interesting since it suggests that the chain folding may exist in the preceding smectic phase.

Firstly, the theoretical discussion on hairpin folding (hairpin theory) submitted by de Gennes and Warner is reviewed in Section 3.2. Secondly, in Section 3.4, the solid state morphology of BB-6 was studied in more detail by the small-angle X-ray scattering (SAXS) method to discuss the chain configuration of the main-chain LCP in the smectic A phase. It is showed that the chain folding exist at a thermodynamic equilibrium in the smectic A phase. Thirdly, in Section 3.5, the study of the crystalline state morphology is extended for four BB-*n* polyesters, namely, BB-6, BB-8, BB-10 and BB-12. The extreme trend in the lamellar spacing was found in the LC polymers of BB-6 and BB-8. It is explainable if the chain foldings exist at a thermodynamic equilibrium as an entropy effect in the preceding smectic phase.

3.2. Review of Hairpin Theory[7,9]

3.2.1. Introduction

What we have in mind here is the chain with mesogens connected by spacers, namely main-chain liquid crystalline polymer (LCP). This section reviews the statics of the polymer chain embedded in nematic field theoretically discussed by de Gennes[7] and later by Warner[9].

The main-chain LCP has the internal molecular degree of freedom. The existence of orientation order of LC, causes a distortion in the constituent chains and the consequent loss of freedom causes the free energy to rise. The coupling of the order to the internal degree of freedom of the chain causes a

change in chain statistics. The complexity and subtlety in the main-chain LCPs come from the interplay between long-range orientational order of the liquid crystal and the polymeric tendency to maximize entropy. de Gennes first pointed out that a semiflexible long chain in the nematic phase may recover some part of the entropy lost due to the ordering of the mesogenic units by forming 'hairpin' where the chain executes a counter-reversal (180°) with respect to the director. The chain stiffness implies that the polymer pays an energy penalty for bending, and the nematic elements mean that the polymer pays an energy penalty for swimming across the nematic direction. They represented the polymer of length L in two dimensions by the trajectory of the angle it makes with the x axis, $\theta(s)$ where s is the arc length measured from one end of the polymer. The nematic director is assumed to point in the $\pm x$ direction. The energy may be written as a functional of $\theta(s)$

$$U[\theta(s)] = \frac{1}{2}\int_0^L ds\left[\varepsilon\left(\frac{d\theta(s)}{ds}\right)^2 + 3aS\sin^2\theta(s)\right] \tag{1}.$$

Here S is the order parameter of the nematic field and ε and a are the elastic bend and nematic mean field coupling constants, respectively. The first term comes from the elastic energy bending the polymer chain. The second term is associated with the potential energy of the nematic mean field, V

$$\begin{aligned} V(\cos\theta) &= -aSP_2(\cos\theta) \\ &= \tfrac{3}{2}aS\sin^2\theta - aS \end{aligned} \tag{2}.$$

Thus the first term depending on s is encountered in eq. 1.

To minimize the energy of the system, the polymer molecule should lie entirely along the nematic direction. For the polymeric system at a finite temperature, on the other hand, its tendency to maximize its entropy must be

considered. The polymeric molecules tend to take random coil configuration to increase their entropy. The polymeric nature and the liquid crystalline alignment of the mesogens in the polymer backbone arises complexity and subtlety of the chain configuration. The polymer chains would fold in the nematic field and that the energic cost of the chain folding would be counter-balanced by the entropy gained with folding the chain. They had chosen here to work in two dimensions because the chain foldings are essentially two dimensional objects.

3.2.2. Infinite Long Chain

de Gennes described the conformations of chains at finite temperature ($T \neq 0$) by minimizing the energy given with eq. 1 and putting the resultant minimum energy in a thermal distribution function. The trajectories of $\theta(s)$ are obtained by the Euler-Lagrange minimization of the energy. The equation of mechanical equilibrium obtained is

$$\varepsilon \frac{d^2\theta(s)}{ds^2} = 3aS\sin\theta(s)\cos\theta(s) \qquad (3).$$

The coordinate system used here is shown in Figure 3.1. The free ends of the polymer imply that the appropriate boundary conditions are $d\theta(s)/ds = 0$ at both ends of the worm. For a chain with infinite length, the boundary conditions are

$$d\theta(s) / ds = 0, \ \theta = 0, \pi \quad \text{at } s = \pm \infty \qquad (4).$$

The differential equation of eq. 3 with the boundary conditions of eq. 4 gives the trajectories of $\theta(s)$ as

$$\tan\frac{\theta}{2} = \exp\left(\frac{s}{\lambda}\right) \qquad (5)$$

where

$$\lambda = \sqrt{\frac{\varepsilon}{3aS}}$$

(6).

The energy is

$$U_h = \frac{1}{2}\int_{-\infty}^{+\infty} 2\sqrt{\varepsilon \cdot 3aS}\,\frac{d\theta}{ds}\sin\theta\, ds$$
$$= 2\sqrt{\varepsilon \cdot 3aS}$$

(7).

The trajectory is shown in Figure 3.1. A chain forms a hairpin with a length of 2λ. λ is less than or the order of the persistence length of the chain, ε / (k_BT). The simple theory gives a probability per unit length of thermally excited hairpin (P_h) proportional to

$$P_h \propto \exp(-U_h / k_B T)$$

(8).

3.2.3. Finite Long Chain

3.2.3.1. Single Hairpin in a Finite Long Chain

Here we consider a chain with a finite length which folds at $s = 0$ in the same coordination shown in Figure 3.1. The boundary condition is

$$d\theta(s) / ds = 0, \quad \theta = \theta_0, \pi - \theta_0 \qquad \text{at } s = \pm L/2$$

(9).

Under this condition, the differental equation gives

$$\int_{\pi/2}^{\theta} \frac{d\theta}{\sqrt{\cos^2\theta_0 - \cos^2\theta}} = \int_0^s \frac{1}{\lambda}\, ds$$

(10)

where it is assumed that $S = 1$ for simplicity. Eq. 10 is rewrote as

$$\int_0^{\frac{\cos\theta}{k}} \frac{dt}{\sqrt{1-t^2}\sqrt{1-k^2t^2}} = \frac{s}{\lambda}$$

(11)

where $k = \cos\theta_0$ and $\cos\theta = -kt$. The right side of eq. 11 is Jacobian elliptic integral of

$$u = \int_0^y \frac{dt}{\sqrt{1-t^2}\sqrt{1-k^2t^2}}$$

Thus $\theta(s)$ is presented as follows with using the inverse function of the Jacobian elliptic function, $y = \mathrm{sn}(u, k)$,

$$\theta(s) = \cos^{-1}\left(k\,\mathrm{sn}\left(\frac{s}{\lambda}, k\right)\right)$$

(12).

Integrating eq. 10 in the period of $0 \le s \le L/2$ gives

$$\int_0^1 \frac{dt}{\sqrt{1-t^2}\sqrt{1-k^2t^2}} = \frac{L}{2\lambda}$$

(13).

The left side in eq. 13 is the complete form of Jacobian elliptic integral represented as $K(k)$. Thus

$$K(k) = \frac{L}{2\lambda}$$

(14)

where

$$k = \cos\theta_0 = \cos\theta\left(-\frac{L}{2}\right) = -\cos\theta\left(\frac{L}{2}\right)$$

(15)

as mentioned before.

The complete form of Jacobian elliptic integral, $K(k)$ has a value range of $K(k) \geq \pi/2$. Thus,

$$K(k) = \frac{L}{2\lambda} \geq \frac{\pi}{2} \tag{16}$$

It shows that the hairpin configuration is obtained only in the case of $L \geq \pi\lambda$, consisting with the qualitative discussion of de Gennes; a short chain is nearly elongated. In contrast, if the molecular weight of the chain is very high, the chances of finding a hairpin become significant. In this case, k is approximated to be 1, and eq. 11 is rewrote as

$$\int_{\frac{\pi}{2}}^{\theta} \frac{d\theta}{\sqrt{1-\cos^2\theta}} = \int_0^s \frac{1}{\lambda} ds \tag{17}.$$

Integrating the both sides of eq. 17 gives immediately

$$\theta = 2\tan^{-1}\left[\exp\left(\frac{s}{\lambda}\right)\right] \tag{18}.$$

Eq. 18 corresponds to Eq. 5 obtained for the infinite length chain, showing that the solution for the infinite length chain is a good approximation to the trajectory for the finite length chain. The condition for this approximation is satisfied exponentially with increment in L as shown in the follows.

In the case of $k \approx 1$, $K(k)$ is approximated to

$$K(k) \cong \ln\frac{4}{\sqrt{1-k^2}} \tag{19}$$

Referring to eq. 14, one obtains

$$k^2 \cong 1 - 16e^{-L/\lambda} \tag{20}$$

thus

$$\theta_0 \cong 4e^{\frac{-L}{2\lambda}} \tag{21}$$

As seen in eq. 21, θ_0 decreases exponentially with increment of L and reaches to zero, meaning that the end of the chain is parallel to the director.

3.2.3.2. Plural Hairpins in a Finite Long Chain

Here, the consideration is expanded to the case that a finite long chain includes plural hairpins. Firstly, the origin for the coordinate of the counterlength along the chain, s, need to be moved to the end of the chain. Eq. 12 should be rewritten as

$$\cos\theta(s) = k\,\mathrm{sn}(K - s/\lambda, k) \tag{22}$$

Eq. 22 is simplified as

$$\sin\theta(s) = \mathrm{dn}(K - s/\lambda, k) \tag{23}$$

with using the relationship in the Jacobian elliptic functions

$$k^2\,\mathrm{sn}\,u + \mathrm{dn}^2\,u = 1 \tag{24}$$

and the simple relationship in trigonometric functions of $\cos^2\theta + \sin^2\theta = 1$. Here dn u is the Jacobian elliptic function associated with the second class elliptic integral defined as

$$\int_0^y \sqrt{\frac{1-k^2t^2}{1-t^2}}\,dt = \int_0^{\varphi} \sqrt{1-k^2\sin^2\theta}\,d\theta = \int_0^{u1} \mathrm{dn}^2 u\,du \tag{25}$$

As shown in Figure 3.2, it is assumed that plural hairpins in a chain can be devided into a hairpin included in a finite long chain discussed in section 3.3.1.

Eq.14 hence should be revised as

$$K(k) = \frac{L}{2n\lambda}$$

(26).

Thus the maximum number of the hairpin included in a chain with a length of L is given from the value range of the complete form of Jacobian elliptic integral, $K(k) \geq \pi/2$.

$$n_{\max} = \left[\frac{L}{\pi\lambda}\right]$$

(27)

where $[x]$ is the largest integer equal or less than x.

These solutions are very closely related to the single hairpin solution. As seen in eq. 26, $K(k)$ and k only depend on L/n. eq. 22 and eq. 23 show that $d\theta/ds = 0$ at a point between the hairpins. This implies that they may be cut at that point and the free end boundary conditions still are satisfied. Thus, a chain of length L with n hairpins is exactly equivalent to n chains of length L/n with a single hairpin smoothly jointed to each other. The hairpin energy is divided into two terms, nematic energy and bending energy corresponding to the second and first terms of the right-hand side of eq. (1). The nematic energy is

$$U_{nem}(n) = \tfrac{1}{2} n \int_0^{L/n} 3a\sin^2\theta(s)\, ds$$
$$= n\sqrt{3a\varepsilon}\, E(k)$$

(28)

where $E(k)$ is the complete normal elliptic integral of the second kind defined as

$$\int_0^{\pi/2} \sqrt{1 - k^2 \sin^2\theta}\; d\theta = \int_0^K \mathrm{dn}^2\, u\, du = E(k)$$

(29).

The bending energy is

$$U_{bend}(n) = \frac{1}{2} n \int_0^{L/n} \varepsilon \left(\frac{d\theta}{ds} \right)^2 ds$$
$$= n\sqrt{3a\varepsilon} E(k) + \frac{3aL}{2}(k^2 - 1)$$
$$= U_{nem} + \frac{3aL}{2}(k^2 - 1)$$

(30).

The hairpin energy is

$$U(n) = U_{nem} + U_{bend}$$
$$= \frac{3a}{2} L \left\{ \frac{4n\lambda}{L} E(k) + k^2 - 1 \right\}$$

(31).

The dependence of these energies on the number of hairpins are shown in Figure 3.3. For $n \ll n_{max}$, $k \cong 1$ and $E(k) \cong 1$ yields $U(n) = nU_h$: the total energy is merely n times the energy of a single hairpin included in a infinite long chain. As the number of hairpins is increased, the energy increase on adding additional hairpins become smaller, implying that the hairpins attract one another, in other words, two hairpins may lower their energy by coalescing into one larger hairpin.

The above analysis has shown that the non-trivial solutions of the equation of mechanical equilibrium are hairpins. However it is not clear whether hairpins are at the ground state or whether they are saddles. The potential energy of the hairpin depends on a finite number of variables $\theta = \{\theta_1, ..., \theta_N\}$, where a chain consists N rigid segments making a angle of θ_i with the director. The stability of the solution is determined with the signs of the eigenvalues of the matrix of second derivatives of the energy. It is too involved in mathematics a subject to be treated here in detail. The analysis proofs that an infinite hairpin is stable against any small perturbations and that any finite hairpin is unstable. However, the hairpins on a chain with $L/\lambda \gg 1$ will have a

very long life. This is because the lifetime of the potential-driven decay will scale initially like $\tau \sim f(L)/\sigma^{(1)}$ where $f(L)$ is a function related to the friction experienced by the chain which scales roughly as L, and $\sigma^{(1)} = -3a \times (1 - k^2)$ is the smallest eigenvalue for a single hairpin in a finite long chain. As noted above, for large L/λ, $1 - k^2 = 16 \exp(-L/(n\lambda))$ so that the decay time grows at least exponentially with the length. Thus it can be said that long hairpins are quasi-stable and the stability of the infinite hairpin is approached very rapidly.

3.3. Experimental Section

BB-*n* polyesters were synthesized by melt transesterification from dimethyl p,p′-bibenzoate and diols with isopropyl titanate as catalyst. The inherent viscosities of the samples, η_{inh}, were measured at 30°C by using 0.5 g dL^{-1} solutions in 60/40 w/w mixture of phenol and tetrachloroethane. The number average molecular weights, M_n, were determined by gel permeation chromatography (Polymer Laboratories Mixed-C with a JASCO 830-RI detector) in a 25/75 v/v mixture of pentafluorophenol and chloroform at 50 °C on the basis of calibration of standard polystyrene. Differential scanning calorimetric (DSC) measurements were carried out with a Perkin-Elmer DSC II under a flow of dry nitrogen. The wide-angle and small-angle X-ray measurements were performed using a Rigaku-Denki X-ray generator, RU-200 BH, with Ni-filtered Cu Kα radiation. The lamellar spacings from the small angle X-ray measurements were evaluated with a possible error of ± 5 Å.

3.4. Chain Folding in the Smectic Phase of BB-6

3.4.1. Characterization of BB-6 Polymers

Six specimens with different molecular weights, BB-6-I to BB-6-VI, were prepared by controlling the reaction period of melt transisterification. All the polymers exhibit the well-defined transition behavior, as found in the DSC thermogram of Figure 3.4 where the two enantiotropic transitions are included. The two transitions at T_m and T_i can be assigned to the crystal melting to smectic A and the isotropization of the smectic A phase, respectively.[2] The inherent viscosities, M_n, M_w/M_n, and thermodynamic data are listed in Table 3.1.

Parts a and b of Figure 3.5 show the wide-angle X-ray patterns taken for the oriented smectic A and crystalline phase of BB-6-III, respectively. The oriented smectic A phase exhibits the characterictic X-ray pattern which includes the sharp inner reflection with a spacing of 18.3 Å on the meridian and the outer broad reflection with a spacing of around 4.5 Å on the equator. The smectic type of structure has been identified from this characteristic reflection geometry.[2]

For the crystal prepared by cooling the smectic A phase of Figure 3.5a, the X-ray pattern is also highly oriented and ordered, as shown in Figure 3.5b; the amorphous halo is nearly absent, and significant peaks are measured up to $2\theta = 30°$ with about 20 peaks. The unit cell of the crystal has been reported to be monoclinic with $a = 10.98$ Å, $b = 11.47$ Å, $c = 19.62$ Å, and $\beta = 89.7°$.[15]

3.4.2. Stacked Lamellar Structure in the Crystalline Phase

Figure 3.6 shows the SAXS pattern taken for the same oriented crystal as in Figure 3.5b. Clear reflection maxima with a spacing of around 250 Å can be seen on the meridian, showing that the long period exists along the chain axis. The spacing of the long period exists along the chain axis. The spacing of the

long period, L, is obviously smaller than the entire extended molecular length of the polymer, l (see Table 3.2). These results show that the lamellar type of crystal structure with the chain foldings is formed. Takahashi and Nagata[14] have reported a similar observation for the same BB-6 sample and concluded the formation of the stacked lamellar structure by giving more decisive evidence from electron microscopy in which the 250 Å thick lamellae showing characteristic smectic-like texture and defects are observed with high contrast and resolution. Thomas et al.[16,17] and Kleman et al.[18] have also reported a similar morphology for the other type of main-chain LC polymer. The stacked lamellar structure with chain foldings is common in linear polyesters, poly(ethylene terephthalate) and poly(butylene terephthalate), so it is reasonable that the present BB-6 polyester could accommodate folds.

The long spacings by SAXS were determined for all the polymers. Those are listed in Table 3.2 and plotted against the molecular weight in Figure 3.7. In an effort to prevent a thermal prehistory, the data were collected for the crystals cooled at a rate of 10°C min^{-1} after 5 min of annealing in the isotropic melt. The long spacing, L, is distributed around 250 Å, increasing somewhat with an increase of molecular weight. This trend is discussed in Section 3.5. The correlation length between foldings thus corresponds to approximately 15 times the length of the repeat unit. The values for the average number of foldings in a chain, F, are listed in Table 3.2 as calculated from the equation. $F = l/L - 1$. It was found that several foldings are included in a chain.

Figure 3.8 shows the dependence of the lamellar spacing on annealing time at respective temperatures below T_m. Initially, the spacing increases very rapidly in the first 10 min of annealing and thereafter changes very little. Figure 3.9 shows the temperature dependence of L values with were collected at a constant annealing time of 60 min. As with other crystalline polymers,[19,20] the

long spacing increases with the increase of annealing temperature. These features are also expected for chain-folded lamellar crystals.

3.4.3. Chain folding in the Smectic A Phase

What is interesting here is that the crystallization of the present BB-6 polymer takes place from the smectic melt. This situation is completely different from that encountered in the conventional polymers in which the crystallization take place from the isotropic liquid. In a liquid state, a polymer molecule is capable of assuming a large number of configurations because of freedom of rotation of the individual chain atoms about their connecting bonds. There is no significant correlation between the configurations assumed by the individual molecules so that the liquid state is characterized by random, haphazard arrangements of the polymer chain units. On the other hand, the smectic A phase has a long range orientational order due to the extended configuration of polymer molecules. Further, it has an additional one-dimensional positional (smectic layer) order with the layer spacing nearly equal to the repeat length of the polymer in a fully extended form.[1,21] It can be thus envisaged that the crystallization to achieve full three-dimensional order takes place more easily and steadily from the smectic melt than from the isotropic melt, since it does not require a significant migration of the molecules and significant change of the molecular configuration. From a comparison of the X-ray patterns in Figure 3.5a and b, in practice, one can recognize that the orientational order of the smectic phase is completely sustained on crystallization and the resulting crystal has a high degree of crystallinity. Solid state morphology of the crystalline phase, hence, should reflect the morphology of the preceding smectic A phase, and it can be concluded that the chain folding

observed in the crystalline phase already existed in the preceding smectic A phase.

A significant question arises as to whether the chain folding in the smectic A is thermodynamically stable or is attributable to kinetic factors arising at the isotropic to smectic phase transformation. To examine this point, the lamellar spacing was measured for the crystal specimens of BB-6-III which were annealed for a certain period in the smectic A phase and then cooled down at a rate of 10°C min^{-1}. In Figure 3.10, the lamellar spacings thus determined are plotted against the annealing time. Here, the crystal specimens with various lamellar sizes were initially prepared by annealing at temperatures below T_m (refer to Figure 3.9) prior to heating to the smectic A phase for annealing. For the specimens with the lamellar spacing larger than 250 Å, the lamellar spacings changed drastically for the initial 5 min of annealing and finally reached a constant value of around 250 Å. This result leads to a significant conclusion that the chain foldings exist as a thermodynamic equilibrium state in the smectic A phase.

The next question that arises is, how are the chain foldings accommodated in the smectic A phase? Are the chain foldings positioned randomly or segregated in a certain confined position to result in the lamellar type of domain boundaries like in the crystalline phase? The two possible schematic diagrams reflecting the key features of the respective models are shown in Figure 3.11a, b. To this argument, it is interesting to note that the smectic phases of the main-chain polymers shows the anomalous orientation behavior on either applying shear flow deformation which was first observed by Krigbaum and Watanabe[21] or drawing the smectic melt (cf. Sect. 2.4). Shear flow orients the polymer chains perpendicular to its flow direction; in other words it orients the smectic layers parallel to the flow direction. An example can be seen Figures 3.5 and 3.6 where the oriented film sample has been prepared by taking advantage of

this flow behavior of the smectic A phase. These orientation behaviors are completely different from that in a nematic phase, where the polymers tend to orient parallel to the flow direction, and can be understood if the lamellar type structure exists such that the chain folding parts are limiting the boundaries of the flow domains,[21] as illustrated in Figure 3.11b. However, it should be also noted that the reflection maxima in SAXS leading to the lamellar type domains have never been observed in the smectic A glass. A similar observation has been reported by Takahashi and Nagata.[14] Thereby, at this stage, no decisive evidence that favors either model can be given. But the characteristic orientation behaviors in which the polymer chains orient perpendicular to either the shear direction or the fiber axis strongly suggest that the chain folding sites are segregated to form the flow domain boundaries, as shown in Figure 3.11b.

3.5. Long Spacings in Solid State of BB-*n* Polyesters Crystallized from Smectic A.

3.5.1. Long Spacings of the Solid Prepared by Cooling the Preceding Phase

In the previous section (Sect. 3.4), the solid state morphology of the BB-6 polyester examined by small angle X-ray scattering (SAXS) method. The BB-6 polyester forms isotropic, S_A and crystal phases in order of decreasing temperature, thereby its crystallization takes place from the S_A phase. SAXS for the crystalline specimens prepared by cooling the smectic melt shows well-defined reflection maxima which are attributable to a stacked lamellar structure. The lamellar spacings are distributed around 250 Å so that an appreciable number of chain foldings are included in a chain. Since we can hardly consider that the chain folding takes place on the crystallization from the S_A phase, it was

suggested that it already exists in the smectic field. Thus, the study has generated much interest because of the challenge of understanding the polymer configuration on a liquid crystalline field.

In this work, the study of the crystalline state morphology was extended to four BB-*n* polyesters, namely, BB-6, BB-8, BB-10 and BB-12, and it was found that in BB-6 and BB-8 forming S_A phase the crystallization temperature decreased with an increase of the cooling rate but the lamellar spacing increased. This trend in the lamellar spacing is opposed to that observed for BB-10 and BB-12 polyesters which crystallized from isotropic liquid like in conventional polymers. Some explanation for this trend will be given a relation to the chain configuration in the preceding S_A phase.

Figure 3.12 shows DSC curves of the BB-*n* polyesters. BB-6 exhibits two enantiotropic transitions at T_m and T_i which are assigned to the crystal melting to S_A and the isotropization of S_A, respectively. For BB-8, only a peak is observed on heating, which corresponds to the crystal melting to isotropic liquid. On cooling, two peaks appear and hence a monotropic S_A phase is formed between the two. In BB-6 and BB-8, thus, the crystallization takes place from the S_A phase. On the other hand, BB-10 and BB-12 show only one peak both on heating and cooling; they can form no mesophase because of the longer flexible spacer. Thus, the crystallization of BB-10 and BB-12 occurs directly from the isotropic liquid as in conventional polymers. The Thermodynamic data as well as the inherent viscosities are listed in Table 3.1.

The crystalline BB-*n* specimens were prepared by cooling the preceding phase at various rates in the DSC sample room. In an effort to prevent a thermal prehistory, all the specimens were heated to the isotropic melt before experiment. After these were kept for 10 minutes in the preceding phase (the S_A phase for BB-6 and BB-8 and the isotropic phase for BB-10 and BB-12), the crystallization process during cooling at various rates of 1.25 to 40°C min^{-1} was

monitored by DSC to determine the crystallization temperature, T_c, and the enthalpy, ΔH_c from the exothermic crystallization peak. Here, the peak temperature was regarded as T_c since the exothermic peak is appreciably sharp. After the whole peak was observed, the specimens were quenched to room temperature and took put from the DSC sample pan for SAXS measurements.

The SAXS pattern of all the specimens include clear reflection maxima with a spacing (L) within a range of 200 - 300 Å, showing that the long period exists in crystals. For BB-6, the long period was attributed to the stacked lamellar structure with chain foldings. Hence it is reasonable that the other BB-n polyesters with longer methylene spacers could accommodate chain foldings and form the stacked lamellar structure with a lamellar spacing, L.

Parts a, b, and c of Figure 3.13 shows the dependence of T_c, ΔH_c and L, on the cooling rate, respectively. As shown in Figure 3.13a, T_c is decreased with an increase in cooling rate for all specimens owing to supercooling. Some decrease is also observed in ΔH_c but it is not so significant (see Figure 3.13b), meaning that the degree of crystallinity is not much altered from sample to sample. On the other hand, the variation of L is completely different between the samples crystallized from isotropic liquid and those from smectic phase (see Figure 3.13c). In the BB-10 and BB-12 crystallized from isotropic melt, the lamellar spacing decreases with an increase in cooling rate, namely, with a decrease of T_c, which can be understood from the kinetical criteria as considered in conventional polymers. On the other hand, the lamellar spacing increases with an increase in cooling rate for BB-6 and BB-8 crystallized from S_A. This contrary dependence shows that chain foldings result from the origin completely different from that in conventional polymers.

The S_A phase has a long range orientational order due to the extended configuration of polymer molecules. Further, it has a one-dimensional

positional order with the layer spacing nearly equal to the repeat length of a fully extended polymer so that a significant migration of the molecules and significant change of the molecular configuration are not required on crystallization from S_A phase. Thus it is speculated that the chain foldings observed in the crystalline phase are not newly formed on crystallization but already exist in the preceding S_A phase. If this is the case, fold length (the distance between consecutive chain foldings) in the crystalline phase should corresponding qualitatively to that in the S_A phase at the temperature just above T_c, and the unusual dependence of the lamellar size on T_c in BB-6 and BB-8 crystals can be interpreted according to the theoretical prediction on polymer chain configuration in liquid crystalline (LC) field.

Polymer configuration in LC field has been initially debated theoretically by de Gennes. The chain folding is considered to arise as a result of the counterbalance between its energical cost and entropy gain. In other words, to produce the orientational and positional orders in a LC phase, the obvious configuration form a polymer molecule to assume in order to minimize its energy is for it to lie entirely along the director, but a semiflexible long chain may recover some part of entropy loss due to the ordering of the mesogenic units by forming hairpin folding where the chain executes a counter reversal (180°) with respect to the director. Such an entropy effect leads to the prediction that the fold length increases with decreasing temperature and hence that the lamellar thickness in the resulted crystal increases with decreasing crystallization temperature. The present result corresponds to this prediction.

Along the line of the chain folding (hairpin) theory, Warner and coworkers[11, 12] have developed statics and dynamics of chain foldings in worm like chains and given the simple theory in which the fold length is proportional to $\exp(U_h / k_B T)$, where $U_h = 2\sqrt{3}aS\varepsilon$ is the hairpin energy; S, the order parameter

of the LC field, ε, the elastic bend constant, and a, the LC field coupling constant. To clarify this proportionality, the logarithmic lamellar spacing are plotted against the reciprocal of absolute temperature in Figure 3.14 for BB-6 and BB-8. A linear relationship between the two can be seen as expected from the above equation. Here, it is reasonable that the slope of the line of BB-6 is larger than that of BB-8 since it reflects the chain rigidity estimated by ε in the above equation. The hairpin theory for the preceding LC phase thus explicates the variation of lamellar size in BB-6 and BB-8 crystals.

Here, the effect of molecular weight on the lamellar size for BB-6 reported in the previous section is reconsidered. Six specimens of BB-6 with different molecular weights, BB-6-I to BB-6-VI, which were prepared and characterized in a previous section are listed in Table 3.1 with the inherent viscosity and thermodynamic data collected on cooling process. All samples were cooled from S_A phase to room temperature at a constant rate of 10°C min^{-1} and the lamellar size was determined. The lamellar size was also listed in the ninth column of Table 3.3. The data is plotted in Figure 3.14 with closed circles, showing the identical linear relationship with the data collected in this work. It is hence reasonable to assert that the lamellar spacing depends on the crystallization temperature rather than the molecular weight.

3.5.2. Long Spacings of the Solid Prepared by Isothermal Crystallization

This section mentions the morphology of crystals which grows isothermally in the preceding phase. A Perkin-Elmer DSC-II apparatus was used to prepare the BB-6 and BB-10 crystalline specimens with the following standard procedure. The samples (about 15 mg) were maintained at the isotropic liquid state in order to eliminate any thermal history of the sample.

After holding the samples in the preceding phase for 10 min (the S_A phase for BB-6 and the isotropic phase for BB-10), they were rapidly cooled (80°C min^{-1}) to the crystallization temperature, T_c, and maintained at that temperature until the DSC signal reached a constant with time. After the whole exothermic peak was observed, the specimens were quenched to room temperature immediately and removed from the DSC sample pan for SAXS measurements in an effort to prevent isothermal thickening of the crystalline lamella.

The SAXS pattern of all the specimens includes clear reflection maxima. Figure 3.15 shows the dependence of the long spacing (L) on the crystallization temperature. The variation of L is different between the sample crystallized from isotropic liquid and that from smectic phase. In the BB-10 crystallized from isotropic melt, the lamellar spacing increases with T_c, which can be understood from the kinetical criteria as considered in conventional polymers. On the other hand, the lamellar spacing of BB-6 shows slightly decrease with an increment in T_c. The slight dependence on T_c in BB-6 is expected. Once a thin liquid crystalline lamellar at a high temperature crystallize, it should thicken more rapid as the T_c is higher. Moreover, the thickening of the lamella takes more time as T_c is a higher temperature. Accounting the isothermal thickening of the lamella, the initial lamellar spacing must decrease with an increment in T_c. This contrary dependence is identical with that in found in Section 3.5.1.

3.6. Concluding Remarks

The solid state morphology in BB-6, BB-8, BB-10 and BB-12 polyesters prepared by crystallizing the preceding phase exhibit well-defined SAXS maxima attributable to the chain folded lamellar. The following two results lead to the most significant result that the chain folding is formed at thermodynamic equilibrium as an entropy effect in the foregoing smectic A phase. (1) The lamellar size was increased by annealing the crystal like in other crystallizable polymers. In contrast, it is not altered by annealing the smectic A phase. Moreover the lamellar size (L) increased by annealing the crystal decreased and reached a constant value by annealing at the smectic A phase. (2) The variation in lamellar size with the crystallization temperature depends strongly on the preceding phase. In BB-10 and BB-12 which crystallize from the isotropic liquid as in conventional polymers, longer L value were observed form samples which crystallized at a higher temperature. In contrast, crystals BB-6 and BB-8 which were prepared from the smectic A phase exhibit the unusual trend where larger value of L were observed for samples crystallized at a lower temperature. This contrary trend in L can be explained by the hairpin theory based on which the chain folding exists at thermodynamic equilibrium as an entropy effect in the preceding smectic A phase.

References

(1) Watanabe, J.; Hayashi, M. *Macromolecules* **1988**, *21*, 278.

(2) Watanabe, J.; Hayashi, M. *Macromolecules* **1989**, *22*, 4083.

(3) Watanabe, J.; Kinoshita, S. *J. Phys. II (France)* **1992**, *2*, 1237.

(4) Watanabe, J; Nakata, Y.; Shimizu, K. *J. Phys. II (France)* **1992**, *2*, 1237.

(5) Nakata, Y.; Watanabe, J. *J. Mater. Chem.* **1994**, *4*, 1699.

(6) Watanabe, J.; Hayashi, M.; Morita; A.; Niori, T. *Mol. Cryst. Liq. Cryst.* **1994**, *254*, 221.

(7) de Gennes, P. G. In Polymer Liquid Crystals, A. Cifferri, W. R. Krigbaum, and R. B. Mayer Eds., Academic Press, New York, 1982; p124.

(8) Wang, X. J.; Warner, M. *J. Phys. A* **1986**, *19*, 2215.

(9) Williams, D. R. M.; Warner, M., *J. Phys. Fr.* **1990**, *51*, 317.

(10) D'Allest, J. F.; Sxiou, P; Blumstein, A.; Blumstein, R. B. *Mol. Cryst. Liq. Cryst* **1993**, *155*, 581.

(11) Arrighi, V.; Higgins, J. S.; Weiss, R. A.; Cimecioglu, A. L. *Macromolecules* **1992**, *25*, 5297.

(12) Li, M. H.; Brulet, A.; Davidson, P.; Keller, P.; Cotton, J. P. *Phys. Rev. Lett.* **1993**, 70, 2293.

(13) Li, M. H.; Brulet, A.; Cotton, J. P.; Davidson, P.; Strazielle, C.; Keller, P. *J. Phys. II (France)* **1994**, *4*, 1843.

(14) Takahashi, T.; Nagata, F. *J. Macromol. Sci. Phys.* **1989**, *B28*, 34.

(15) Li, Xiaodongand; Brisse, F. *Macromolecules* **1994**, *27*, 7725.

(16) Thomas, E. L.; Wood, B. A. *Faraday Discuss. Chem. Soc.* **1985**, 79, 229.

(17) Hudson, D.; Vezie, D. L.; Thomas, E. L. *Makromol. Chem., Rapid Commun.* **1990**, *11*, 657.

(18) Mazelet, G.; Kleman, M. *J. Mater. Sci.* **1988**, 23, 3055.

(19) Fisher, E. W.; Schmidt, G. F. *Angew. Chem., Int. Edit. Engl.* **1962**, *1*, 488.

(20) Barham, P. J.; Chivers, R. H.; Keller, A., Martines-Salazar, J.; and Organ, S. J. *J. Mater. Sci.* **1985**, *20*, 1625.

(21) Krigbaum, W. R.; Watanabe, J. *Polymer* **1983**, *24*, 1299.

(22) Barham, P. J.; Keller, A. *J. Polym. Sci. Phys. Ed.* **1989**, 27, 1029.

Table 3.1. Characterization of BB-*n* polyesters

		Calorimetric Data[a]					
		Transition temperatures				Transition enthalpies	
		Heating		Cooling			
Sample	η_{inh} /dL g^{-1}	T_m /°C	T_i /°C	T_c /°C	T_i /°C	ΔH_c /kcal mol^{-1}	ΔH_i /kcal mol^{-1}
BB-6-I	0.26	210	231	187	218	3.12	1.99
BB-6-II	0.34	213	238	167	228	2.09	2.31
BB-6-III	0.40	216	239	166	227	2.09	1.97
BB-6-IV	0.49	214	240	165	229	1.90	2.01
BB-6-V	0.67	220	241	161	227	1.84	2.13
BB-6-VI	0.92	213	239	155	224	1.96	2.15
BB-8	0.70	193		153	180	1.62	2.27
BB-10	0.84	171		151		3.88	
BB-12	1.05	164		141		4.71	

[a] Based on DSC data measured at a scanning rate of 10°C min^{-1}.

Table 3.2. Parameters for the lamellar structure formed by folded chains of BB-6

Sample	M_n (10^4)	M_w/M_n	Chain length l^a /Å	Lamellar size L^b /Å	Number of chain folding F^c
BB-6-I	1.28	2.41	7.8×10^2	225	2.5
BB-6-II	1.36	2.39	8.3×10^2	244	2.4
BB-6-III	1.52	2.03	9.2×10^2	251	2.7
BB-6-IV	1.70	2.46	1.0×10^3	247	3.2
BB-6-V	2.15	2.38	1.3×10^3	267	3.9
BB-6-VI	3.23	2.30	2.0×10^3	294	5.5

[a]Calculated by using the repeating length of 19.6Å in the crystalline state.
[b]Observed for the crystal sample which was cooled from the isotropic melt at a rate of 10°C min^{-1}.
[c]$F = l / L - 1$.

Figure Captions

Figure 3.1. Coordinate system used for calculating the trajectory of a single hairpin in an infinity long chain. The chain bends over a distance of a few times its persistence length and the remain is aligned very closely with the nematic director, **n**.

Figure 3.2. Coordinate system used for calculating the trajectory of plural hairpins in a finite long chain.

Figure 3.3. Plots of the energy in units of the hairpin energy, U_h versus the number of hairpins for a typical case of $L/l = 100$. Asterisks are the total energy, which increases linearly with the number of hairpins. Solid squares are the nematic contribution of the energy, and open circles are the bending contribution.

Figure 3.4. DSC heating and cooling thermograms of BB-6-III measured at a rate of 10°C min^{-1}.

Figure 3.5. Wide angle X-ray patterns of (a) the oriented smectic A and (b) the crystalline phase of BB-6-III. Here, the oriented film specimen was prepared by shear flowing the smectic A phase between thin glass plates. The flow direction is horizontal.

Figure 3.6. Small angle X-ray pattern for the oriented crystal of Figure 3.5b.

Figure 3.7. Molecular weight dependence of the lamellar spacing elusidated for the crystalline specimens which were prepared by cooling the isotropic melt at a rate of 10°C min^{-1}.

Figure 3.8. Dependence of the lamellar spacing on the time of annealing in the crystalline phase. The crystalline specimens of BB-6-III were initially prepared by cooling the isotropic melt at a rate of 10°C min^{-1} and annealed at respective temperatures below T_m.

Figure 3.9. Dependence of the lamellar spacing on the annealing temperature below T_m. The data were collected after 60 min of annealing (refer to Figure 3.8).

Figure 3.10. Dependence of the lamellar spacing on the annealing time in the smectic A phase. Here, the crystalline specimens of BB-6-III with the different lamellar sizes of 320, 290, and 248 Å were initially prepared by annealing at temperatures below T_m (refer to Figure 3.9) and heated to the smectic A phase (at 225°C) for annealing. After an appropriate time of annealing, the specimen was cooled to room temperature at a rate of 10°C min^{-1} and the lamellar size determined in its crystalline phase.

Figure 3.11. Two possible schematic diagrams showing the different accommodation of the chain folding sites into the smectic structure. In (a), the folding sites are randomly placed, while in (b), they are segregated to form domain boundaries.

Figure 3.12. DSC thermograms of (a) BB-6-IV, (b) BB-8, (c) BB-10 and (d) BB-12 measured at a scanning rate of 10°C min^{-1}.

Figure 3.13. (a) Crystallization temperature (T_c), (b) crystallization enthalpy (ΔH_c) and (c) lamellar spacing (L) as a function of the cooling rate observed for BB-6-IV (circles), BB-8 (triangles), BB-10 (squares) and BB-12 (lozenges). The data points of BB-8 measured at cooling rates 1.25 and 2.5°C min^{-1} are omitted because of significant overlapping of the two peaks due to the isotropic S_A and S_A to crystal transitions.

Figure 3.14. Plots of logarithmic lamellar spacing against the reciprocal of the crystallization temperature (T_c) for BB-6-IV (circles) and BB-8 (triangles). The data points given by the open symbols are those observed in Figure 3.13. Also included are the data points given by solid symbols which were collected for the BB-6 polyesters with different molecular weights in Section 3.4.

Figure 3.15. Dependence of the lamellar spacing on the isothermal crystallization temperature. The data were collected for the sample quenched just after the exothermic peak in the DSC curve ended.

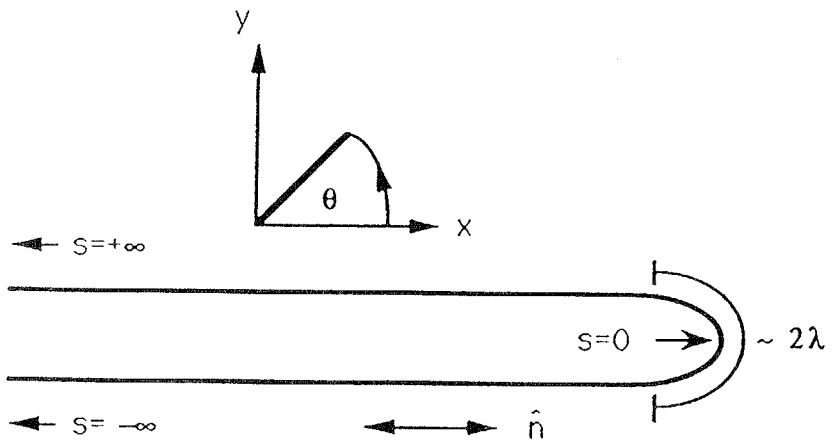

Figure 3.1. Coordinate system used for calculating the trajectory of a single hairpin in an infinity long chain. The chain bends over a distance of a few times its persistence length and the remain is aligned very closely with the nematic director, **n**.

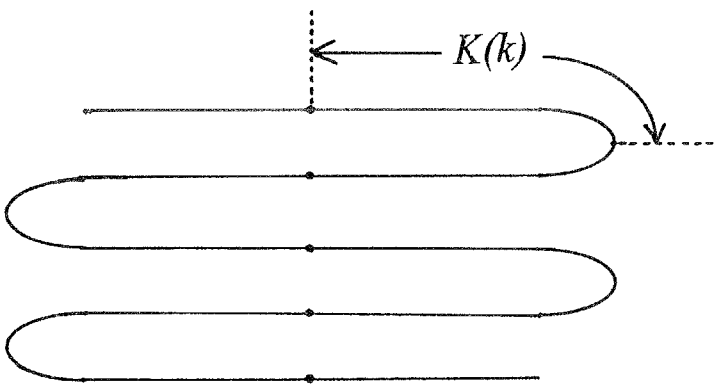

Figure 3.2. Coordinate system used for calculating the trajectory of plural hairpins in a finite long chain.

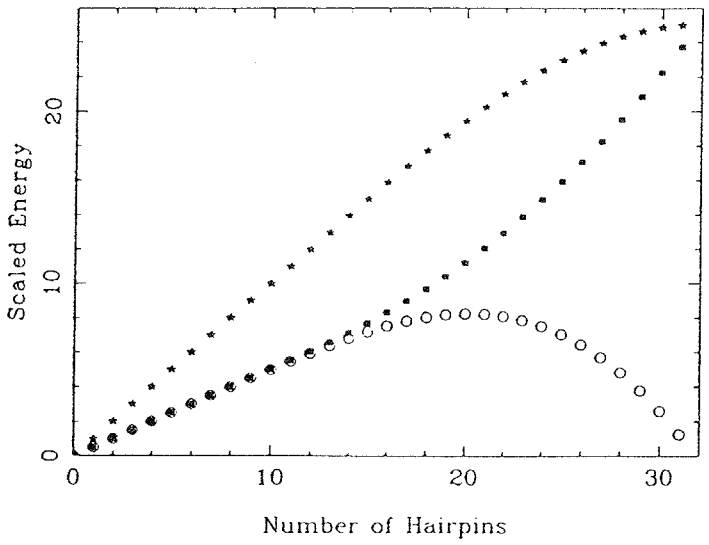

Figure 3.3. Plots of the energy in units of the hairpin energy, U_h versus the number of hairpins for a typical case of $L/l = 100$. Asterisks are the total energy, which increases linearly with the number of hairpins. Solid squares are the nematic contribution of the energy, and open circles are the bending contribution.

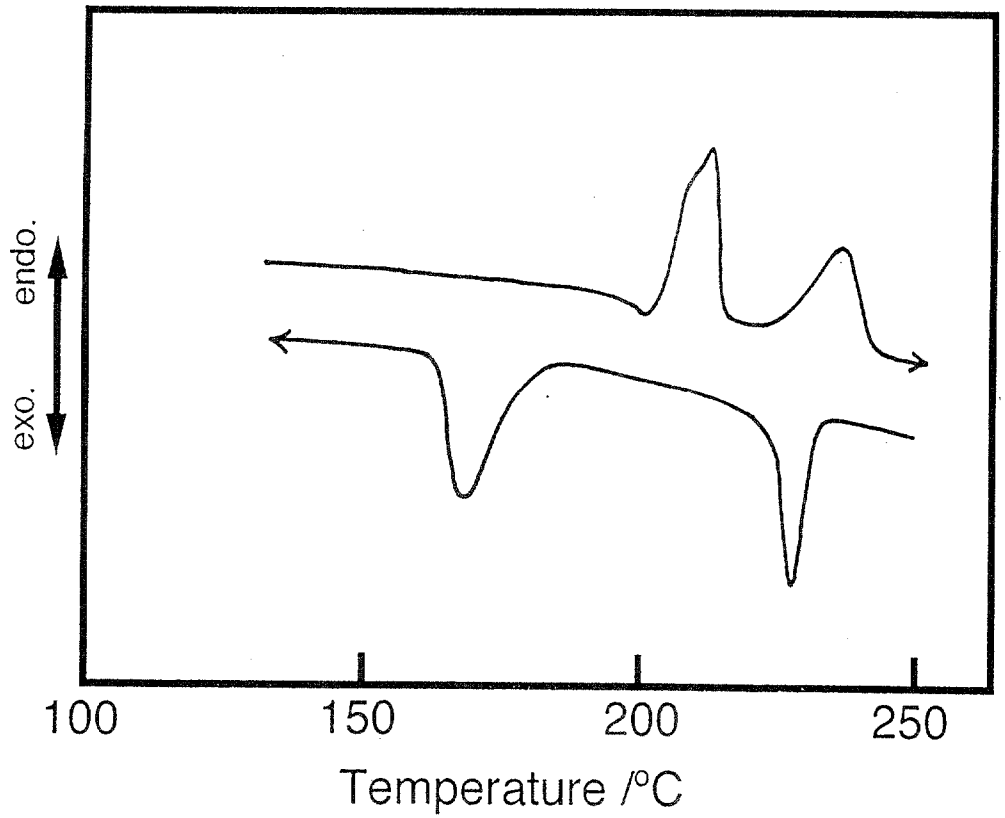

Figure 3.4. DSC heating and cooling thermograms of BB-6-III measured at a rate of 10°C min^{-1}.

(a)

(b)

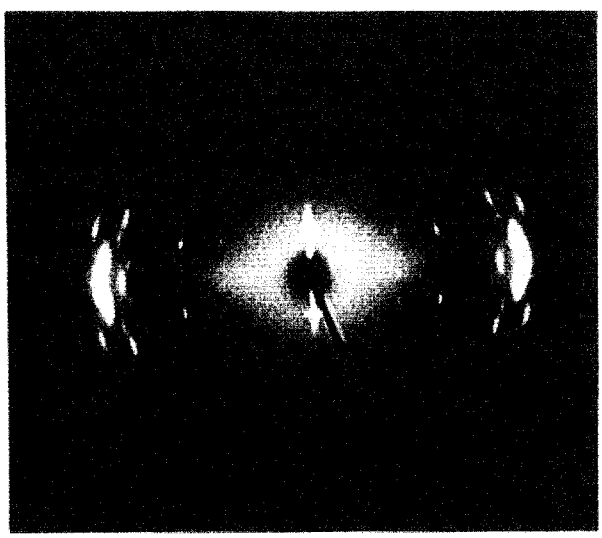

Figure 3.5. Wide angle X-ray patterns of (a) the oriented smectic A and (b) the crystalline phase of BB-6-III. Here, the oriented film specimen was prepared by shear flowing the smectic A phase between thin glass plates. The flow direction is horizontal.

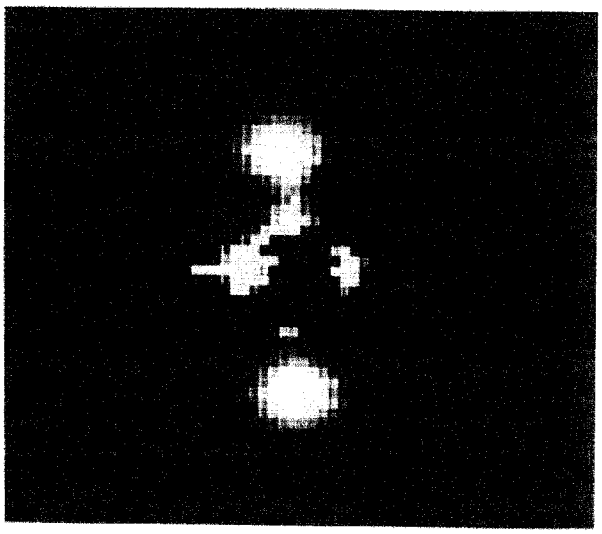

Figure 3.6. Small angle X-ray pattern for the oriented crystal of Figure 3.5b.

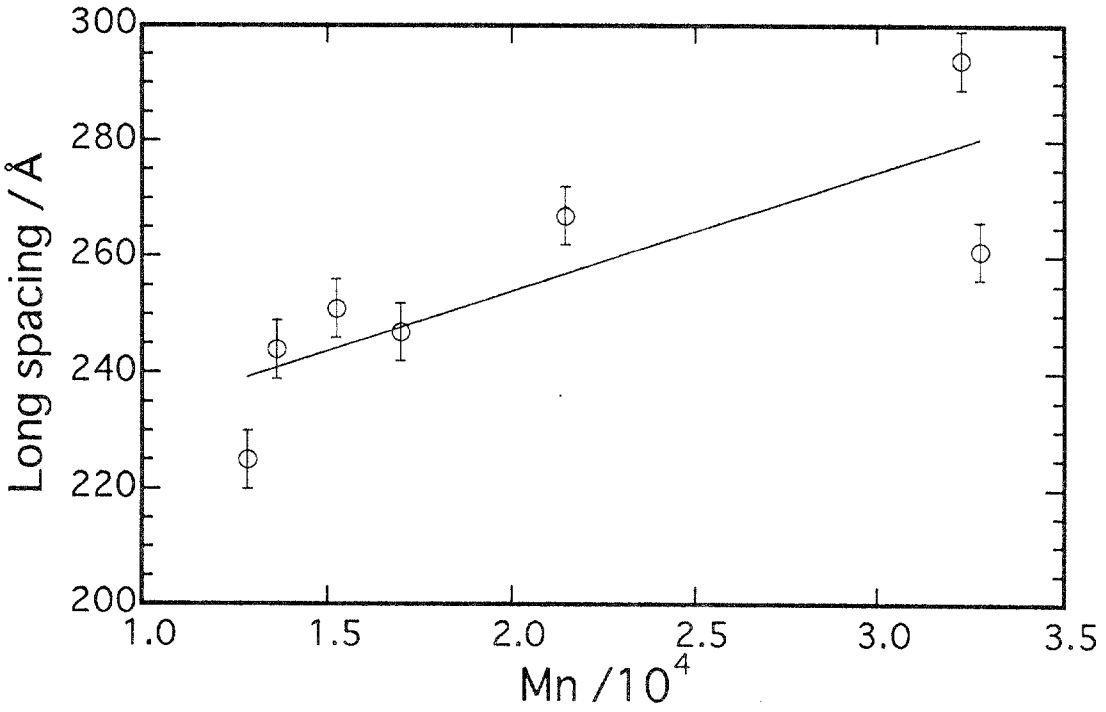

Figure 3.7. Molecular weight dependence of the lamellar spacing elusidated for the crystalline specimens which were prepared by cooling the isotropic melt at a rate of 10°C min^{-1}.

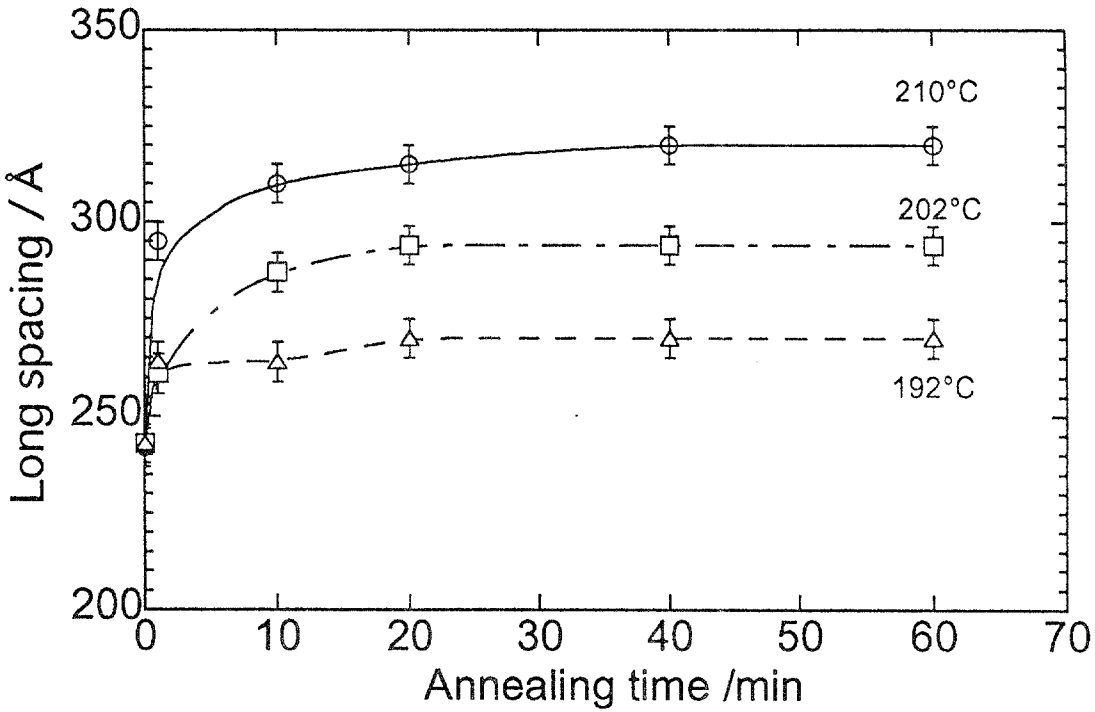

Figure 3.8. Dependence of the lamellar spacing on the time of annealing in the crystalline phase. The crystalline specimens of BB-6-III were initially prepared by cooling the isotropic melt at a rate of 10°C min^{-1} and annealed at respective temperatures below T_m.

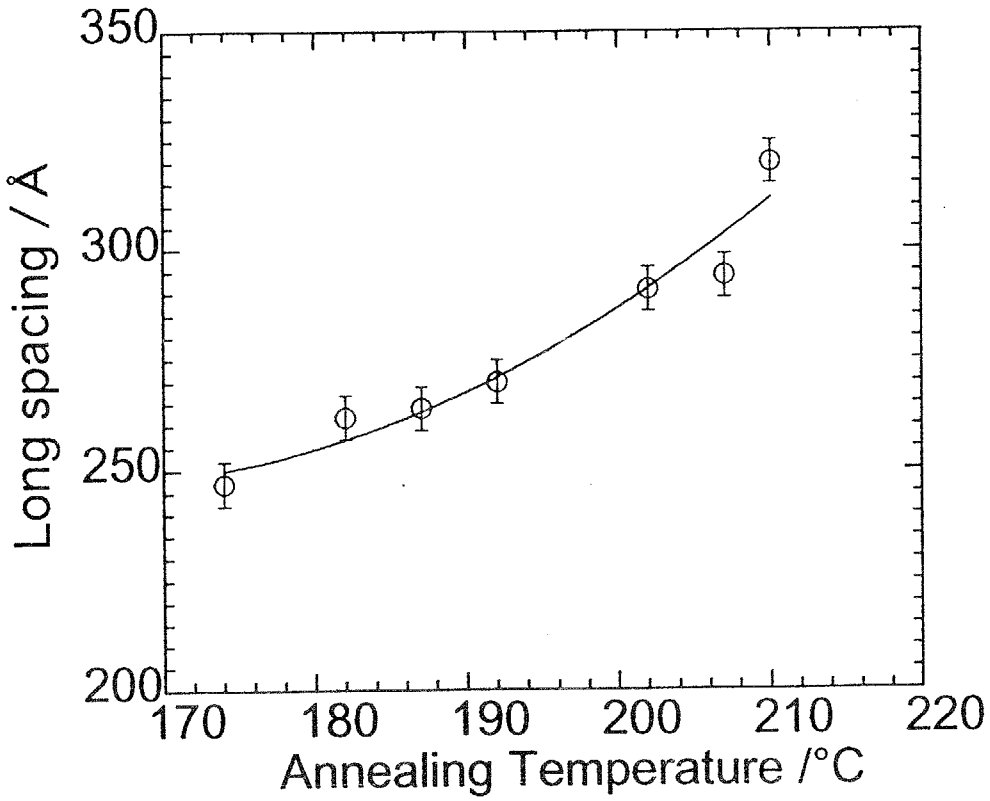

Figure 3.9. Dependence of the lamellar spacing on the annealing temperature below T_m. The data were collected after 60 min of annealing (refer to Figure 3.8).

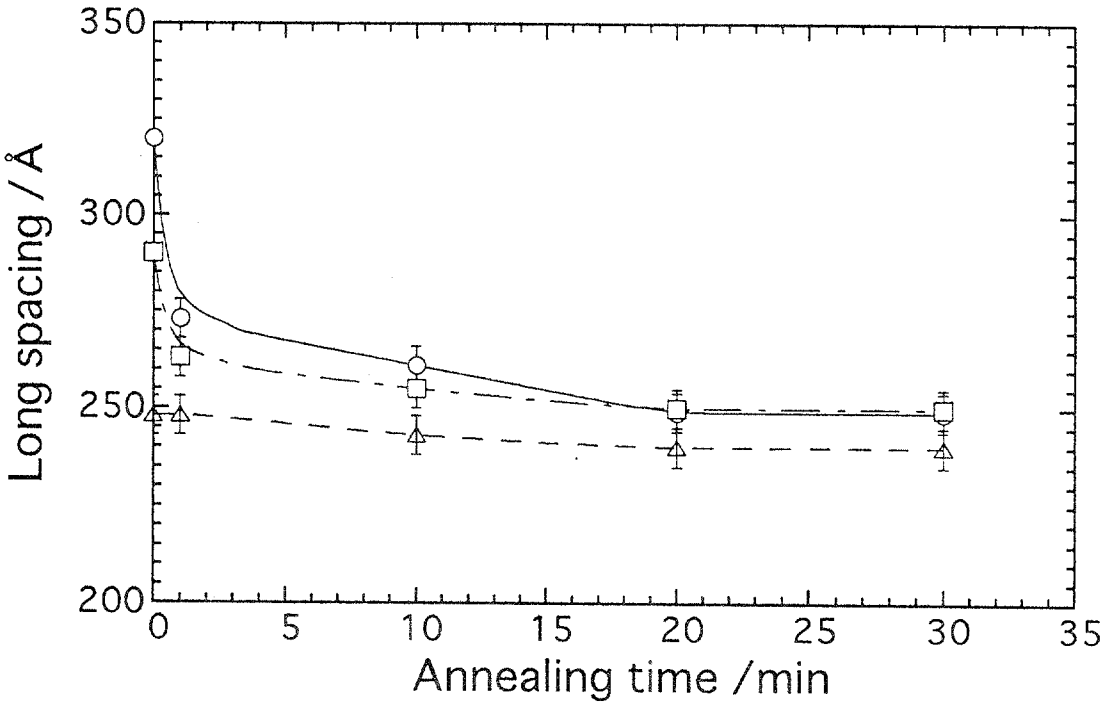

Figure 3.10. Dependence of the lamellar spacing on the annealing time in the smectic A phase. Here, the crystalline specimens of BB-6-III with the different lamellar sizes of 320, 290, and 248 Å were initially prepared by annealing at temperatures below T_m (refer to Figure 3.9) and heated to the smectic A phase (at 225°C) for annealing. After an appropriate time of annealing, the specimen was cooled to room temperature at a rate of 10°C min^{-1} and the lamellar size determined in its crystalline phase.

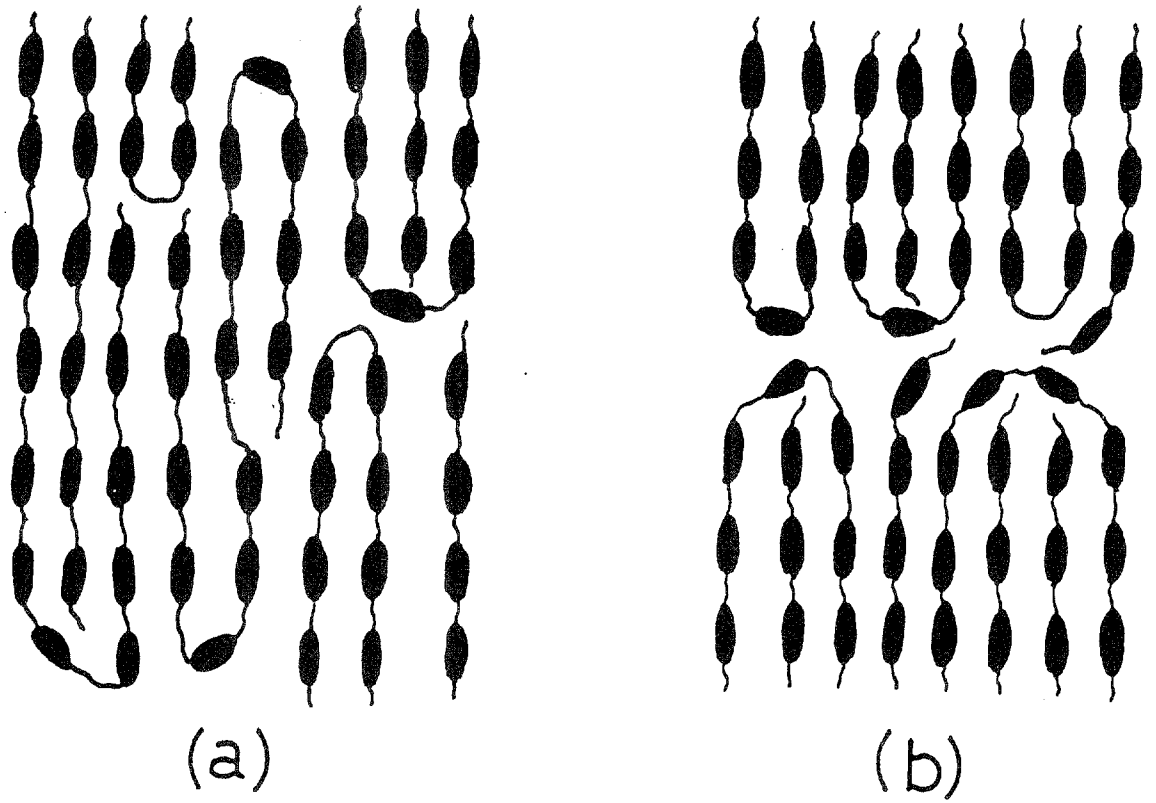

Figure 3.11. Two possible schematic diagrams showing the different accommodation of the chain folding sites into the smectic structure. In (a), the folding sites are randomly placed, while in (b), they are segregated to form domain boundaries.

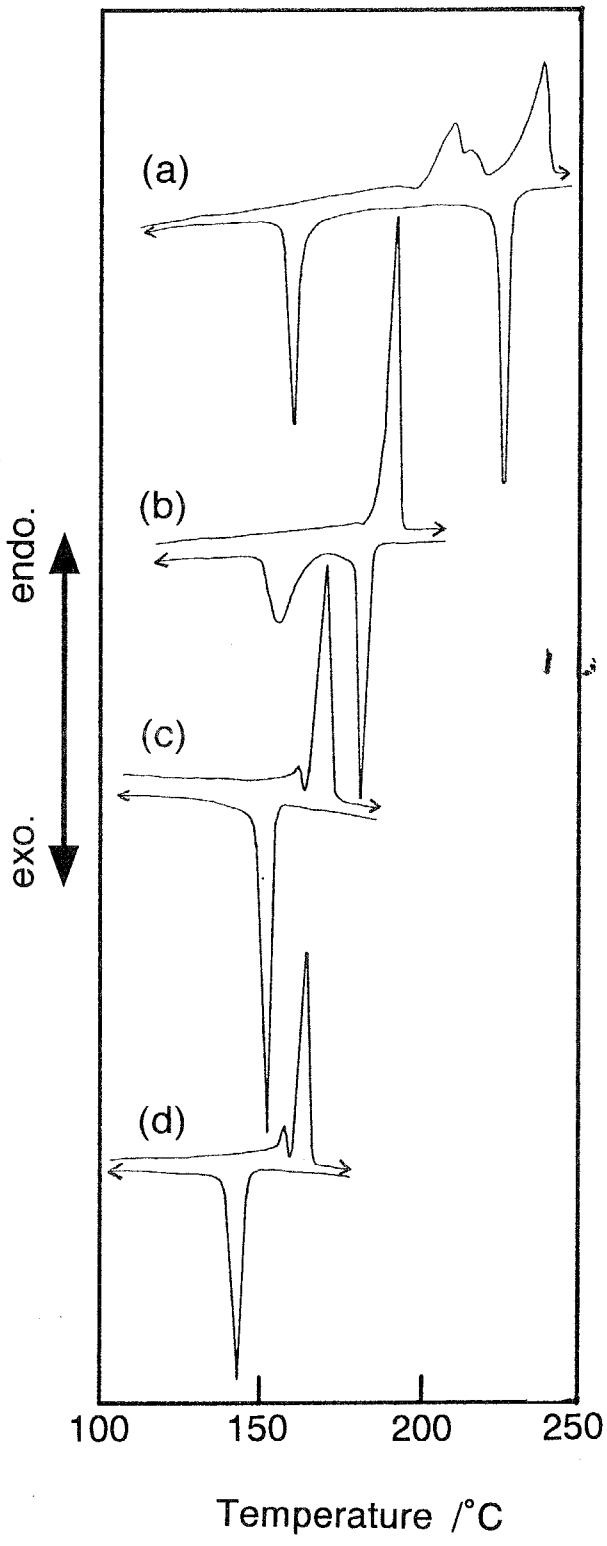

Figure 3.12. DSC thermograms of (a) BB-6-IV, (b) BB-8, (c) BB-10 and (d) BB-12 measured at a scanning rate of 10°C min^{-1}.

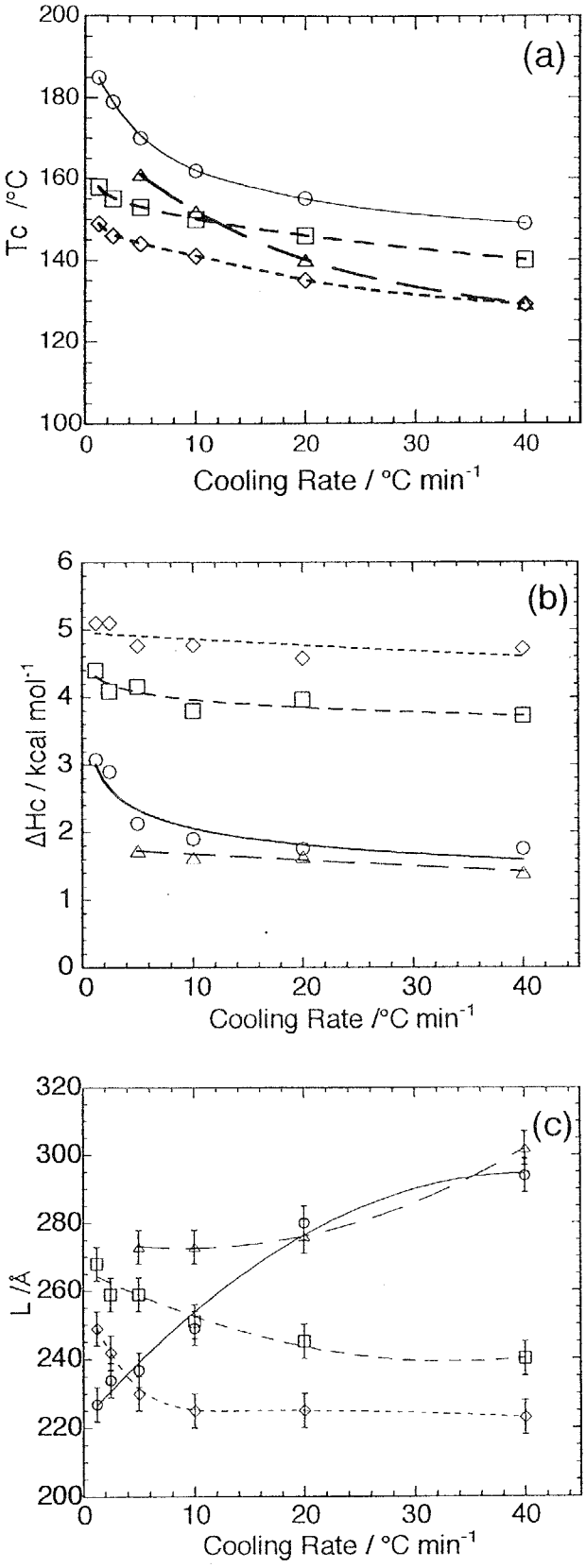

Figure 3.13. (a) Crystallization temperature (T_c), (b) crystallization enthalpy (ΔH_c) and (c) lamellar spacing (L) as a function of the cooling rate observed for BB-6-IV (circles), BB-8 (triangles), BB-10 (squares) and BB-12 (lozenges). The data points of BB-8 measured at cooling rates 1.25 and 2.5°C min^{-1} are omitted because of significant overlapping of the two peaks due to the isotropic S_A and S_A to crystal transitions.

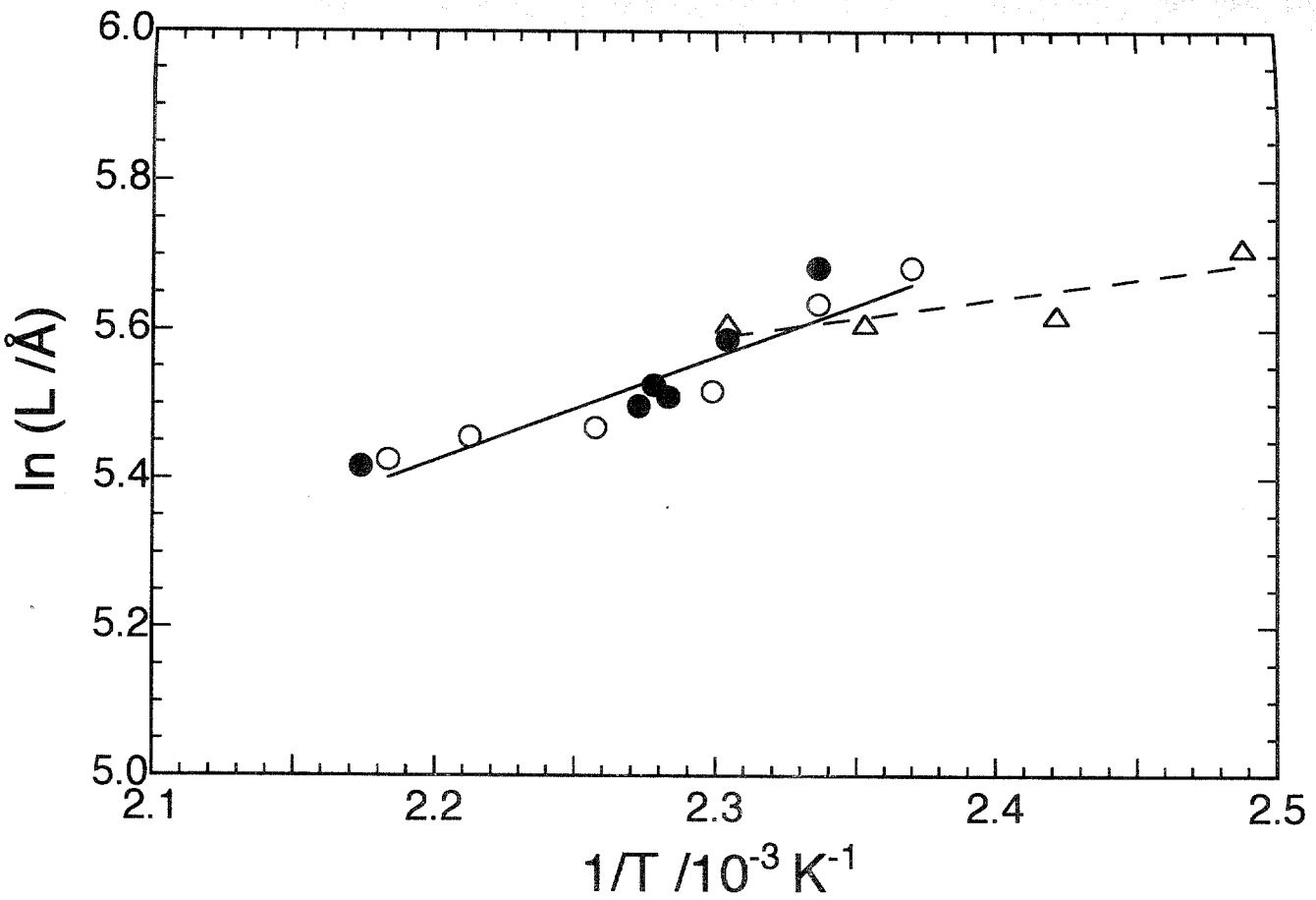

Figure 3.14. Plots of logarithmic lamellar spacing against the reciprocal of the crystallization temperature (T_c) for BB-6-IV (circles) and BB-8 (triangles). The data points given by the open symbols are those observed in Figure 3.13. Also included are the data points given by solid symbols which were collected for the BB-6 polyesters with different molecular weights in Section 3.4.

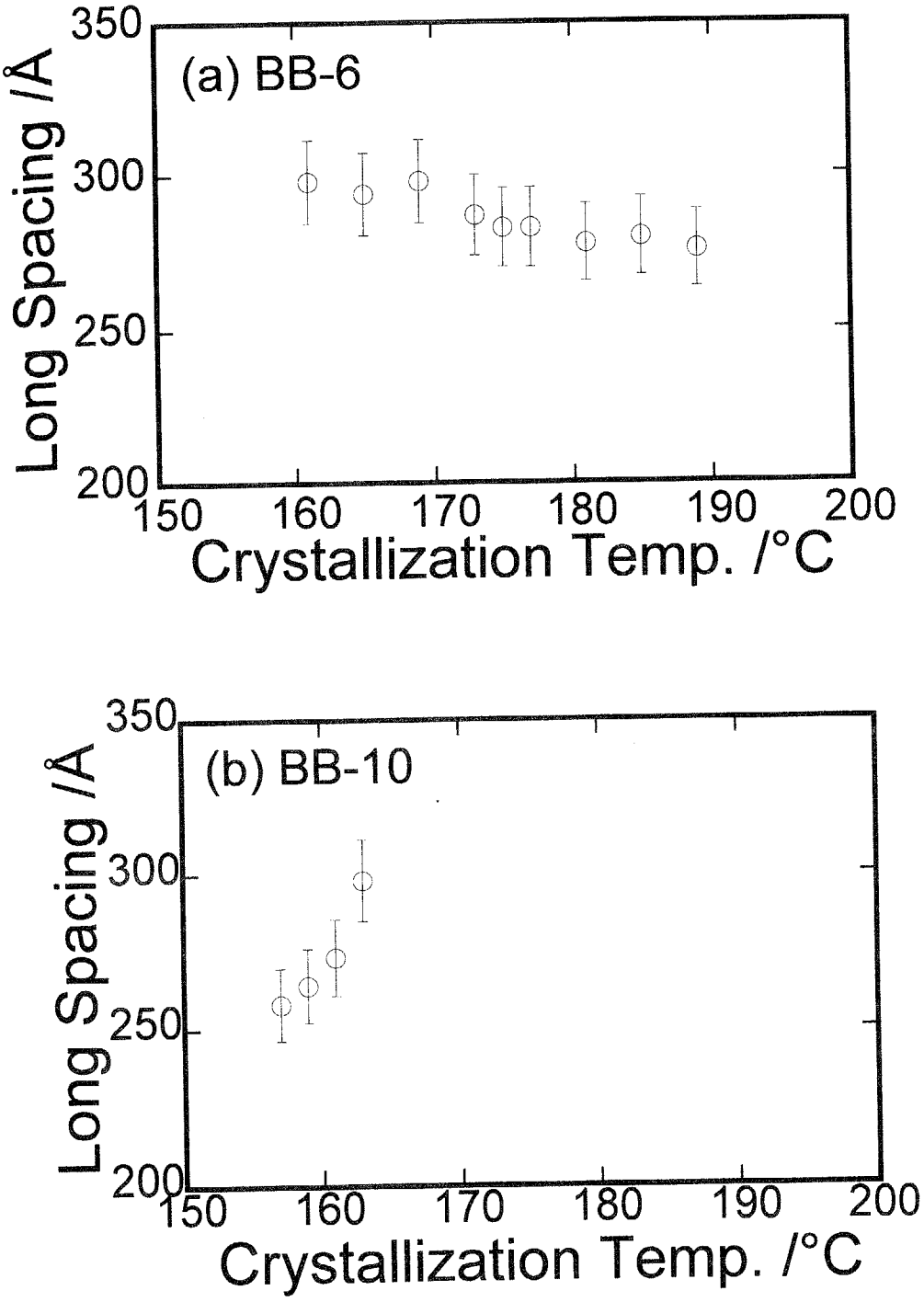

Figure 3.15. Dependence of the lamellar spacing on the isothermal crystallization temperature. The data were collected for the sample quenched just after the exothermic peak in the DSC curve ended.

Chapter 4

Smectic Liquid Crystalline Glass

ABSTRACT: From examination of transition behavior in poly(pentamethylene 4,4′-bibenzoate) (BB-5) forming crystal, S_{CA} and isotropic phases, it was found that the liquid crystallization proceeds promptly and completely from the isotropic phase while the crystallization takes place partly even from the ordered smectic phase. The solid state of liquid crystal (LC) polymer is thus composed of crystal and smectic LC glass. Similarly as in the isotropic liquid glass of conventional polymers, the glass transition of the smectic LC glass is detected as an α-relaxation which appears at around T_α = 50°C by a dynamic mechanical method. The α-relaxation shows considerable mechanical anisotropy such that the *tan δ* peak measured in a direction parallel to the layer is larger than that in a perpendicular direction. This anisotropy can be explained according to the structural characteristics of the smectic phase. Dynamic mechanical properties were also examined for a series of BB-*n* polyesters with *n* of 5-12 and compared to those for poly(alkylene 2,6-naphthalene dicarboxylate)s (N-*n*) with the identical values of *n*. The smectic LC glass formed from BB-*n* polyesters with *n* of 5 - 9 have the lower T_α than the isotropic liquid glass of N-*n* polyesters with the corresponding *n*. Similar trend is observed in BB-6-*co*-N-6 copolymer system in which the S_A phase can be formed only from the copolymers with the N-6 compositions less than 60%. It is thus concluded that the glass transition temperature of the smectic LC glass is lower than that of the isotropic liquid glass. The temperature of γ-relaxation due to the local motion of alkylene spacer is relatively higher in the smectic LC glass than that in the isotropic liquid glass. This may reflect the more stretched conformation of the flexible spacer in the smectic structures.

4.1. Introduction

The thermotropic liquid crystalline behavior of polymers with rigid mesogenic units interconnected through flexible spacers is well known from reports over the past two decades. The polymers are termed main-chain liquid crystalline (LC) polymers, which have generated much interest because of challenge of understanding such systems and their many industrial and commercial applications.

In this series of studies,[1-9] we have treated the following main-chain LC polyesters, poly(alkylene 4,4'-bibenzoate)s:

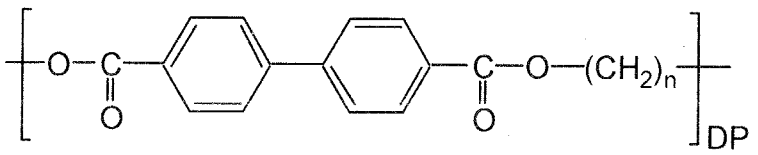

The polymers are designated as BB-*n* (*n*; carbon number of the methylene spacer). These BB-*n* polyesters invariably form smectic mesophases when *n* varies from 3 to 9. In BB-*n* with an even *n*, a S_A phase is formed with both axes of the polymer chain and biphenyl mesogen lying perpendicular to the layers. In contrast, the smectic structure of BB-*n* with an odd *n* was identified as a S_{CA} phase, in which the tilt direction of the mesogenic group is the same in every second layer but opposite between neighboring layers.[2, 3, 6, 9]

Despite detailed studies on liquid crystals, the structure and properties of solid films and fibers in BB-*n* polyesters are relatively little known.[7-13] Assuming that the formation of a smectic phase takes place completely from the isotropic melt, BB-*n* polyesters include the smectic LC glass instead of the isotropic liquid glass. Here, isotropic liquid glass and smectic LC glass are defined as the glassy states of isotropic liquid and smectic liquid crystal, respectively. The smectic LC glass possesses long-range orientational and positional orders and so its properties are completely different from those of the isotropic liquid glass. This study clarifies the solid state morphology for the LC

BB-*n* (*n* =5, 6, 7, 8, 9) and shows the dynamic mechanical properties of the smectic LC glasses. The mechanical properties of the smectic LC glasses are compared with those of the isotropic liquid glasses observed in BB-*n* with *n* of 10-12 and poly(alkylene 2,6-naphthalene dicarboxylate)s (N-*n*) with *n* = 5-12,

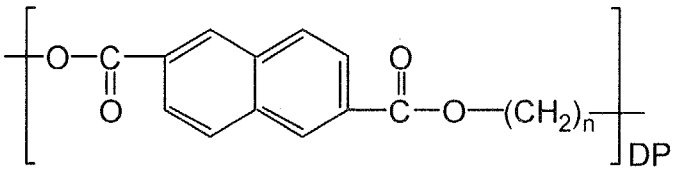

which form no mesophase and solidify directly from isotropic liquid.

4.2. Experimental Section

The polyesters were synthesized by melt transesterification of dimethyl 4,4′-bibenzoate and dimethyl-2,6-naphthalene dicarboxylate with n-alkane diols. Isopropyl titanate was used as catalyst. The inherent viscosities of the sample, η_{inh}, were measured at 30°C by using 0.5 g dL^{-1} solutions in a 60/40 w/w mixture of phenol and tetrachloroethane, and the polyesters with the inherent viscosities ranged from 0.6 to 1.5 dL g^{-1} were used.

Differential scanning calorimetric (DSC) measurements were carried out with a Perkin-Elmer DSC II under a flow of dry nitrogen. Wide-angle X-ray measurements were performed using a Rigaku-Denki RU-200 BH with Ni-filtered CuKα radiation. Dynamic mechanical measurements were carried out with a Seiko Instruments DMS 210 working in the tensile mode. The solid specimens were prepared by quenching the preceding phase (i.e. the smectic phase for the LC polyesters and the isotropic phase for the non-LC polyesters). After the thermal treatments, the sample was cut out into a rectangular strip of 20 mm length, 2 mm wide and 0.2 mm thickness. The complex moduli and loss tangent were determined at frequencies of 0.01 to 20 Hz under a dry nitrogen

atmosphere. The temperature was varied from -150°C to 250°C at a rate of 3°C min^{-1}.

4.3. Results and Discussion

4.3.1. Characterization of Polyesters

Two series of homopolyesters, BB-*n* and N-*n*, were prepared with the carbon numbers of the methylene spacer from 5 to 12 and their thermotropic behavior was analyzed from DSC thermograms.

BB-*n* polyesters with *n* of 5 - 9 exhibit the two transitions at T_m and T_i assigned to the crystal-LC phase transition and the isotropization of the LC phase, respectively. As mentioned in Introduction, the S_A and S_{CA} phases are formed from BB-6 and BB-8 and from BB-5, BB-7 and BB-9, respectively. BB-*n* with *n* of 10 - 12 form no mesophase, showing one peak of crystal melting on both the heating and cooling DSC thermograms.

N-*n* polyesters with even *n* show one peak of crystal melting while the odd-numbered N-*n* polyesters do not show any peak but a clear step in heat capacity associated with the glass transition. All the N-*n* polyesters with *n* of 5 - 12 thus form no mesophase and solidify directly from isotropic melt.

A series of BB-6-*co*-N-6 copolyesters having the molar ratios of BB-6:N-6 = 75:25, 50:50, 40:60 and 25:75

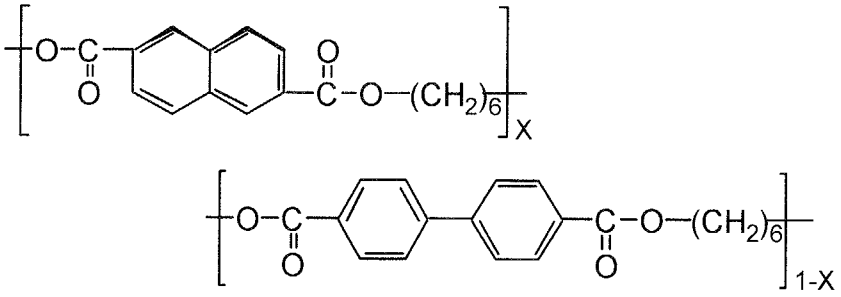

were prepared. The transition temperatures from the cooling DSC data are plotted against the content of N-6 unit in Figure 4.1. Only the copolymers with N-6 contents less than 60 % form a S_A phase and so solidify from the S_A phase, while the copolymers with the N-6 contents above 60 % solidify directly from isotropic liquid state.

The inherent viscosities and thermodynamic data of the homopolymers and copolymers are listed in Table 4.1.

4.3.2. Representative Smectic LC Glass Prepared from BB-5 and its Thermal and Mechanical Properties

Thermotropic LC polymers form isotropic liquid, LC, and crystal phases in order of decreasing temperature. In the liquid state, a polymer molecule is capable of assuming a large number of conformations due to the rotational freedom of individual chain atom about their connecting bonds. There is no significant correlation between the conformations assumed by the individual molecules so that the liquid state is characterized with random, haphazard arrangements of the polymer chain segments. In the LC phase, a long range orientational order requires polymer molecules to take some extended conformations. Starting from coiled, mutually interpenetrating macromolecules, these specified conformations in the LC phase seem to be hardly achieved instantaneously from purely kinetic reasons. We thus have a significant question as to whether the isotropic phase can be transformed to the LC phase completely or not in the polymeric system.

To examine this point, the isotropization enthalpy, ΔH_i, was measured for the S_{CA} phase of BB-5 formed under an isothermal condition. On this measurement, BB-5 polyester was preheated for 5 min at isotropic temperature of 230°C to eliminate the effect of thermal history. The sample was then

quenched to the S_{CA} phase of 185°C. After the isothermal formation of the S_{CA} phase at this temperature for a certain period, isotropizaion enthalpy, ΔH_i, was measured at a heating rate of 10°C min^{-1}. The crystallization behavior from the smectic phase was also examined with a similar procedure. After the sample was annealed at the S_{CA} temperature of 185°C for 30 min, it was quenched to the room temperature, heated up to 140°C, and maintained for a certain period for crystallization. The melting enthalpy of the crystal, ΔH_m, was measured at a heating rate of 10°C min^{-1}.

In Figure 4.2, ΔH_i and ΔH_m thus determined are plotted against the time of the isothermal transformation, respectively. ΔH_i is relatively constant independent on the transformation time which was varied from 1 to 330 min. This feature of the liquid crystallization is in contrast to that for the crystallization where ΔH_m decreases significantly with a decrease of the crystallization time. Thus, it is likely that the perfect transformation of the isotropic phase to smectic phase takes place in a short period even in the polymeric system. This is reasonable since in the smectic phase the molecules are mobile and can be packed without significant defects although some deformation might be included with respect to the orientation of n- and c-directors. The crystallization does not proceed completely in a short period even if it takes place from the ordered S_{CA} phase. This may be due to the fact that the structural order of the S_{CA} phase is fairly less than that of the crystal. Such a characteristic transformation results in the interesting solid morphology in which no isotropic liquid glassy phase is included. In other words, the solid of LC polymers is composed of two phases, LC glass and crystal while the solid of the conventional polymers is composed of isotropic liquid glass and crystal.

Because of a very late crystallization, it is possible to prepare the BB-5 solid composed only of the glassy smectic phase by quenching the smectic

phase to the room temperature. This can be clearly recognized from the X-ray photograph as shown later in Figure 4.6, where the pattern characteristic of the mesophase is still observed. DSC thermogram of this sample shows the typical jump of the heat capacity at around 45°C (see Figure 4.3) and dynamic mechanical analysis (DMA) shows the relaxations characteristic to the glass transition as stated in details below.

Figure 4.4 shows the temperature dependence of the storage tensile modulus (E'), the loss modulus (E'') and the mechanical loss tangent ($tan\ \delta$) for a glassy smectic film of BB-5. Data were obtained with a forced oscillation at a frequency of 10 Hz. Three relaxations can be detected at around 50, -60 and -120 °C, and designated here as α-, β- and γ-processes, respectively. Since the temperature of α-relaxation corresponds to the glass transition temperature (T_g) detected by DSC, α-relaxation can be connected to the glass transition and attributed to the segmental motion of molecules. The β-process can be connected with the motion of the aromatic part including the ester group.[11-13, 15] The γ-process is attributed to local rotation of methylene group commonly observed for polymers containing methylene sequences.[14, 16] These mechanical relaxations are similar to those observed in the isotropic liquid glass of the conventional polymers. The activation energies estimated from the frequency dependence of the relaxation temperature are 75, 35 and 10 kcal/mol for the α-, β- and γ-relaxations, respectively.

The dependence of the strength of α-relaxation on the degree of crystallinity was examined as shown in Figure 4.5. The BB-5 sample was quenched from the S_{CA} phase and annealed at 140°C for a certain period for controlled enhancement of the crystallinity (refer to Figure 4.2(b)). Since the sample became brittle as the crystallization proceeded more and more, β- and γ-

transitions could not be measured. Increasing crystallinity results in decrease of the loss signal, indicating that the α-process is attributed to a smectic LC glass.

The use of oriented specimens is a further step to understand molecular relaxation. Two smectic LC glassy fibers of BB-5 with different orientation were produced by the two methods of spinning. Fiber A was prepared by drawing the isotropic melt at a high rate of about 1 m sec^{-1}. The X-ray pattern of fiber A shows that the polymer chains lie parallel to the axis and hence that the smectic layers arrange perpendicular to the fiber axis as found in part (a) of Figure 4.6. Drawing the smectic melt at a low rate of about 1 cm sec^{-1} produced fiber B in which the smectic layers lie parallel to the fiber axis, i.e., the polymer chains lie perpendicular to the axis (see part (b) of Figure 4.6). The orientation of fiber B is unusual, but can be explained by a chain folded lamellar structure such that the lamellae lie preferentially in a direction parallel to the elongation flow.[7-9] The results of DMA obtained for the two oriented fibers of A and B are shown in Figure 4.7, where only *tan* δ are presented because the small cross section of the fibers prevents to determine the accurate value of Young's modulus from being obtained. Considerable mechanical anisotropy with *tan* δ of fiber B larger than that of fiber A can be seen for the α-relaxation while the intensities of β and γ relaxations are similar. The ratio of *tan* δ peak height is around 3. This anisotropy is simply explained according to the layered characteristics of the smectic structure as following. In the S_{CA} phase, the mesogenic groups lie with one-dimensional positional order along the polymer chain axes and so form the layers. Along each layer, their centers of gravity have no positional order, i.e. the mesogens are laterally packed with liquid-like nature. Hence, the motion of the chain in the direction perpendicular to the layer is restricted while relatively free motion is allowed in the parallel direction.

Anisotropy in mechanical properties is also observed with respect to the terminal flow behavior in the fibers. As seen in Figure 4.7, the temperature at which the terminal flow takes place and so that *tan* δ diverges to infinity, corresponds to T_i (210°C) for fiber A while it corresponds to T_m (170°C) for fiber B. This can be also explained in terms of the structural features of smectic phase as mentioned above.

4.3.3. Dependence of Glass Transition Temperature on Carbon number

It is interesting to examine how T_g of the LC glass depends on the carbon number of flexible spacer. With respect to this, we first refer to T_g of the isotropic liquid glass observed in the N-*n* polyesters with n = 4 - 12. These polyesters form no mesophase so that crystallization takes place directly from the isotropic melt like in the conventional polymers. T_g temperatures as determined by DSC are plotted against n by closed circles in Figure 4.8. Figure 4.9 shows the typical viscoelastic properties observed in N-6. As observed in BB-5, three α, β and γ-relaxations can be observed. The temperatures of these relaxations are plotted against n by closed marks in Figure 4.10. Here, it should be noted that the β-relaxation temperature was determined with a significant error because of the overlapping with α-relaxation. T_g and T_α showing the odd-even oscillation decrease steadily with an increases of n. T_β also decreases with n although T_γ is relatively constant at around -130°C.

T_g in BB-*n* determined by DSC are plotted against n by open circles in Figure 4.8. The mechanical α, β and γ-relaxation temperatures are given by open marks in Figure 4.10. It must be noted that the BB-*n* polyesters show an unusual variation of T_g and T_α on n. The LC BB-*n* polyesters with n of 5 - 8 forming the smectic phase show the lower T_g and T_α than the non-LC BB-*n*

with n of 10-12 despite of the higher chain stiffness. This variation is contradictory to that observed in N-n polyesters, in which T_g decreases steadily with increase of chain flexibility.[16] Since T_g and T_α are almost same between non-LC BB-n and N-n with n of 10 - 12, this anomalous variation can be understood if the smectic LC glass shows the lower T_g and T_α than the isotropic liquid glass.

Let us now expand the observation to the copolymers of BB-6-*co*-N-6. As observed in the homopolymers of BB-n and N-n, the copolymers show up three α-, β- and γ-relaxations. The relaxation temperatures, T_α, T_β and T_γ, are plotted against the molar content of N-6 units in Figure 4.11. The glass transition temperatures in a copolymer system is related to its composition as described in many cases successfully and simply with the 'Fox-Flory' equation where the glass transition temperature is represented with a continuous function of the volume fractions. In this series of copolymers, T_α remains almost constant around 50°C up to a N-6 content of 60%. For higher N-6 content, T_α rises discontinuously to 70°C. On comparing this feature with the phase behavior of Figure 4.1, one can find that the lower T_α is observed for the copolymers forming the S_A phase.

The overall results thus lead to the conclusion that a LC glass shows a lower transition temperature than the isotropic liquid glass. Similar conclusion has been deduced in the aromatic copolyesters forming nematic liquid crystal by Zachmann, et al.[17,18] Lower T_g of LC glass is explainable, as reported by Zachmann, et al.,[17] if the change of the volume on the isotropic-smectic transition at T_i is smaller than the volume difference between the smectic LC and isotropic liquid glasses. Such a situation can be expected since the free volume necessary to promote the restricted motion in the smectic LC glass is

considerably smaller than the one which allows segmental motion in the isotropic liquid glass.

4.3.4. Local Motion of Polyesters Associated with β- and γ-Relaxations

With respect to the β-relaxation, we find that T_β of N-*n* is fairly higher than that of BB-*n* (see Figure 4.10). This means that the rotational motion of the naphthalene moiety is more restricted than that of biphenyl moiety. T_β decreases with increase of *n* in both the BB-*n* and N-*n* polymers although T_β of the smectic LC BB-*n* with *n* of 5 to 9 shows some odd-even oscillation. In the BB-6-*co*-N-6 copolymers, as seen in Figure 4.11, T_β increases continuously with molar content of N-6 unit, suggesting that the β-relaxation is not closely associated with the structure of the glassy state.

T_γ of LC BB-*n* polymers with *n* of 5-9, showing some odd-even oscillation, is relatively higher than that in non-LC N-*n* polymers with identical *n* (see Figure 4.10). Higher T_γ of the LC glass can be also observed in the copolymer system as found in Figure 4.11. T_γ is around -110°C for the LC copolymers while -140°C for the non-LC copolymers. This may be caused by the extended conformation of polymethylene units in the smectic structures.

4.4. Conclusions

The transformation behavior from isotropic liquid to smectic phase was examined for the BB-5 polyester. The transformation proceeds promptly and completely even in the polymeric LC while the crystallization occurred partly even from the smectic phase. The solid state of LC polymer is thus composed of crystal and smectic LC glass. The glass transition of the smectic LC glass was detected as a jump of heat capacity by the DSC and the related segmental motion was observed as an α-relaxation by the dynamic mechanical method. The α-relaxation of the BB-5 polyester showed considerable mechanical anisotropy. *Tan δ* of α-relaxation measured in the direction parallel to the layer was larger than that in the perpendicular direction. Structural characteristics of the smectic phase can explain this anisotropy.

Dynamic mechanical properties of BB-*n* polyesters with *n* of 5-12 were studied and compared with those for N-*n* polyesters with the corresponding *n*. The smectic LC glass prepared from BB-*n* polyesters with n of 5 - 9 had relatively lower T_α than the isotropic liquid glass of polyesters of BB-*n* with *n* of 10 - 12 and N-*n* polyesters with the identical *n*. The same was found for BB-6-*co*-N-6 copolymers which form a S_A phase depending on the composition. We thus conclude that the glass transition temperature of the smectic LC glass is lower than that of the isotropic liquid glass.

The temperatures of γ-relaxation due to the local motion of alkylene spacer are relatively higher for the smectic LC glass than that for the isotropic liquid glass. This may be due to more stretched conformation of the flexible spacer in the smectic LC glass.

References

(1) Watanabe, J.; Hayashi, M. *Macromolecules* **1988**, *21*, 278.

(2) Watanabe, J.; Hayashi, M. *Macromolecules* **1989**, *22*, 4083.

(3) Watanabe, J.; Kinoshita, S. *J. Phys. II (France)* **1992**, *2*, 1237.

(4) Watanabe, J.; Nakata, Y.; Simizu, K. *J. Phys. II (France)* **1994**, *4*, 581.

(5) Nakata, Y., Watanabe, J. *J. Mater. Chem.* **1994**, *4*, 1699.

(6) Watanabe, J.; Hayashi, M.; Morita, A.; Niori, T. *Mol. Cryst. Liq. Cryst.* **1994**, *254*, 221.

(7) Tokita, M.; Takahashi, T.; Hayashi, M.; Inomata, K.; Watanabe, J. *Macromolecules* **1996**, *29*, 1345.

(8) Tokita, M.; Osada, K.; Watanabe, J. *Liq. Cryst.* **1997**, *23*, 453.

(9) Watanabe, J.; Hayashi, M.; Niori, T.; Tokita, M.; Nakata, Y. *Prog. Polym. Sci.* **1997**, *22*, 1053.

(10) Li, X.; Brisse, F *Macromolecules* **1994**, *27*, 7725.

(11) Frosini, V.; Petris, S.; Chiellini, E.; Galli, G.; Lenz, R. W. *Mol. Cryst. Liq. Cryst.* **1983**, *98*, 223.

(12) Benavente, R.; Perena, J.M.; Perez, E.; Bello, A.; Lorenzo, V. *Polymer* **1994**, *35*, 3686.

(13) Benavente, R.; Zhu, Z.; Perena, J.M.; Bello, A.; Perez, E. *Polymer* **1996**, *37*, 2379.

(14) Heaton, H. J.; Benavente, R.; Perez, E.; Bello, A.; Perena, J. M. *Polymer* **1996**, *37*, 3791.

(15) Farrow, G.; McIntosh, J.; Ward, I. M. *Makromol. Chem.* **1960**, *38*, 147.

(16) McCrum, N. G.; Read, B. E.; Williams, G. *Anelastic and Dielectric Effects in Polymeric Solids*, Wiley, New York, 1967.

(17) Chen, D.; Zachmann, H. G. *Polymer* **1991**, *32*, 1612.

(18) Ahumada, O.; Ezquerra, T. A.; Nogales, A.; Balta-Callenja; Zachmann, H. G. *Macromolecules* **1996**, *29*, 5002.

Table 4.1. Characterization of Polyesters

Sample	η_{inh} /dL g^{-1}	Calorimetric data[a]						
		Transition temperatures						
		Heating process			Cooling process		Transition enthalpy[b]	
		T_g /°C	T_m /°C	T_i /°C	T_m /°C	T_i /°C	ΔH_m /kcal mol^{-1}	ΔH_i /kcal mol^{-1}
BB-5	0.91	43	173	212	86	196	0.60	1.27
BB-6	1.33	40	210	240	154	223	1.66	2.19
BB-7	0.77	35	165		97	139	2.52	3.10
BB-8	1.00	34	195		160	180	1.84	2.23
BB-9	0.65	37	154		111	115	3.11[c]	
BB-10	0.64	40	171		152		3.97	
BB-11	0.73	36	149		107		2.89	
BB-12	0.70	35	161		138		4.41	
N-5	0.60	39						
N-6	0.62	55	213		175		3.50	
N-7	0.95	36						
N-8	0.69	46	181		141		3.32	
N-9	0.75	37						
N-10	0.77	37	144		106		3.57	
N-11	0.95	35						
N-12	0.74	32	139		102		3.67	
BB-6-*co*-N-6								
75:25	1.27	36	184	216	100	198	0.88	1.87
50:50	0.63	38	178	187	140	173	0.73	1.76
40:60	0.66	42	185		157[c]		2.75[c]	
25:75	1.53	61	190		157		1.85	

[a] Based on DSC data measured at a rate of 10°C min^{-1}. [b] Based on cooling DSC data. [c] Significant overlapping of the two peaks due to the isotropic to smectic and smectic to crystal transition.

Figure Captions

Figure 4.1. Transition temperatures and phase behavior of BB-6-*co*-N-6 copolyesters. Transition temperatures were determined from the cooling DSC curves measured at a rate of 10°C min^{-1}.

Figure 4.2. Variation in isotropization enthalpy, ΔH_i (rectangles), and the crystal melting enthalpy, ΔH_m (circles), for BB-5 with the isothermal formation time. ΔH_i (or ΔH_m) was measured for the sample which was quenched from the isotropic (or S_{CA}) phase and held at 185°C (or at 140°C) during a certain period for isothermal formation of the S_{CA} (or crystal) phase.

Figure 4.3. DSC thermograms showing the glass transition of S_{CA} LC phase in BB-5.

Figure 4.4. Storage modulus, loss modulus and loss tangent as a function of temperature at 10 Hz for BB-5 specimen quenched from smectic melt.

Figure 4.5. Loss tangent as a function of temperature at 10 Hz for BB-5 samples with different degrees of crystallinity. The crystallinity was controlled by annealing the specimen at 140°C for a certain period of (a) 0 min (as quenched from S_{CA}), (b) 1 min, (c) 5 min, (d) 10 min, (e) 30 min and (f) 60 min (refer to Figure 4.2).

Figure 4.6. X-ray photographs for (a) fiber A drawn from the isotropic melt of BB-5 at a rate of around 1 m sec^{-1} and (b) fiber B drawn from the smectic melt of BB-5 at a rate of 1 cm sec^{-1}. The fiber axis is in the vertical direction. The molecular arrangements deduced from the X-ray patterns are also illustrated.

Figure 4.7. Temperature dependence of loss tangent measured at 10 Hz for the two different BB-5 fibers; (a) solid curve for fiber A and (b) dashed curve for fiber B (refer to Figure 4.6).

Figure 4.8. Variation in DSC glass transition temperatures in BB-*n* (open circles) and N-n (closed circles) polyesters with *n*.

Figure 4.9. Temperature dependence of storage modulus, loss modulus and loss tangent for N-6 specimen quenched from isotropic melt. Frequency was 10 Hz.

Figure 4.10. Variation in α-, β- and γ-relaxation temperatures for BB-*n* (circles) and N-*n* (rectangles) polyesters with n. The temperatures were determined from the peak of loss modulus, *E″*, measured at 10 Hz.

Figure 4.11. Variation in α-, β- and γ-relaxation temperatures of BB-6-*co*-N-6 copolyesters with the molar content of N-6. Temperatures were determined from the peak of loss modulus, *E″*, measured at 10 Hz.

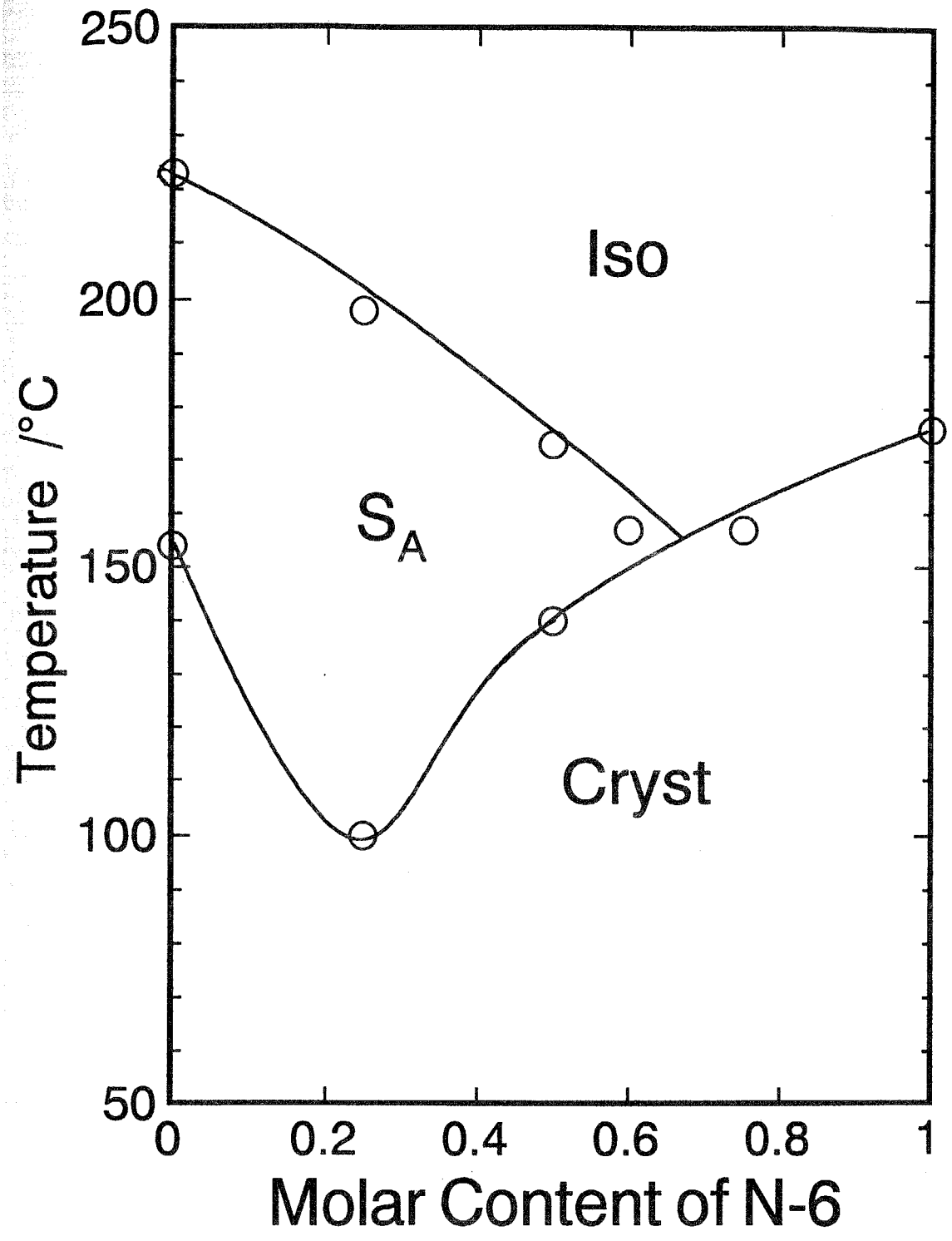

Figure 4.1. Transition temperatures and phase behavior of BB-6-*co*-N-6 copolyesters. Transition temperatures were determined from the cooling DSC curves measured at a rate of 10°C min^{-1}.

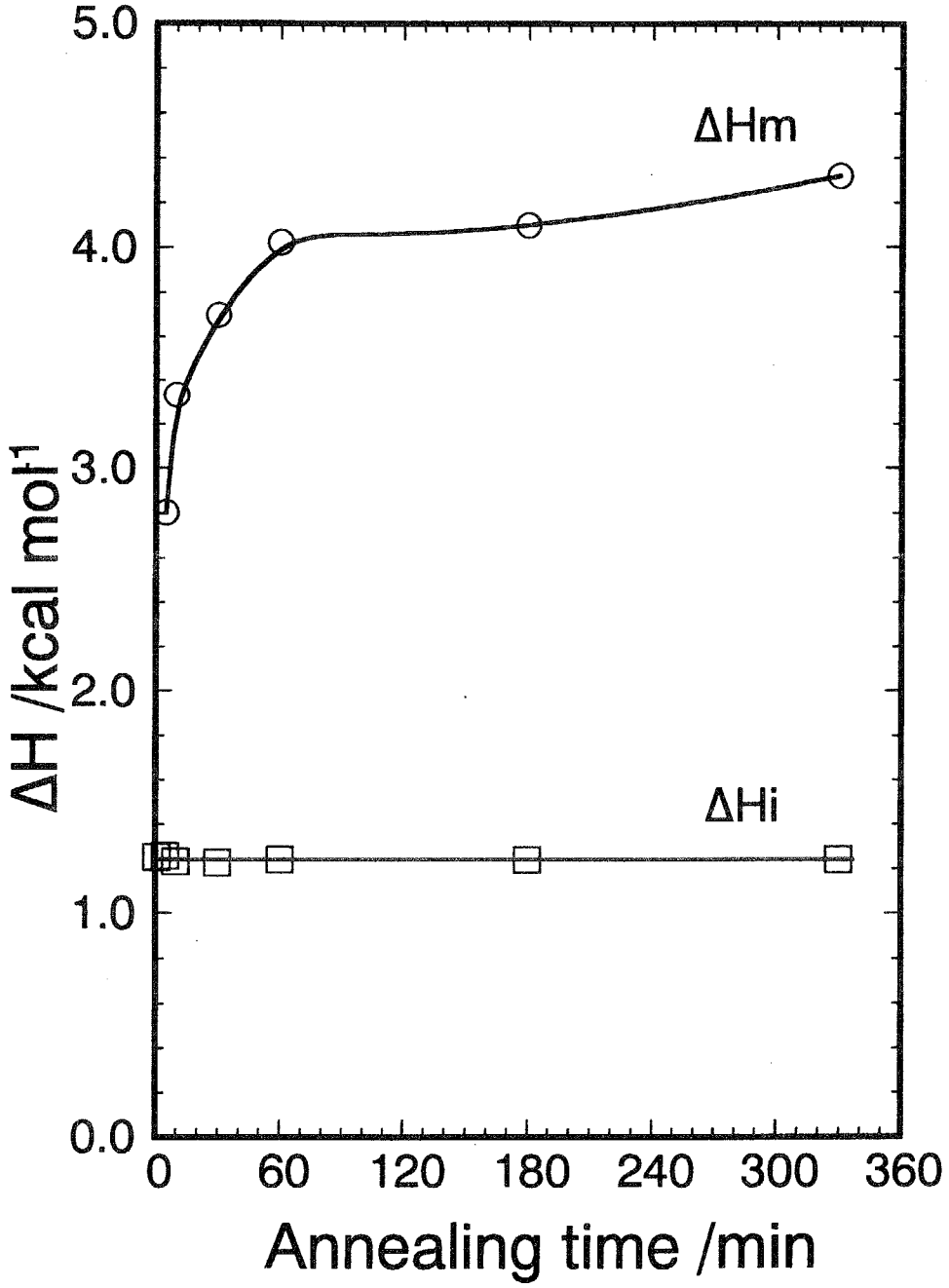

Figure 4.2. Variation in isotropization enthalpy, ΔH_i (rectangles), and the crystal melting enthalpy, ΔH_m (circles), for BB-5 with the isothermal formation time. ΔH_i (or ΔH_m) was measured for the sample which was quenched from the isotropic (or S_{CA}) phase and held at 185°C (or at 140°C) during a certain period for isothermal formation of the S_{CA} (or crystal) phase.

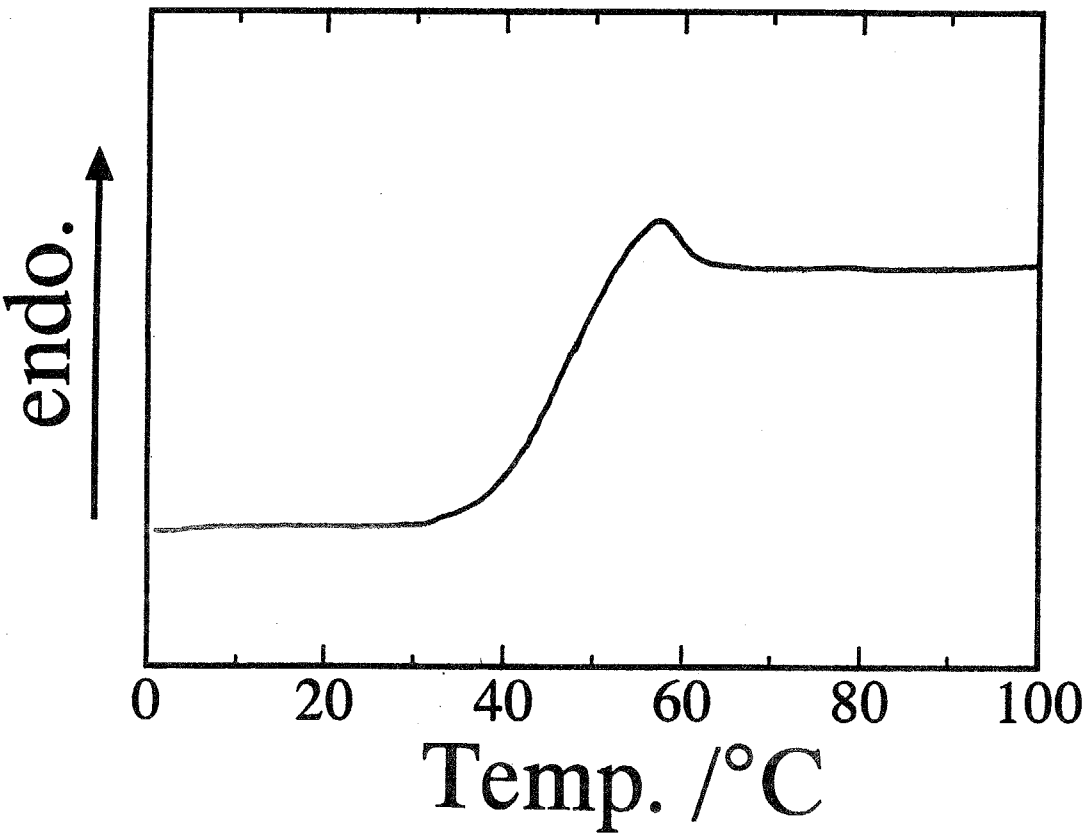

Figure 4.3. DSC thermograms showing the glass transition of S_{CA} LC phase in BB-5.

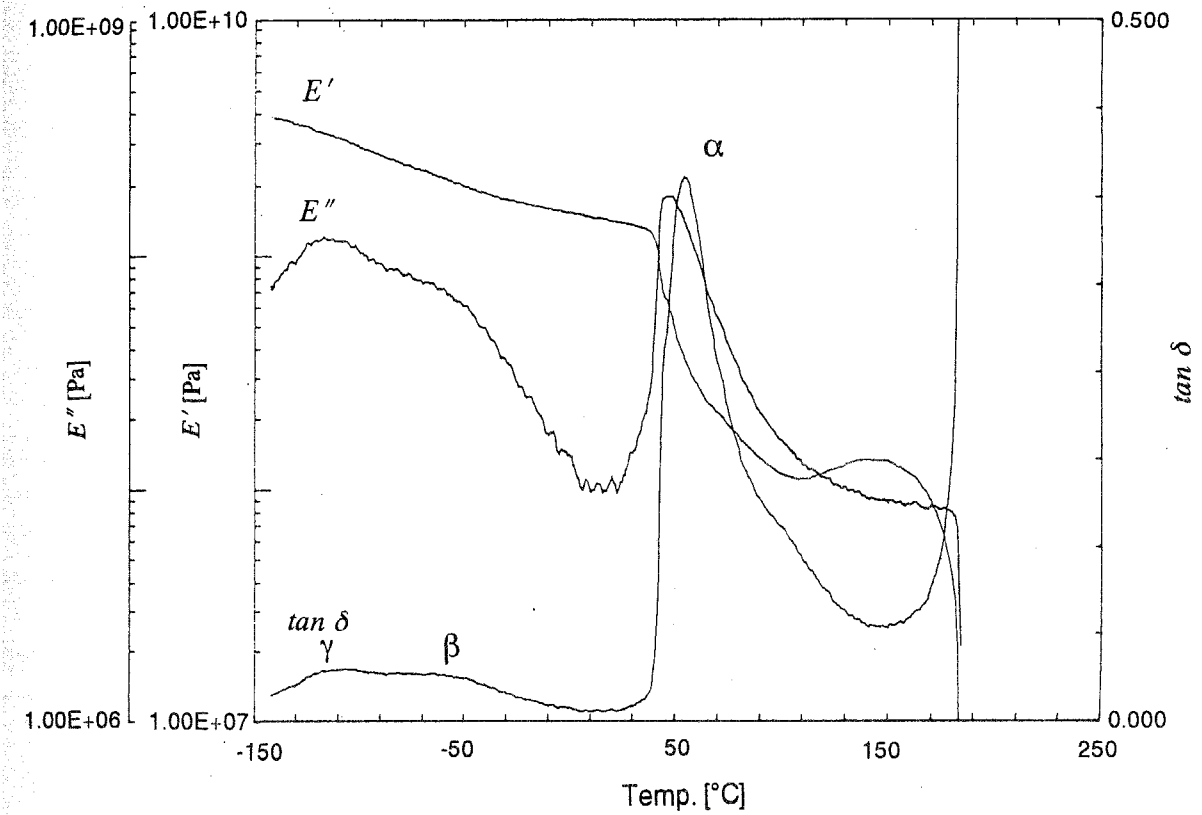

Figure 4.4. Storage modulus, loss modulus and loss tangent as a function of temperature at 10 Hz for BB-5 specimen quenched from smectic melt.

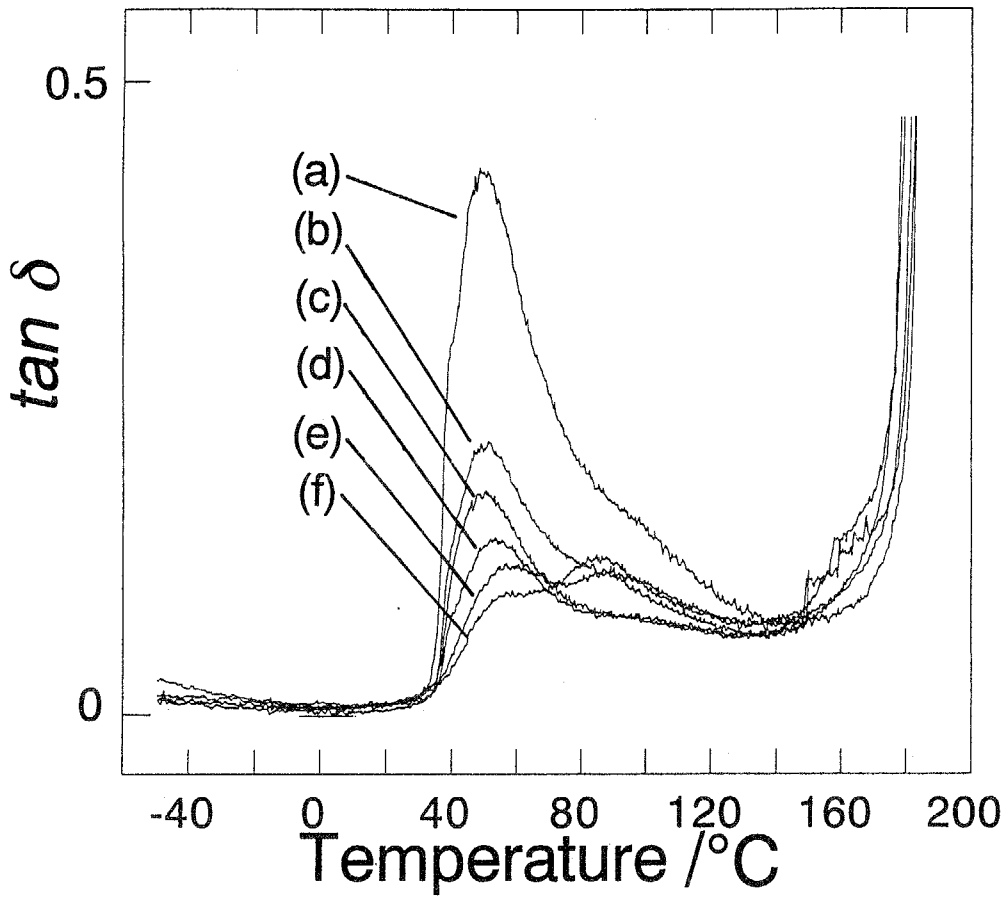

Figure 4.5. Loss tangent as a function of temperature at 10 Hz for BB-5 samples with different degrees of crystallinity. The crystallinity was controlled by annealing the specimen at 140°C for a certain period of (a) 0 min (as quenched from S_{CA}), (b) 1 min, (c) 5 min, (d) 10 min, (e) 30 min and (f) 60 min (refer to Figure 4.2).

(a) Fiber A

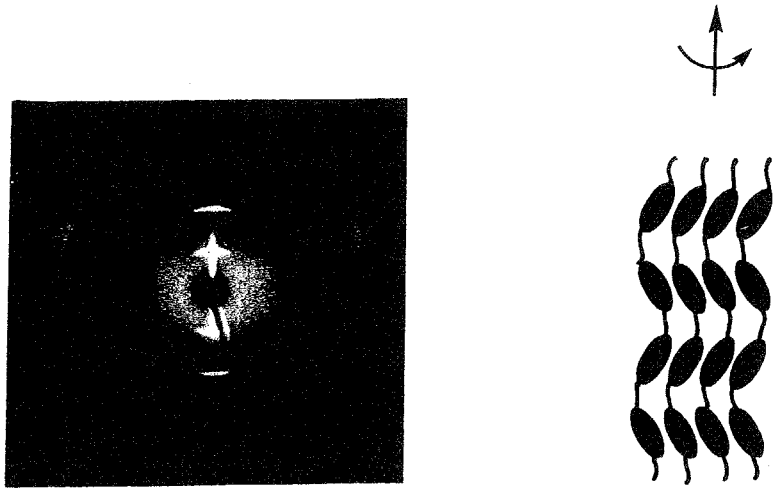

(b) Fiber B

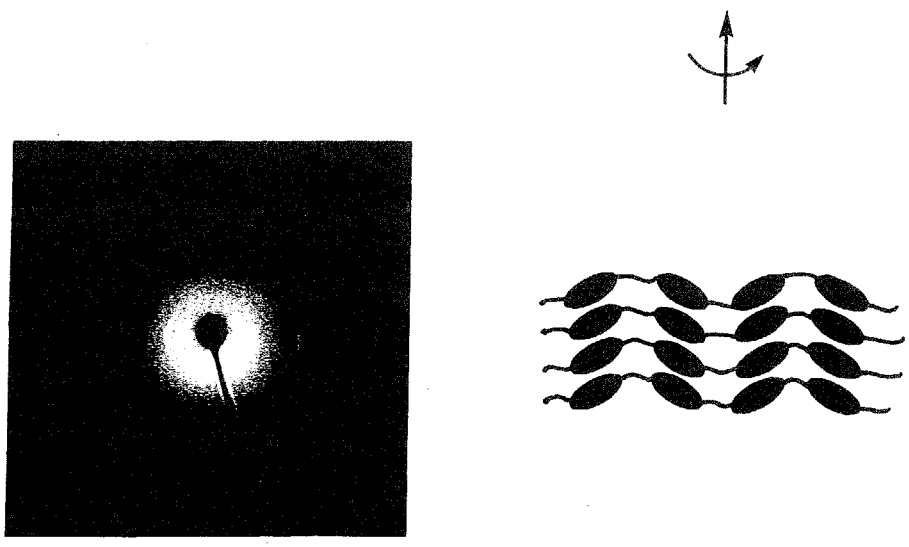

Figure 4.6. X-ray photographs for (a) fiber A drawn from the isotropic melt of BB-5 at a rate of around 1 m sec^{-1} and (b) fiber B drawn from the smectic melt of BB-5 at a rate of 1 cm sec^{-1}. The fiber axis is in the vertical direction. The molecular arrangements deduced from the X-ray patterns are also illustrated.

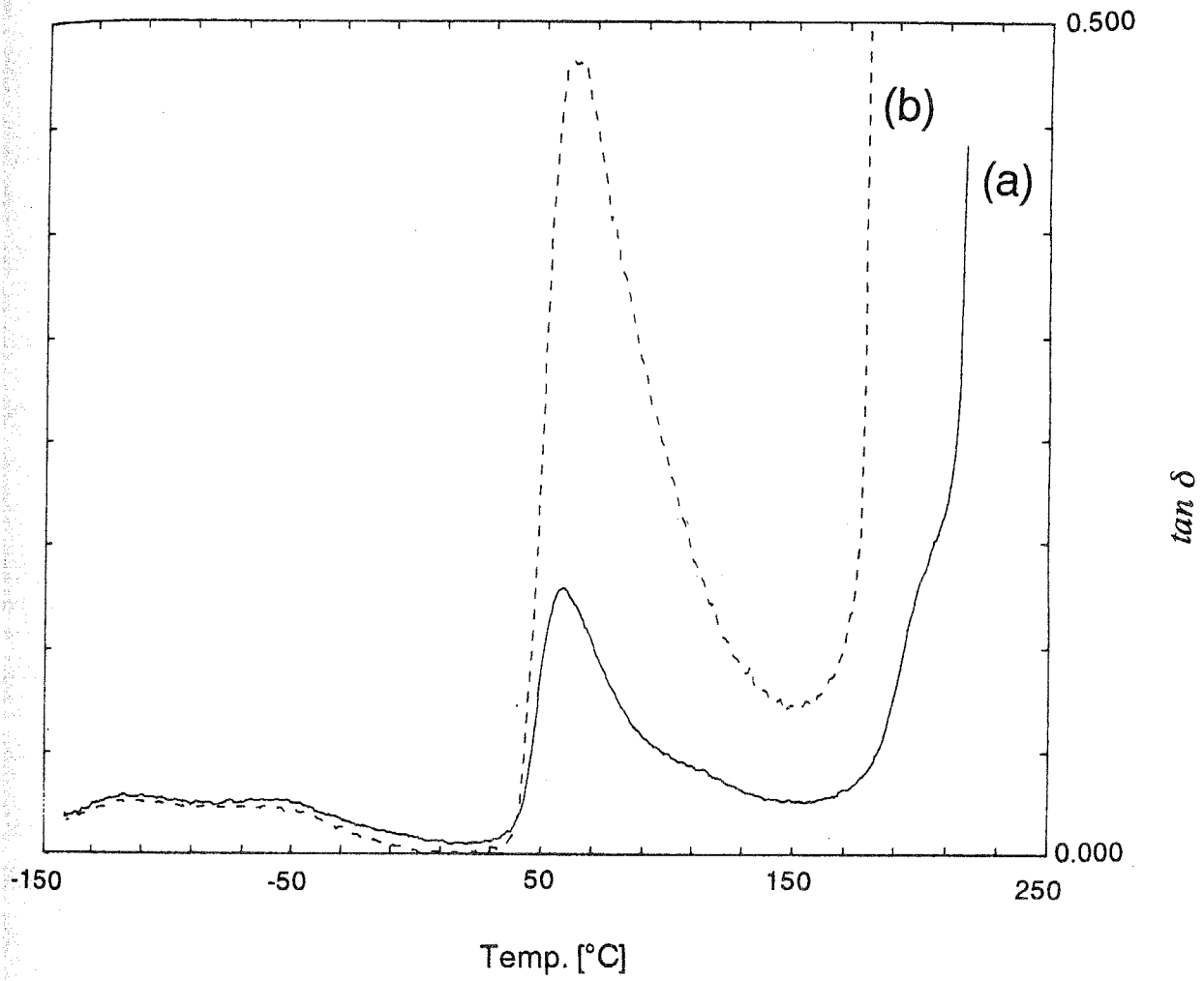

Figure 4.7. Temperature dependence of loss tangent measured at 10 Hz for the two different BB-5 fibers; (a) solid curve for fiber A and (b) dashed curve for fiber B (refer to Figure 4.6).

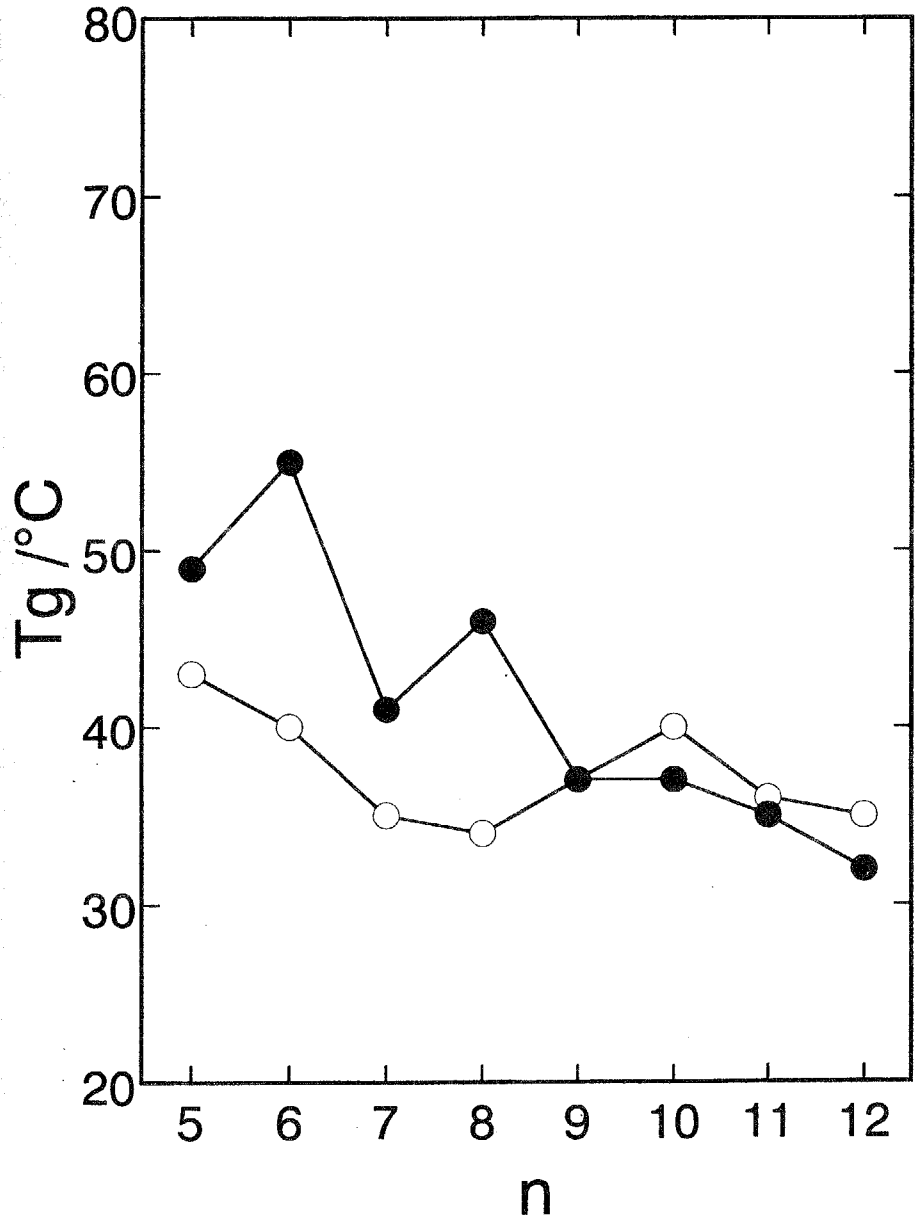

Figure 4.8. Variation in DSC glass transition temperatures in BB-*n* (open circles) and N-n (closed circles) polyesters with *n*.

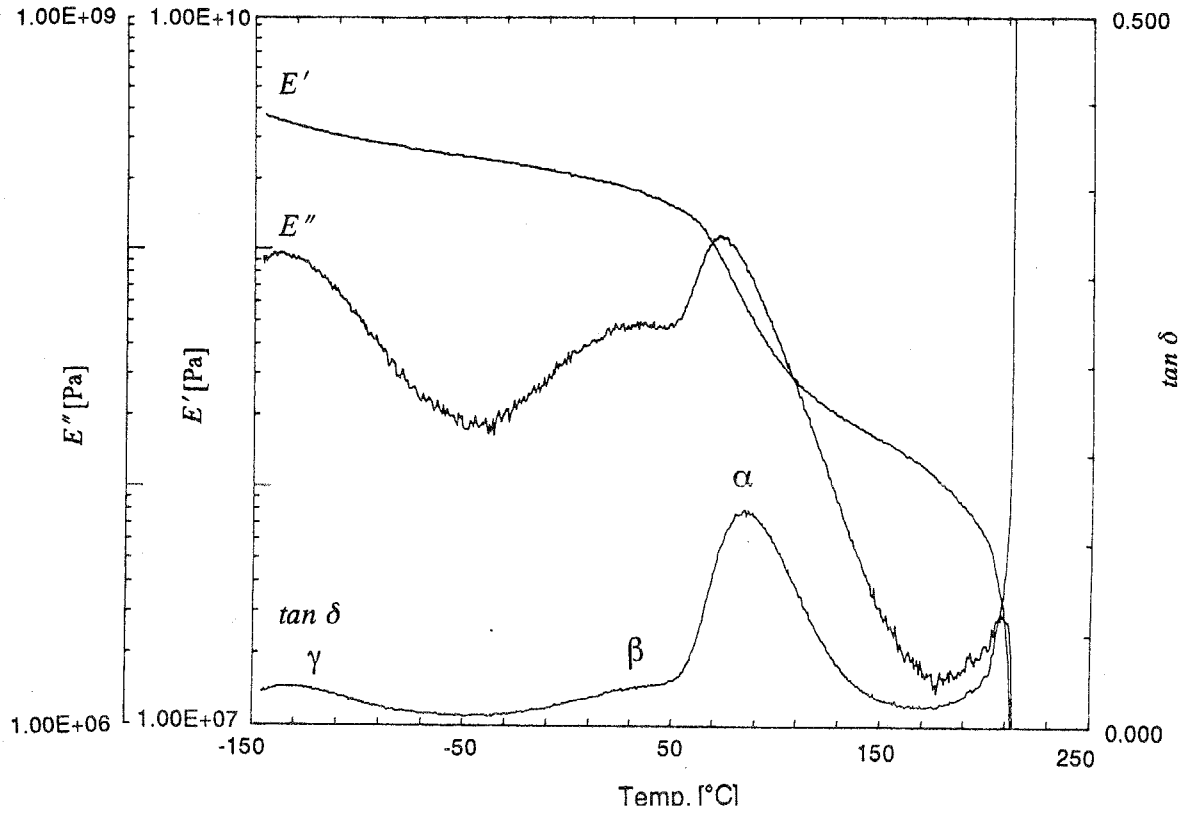

Figure 4.9. Temperature dependence of storage modulus, loss modulus and loss tangent for N-6 specimen quenched from isotropic melt. Frequency was 10 Hz.

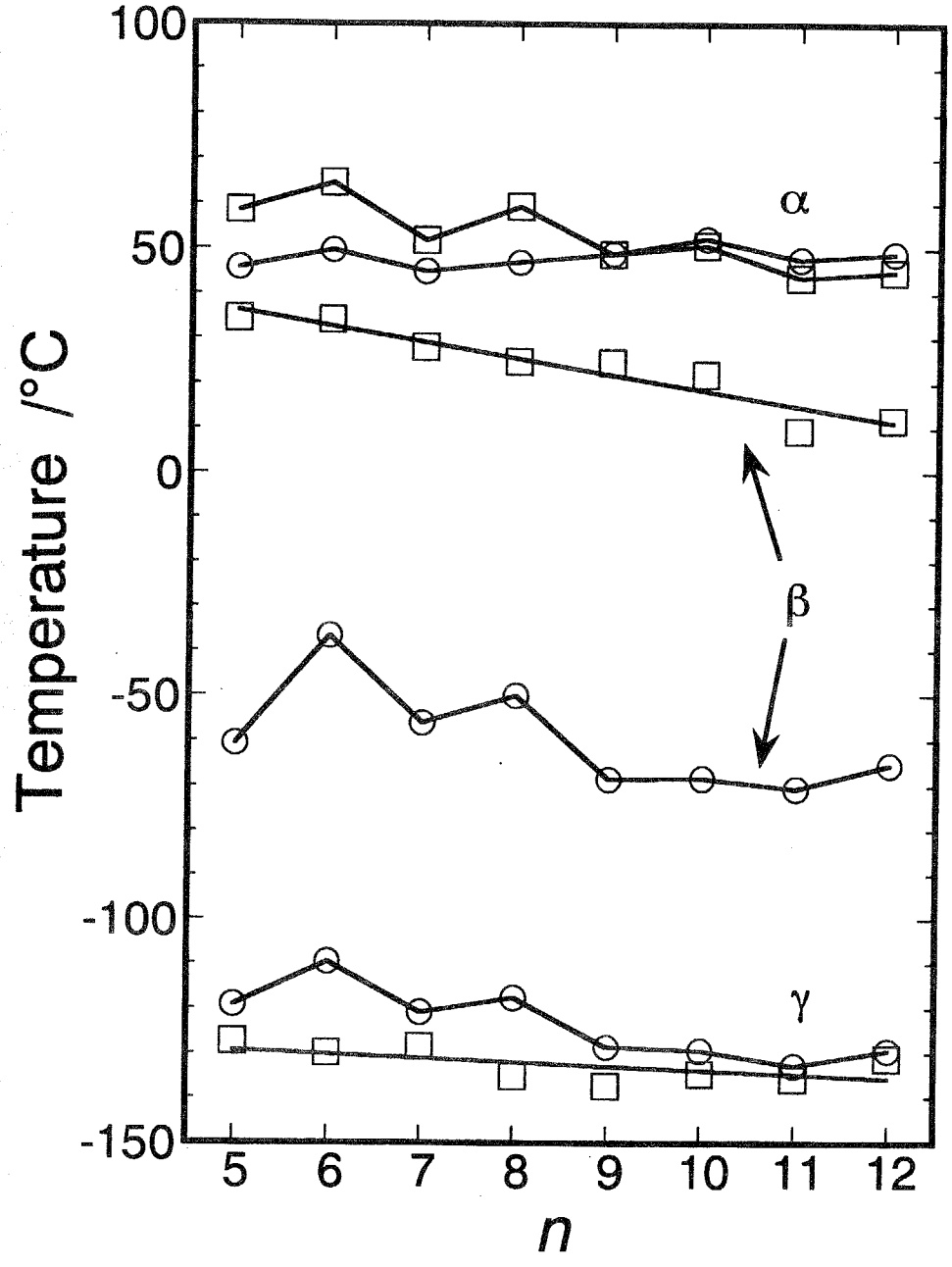

Figure 4.10. Variation in α-, β- and γ-relaxation temperatures for BB-*n* (circles) and N-*n* (rectangles) polyesters with n. The temperatures were determined from the peak of loss modulus, *E″*, measured at 10 Hz.

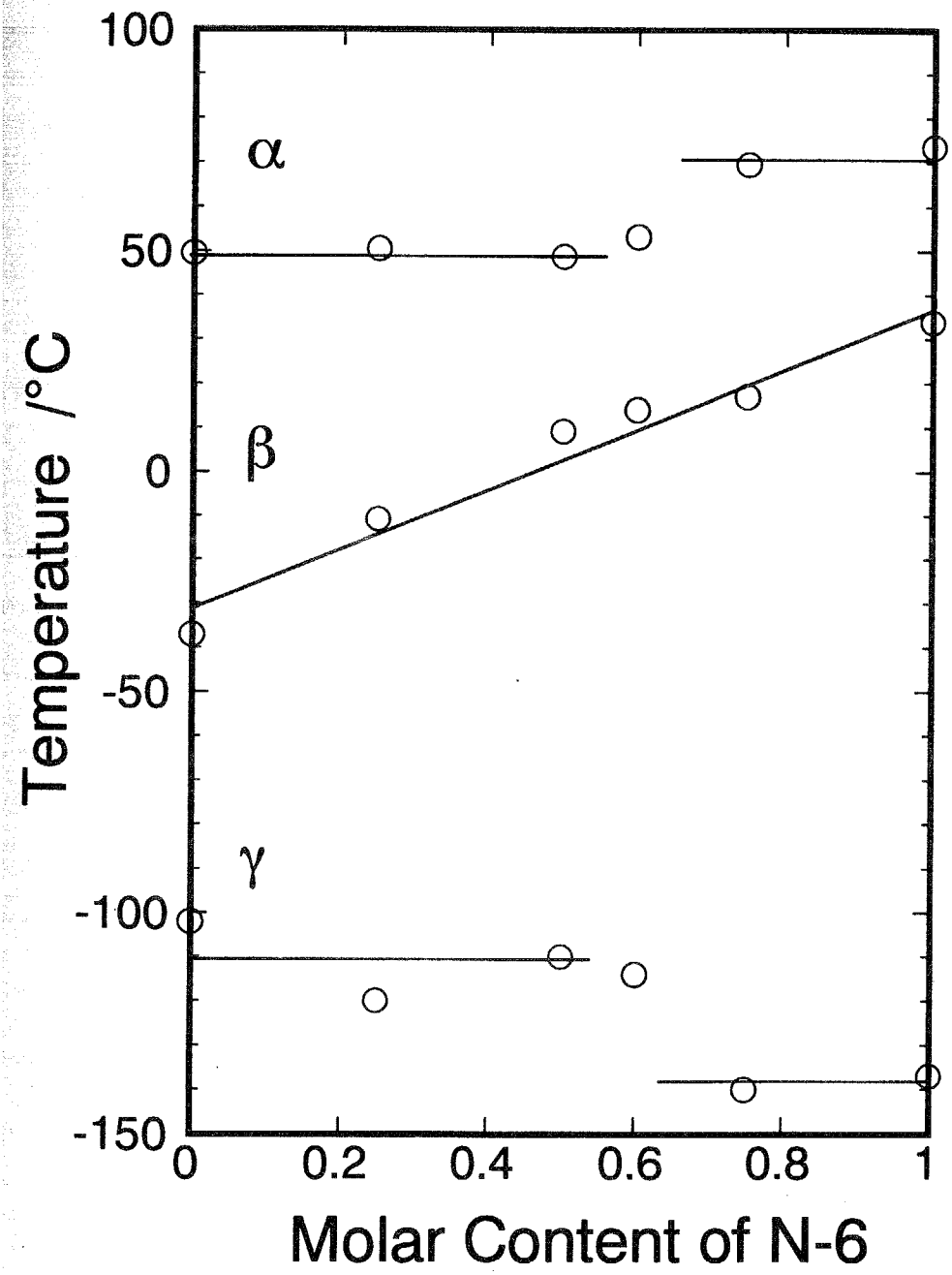

Figure 4.11. Variation in α-, β- and γ-relaxation temperatures of BB-6-*co*-N-6 copolyesters with the molar content of N-6. Temperatures were determined from the peak of loss modulus, *E″*, measured at 10 Hz.

Chapter 5

Smectic Liquid Crystal and Crystalline Structures in PB-*n* Polyesters

ABSTRACT: The thermotropic PB-*n* polyesters consisting of 4,4′-dihydroxybiphenyl and aliphatic dibasic acid with an even number of methylene show a smectic H mesophase. Information on structure and conformation for the crystalline and smectic phases of even-membered PB-*n* polyesters were investigated by means of wide-angle X-ray diffraction, fluorescence, and high resolution solid-state ^{13}C NMR spectra.

Another type for main-chain liquid crystalline polymers based on the biphenyl mesogen is PB-*n* polyesters,

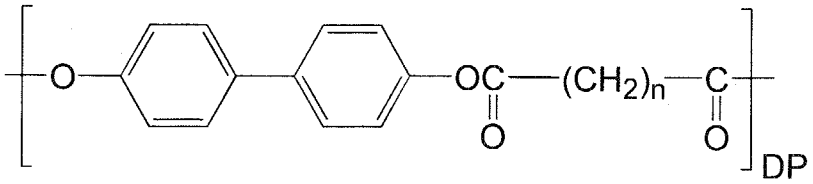

where n = 6 - 20 is the number of methylene units in the spacer.[1-3] PB-*n* polyesters exhibit a unique odd-even effect in that the mesophase is nemaic for the odd-membered polymers and smectic H (S_H) for the even-membered polymer. This chapter presents the structural characteristics of the smectic H, crystalline phases of the PB-*n* polyesters investigated by wide-angle X-ray scattering, fluorescence, and high resolution solid-state ^{13}C NMR spectra.

5.1. Phase Transitions of PB-*n* Polyesters

The PB-*n* polyester was prepared by melt condensation of 4,4'-diacetoxybiphenil and dioic acid. The inherent viscosity of the sample of 0.6 - 1.2 dL g^{-1} was determined at 30°C using a 0.5 g dL^{-1} solution in a 60/40 mixture by weight of phenol and tetrachloroethane.[1] The calorimetric behavior was investigated with a Perkin-Elmer DSC II calorimeter at a rate of 10°C min^{-1} under a flow of nitrogen. The wide-angle X-ray measurement was performed using a Rigaku-Denki RU-200 BH X-ray generator with Ni- filtered Cu Kα radiation. The sample temperature was measured and regulated with an accuracy of 0.2°C by using a Mettler FP-80 hot stage.

DSC thermograms of the even-membered PB-*n* polyesters with n of 8 - 20 include several peaks in the heating and cooling processes (see Figure 5.1). The DSC thermograms of PB-*n* with n of 8 - 12 show two sharp peaks

corresponding to crystal (K) - S_H and isotropization of the S_H, respectively.[2] On the other hand, in the DSC thermograms for PB-*n* with *n* of 14 - 20, an additional broad peak appears just below the sharp peak for the crystal - S_H transition. It corresponds to a crystal - crystal transition, K_1 - K_2. These transitions have been determined with the change in the d-spacing of the X-ray diffraction as illustrated in Figure 5.2. At the transition from the crystal to the S_H phase in all the specimens, the layer spacing drops suddenly. In K_1 - K_2 transition of the samples with *n* of 14 - 20, the layer spacing gradually increases with rising temperature in the crystalline state. The oriented sample of PB-*n* polyesters is not obtainable even for a high molecular weight sample. Thereby the unit-cell dimension and the chain packing in the crystals and the S_H phase have been estimated with Bragg-spacings of an unoriented sample as described in the following sections.

5.2. Identification for the Structures of Phases in PB-*n* Polyesters with Wide-angle X-ray Diffraction

5.2.1. S_H Phase

It is often possible to distinguish between the nematic and smectic phases from the textures seen in the polarizing microscope. The identification of a particular smectic polymorph is a more difficult even for low-molecular weight materials. X-ray diffraction provides information concerning the arrangement and mode of packing of molecules and the types of order present in a mesophase. For powder samples, the well-known Debye-Scherrer technique is used. This method gives all the reticular spacing but no information about the spacial orientation of these planes. If a sample can be obtained in the form of an oriented monodomain, it is possible to extract more detailed structural

information from its diffraction diagram. However, for PB-*n* polyesters, their oriented sample is not obtainable.

The two main diffraction effects usually observed on the X-ray diffraction pattern of a powder sample are the inner ring(s) (close to the center of the diffraction pattern, and corresponding to a diffraction angle θ of only a few degrees) and the outer ring(s) (much farther out in the diffraction pattern and corresponding to a diffraction angle about 10°).[4] The inner rings are indicative of longer layer spacings. The outer rings correspond to shorter preferred spacing occurring in the lateral packing arrangement of the molecules. The appearance of a broad halo or a sharp ring furnishes a qualitative indication of the degree of order.

The X-ray patterns of nematic and smectics differ mainly in their characteristics at small diffraction angles. Nematic patterns present a diffuse ring, indicating that there is no order in the direction of the molecular long axes. In contrast, smectic patterns present one or several sharp rings, showing the existence of layer-like correlations. These diffraction maxima provide direct information about the layer thickness.

Smectic mesophases can be divided into three groups according to the characteristics of their X-ray patterns at large diffraction angles. In the first group, we find the S_A and S_C phases whose diffraction patterns show only one broad, diffuse halo indication a lack of periodic lateral order: the distribution of the molecular centers of mass is random. The second group is composed of the crystalline smectics (S_B, S_E, S_G, S_H, S_J and S_K). Their diffraction patterns show a single or several sharp outer rings which are related to the high degree of order within the layers. If the molecules form a hexagonal close-packing of cylinders as in the S_B phase, the distances between neighbouring molecules are equal, and there is only one sharp diffraction maximum corresponding to the

nearest-neighbour distances. If there is more than one such maximum, then there must be also more than one value for these distances, and packing can no longer be hexagonal. Thus, the number of maxima gives information about the type of the molecular packing. The S_{BHex}, S_F and S_I phases are intermediate between these two groups.

These diffraction maxima provide direct information about the layer thickness. For orthogonal phases, i.e. phases in which the director is perpendicular to the smectic layer, it has been generally found that the layer spacing, *d*, is closely equal to the molecular length, *L*. For tilted phases, the difference between *d* and *L* is used to calculate the tilt angle. However, there is the possibility of some ambiguity because of unknown molecular conformation.

Figure 5.3 shows the diffraction pattern of the mesophase of PB-18 taken at 190°C. It has one sharp inner ring and two sharp outer rings, which eliminates S_A, S_C, S_F (diffuse outer ring) and S_B (one sharp outer ring). The Bragg spacings observed for the smectic phases of even-membered PB-*n* polyesters have been interpreted upon the following assumptions:

(1) The molecule including the hydrocarbon portion of the dibasic acid residue is in its most highly extended form.

(2) In such a homologous series, the outer reflections with spacings that are independent upon the number of methylene units in the diacid can be attributed to the lateral packing in the plane perpendicular to the molecular axis.

(3) For the smectic phases, the spacing corresponding to the innermost ring can be assigned as the thickness of the smectic layer.

The Bragg spacing of PB-8 corresponding to the inner ring, 16.5 Å, is significantly shorter than the length of the repeat unit, 22.0 Å, indicating a tilted phase. This observation indicates the smectic phase is either S_G or S_H. The smectic phase generally exhibits only two outer rings with spacings of 5.0 and 4.5 Å; however homologous PB-6 shows several additional reflections which

are accountable an oblique lattice containing two chains is indicated. By analogy with the structure for PB-6, the following can be suggested for the smectic phases of even-membered PB-*n* polyesters, a′ = 9.0 Å, b′ = 6.15 Å, and γ′ = 90°. Since this is not hexagonal, S_I and S_G are eliminated, and the X-ray results are sufficient, standing alone, to determine that the smectic phase of the even-membered PB-*n* is S_H.[2]

The smectic layer spacings observed in the S_H phase of the even-membered PB-*n* polyesters (*n* = 8 - 20) are plotted against the number of the methylene unit in the diacid in Figure 5.4. The smectic layer spacing increases from 16.5 Å to 29.8 Å with increment in the spacer length, while the spacings of the two outer rings are essentially constant, indicating that a lateral packing common to all members. Comparing the smectic layer spacing with the extended length of the repeat unit gives the angle between the polymer chain axis and the layer normal of 41°. The incremental increase in the smectic layer spacing per methylene unit is 1.07 Å is smaller than the projected length of a methylene unit along the chain direction, 1.26 Å, indicating the methylene units of dibatic acid makes an angle of 30° with respect to the layer normal. Figure 5.5(a) illustrates the approximate molecular arrangements of PB-8 in the S_H phase.[2] The biphenyl moiety is tilted with an angle of 65° to the layer normal. This suggests weak interactions between the aromatic rings, which would permit easier translation and rotation of the molecules in the mesophase.

5.2.2. Crystalline Phases

PB-*n* with *n* of 8 - 12 forms one crystalline phase, while that with *n* of 14 - 20 forms two crystalline phases, K_1 and K_2. The d spacings of these crystalline phases estimated from WAXD are plotted against the number of methylene units in the spacer, *n*, in Figure 5.4. The spacer length dependence of the d

spacing for the crystalline phase of PB-*n* with *n* of 8 - 12 is identical with that for the K_1 phase of PB-*n* with *n* of 14 - 20. It indicates that the crystal structure of PB-*n* with a shorter spacer is equivalent with the structure of K_1 crystal in PB-*n* with a longer spacer.

K_1 Crystal The spacings of five of outer reflections in WAXD (about 5.0 Å, 4.6 Å, 4.2 Å, 4.0 Å, and 3.8 Å) are common to most of polymers. These can be accounted for by an oblique lattice with $a' = 8.59$ Å, $b' = 5.06$ Å, and $\gamma' = 100°$ containing two molecules.[2] It can be assumed that the homologous polymers have a similar lateral packing in the K_1 crystal. Smectic layer spacing corresponding to inner reflection increases by 0.88 Å per methylene unit (see Figure 5.4). The value of the increment in the spacing is smaller than the projected length of a methylene unit along the chain direction 1.26 Å, indicating the spacer moiety makes an angle of 45° with respect to the layer normal. The spacing extrapolated for $n = 0$ is 11.5 Å. The value corresponds approximately with the length of the mesogenic moiety along the long axis of 11.3 Å, indicating that the long axis of the mesogenic moiety is parallel to the layer normal. Figure 5.5(b) illustrates the approximate molecular arrangement of PB-8 in K_1 phase.

K_2 Crystal The number of outer rings in WAXD pattern for K_2 crystal is not enough to determine the lattice constants. Since the K_2 crystal is the mesophase between K_1 and S_H where an oblique lattice is formed, it can be assumed that the two polymer chains are packed in an oblique lattice. On the other hand, the layer structure can be presumed from the variation of the d spacing of the inner reflection in WAXD upon the number of methylene units in a spacer. The layer spacing increases by 1.13 Å with per a methylene unit and shows the extrapolated value of 9.4 Å for the mesogenic unit. Thus we can picture the layer that the mesogenic part and spacer moiety are tilted with the

layer normal at an angle of 34°, and at an angle of 27°, respectively (see Figure 5.5(c)).

5.3. Fluorescence Study on Intermolecular Complex Formation between Mesogenic Moieties in S_H and Crystalline Phases of PB-*n*

The microstructure of a liquid crystal affects the intermolecular interaction between mesogenic moieties. Various fluorescent species in molecules, such as monomeric chromophores, excimers, and ground-state complexes, are demonstrated to originate in the difference in formation of molecular interaction between moieties in the molecule. The change in molecular interaction can be elucidated by investigating the change in fluorescence behavior of fluorescing complexes. Thus, the fluorescence is an effective method for investigating microstructure of the liquid crystal. Based on this concept, the fluorescence of PB-*n* was studied in order to obtain more detailed structural information for the S_H and crystalline phases.

Steady-state fluorescence spectra were measured with a Hitachi 850 fluorescence spectrophotometer equipped with a 30 kV xenon lamp. The bandpasses were 5 nm for both excitation and emission monochromators. The fluorescence and its excitation spectra were measured in a front-face arrangement to minimize the self-absorption. The temperature was controlled with an Alpha Engineering thermostat coupled with a temperature controlling unit.

5.3.1. Fluorescence from Fully Overlapping Biphenyl Groups

Biphenyl has a fully overlapping molecular arrangement in the crystal.[10-14]

4,4′-diacetoxybiohenyl (DABP) of the mesogenic moiety of PB-*n* and biphenyl for the standard material were used to investigate the fluorescence of the fully overlapping biphenyl group. Figure 5.6 shows the fluorescence spectra and its excitation spectra for DABP and biphenyl in their crystal state (a and b) and in dilute solution (a* and b*). DABP and biphenyl in dilute solutions (10^{-4} M) show a monomer fluorescence at 323 and 315 nm, respectively. DABP crystal shows a fluorescence peak at 362 nm, besides the monomer fluorescence at 322 nm. Similarly, the biphenyl crystal shows fluorescence at 360 nm, besides the monomer fluorescence at 321 nm. It indicates that the fluorescence at about 360 nm is due to two fully overlapping biphenyl groups. The fluorescence excitation spectra for DABP crystal (a_1' and a_2' in Figure 5.6(a)) and biphenyl crystal (b_1' and b_2' in Figure 5.6(b)) are all distorted by monomer self-absorption and the multiscattering effect, while their monomer fluorescence excitation spectra (a_1' and b_1') are not in accord with those monitored at 360 nm (a_2' and b_2'), indicating that the fluorescence at about 360 nm does not originate from an excimer but is due to the emission from an intermolecular ground-state complex. These results lead to a conclusion that the fluorescence of two fully overlapping biphenyl moieties at about 360 nm is attributed to an intermolecular ground-state complex.

5.3.2. Fluorescence Spectra of PB-*n* polyesters

Figure 5.7 shows the fluorescence (right) and its excitation spectra (left) at room temperature for PB-*n*. The identical fluorescence is found at around 340 nm (curves a in Figure 5.7). The fluorescence at around 340 nm shows a longer wavelength than the monomer fluorescence of DABP crystal (322 nm) and shows no excitation wavelength dependence. Thus it is attributed to the monomer fluorescence. On the other hand, various fluorescence at 360 - 475

nm (b - i) depends strongly on excitation wavelength. Moreover, the shapes of fluorescence excitation spectra for the fluorescence at 360 - 475 nm (b′ and c′) disagree with those for the monomer (a′). This indicates that the fluorescence at 360 - 475 nm is not due to excimer or exciplex but to various intermolecular ground-state complexes. In other words, the solid of PB-*n* contains various kind of molecular packing and low uniformity.

The fluorescence and its excitation spectra of PB-*n* during heating change corresponding to the phase transitions. The fluorescence spectra of PB-18 excited at various excitation wavelength during heating are shown in the right part of Figure 5.8. The wavelength of fluorescence peak excited at 320 nm (curve b in Figure 5.8), which corresponds to the aggregation structure of two fully overlapping biphenyl moieties as deduced from WAXD for the K_1 crystal, shifts gradually from 360 to 418 nm during heating. The shift of the peak may be attributable to the gradual alternation in the arrangement of the lateral mesogenic moieties from fully overlapping one to partially overlapping one, as elucidated from the WAXD method. The main intermolecular interaction between mesogenic moieties changes from one between tow fully overlapping biphenyl group to a biphenyl and an ester moieties, and alters the electronic distribution between mesogenic moieties to strengthen molecular interaction leading to a red-shifted fluorescence. Other fluorescence wavelengths (curves c - f in Figure 5.8) do not shift as much as that associated to the two fully overlapping biphenyl groups (curve b). They are assumed to be related to intermolecular ground-state complexes composed by the two biphenyls overlapping with the various degrees. The smaller overlap packing of mesogens is more favorite at the higher temperature, so the related fluorescence peaks do not change so much.

The monomer fluorescence peak at 337 nm and emission at 448 - 466 nm

(curves g - i) are observed almost invariably during heating. It is reasonable that the monomer fluorescence peak does not shift during heating considering the consistency of the electronic distribution in an independent mesogenic moiety.

The fluorescence excitation spectra during heating are depicted in the left part of Figure 5.8. The spectra monitored at 450 nm (curve c') show a broad shoulder around 390 nm, suggesting that the fluorescent species at high wavelengths become the main ones at high temperatures and that the change in the fluorescence peak wavelengths is not only due to the change in the excited state but also the change in he ground state. The change in fluorescence and its excitation spectra mentioned above have been observed for other PB-*n* polyesters.

Figure 5.9 shows the fluorescence (right) and its excitation spectra (left) of PB-n in isotropic phase. As can be seen in their fluorescence spectra, except for the monomer fluorescence (curve a) and fluorescence at 445 - 475 nm (curves g -i), fluorescence excited at 320 - 360 nm (b - f) show only a broad structureless band around 415 - 430 nm, in contrast to the fact that these fluorescent species show strong excitation wavelength dependence in crystalline and S_{II} phase. Thus all PB-*n* show only one kind of ideal steady-state molecular interaction between biphenyl moieties in the isotropic phase. This is reasonable because the mobile surroundings around chromophores in isotropic phase of PB-*n* have no correlation to the spacer length.

5.3.3. Phase Transition Behavior

The changes in fluorescence peak wavelengths excited at various excitation wavelengths during heating for PB-*n* polyesters are plotted in Figure 5.10. The peak wavelength change for fluorescence excited at 320 nm (closed

lozenges) is the largest one. It is reasonable since two fully overlapping biphenyl groups at room temperature change their interaction structure most clearly during heating. The plot for PB-8 shows two breaks at 158 and 283°C. It indicates that the packing of the mesogenic moiety change begins at 158°C. This temperature is significant lower than the K_1 - S_H transition temperature of 215°C determined by DSC and WAXD, suggesting that the phase transition starts in a local microstructure level, i.e., molecular interaction between mesogenic moieties, and then extends to the macrostructure change (the entire phase transition. The second break in the plot appears at 283°C which corresponds to the S_H - isotropic transition temperature of 284°C. This result indicates that the temperature dependence of the change in molecular interaction for the three phases (crystal, S_H and isotropic phases) are different. The similar result was obtained for PB-10 (see Figure 5.10b). For PB-*n* with longer spacer lengths, temperature dependence of fluorescence excited at 320 nm of PB-16 (closed lozenge in Figure 5.9c) shows breaks at 163 and 206°C. The temperature of 163°C is lower than the K_1 - K_2 transition temperature of 177°C determined by DSC and WAXD, while that of 206°C is near the S_H - isotropic transition temperature of 210°C. The similar result was obtained for PB-18 (see Figure 5.10d). It suggests that microscopic pretransition takes place before K_1 - K_2. On the other hand, the break does not appear around the K_2 -S_H transition temperature.

During heating from room temperature to the crystal - S_H transition temperature, the fluorescence peak excited at 320 nm red-shift about 14, 16, 26, 36 nm for PB-8, PB-10, PB-16 and PB-18, respectively as shown in Figure 5.10 with shadow area. PB-*n* with the longer spacer shows the more red shift. The degrees of overlap between two biphenyl moieties of PB-16 and PB-18 decrease much more before crystalline - S_H transition than PB-8 and PB-18 do. The

increment in the red-shift for PB-16 and PB-18 is associated with the increment in their layer spacing in K_1 - K_2 transition.

5.3.4. Molecular Arrangements between Mesogenic Moieties

The degree of overlap between mesogenic moieties are different in the S_H phase of PB-*n* with various spacer length. The change in fluorescence peak wavelength excited at 320 nm (λ_f) and averaged λ_f in S_H phase and the illustration of tentative molecular arrangements between two neighbouring mesogenic moieties are shown in upper part of Figure 5.10. The degree of overlap between two biphenyl moieties in SH phase of PB-*n* decreases with increasing in the spacer length.

Based on the fluorescence results, the approximate molecular arrangements between mesogenic moieties of PB-18 as an example in the three phases are illustrated in Figure 5.11. λ_f of around 360 nm for K_1 phase corresponds to the fluorescence of the fluorescence from two fully overlapping biphenyl groups, so the mesogenic moieties is depicted to be a fully overlapping arrangement which corresponds to that elucidated from the WAXD method. λ_f for K_2 of around 390 nm longer than K_1 phase is due to the change in electronic distribution between a biphenyl moiety and an ester moiety, indicating that the degree of overlap between two biphenyl moieties in K_2 phase is lower than that in K_1 phase. For the S_H phase, λ_f shows much longer fluorescence peak wavelength than those in K_1 and K_2 phase. Therefore, the degree of overlap between two biphenyl moieties in S_H phase is lowest between the three phases. These deduced arrangement is comparable with that elucidated from WAXD; the mesogenic unit is tilted with the lager angle in the order of K_1, K_2 and S_H phases.

5.4. High Resolution Solid State ^{13}C-NMR Studies for Crystalline and Liquid Crystalline Phases of PB-18

The objective of this work is to clarify the conformations of the mesogenic and spacer moieties in the two crystalline and S_{II} phases of PB-18 polyesters by the use of high resolution solid state ^{13}C NMR. An attempt has been made to estimate the conformation of the mesogenic moiety by considering the ^{13}C NMR shieldings using the finite perturbation theory (FPT) method within the INDO framework.[14-17] Furthermore, the solid state NMR proved to be a very good technique for delineating the conformations of the spacer groups in the mesophase.

^{13}C MAS NMR spectra were obtained on a JNM GSX-270 NMR spectrometer operating at 67.8 MHz with cross polarization/magic angle spinning (CP/MAS) and variable temperature (VT) accessories. Samples were contained in a cylindrical rotor composed of zirconia with an O-ring and spun at a speed of 4.0 kHz given by a spinning controller. The contact time was 2.0 ms and the repetition time was 3 s. The ^{1}H radio frequency (rf) field strength was 60 kHz. Spectra were observed by the accumulation of 1200 scans so as to achieve a reasonable signal to noise ratio. The ^{13}C chemical shifts were calibrated indirectly with adamantane as the external standard (29.5 ppm relative to tetramethylsilane).

The ^{13}C NMR shielding calculations for a model compound were performed using the INDO method incorporated with the FPT method[14-17] by a SUN SPARC station 5.

5.4.1. Solid-State ^{13}C NMR Spectra of PB-18 Polyester

The solid-state ^{13}C NMR spectra of PB-18 polyester were found to be rather complicated with a large number of spinning side bands resulting from

large anisotropy of the shielding tensors. In order to eliminate the spinning side bands, total suppression of spinning side band (TOSS) spectra were recorded. The spectra for the three phases of PB-18 polyester are shown in Figure 5.12, where the peaks in the region of 100 - 180 ppm can be assigned to the aromatic carbons in the mesogenic moiety and the peaks in the region of 10 - 80 ppm to the carbons in the aliphatic spacer part. For the accurate assign of the peaks, the NMR spectra for the crystalline phases were measured using the dipolar dephasing method. These data and reference data[19] allow a well defined assignment of the peaks, which are summarized in Table 5.1. Assuming that the influence of intermolecular interactions on the ^{13}C NMR chemical shift values is negligible,[24] the chemical shifts varying from a phase to a phase lead to a preliminary conclusion that three phases are different in the conformation of the ester, biphenyl and spacer parts.

5.4.2. Conformation of the Mesogenic Moiety

At first, we shall discuss on the conformation of the mesogenic moiety. Figures 5.13 and 5.14 show the expanded aromatic region of the ^{13}C CP/MAS NMR spectra and the schematic chemical shifts with their assignments respectively for K_I, K_2 and S_H phases. In order to estimate the conformation of the mesogenic moiety in the three phases of PB-18 polyester, the chemical shift values at the peak top of the focused carbons are discussed with the ^{13}C NMR shielding calculated for a model compound.

Calculation of ^{13}C NMR Shielding. There are a few reports on the relationship between the conformation of aromatic ester bond and the ^{13}C NMR chemical shift.[9] ^{13}C NMR shieldings calculation of the model compound, hence might provide detailed information on the relation. The FPT INDO calculations were carried out for the model compound of Figure 5.15 were performed as a

function of the two torsion angles, ϕ and ψ, which correspond to the angles between the two phenyl rings of the biphenyl moiety and between the phenyl rings in the biphenyl and ester bonds, respectively (refer to Figure 5.16). The geometric parameters given in Figure 5.15 are based on the X-ray diffraction data of aromatic ester compounds.[18] The shielding constants were calculated with varying one of the two angles under fixing the other angle at 60°, presuming that the interactions between the central and the third or forth nearest neighboring segments were negligible. Figures 5.17 and 5.18 show the calculated ^{13}C NMR shieldings with the torsion angles, ϕ and ψ, respectively. These results give the following information on the relationship between the two angles, ψ and ϕ, and the chemical shifts of the carbons. (1) ϕ and ψ affect independently on the ^{13}C NMR chemical shift of the carbons. (2) The increment of ϕ makes the C1 carbon peak shift to a lower field. (3) The decrease of ψ leads the C3 carbon peak into a large splitting with two distinct components at higher and lower fields and the C2 carbon peak into only a small splitting. These results consist with that in a previous study[9] where the two angles were varied under the condition of $\phi = 2\psi$, whereas in this study the two angles were varied independent. It can be said that the results are available for the qualitative estimation of the conformation of the mesogenic moiety with ^{13}C NMR chemical shifts, as discussed below.

K_1 and K_2 Phases As shown in Figures 5.12 and 5.13, the carbonyl carbon has two sharp peaks at 173.3 and 171.9 ppm in K_1, whereas a single sharp peak at 171.3 ppm in K_2. The peak at 123.2 ppm in K_1 attributed to C3 carbon splits into two peaks at 126.0 and 122.4 ppm in K_2. The peak for C2 carbon shifts to lower field from 126.5 ppm in K_1 to 128.2 ppm in K_2. The calculated ^{13}C NMR shielding constants connect these variations of the chemical shifts reasonably with the difference of the conformation in K_1 and K_2. The dihedral angle ψ

between the phenyl ring and the carbonyl group is smaller in K_2 than that in K_1. The lower field shift of the peak for C1 carbon from 132.4 ppm in K_1 to 133.6 ppm in K_2 suggests that the torsion angle ϕ between the two phenyl rings in the biphenyl moiety is larger in K_2 than that in K_1. The results lead to submit the two distinct conformations of the mesogenic moieties in two crystalline phases. In K_1 crystal, the phenyl rings assume a nearly coplanar conformation and the ester bond is twisted respect to the neighbor biphenyl moiety. In K_2 crystal, the phenyl rings are twisted and the ester bond is closely coplanar.

S_H Phase The chemical shifts for the carbonyl and C3 carbons in the S_H phase of 171.6 and 151.6 ppm, respectively are in higher field than that in the K_1 crystal, indicating that the dihedral angle ψ between the ester bond and the phenyl ring in the S_H phase is larger than that in the K_1 crystal. The sharpness of the peak of C3 carbon also supports this estimation. The peak for C1 carbon at lower field of 137.1 ppm than that in the K_2 crystal shows that the phenyl rings of the biphenyl moiety are more twisted than that in the K_2 crystal. Thus the both angles, ψ and ϕ in the S_H phase is the largest in that for the three phases of PB-18.

Here it is worth mentioning the shape of the peaks for the mesogenic carbons in the S_H phase. The peaks of C2 and C3 carbons are sharp while that of C1 and C4 carbons are broad and asymmetrical. The broadening and asymmetry of the peaks can attribute to the restricted rotational motion of the phenyl rings in which the angle ϕ varies, because the chemical shifts of C1 and C4 depends on ϕ, while that of C2 and C3 do not. The peak of C1 is asymmetric with the top in the lower magnetic region, indicating a slow exchange between the two conformational states. If the exchange was not limited to a confined angle, the peak would appear symmetrical.

5.4.3. Conformation of Spacer Part

The position of the peaks changes among the phases in the aliphatic region as well as in the aromatic one as shown in Figure 5.12. Here we look closely on the peak for the interior carbons in the spacer moiety. In the crystalline phases of K_1 and K_2, the peak consists with two components and the observed chemical shifts are different in the two phases, while it is sharp and consists with one component in the S_H phase (refer to Table 5.1). The difference of the feature of the peak in the NMR spectra suggests that the conformation of the spacer part is different in the three phases.

The relationship between the chemical shift of the interior methylene carbons and the conformation was investigated for the *n*-alkane where the chemical shifts of 30.0 and 34.2 ppm are observed for the amorphous chain and the trans zigzag chain, respectively. Ishikawa, et al.[19] have reported the chemical shifts for the crystalline phases of *n*-alkane. The signals methylene carbons loaded in the interior of the chain appear at 32.8, 34.2 and 33.2 ppm for the orthorhombic crystal, the triclinic crystal and the rotator phase, respectively. These reference data is available for the discussion on the conformation of the spacer moiety. The chemical shifts of 34.2 and 33.6 ppm observed for the K_1 and K_2 phases respectively shows that the alkyle spacer takes the same conformation as that for the triclinic crystal in K_1 and as that for the rotator phase in K_2, respectively. On the other hand, the chemical shifts of 31.8 and 31.1 ppm for the crystalline phases suggest that the part of the spacers takes a mixed conformation of gauche and some amount of trans, which may be attributable to folding sites in a polymer chain which discussed in the next chapter of this thesis.

The peak with one component with its chemical shift value of 32.1 ppm for the S_H phase is located between the trans zigzag conformation and the

amorphous state, and suggests that trans and gauche conformers exchange rapidly with a fraction of gauche conformars of 0.208.[19,25] In other words, the spacer mostly extends as estimated with wide-angle X-ray diffraction data[2,3], but includes traces gauche conformers in the smectic phase.[20-23]

5.5. Phase Transition Behavior in Random Copolymers of Even-membered PB-*n* Polyesters

Isomorphous liquid crystals are considered as equivalent and characterized by the same symbol. Therefore, the mesophases of a new compound can be positively identified by isomorphy with known mesophases of reference compounds. Sackman and his school of at Halle have produced a classification scheme for monomeric liquid crystals based on the criterion of complete miscibility of identical phases.[26] Assuming that the method is applicable to polymeric liquid crystals, the type of mesophase can be determined by establishing the isobaric temperature-composition phase diagram of a binary system composed of the polymer and a reference compound. For the identification of polymeric mesophases, mutual miscibility is the method of choice for nematic and smectic of low order. Thus the attempt to identify from miscibility test the S_H phase of even-membered PB-*n* polyesters is unsuccessful.

Polymeric systems containing two different mesogenic repeating units mixed intimately within a single chain can be prepared by random copolymerization. Thus the phase transition behavior of the binary copolymers with a reference polymer is a useful peace of information to identify the type of the mesophase.

PB-10-co-PB-12[27] As indicated by the phase behavior of PB-10-co-PB-12 shown in Figure 5.19(a), the phases encountered with increasing temperature are crystal (K), smectic H (S_H) and isotropic (I). There is a clear indication of eutectic behavior in the melting temperature of the crystal when the second component is added, while the isotropization temperatures of S_H falls on a smooth curve very nearly corresponding to the arithmetic average of those for the homopolymers. Thus the S_H phase can be formed stable in a wide temperature region. Figure 5.19(b) shows the entropy changes for the K-S_H and S_H-I transitions plotted as a function of copolymer composition. The entropy change for the K-S_H transition is significantly depressed by addition of the second comonomer, which can be interpreted quantitatively in terms of the degree of crystallinity. By contrast, the variation of the S_H-I transition entropy very nearly follows the arithmetic average, as observed for the variation of the S_H-I transition temperature. The X-ray diffraction pattern of the S_H phase was quite clear for all copolymers, indicating that the copolymerization does not disrupt the ordered packing in the S_H phase. The layer spacing is composition-dependent and falls above the dashed line representing the arithmetic average of the homopolymer spacings (Figure 5.19(c)). Thus it appears that both types of repeating unit can be accommodated in the smectic phase of the copolymers.

PB-8-co-PB-12[27] This copolymer has a larger difference between the two repeating units than the preceding case. The phase diagram in Figure 5.20(a) shows a very large depression of the crystal melting temperature upon addition of the second comonomer, so that the temperature region of the smectic phase is broadened. Figure 5.20(c) illustrates the composition dependence of the smectic layer spacings for the crystal and smectic phases. For this copolymer the negative deviation of the smectic layer spacing of the crystal from the arithmetic mean is much more pronounced. The smectic phases of all copolymer gave a well-defined WAXD pattern consisting of one inner and two

outer reflections. Evidently introduction of a second repeating unit, even one differing substantially in length, is much less destructive to the smectic phase than to the crystalline phase. Further supporting evidence for this conclusion appears in Figure 5.20(b), where the composition dependence of the entropy changes for the K-S and S-I transitions are compared. The decrease of $\Delta S_{K\text{-}S}$ is even more pronounced for this copolymer than was the case for PB-10-*co*-PB-12.

PB-16-co-PB-18 The homopolymers, namely PB-16 and PB-18 shows three clear transitions, while the transition peak at the lowest temperature associated with K_I - K_2 transition becomes unclear in adding another component. All the copolymers form K_I, K_2, S_{II}, and isotropic phases in the order of increase in temperature as shown in Figure 5.22(a). The copolymers shows lower transition temperatures and enthalpies for K_I - K_2 and K_2 - S_{II} than the homopolymers, while no significant decrease in the isotropization temperatures and enthalpies of the S_{II} are found for all the copolymers. The d-spacings for the outer ring in the WAXD of the S_{II} phase are constant in the copolymers, showing that the incorporation of the second repeat unit does not affect the lateral packing of the polymer chains in the S_{II} phase. The layer spacing for the copolymer shows different composition dependencies in the three phases as shown in Figure 5.21(c). The layer spacing takes arithmetic average value of the spacings for PB-16 and PB-18 in the K_I phase, smaller value than the arithmetic average in the K_2 phase, and lager value than the arithmetic average in the S_{II} phase, respectively.

PB-14-co-PB-18 In the copolymer of PB-14 and PB-18, the difference in the spacer lengths of the homopolymers are twice as long as that for PB-14-co-PB-16. The phase diagram for PB-14-co-PB-18 is shown in Figures 5.22(a). The K_2 phase disappears with adding another component. Decrease in the transition temperatures and enthalpies for K_I - K_2 and K_2 - S_{II} with adding

another component is more significant than that in PB-16-co-PB-18. On the other hand, decrease in the transition temperature for S_H - isotropic is not as significant as that in the crystal -S_H transition but larger than the isotropization temperature for PB-16-co-PB-18. But the isotropization enthalpy is nearly independent on the composition (Figure 5.22(b)). The variation of the layer spacings in the copolymers shown in Figure 5.22(c) is similar to PB-16-co-PB-18, but the layer spacing for K_1 crystal is smaller than the arithmetic average of the layer spacings for PB-14 and PB-18.

PB-6-co-PB-12[27] This even-even copolymer has the largest difference in the lengths of the two types of repeating unit. The upper temperature transition found in the DSC heating curve is replaced by two transitions in the cooling curve. Optical microscopy observation revealed that the additional transition is due to a monotropic nematic phase. The phase diagram for this copolymer constructed from the cooling DSC data is shown in Figure 5.23(a). In contrast to the preceding copolymers, in this system the crystal-smectic transition exhibits a eutectic. Hence, no crystallization occurs when the repeating units are quite different in length. Further the inner reflection is missing in the smectic phase though the fan-shaped smectic texture was observed in optical microscopy observation. Figure 5.23(b) illustrated the composition dependence of ΔS_{S-I}. Unlike previous copolymers, PB-6-co-PB-12 exhibits a significant depression of ΔS_{S-I} upon addition of the second comonomer. The structure of the smectic phase becomes imperfect when it is forced accept repeating units of much different length.

Thus, incorporation of a second repeating unit of different length in PB-*n* polyesters does not significantly disrupt the smectic structure of the mesophase if the difference in length between the two is not so large. Such random variation may be tolerated in the liquid crystal structure, whereas it could not

occur in the crystalline phase. Hence this observation is one of the evidences that the mesophase of even-membered PB-*n* is a single smectic liquid crystal.

5.6. Conclusions

The structure of S_H and crystalline phases of even-membered PB-*n* polyesters were investigated by means of WAXD, fluorescence, and high-resolution solid-state ^{13}C NMR spectra.

In the S_H phase, two polymer chains are packed in a orthogonal lattice with $a' = 9.00$ Å, $b' = 6.15$ Å and $\gamma' = 90°$ with the mesogenic moiety and spacer moiety tilted by 41° and 34°, respectively to the smectic layer normal. The conformations of the mesogenic moiety are not confined to the S_H phase where the two phenyl rings in the mesogenic moiety rotate along a chain axis in a limited angle. In the spacer moiety, a fast exchange occurs between trans and gauche conformers. The fraction of gauche conformers is estimated as 0.21.

In the K_1 phase, two polymer chains are packed in an oblique lattice with $a' = 8.59$ Å, $b' = 5.06$ Å and $\gamma' = 100°$. It is assumed that the mesogenic moiety is parallel and the spacer moiety is tilted by 45°, respectively to the layer normal. The biphenyl moieties assume a coplanar conformation and the ester bond is twisted with the spacer packed in a triclinic lattice.

In the K_2 crystal, the crystalline lattice cannot be estimated. The mesogenic and spacer moieties are assumed to be tilted by 34° and 27°, respectively to the layer normal. In the mesogenic moiety, the ester bond is closely on the same plane with the neighbouring phenyl ring although the biphenyl moiety is slightly twisted. The spacers are packed as in a rotator phase.

The variation of the tilt angle of the mesogenic moiety in the three phases deduced by WAXD correspond to the change in the degree of overlapping between neighbouring two mesogenic moieties estimated by change in the fluorescence spectra.

References and Notes

(1) Asrar, J.; Toriumi, H.; Watanabe, J.; Krigbaum, W. R.; Ciferri, A. *J. Polym. Sci. Polym. Phys. Ed.* **1983**, *21*, 1119.

(2) Watanabe, J.; Krigbaum, W. R.; Ishikawa, T.; *Macromolecules* **1983**, *16*, 1271.

(3) Maeda, Y.; Mabuchi, T.; Watanabe, J. *Thermochim. Acta.* **1995**, *266*, 189.

(4) Gray, G. W.; Goodby, J. W. *Smectic Liquid Crystal*, Leonard Hill. Grasgouw, 1984.

(5) Sone, M.; Harkness, B. R.; Watanabe, J.; Yamashita, T.; Horie, K. *Polym. J.* **1993**, *25*, 997.

(6) Huang, H. W.; Horie, K.; Yamashita, T. *J. Polym. Sci. Polym. Phys. Ed.* **1995**, *33*, 1673.

(7) Horie, K.; Huang, H. W. *Macromol. Symp.* **1997**, *118*, 229.

(8) Takahashi, H.; Horie, K.; Yamashita, T.; Machida, S.; Hannah, D. H. B.; Sherrington, D. C. *Macromol Chem. Phys.* **1996**, *197*, 2703.

(9) Robertson, G. B. *Nature* **1961**, *191*, 593.

(10) Trotter, J. *Acta Crystallogr.* **1961**, *14*, 1135.

(11) Hargreaves, A.; Rizvi, S. H. *Acta Crystallogr.* **1962**, *15*, 365.

(12) Charbonneau, G. B.; Delugeard, Y. *Acta Crystallogr.* **1976**, *B32*, 1420.

(13) Cailleau, H.; Baudaur, J. L.; Zeyen, C. M. E. *Acta Crystallogr.* **1979**, *B35*, 426.

(14) Ando, I.; Yamanobe, T.; Kurosu, H.; Webb, G. A. *Annu. Rep. NMR Spectrosc.* **1990**, *22*, 205.

(15) Ando, I.; Yamanobe, T.; Asakura, T. *Prog. NMR Spectrosc.* **1990**, *7*, 839.

(16) Kurosu, H.; Webb, G. A.; Ando, I. *Mag. Res. Chem.* **1993**, *31*, 399.

(17) Sone, M.; Harkness, B. R.; Kurosu, H.; Ando, I.; Watanabe, J. *Macromolecules* **1994**, *27*, 2769.

(18) Coulter, P.; Windle, A. H. *Macromolecules* **1989**, *22*, 1129.

(19) Ishikawa, S.; Kurosu, H.; Ando, I. *J. Mol. Struct.* **1990**, *248*, 361.

(20) Abe, A.; Furuya, H. *Macromolecules* **1989**, *22*, 2982.

(21) Abe, A.; Furuya, H. *Mol. Cryst. Liq. Cryst.* **1988**, *159*, 99.

(22) Abe, A.; Furuya, H.; Yoon, D. Y. *Mol. Cryst. Liq. Cyrst.* **1988**, *159*, 151.

(23) Maroncelli, M.; Qi, S. P.; Strauss, H. L.; Snyder, R. G. *J. Am. Chem. Soc.* **1982**, *104*, 6237.

(24) Simmons, A.; Natansohn, A. *Macromolecules* **1992**, *25*, 3881.

(25) The fraction of gauche conformer, f_g was calculated from the equation in ref. 19, $f_g = (\delta_{obs} - 34.2) / (2 \times (-5.3))$ where δ_{obs} is the observed chemical shift.

(26) Sackman, H.; Demus, D. *Mol. Cryst. Liq. Cyst.* **1973**, *21*, 239.

(27) Krigbaum, W. R.; Watanabe, J.; Ishilawa, T. *Macromolecules* **1983**, **16**, 1271.

Table 5.1. Observed ^{13}C NMR chemical shift for PB-18 polyesters in the different phases

Temp.(°C)	C=O	C4	C1	C2	C3	α	int.	β
30 (K1)	173.2 171.9	150.9	132.4	126.6	123.3	35.0	34.2 31.8	26.8
174 (K2)	173.0	151.9	133.6	128.0	125.9 122.4	35.0	33.6 31.1	26.4
185 (S_H)	171.6	151.6	137.1	127.9	122.6	35.3	32.1	26.2

Figure Captions

Figure 5.1. DSC thermogram of PB-*n* polyesters measured at a rate of 10°C min^{-1}.

Figure 5.2. Temperature dependence of some selected spacings for (a) PB-10 and (b) PB-18.

Figure 5.3. Wide-angle X-ray diffraction pattern for PB-18 taken at 190°C

Figure 5.4. Variation of the layer spacing for the inner reflection upon the number of methylene units (*n*) in the spacer part in K_1 (square), K_2 (circle) and S_{II} (triangle) of PB-*n* polyesters.

Figure 5.5. The approximate molecular arrangements of PB-*n* polyesters in the (a) S_{II}, (b) K_1 and (c) K_2 phases.

Figure 5.6. Fluorescence (black curves) and its excitation spectra (gray curves) for (a) DABP crystal, (a*) DABP in 10^{-4} M acetonitrile solution, (b) biphenyl crystal , and (b*) biphenyl in 10^{-4} M acetonitrile solution. (a) a_1, a_2, and a_3 are the fluorescence spectra excited at 260, 320, and 330 nm, respectively; a_1' and a_2' are the fluorescence excitation spectra monitored at 322 and 360 nm, respectively. (a*) The fluorescence spectrum is excited at 260 nm and its excitation fluorescence spectrum monitored at 323 nm. (b) b_1, b_2, and b_3 are the fluorescence spectra excited at 260, 320, and 330 nm, respectively; b_1' and b_2' are the fluorescence excitation spectra monitored at 321 and 360 nm. (b*) The

fluorescence spectrum is excited at 255 nm, and its excitation spectrum is monitored at 315 nm.

Figure 5.7. Fluorescence (right) and its excitation spectra (left) for PB-8 (A, A′), PB-10 (B, B′), PB-16 (C, C′), and PB-18 (D, D′) at room temperature. (a - i) The fluorescence spectra excited at 300, 320, 330, 340, 350, 360, 380, 390 and 400 nm, respectively. (a′ - c′) The fluorescence excitation spectra monitored at 340, 400 and 450 nm, respectively.

Figure 5.8. Fluorescence (right) and its excitation spectra (left) for PB-18 during heating. (a - i) The fluorescence spectra excited at 300, 320, 330, 340, 350, 360, 380, 390 and 400 nm, respectively. (a′ - c′) The fluorescence excitation spectra monitored at 340, 400 and 450 nm, respectively.

Figure 5.9. Fluorescence (right) and its excitation spectra (left) for PB-n polyesters in isotropic phase. (a - i) The fluorescence spectra excited at 300, 320, 330, 340, 350, 360, 380, 390 and 400 nm, respectively. (a′ - c′) The fluorescence excitation spectra monitored at 340, 400 and 450 nm, respectively.

Figure 5.10. Temperature dependence of the fluorescence peak wavelengths excited at 300 nm (●), 320 nm (◆), 330 nm (△), 340 nm (▽), 350 nm (◇), 360 nm (○), 380 nm (+), 390 nm (×) and 400 nm (*) for (a) PB-8, (b) PB-10, (c) PB-16 and (d) PB-18 during heating.

Figure 5.11. Approximate molecular arrangements between mesogenic biphenyl moieties of PB-18 in the K_1, K_2 and S_H phases.

Figure 5.12. ^{13}C TOSS CP/MAS NMR spectra of PB-18 polyesters in K_1, K_2, and S_H phases.

Figure 5.13. Expanded aromatic region of the ^{13}C TOSS CP/MAS NMR spectra of PB-18 polyesters in K_1, K_2 and S_H phases.

Figure 5.14. Diagram of the observed ^{13}C chemical shifts for the carbons of the mesogenic moiety in the K_1, K_2 and S_H phases.

Figure 5.15. Model compound and the geometric parameters for the FPT-INDO calculation.

Figure 5.16. Torsion angles, ϕ and ψ, defined the relative twist between aromatic groups and between aromatic groups and between aromatic group and ester group, respectively.

Figure 5.17. Calculated ^{13}C NMR shielding of the carbons of the biphenyl moiety as a function of the relative torsion angle, ϕ, under the condition that $\psi = 60°$. The negative sign indicates deshielding.

Figure 5.18. Calculated ^{13}C NMR shielding of the carbons of the biphenyl moiety as a function of the relative torsion angle, ψ, under the condition that $\phi = 60°$. The negative sign indicates deshielding.

Figure 5.19. Composition dependence of (a) phase behavior on heating, (b) transition entropy and (c) layer spacing in PB-10-co-PB-12 copolymers. In (b), the open and closed marks denotes S_H - isotropic and crystal - S_H transitions

respectively. In (c), the open and closed marks denotes the layer spacing in S_H and that in crystal respectively.

Figure 5.20. Composition dependence of (a) phase behavior on heating, (b) transition entropy and (c) layer spacing in PB-8-co-PB-12 copolymers. In (b), the open and closed marks denotes S_H - isotropic and crystal - S_H transitions respectively. In (c), the open and closed marks denote the layer spacing in S_H and that in crystal respectively.

Figure 5.21. Composition dependence of (a) phase behavior on heating, (b) transition entropy and (c) layer spacing in PB-16-co-PB-18 copolymers. In (b), the circle, square and triangle marks denotes S_H - isotropic, K_2 - S_H and K_1 - K_2 transitions respectively. In (c), the triangle, circle and square marks denote the layer spacing in S_H, K_2 and K_1 phases, respectively.

Figure 5.22. Composition dependence of (a) phase behavior on heating, (b) transition entropy and (c) layer spacing in PB-14-co-PB-18 copolymers. In (b), the circle and triangle marks denotes S_H - isotropic and K_2 - S_H transitions respectively. In (c), the triangle, circle and square marks denote the layer spacing in S_H, K_2 and K_1 phases, respectively.

Figure 5.23. Composition dependence of (a) phase behavior on cooling and (b) transition entropy in PB-6-co-PB-12 copolymers. In (b), the open and closed marks denotes S_H - isotropic and crystal - S_H transitions respectively.

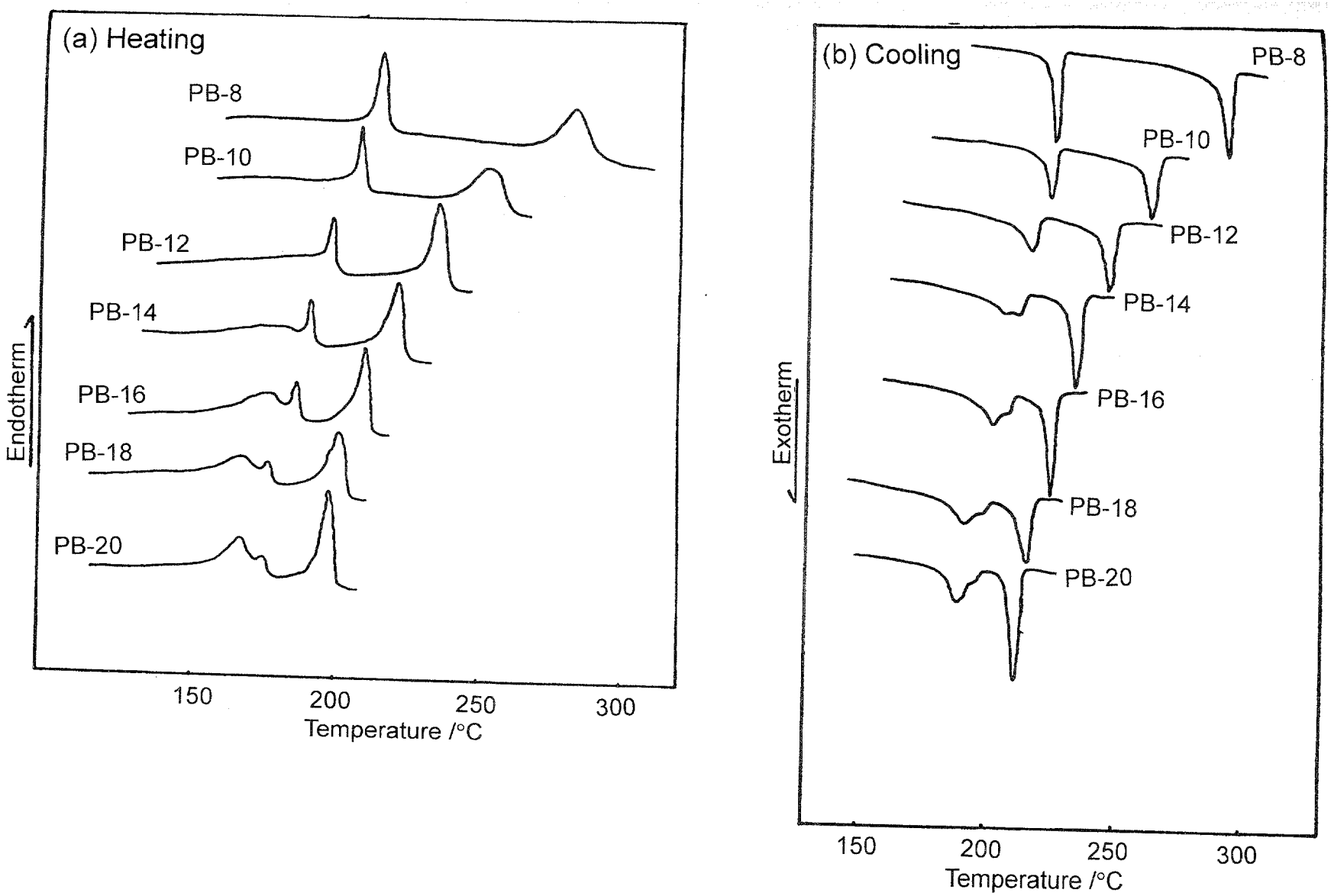

Figure 5.1. DSC thermogram of PB-*n* polyesters measured at a rate of 10°C min^{-1}.

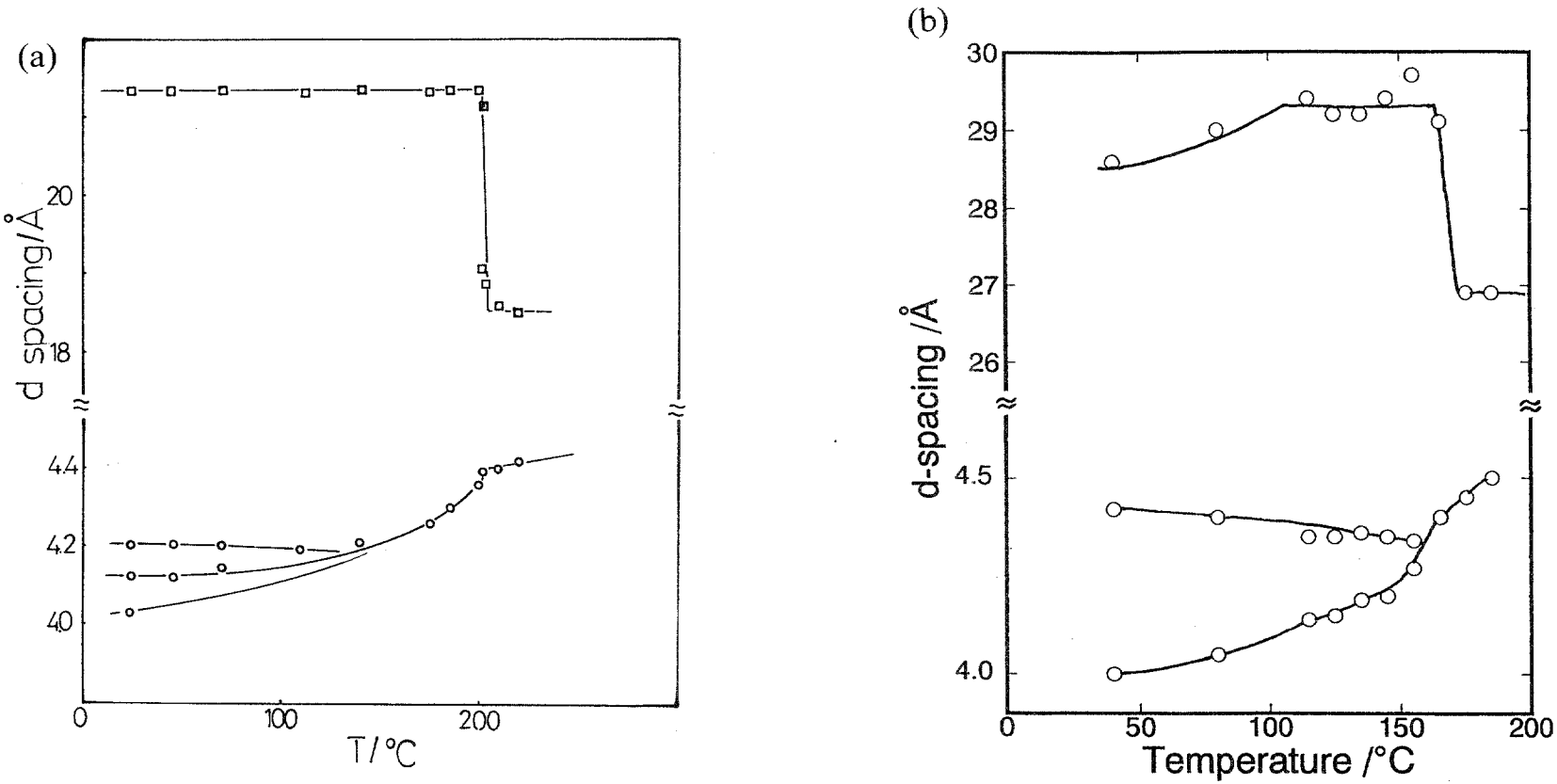

Figure 5.2. Temperature dependence of some selected spacings for (a) PB-10 and (b) PB-18.

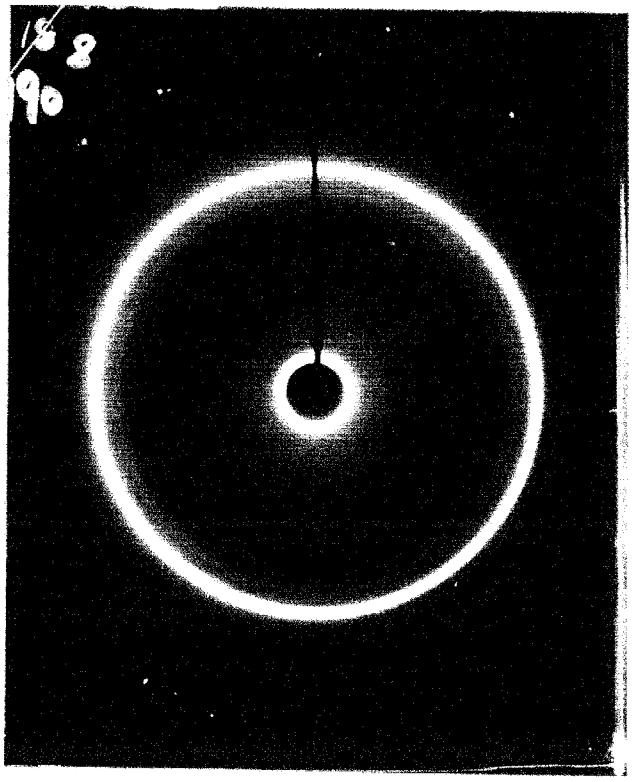

Figure 5.3. Wide-angle X-ray diffraction pattern for PB-18 taken at 190°C

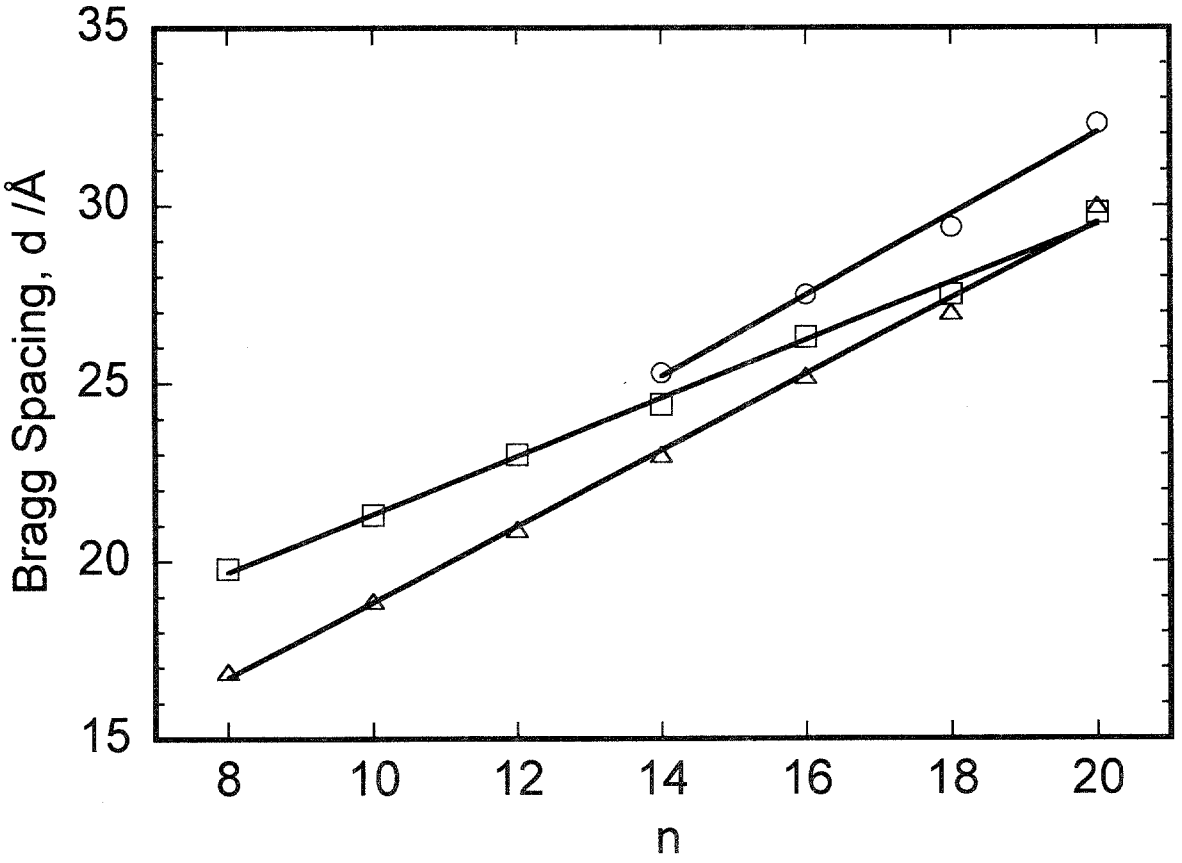

Figure 5.4. Variation of the layer spacing for the inner reflection upon the number of methylene units (*n*) in the spacer part in K_1 (square), K_2 (circle) and S_H (triangle) of PB-*n* polyesters.

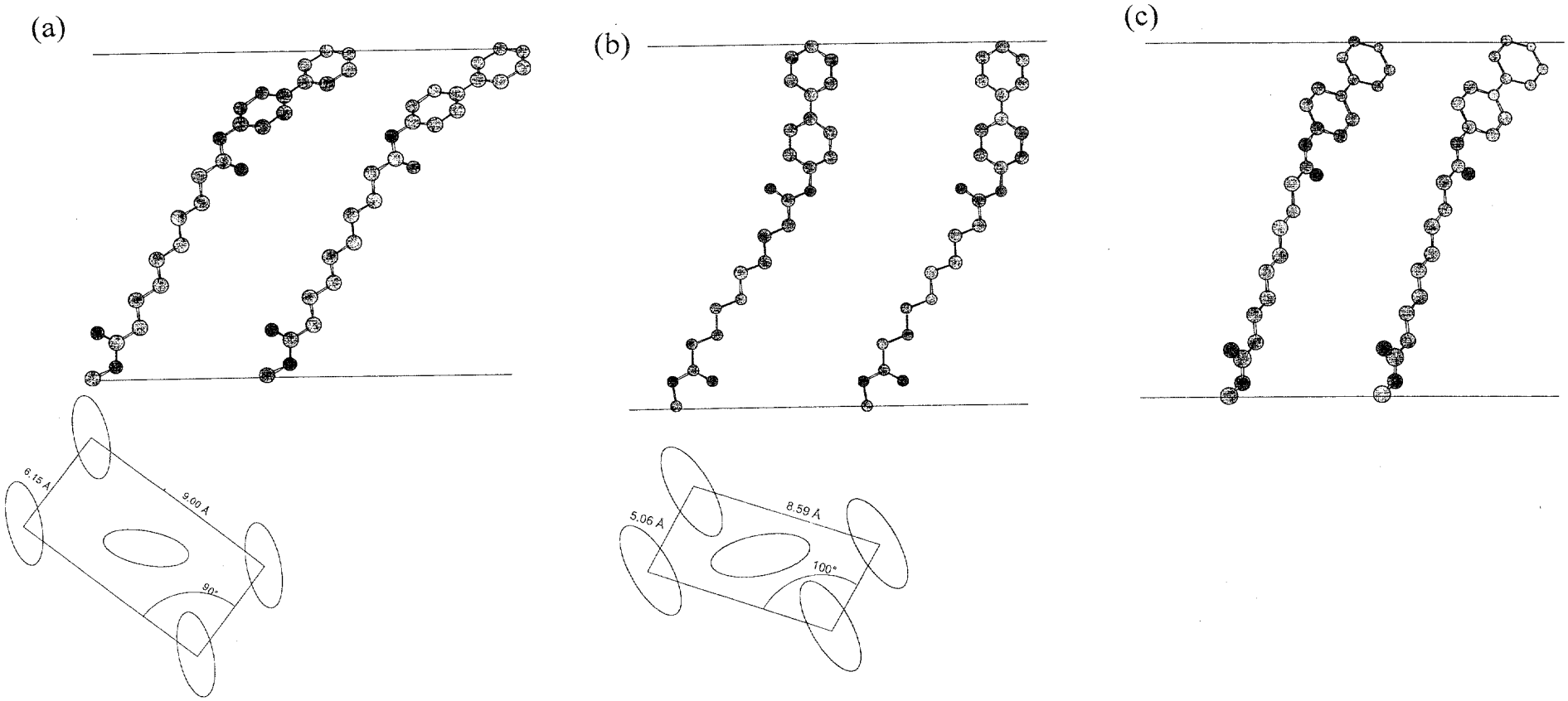

Figure 5.5. The approximate molecular arrangements of PB-*n* polyesters in the (a) S_H, (b) K_1 and (c) K_2 phases.

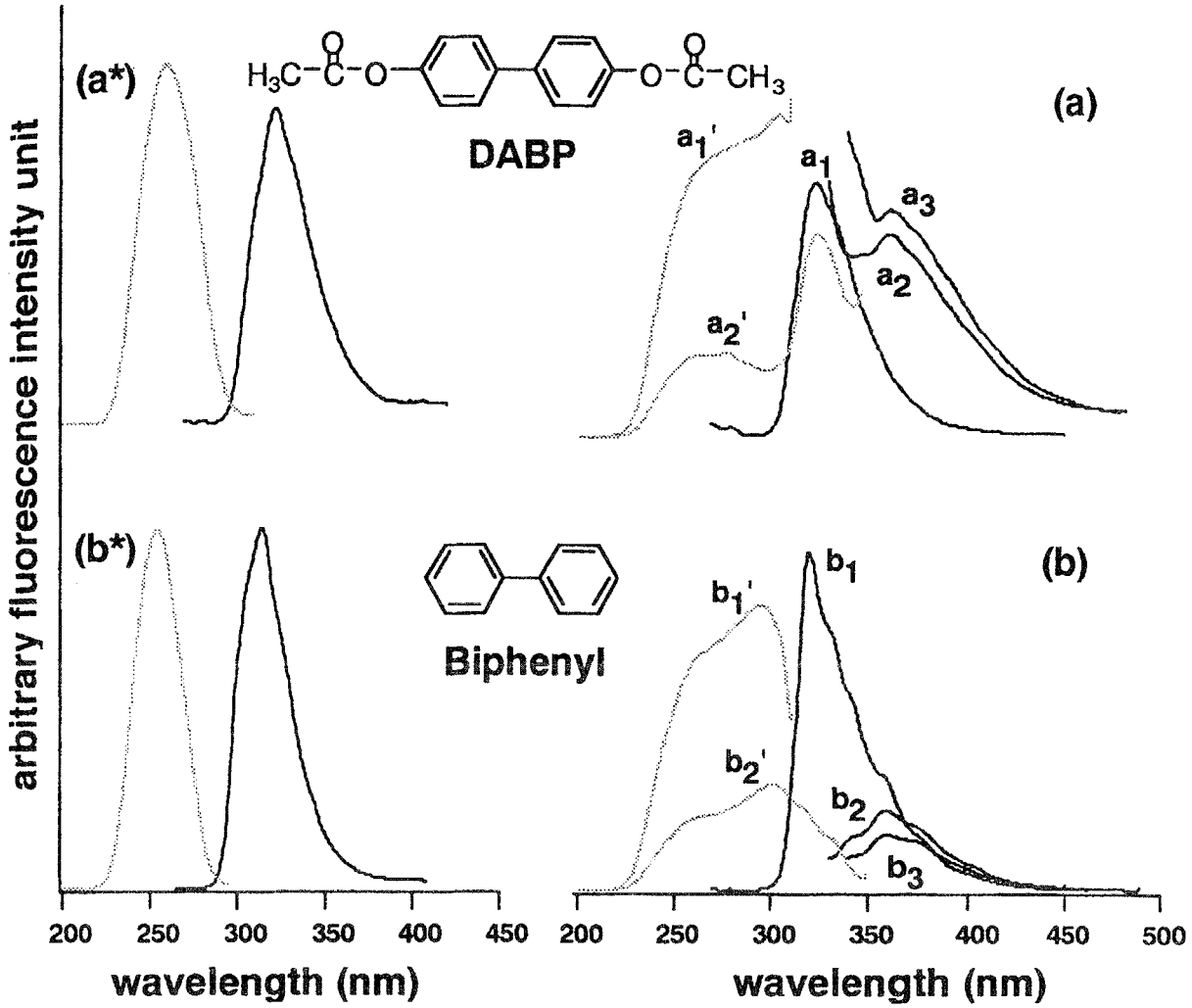

Figure 5.6. Fluorescence (black curves) and its excitation spectra (gray curves) for (a) DABP crystal, (a*) DABP in 10^{-4} M acetonitrile solution, (b) biphenyl crystal , and (b*) biphenyl in 10^{-4} M acetonitrile solution. (a) a_1, a_2, and a_3 are the fluorescence spectra excited at 260, 320, and 330 nm, respectively; a_1' and a_2' are the fluorescence excitation spectra monitored at 322 and 360 nm, respectively. (a*) The fluorescence spectrum is excited at 260 nm and its excitation fluorescence spectrum monitored at 323 nm. (b) b_1, b_2, and b_3 are the fluorescence spectra excited at 260, 320, and 330 nm, respectively; b_1' and b_2' are the fluorescence excitation spectra monitored at 321 and 360 nm. (b*) The fluorescence spectrum is excited at 255 nm, and its excitation spectrum is monitored at 315 nm.

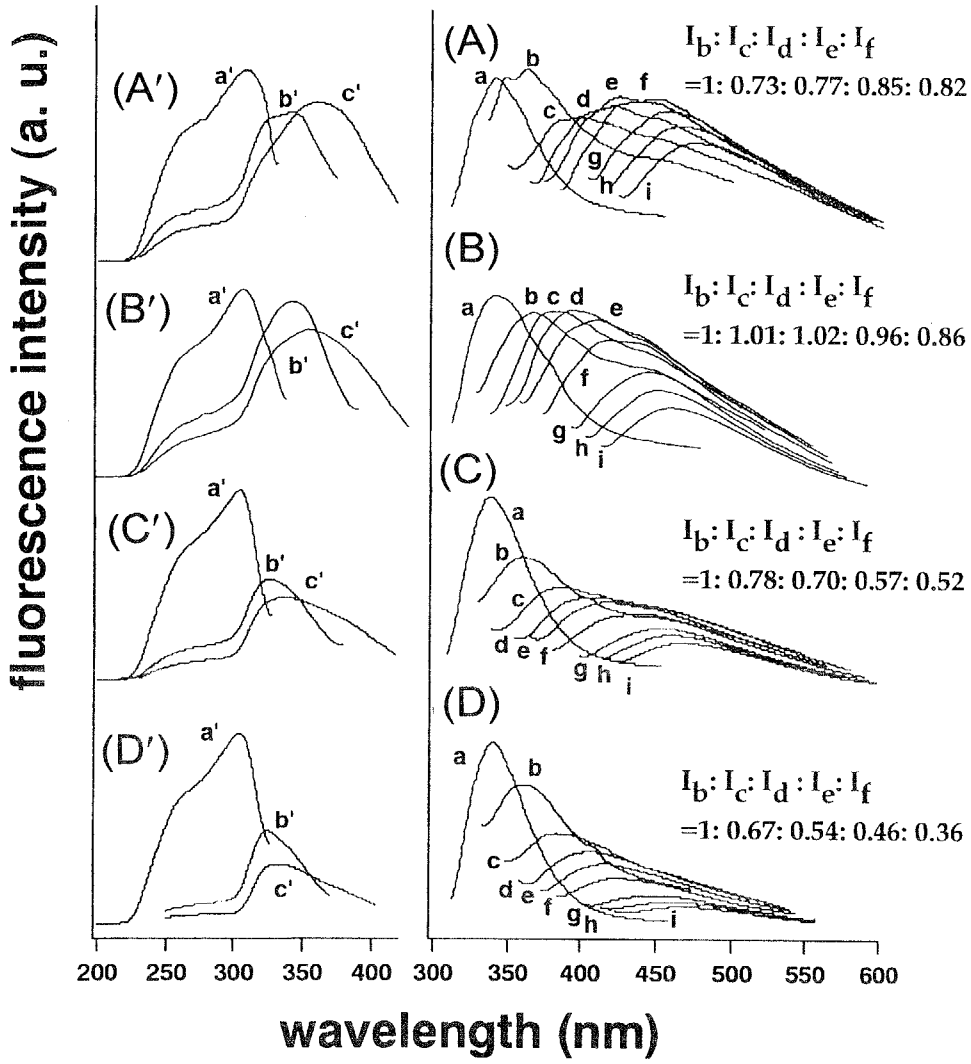

Figure 5.7. Fluorescence (right) and its excitation spectra (left) for PB-8 (A, A′), PB-10 (B, B′), PB-16 (C, C′), and PB-18 (D, D′) at room temperature. (a - i) The fluorescence spectra excited at 300, 320, 330, 340, 350, 360, 380, 390 and 400 nm, respectively. (a′ - c′) The fluorescence excitation spectra monitored at 340, 400 and 450 nm, respectively.

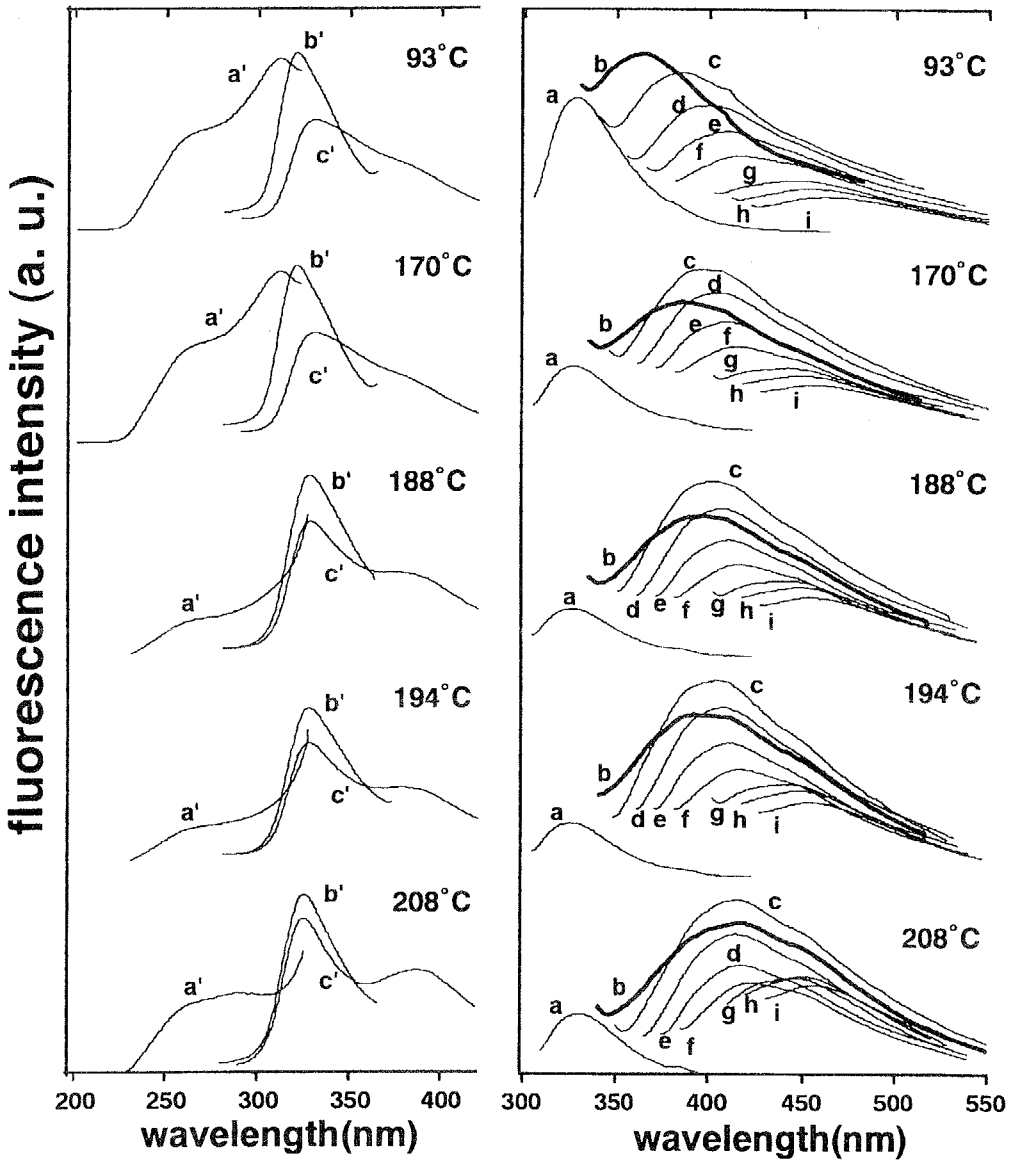

Figure 5.8. Fluorescence (right) and its excitation spectra (left) for PB-18 during heating. (a - i) The fluorescence spectra excited at 300, 320, 330, 340, 350, 360, 380, 390 and 400 nm, respectively. (a′ - c′) The fluorescence excitation spectra monitored at 340, 400 and 450 nm, respectively.

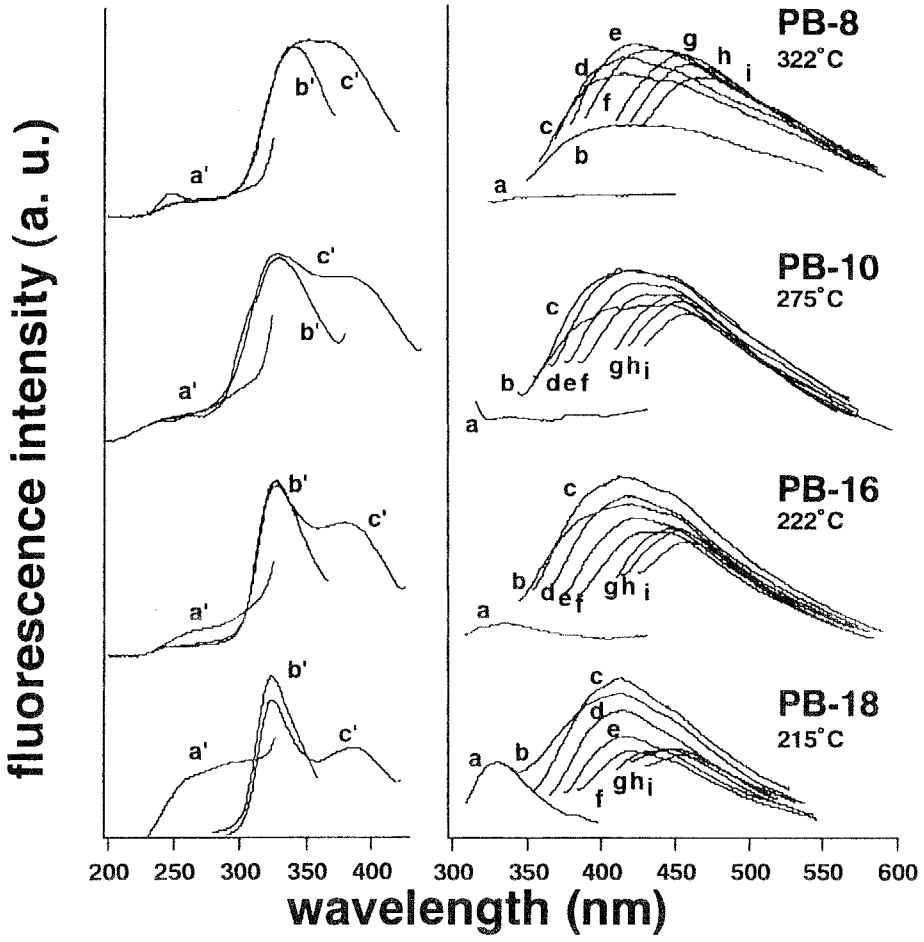

Figure 5.9. Fluorescence (right) and its excitation spectra (left) for PB-n polyesters in isotropic phase. (a - i) The fluorescence spectra excited at 300, 320, 330, 340, 350, 360, 380, 390 and 400 nm, respectively. (a′ - c′) The fluorescence excitation spectra monitored at 340, 400 and 450 nm, respectively.

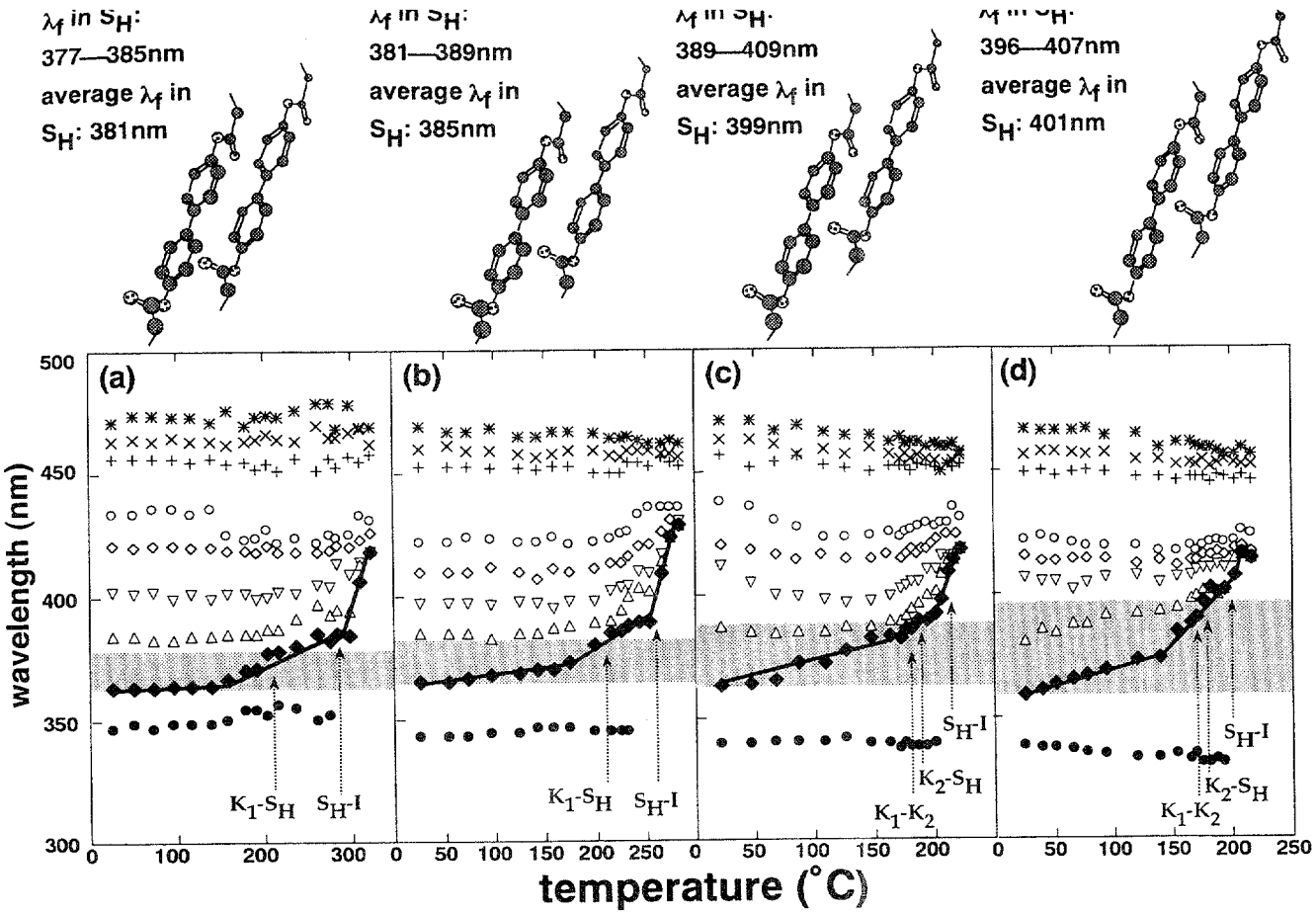

Figure 5.10. Temperature dependence of the fluorescence peak wavelengths excited at 300 nm (●), 320 nm (◆), 330 nm (△), 340 nm (▽), 350 nm (◇), 360 nm (○), 380 nm (+), 390 nm (×) and 400 nm (*) for (a) PB-8, (b) PB-10, (c) PB-16 and (d) PB-18 during heating.

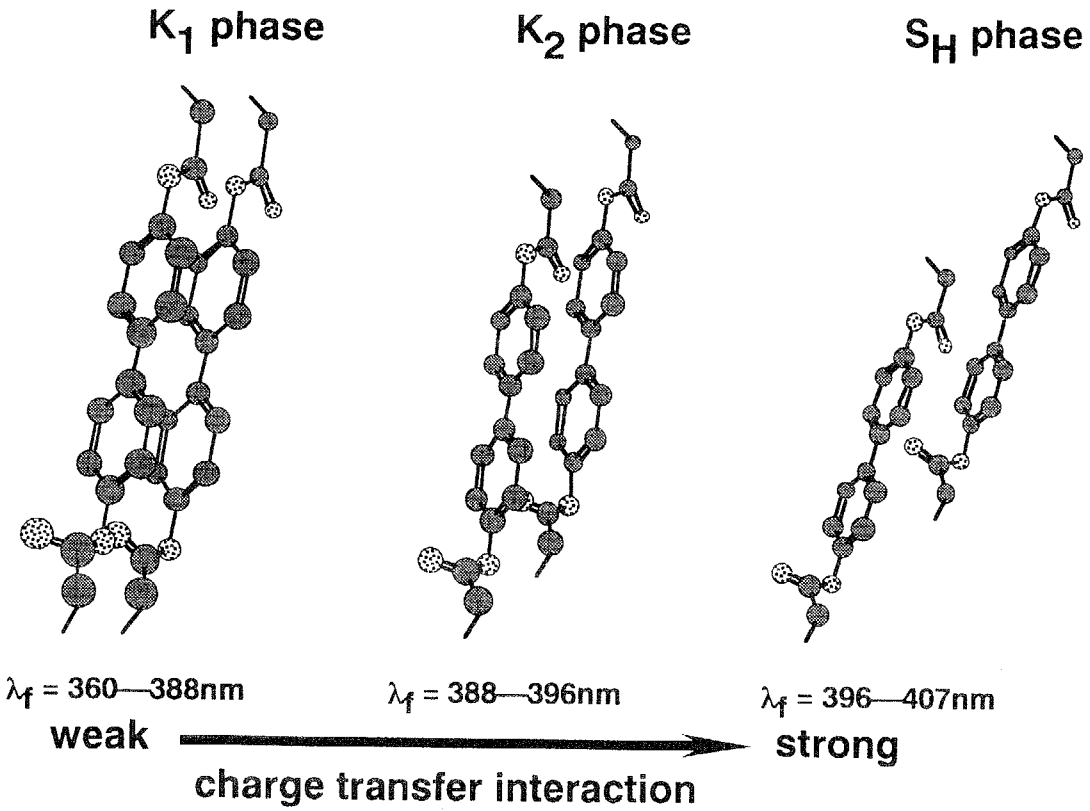

Figure 5.11. Approximate molecular arrangements between mesogenic biphenyl moieties of PB-18 in the K_1, K_2 and S_H phases.

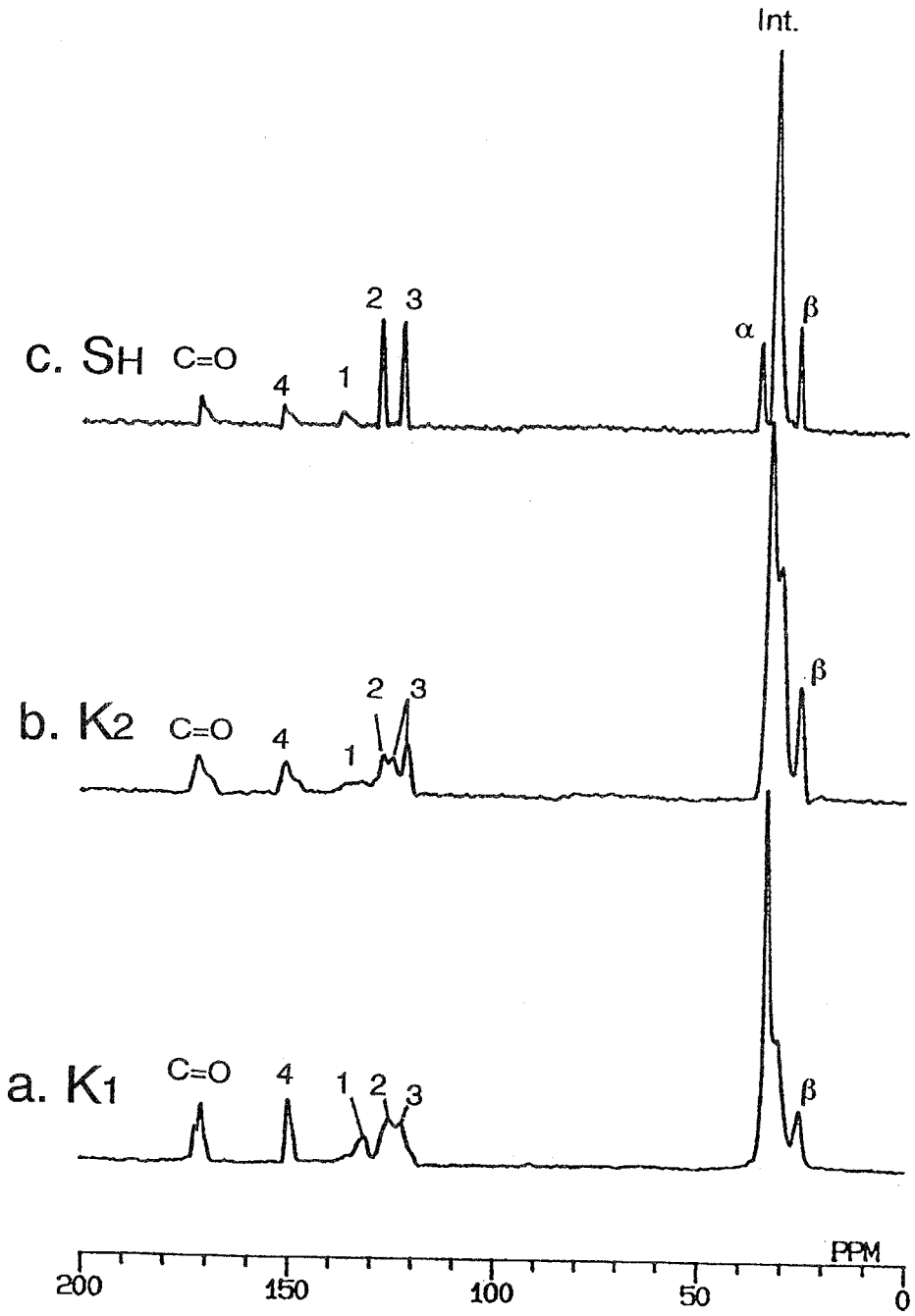

Figure 5.12. ^{13}C TOSS CP/MAS NMR spectra of PB-18 polyesters in K_1, K_2, and S_H phases.

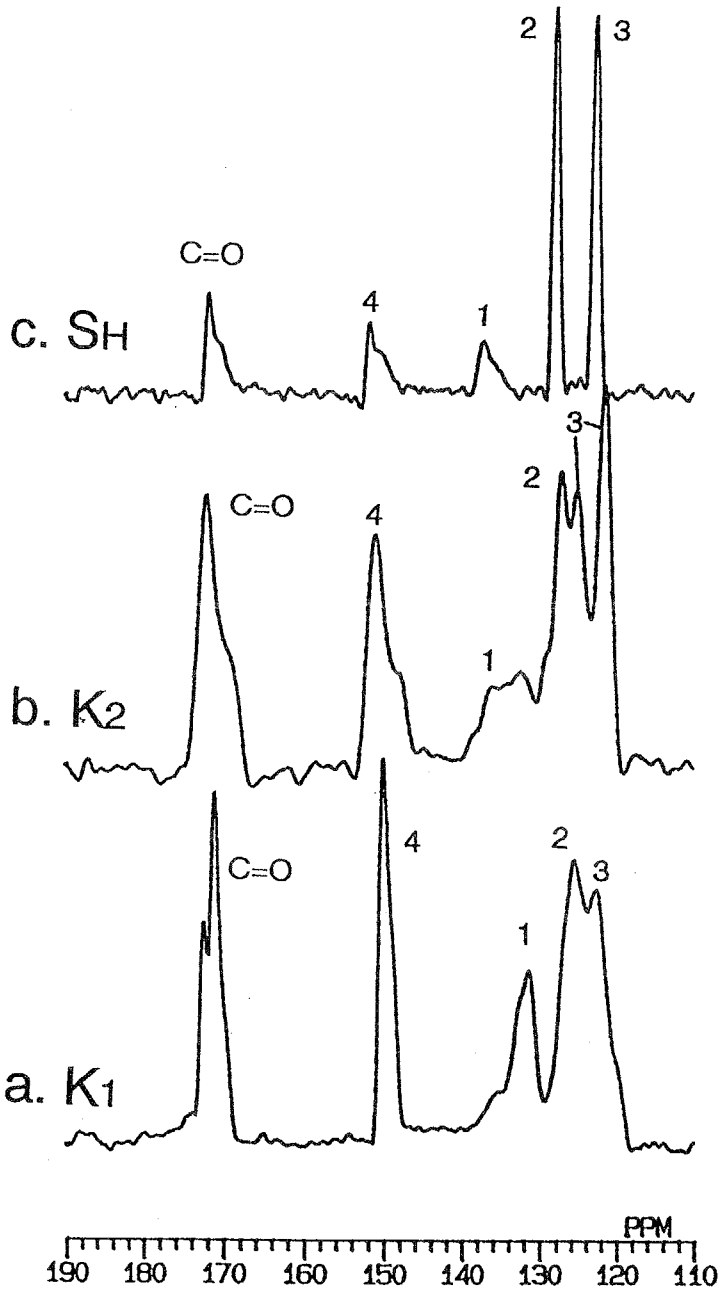

Figure 5.13. Expanded aromatic region of the ^{13}C TOSS CP/MAS NMR spectra of PB-18 polyesters in K_1, K_2 and S_H phases.

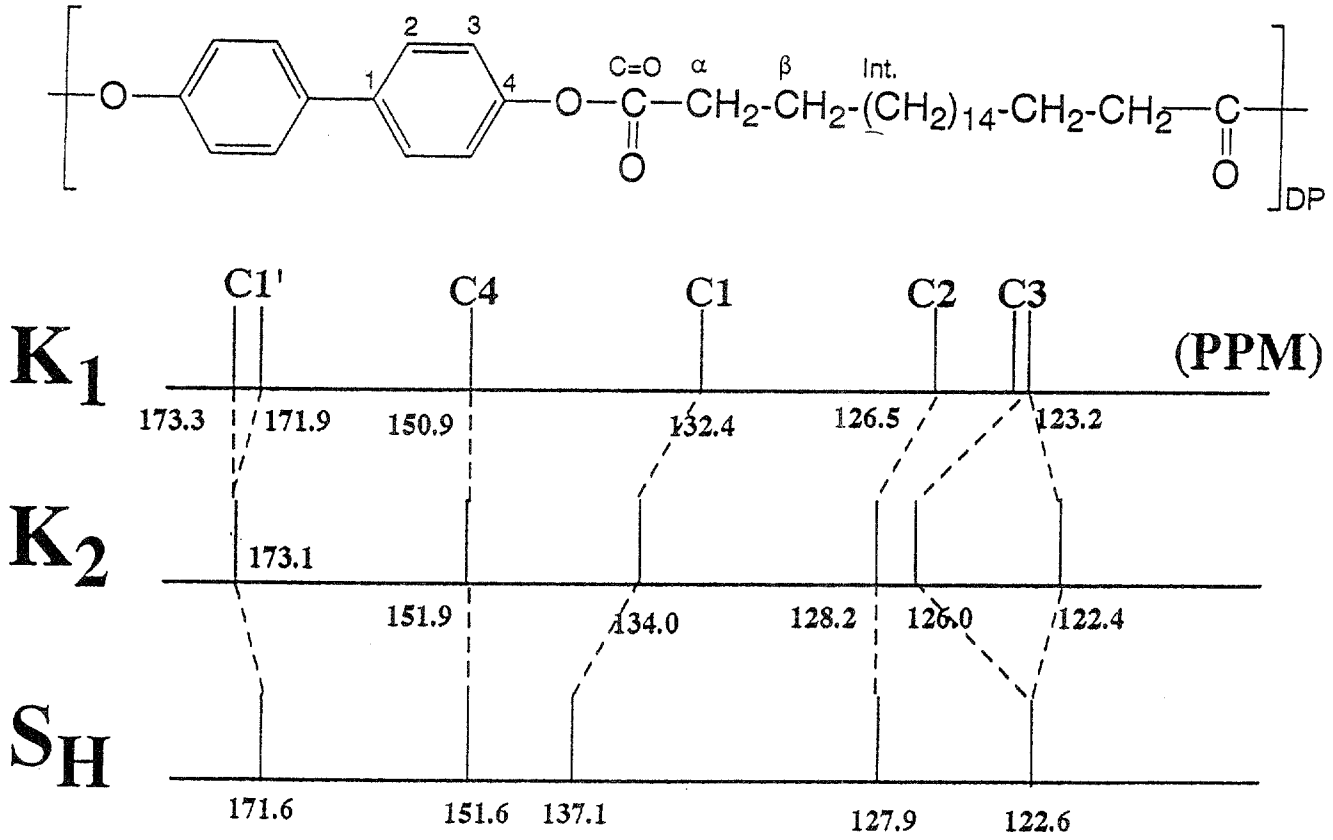

Figure 5.14. Diagram of the observed ^{13}C chemical shifts for the carbons of the mesogenic moiety in the K_1, K_2 and S_H phases.

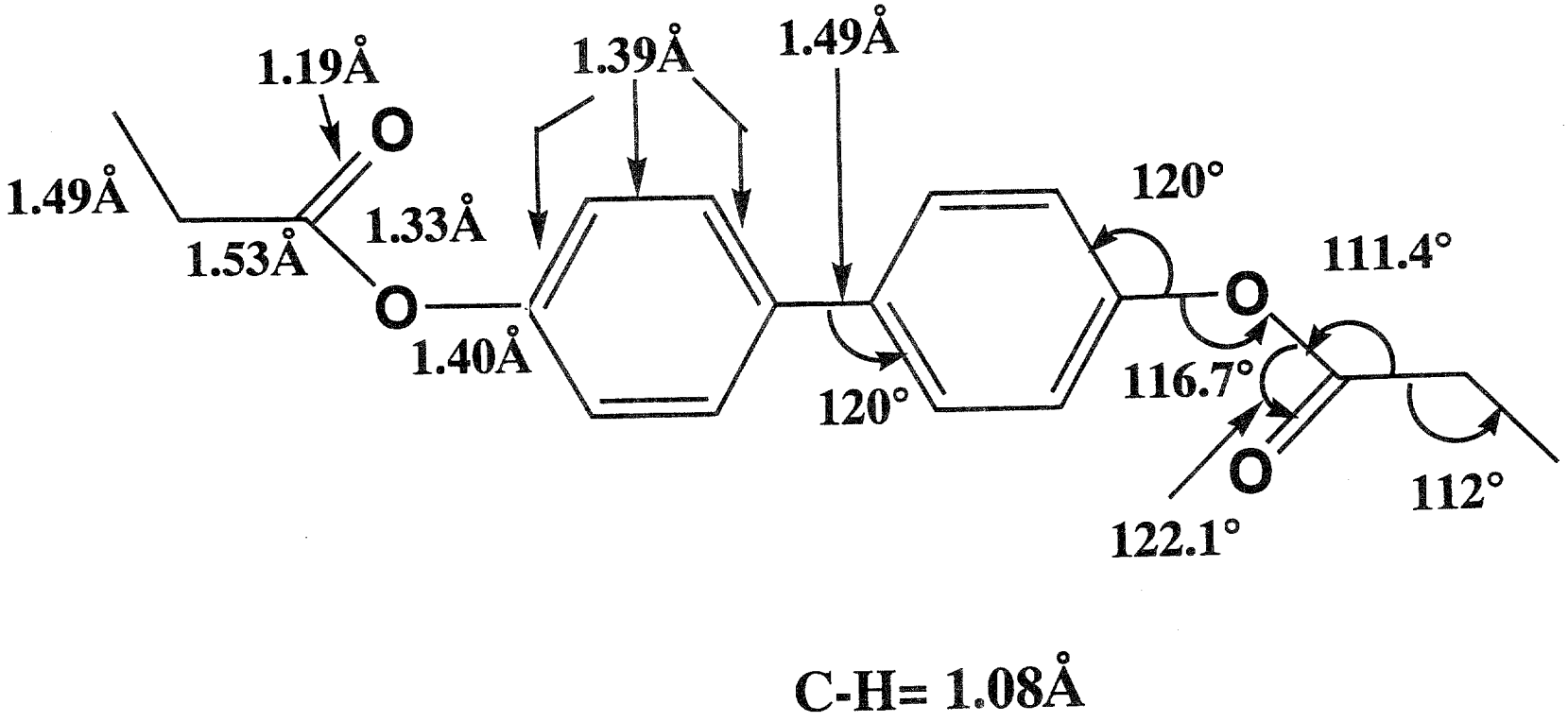

Figure 5.15. Model compound and the geometric parameters for the FPT-INDO calculation.

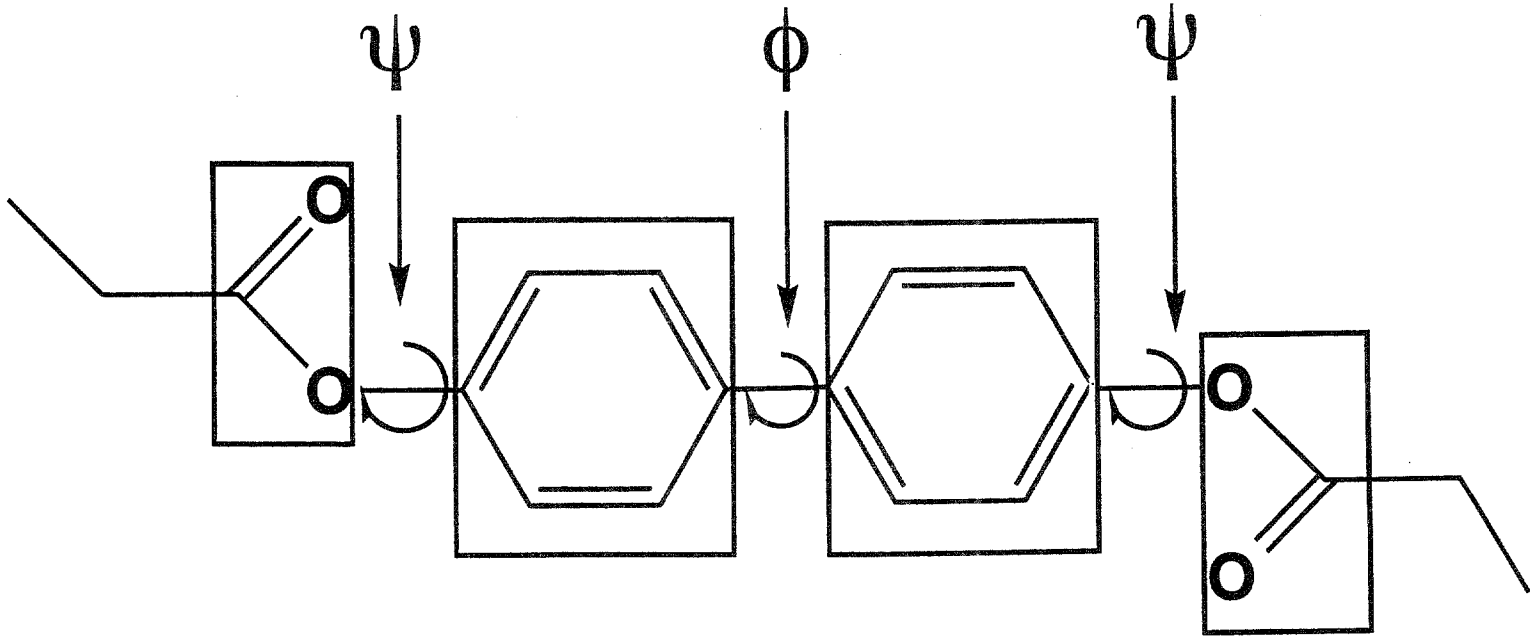

Figure 5.16. Torsion angles, ϕ and ψ, defined the relative twist between aromatic groups and between aromatic groups and between aromatic group and ester group, respectively.

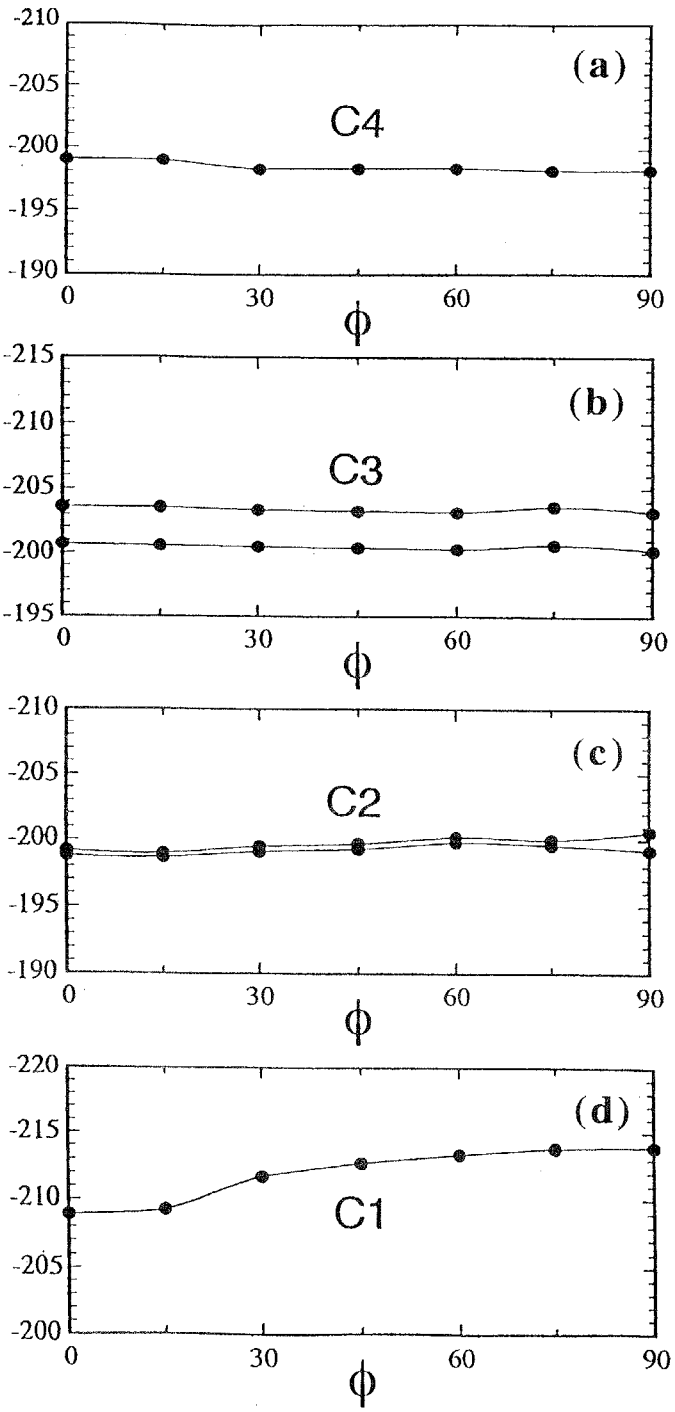

Figure 5.17. Calculated ^{13}C NMR shielding of the carbons of the biphenyl moiety as a function of the relative torsion angle, ϕ, under the condition that $\psi = 60°$. The negative sign indicates deshielding.

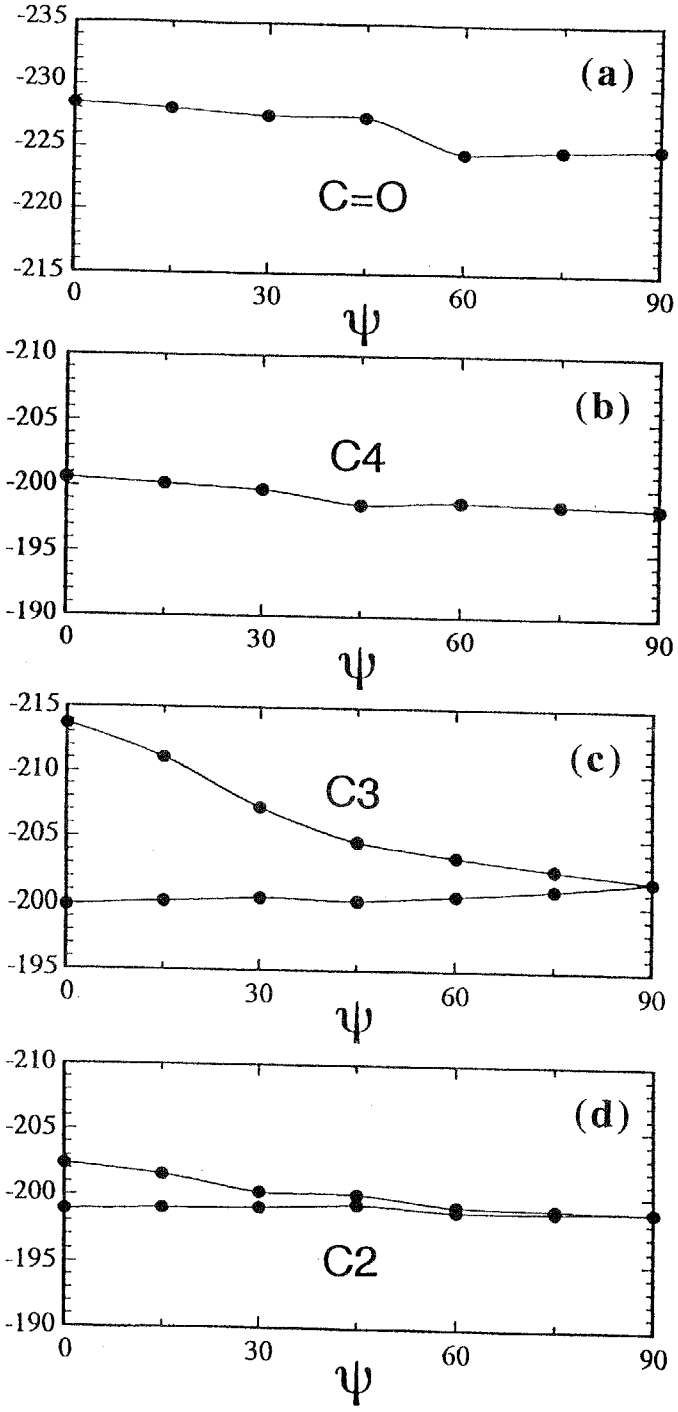

Figure 5.18. Calculated ^{13}C NMR shielding of the carbons of the biphenyl moiety as a function of the relative torsion angle, ψ, under the condition that $\phi = 60°$. The negative sign indicates deshielding.

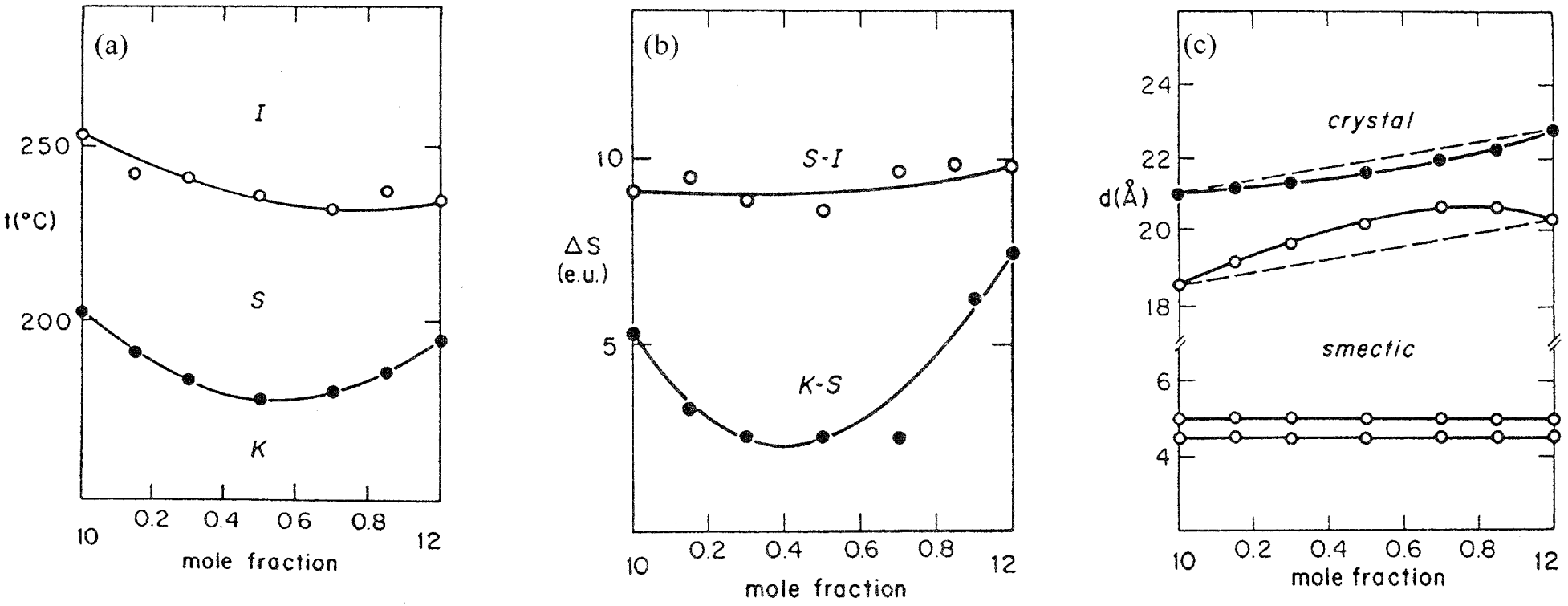

Figure 5.19. Composition dependence of (a) phase behavior on heating, (b) transition entropy and (c) layer spacing in PB-10-co-PB-12 copolymers. In (b), the open and closed marks denotes S_H - isotropic and crystal - S_H transitions respectively. In (c), the open and closed marks denotes the layer spacing in S_H and that in crystal respectively.

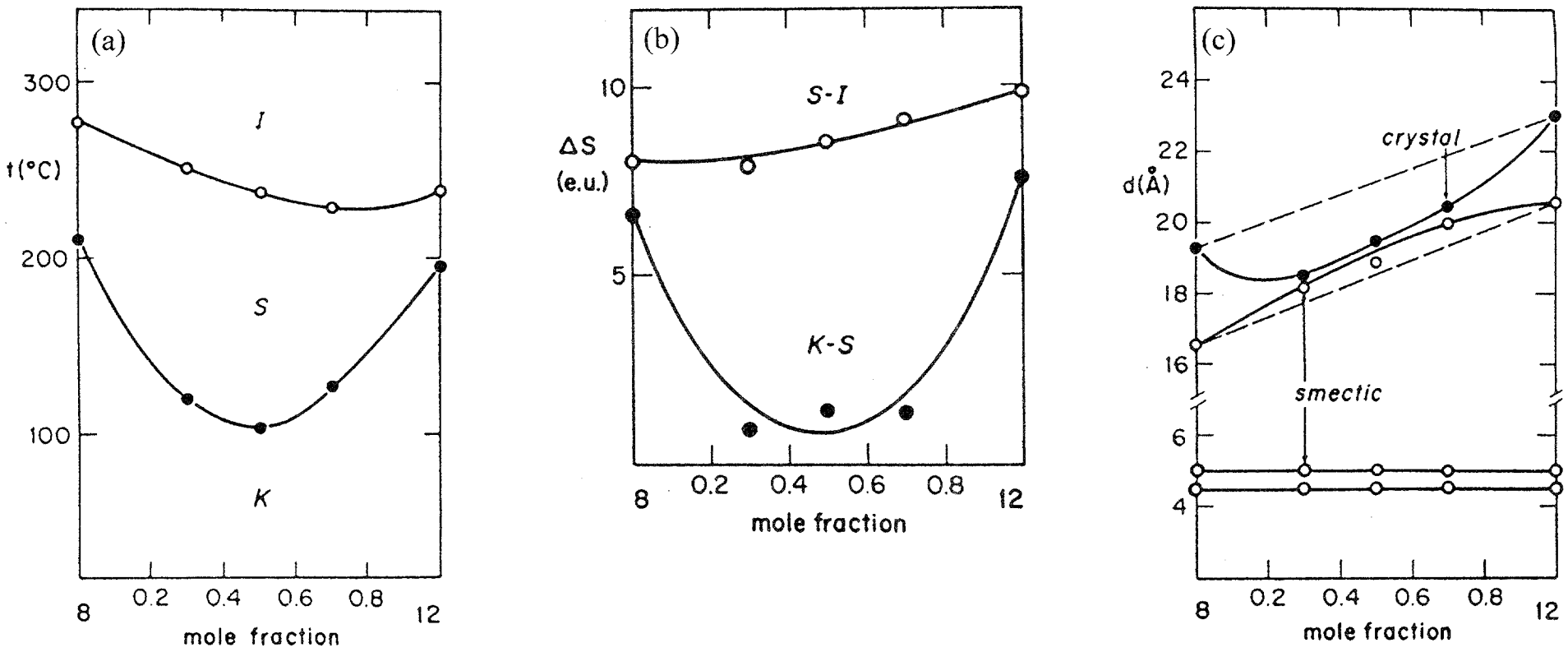

Figure 5.20. Composition dependence of (a) phase behavior on heating, (b) transition entropy and (c) layer spacing in PB-8-co-PB-12 copolymers. In (b), the open and closed marks denotes S_H - isotropic and crystal - S_H transitions respectively. In (c), the open and closed marks denote the layer spacing in S_H and that in crystal respectively.

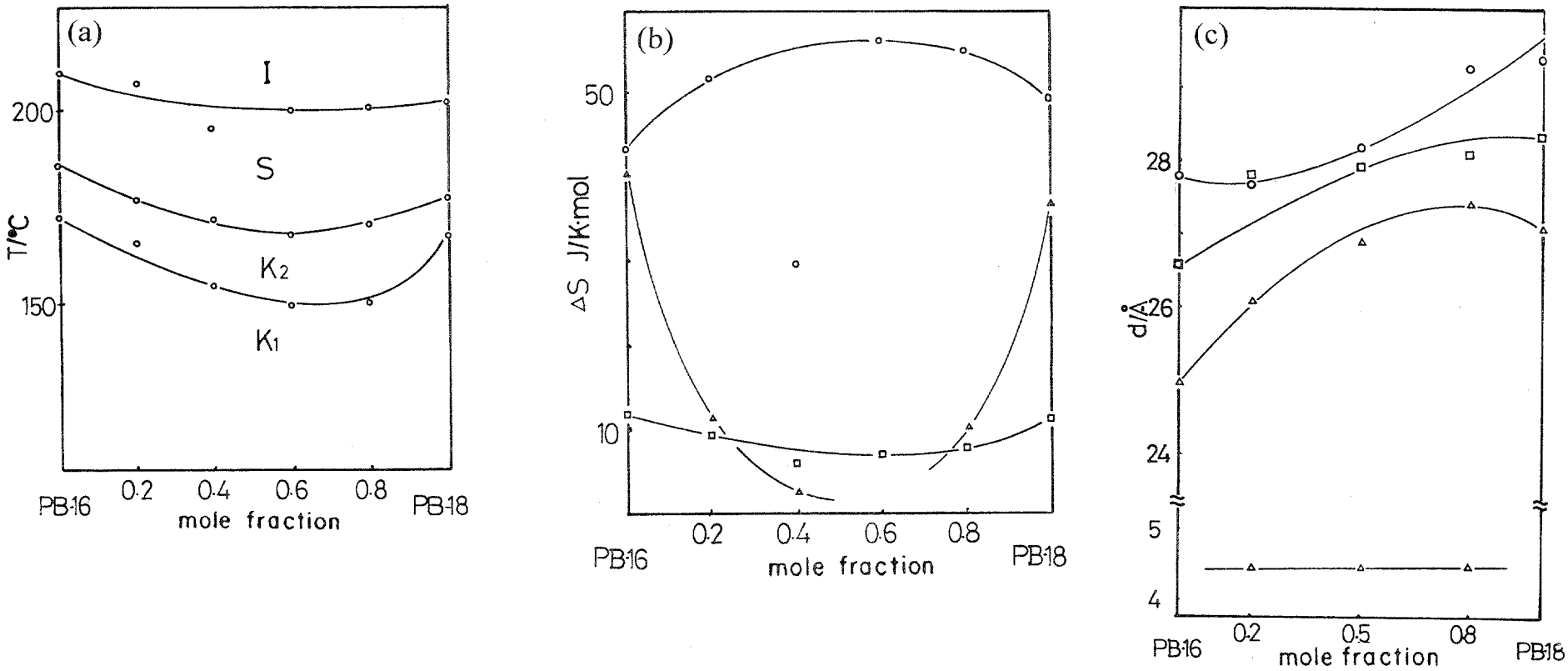

Figure 5.21. Composition dependence of (a) phase behavior on heating, (b) transition entropy and (c) layer spacing in PB-16-co-PB-18 copolymers. In (b), the circle, square and triangle marks denotes S_H - isotropic, K_2 - S_H and K_1 - K_2 transitions respectively. In (c), the triangle, circle and square marks denote the layer spacing in S_H, K_2 and K_1 phases, respectively.

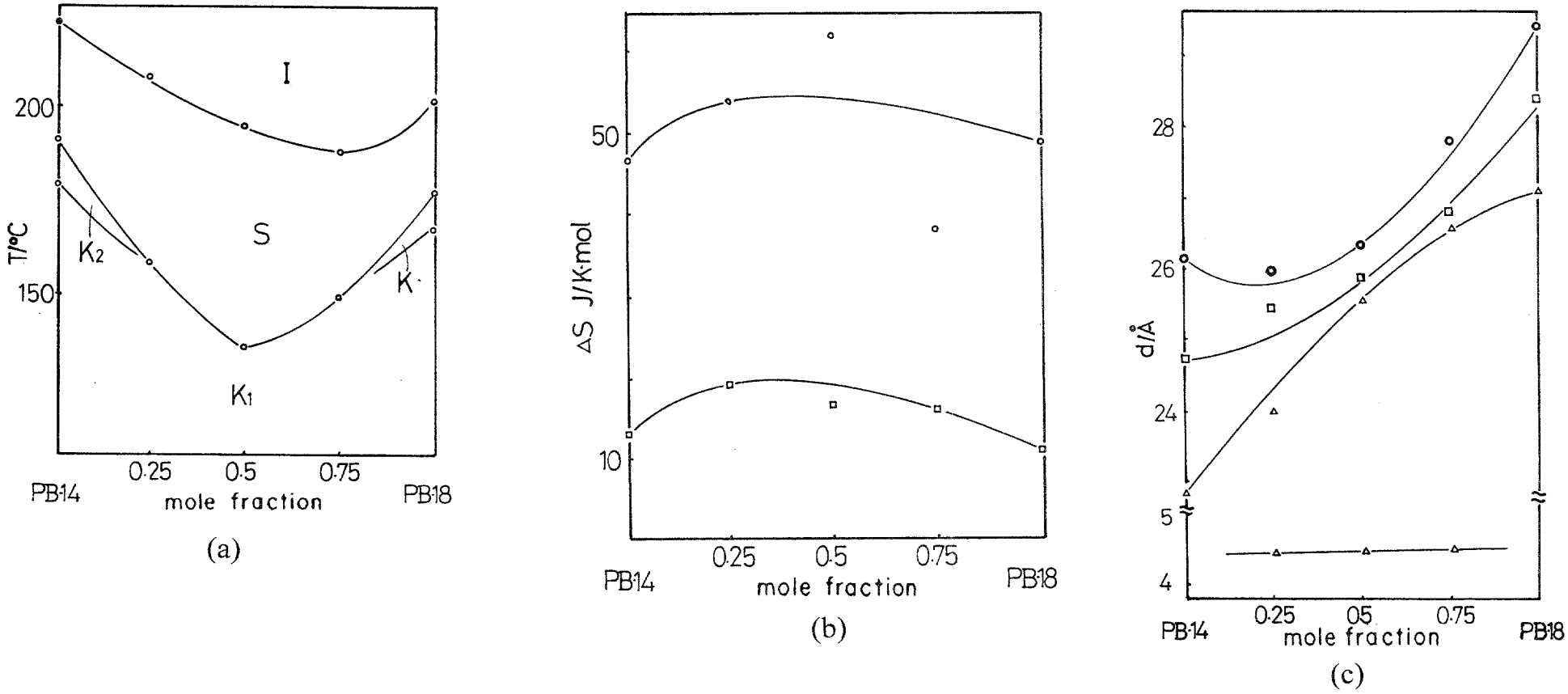

Figure 5.22. Composition dependence of (a) phase behavior on heating, (b) transition entropy and (c) layer spacing in PB-14-co-PB-18 copolymers. In (b), the circle and triangle marks denotes S_H - isotropic and K_2 - S_H transitions respectively. In (c), the triangle, circle and square marks denote the layer spacing in S_H, K_2 and K_1 phases, respectively.

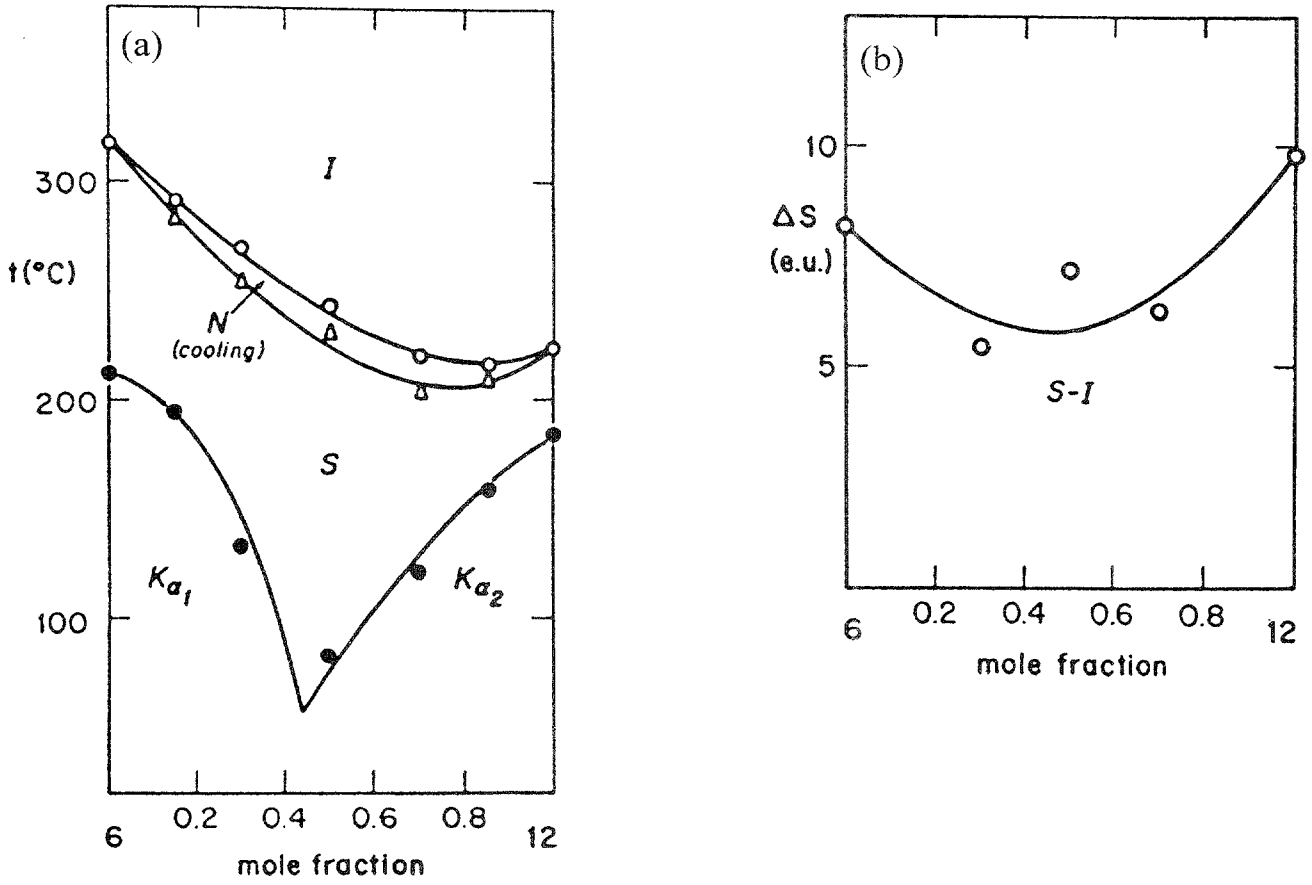

Figure 5.23. Composition dependence of (a) phase behavior on cooling and (b) transition entropy in PB-6-co-PB-12 copolymers.

Chapter 6

Chain-Folded Lamellar Structure in Smectic H Phase of PB-*n* Polyesters

ABSTRACT: Smectic state morphology of the main-chain liquid crystal PB-*n* polyester was studied by the small-angle X-ray scattering (SAXS), differential scanning calorimetry (DSC), and transmission electron microscope (TEM) methods. The PB-*n* polyesters with *n* of 10, 12, 14, 16, and 18 form isotropic liquid (I), smectic H (S_H) and crystalline phases in order of decreasing temperature. SAXS for the S_H phase formed from the isotropic melt showed well-defined reflection maxima which are attributed to the chain-folded lamellar structure. The lamellar size increased from with an increase of the liquid crystallization temperature continuously over the PB-*n* polyesters. The relationship between the lamellar thickness and isotropization temperature is well described by the Thomson-Gibbs equation. According to this relationship, the surface free energy of the lamellae and the equilibrium isotropization temperature of S_H were elucidated. When the sample was annealed at a S_H temperature, the isotropization temperature of the S_H phase increased and simultaneously the enthalpy change increased. These trends can be well explained by the lamellar thickening. The overall results thus indicate that the S_H liquid crystallization at a certain temperature takes place imperfectly in a finite period due to the chain folding and that the succeeding annealing causes the alteration of the chain conformation from a folded form to an extended one as observed in the crystallization of conventional polymers.

6.1. Introduction

Semiflexible homopolymers having rigid aromatic and flexible alkylene segments in a repeating unit are an attractive object of investigation since they form liquid crystalline phases. The polymers are termed main-chain liquid crystalline (LC) polymers. Appearance of a mesophase is a consequence of the existence of an anisotropic intermolecular interaction associated with the anisotropic shape of molecules. The chain backbone can be thus assumed to take an extended configuration at least in a local space of the LC field. [1]

Here, the interesting question arises as to whether the polymer chains are extended or not along the entire length.[1-5] As the first challenge to answer this question, the solid state morphology of the main-chain LC poly(hexamethylene bibenzoate) (BB-6) was studied by the small-angle X-ray scattering (SAXS) method.[6,7] The BB-6 polyester forms isotropic, smectic A (S_A) and crystal phases in order of decreasing temperature, thereby its crystallization taking place from the S_A phase. SAXS for the crystalline specimens prepared by cooling the isotropic melt at a rate of 10°C min^{-1} showed well-defined reflection maxima which were attributed to the stacked lamellar structure. The lamellar spacings were distributed around 250 Å so that an appreciable number of chain foldings were included in a chain. For the film sample which was prepared by applying shear flow in the smectic state, the reflection spots appeared perpendicularly to the shear direction, showing that the shear flow arranged the lamellae parallel to its direction.[6,8,9] This anomalous orientation strongly suggests that the chain folded lamellar structure already exists in the foregoing smectic state, although no SAXS maximum is observed in the smectic state.

In this study, SAXS measurements were performed for another type of smectic phase, namely the smectic H (S_H) phase, formed by the following main-chain PB-*n* polymer (*n* = 10, 12, 14, 16, and 18),[10-14]

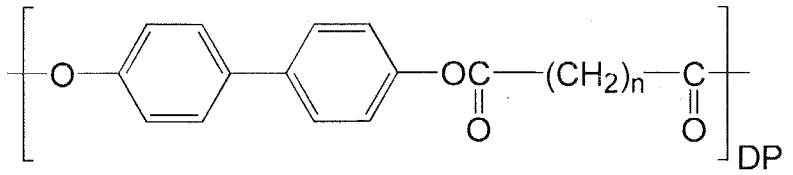

and observed the well-defined reflections attributable to the lamellar structure. According to this observation, the liquid crystal morphology was described in detail.

6.2. Experimental Section

The PB-*n* polyesters were prepared by melt condensation of 4,4′-diacetoxybiphenyl and diacids. Two specimens with different molecular weights, PB-14-I and PB-14-II, were prepared by controlling the reaction period of melt transesterification (see Table 6.1). Inherent viscosities of the samples were determined at 30°C using a 0.5 g dL^{-1} solution in a 60/40 mixture by weight of phenol and tetrachloroethane. The calorimetric behavior was investigated with a Perkin-Elmer DSC-II calorimeter under a flow of dry nitrogen. Wide-angle (WAXS) and small-angle X-ray (SAXS) measurements were performed using a Rigaku-Denki X-ray generator with Ni-filtered CuKα radiation and a flat imaging plate. The sample temperature was measured and regulated with an accuracy of 0.2°C by using a Mettler FP-80 hot stage. The lamellar spacing from the SAXS measurement was evaluated with a possible error of ± 5 Å. TEM observation to clarify the morphology of the polymer was performed by a Hitachi H-500 transmission electron microscope with 100 kV of accelerating voltage. For this observation, an ultrathin section of the polymer was prepared as follows. The bulk polymer was cut into ultrathin sections (700 Å thick) by an ultramicrotome with a diamond knife. The sectioned specimen was stained with the vapor of RuO_4 for 10 min before observation.

6.3. Stacked Lamellar Structure in the S_H Phase of PB-14

6.3.1. Characterization of Polyesters

Figure 6.1 shows the DSC thermogram of PB-14-I. The DSC thermogram includes two sharp peaks and one broad peak in both the heating and cooling curves. The two sharp peaks on heating indicate a K_2 - S_H transition and isotropization of the S_H phase, respectively.[12,14] The additional broad peak at a temperature just below the K_2 - S_H transition shows a crystal - crystal transition, K_1 - K_2.[12,14]

These transitions have also been followed by the change in the d-spacings of the X-ray reflections as illustrated in Figure 6.2. With an increase of temperature in the crystalline region, the spacing of the inner layer reflection increased from 24.6 to 25.2Å and the two outer reflections merged with each other. At the K_2 - S_H transition at 191°C, the layer spacing of 25.2Å drops suddenly to 22.7Å. Although an oriented sample was not obtainable, the reflection spacings indicate that the molecules in the S_H phase are packed into a two dimensional orthogonal unit-cell where $a' = 9.0$ Å, $b' = 6.1$ Å and $\gamma' = 90°$.[10,11] The layer spacing of 22.7Å is appreciably smaller than the repeat length of the polymer (30.1Å). By assuming the most extended chain conformation, the tilt angle of polymer chain to the smectic layer normal was estimated as 41°. Thermodynamic data and inherent viscosity of the two polymers, PB-14-I and PB-14-II, are listed in Table 6.1.

6.3.2. Stacked Lamellar Structure in the S_H Phase

To perform SAXS measurements of the S_H liquid crystal, the sample was first heated to 260°C and maintained at this temperature for about 5 min to ensure isotropization. Then, it was cooled to the predetermined S_H temperature for the liquid crystallization at a rate of 160°C min^{-1}. After annealing for 20 min

at that temperature, the sample was irradiated with X-ray for 40 min. Figure 6.3 shows the SAXS intensity profile of the S_H phase of PB-14-I prepared at 207°C. Two scattering maxima with spacings of 200 and 133 Å can be easily observed. These were attributed to the second and third order reflections, although the first order reflection with a spacing of 400 Å is significantly overlapped with the intense diffuse scattering from the central beam. The well-developed reflection profile thus shows that a stacked lamellar structure with a period of 400 Å exists in the S_H phase.

More insight into the lamellar structure was gained from electron micrographs of the ultrathin sections cut from the bulk sample. Figure 6.4 shows a typical electron microphotograph for the sample quenched from the S_H phase at 207°C. The sections were stained with ruthenium tetraoxide (RuO_4), so the staining agent can be assumed to enter the disordered region. The bright parts, therefore, correspond to the lamellae separated by disordered regions which appear as the dark areas. The laterally large lamellae are formed with a thickness ranging from 300 Å to 400 Å, which roughly corresponds to that elucidated from the X-ray method. Furthermore, it is found that the disordered region is so narrow that the degree of liquid crystallinity is fairly high.

The stacked lamellar structure of the chain folding is common in linear polyesters, poly(ethylene terephthalate) and poly(buthylene terephthalate). The present PB-14 polyester has a much longer flexible spacer than these, and so it is reasonable to conclude that it could accommodate the chain foldings in the smectic phase. The correlation length between foldings is approximate to the lamellar spacing of 400 Å, which corresponds to 13 times the length of the repeating unit.

6.3.3. Dependence of Liquid Crystallization Temperature on Lamellar Thickness

The lamellar sizes (L) of the S_H phase for PB-14-I and PB-14-II were collected at various liquid crystal temperatures as shown in Figure 6.5. Here, the lamellar sizes were determined from the second order reflections in SAXS since the diffraction maxima greater than 350-400 Å cannot be resolved because of a significant overlapping with the central beam. Though the molecular weights are markedly different, the two specimens exhibited an identical dependence of the lamellar size on the liquid crystallization temperature. The lamellar spacing increases continuously with the liquid crystallization temperature. Similar dependence was also observed for the S_H phases of other PB-n polyesters with n of 10 - 20 as described in Section 6.4.

The DSC endotherms for the isotropization of the lamellar S_H liquid crystals were recorded with a Perkin-Elmer DSC II. Here, the S_H samples were prepared in DSC pan under the same condition of liquid crystallization as in the SAXS measurements, and heated to isotropization at a rate of 10°C min^{-1}. The isotropization temperatures (T_i) are presented in Figure 6.6 as a function of reciprocal lamellar spacing ($1/L$) determined by the SAXS measurements. The data are consistent with a straight line and the relationship between T_i and L are described by the equation

$$T_i\,(\mathrm{K}) = T_i^{\circ}\,(1 - a/L) \qquad (1).$$

which corresponds to the Thomson-Gibbs equation expected for a lamellar crystallite of large lateral dimensions and finite thickness.[15,16] The data extrapolates to T_i° of 536K (263°C), which can be regarded as the isotropization temperature of the S_H liquid crystal with an infinite lamellar thickness.[17] The value of a ($= 2\sigma_e/\Delta h_i$) is 22.0 Å, where Δh_i is the bulk heat of fusion and σ_e the top and bottom specific surface free energy. By putting the

values of Δh_i = 6.0 kcal mol^{-1} and the lattice volume v_o = 6.1 × 9.0 × 22.7 Å^3 (two repeat units)$^{-1}$, we could calculate 72 erg cm^{-2} for the value of σ_e. This value is comparable to 87 erg cm^{-2} in the polyethylene lamellar crystal.[15]

6.3.4. Thickening of Lamellae by Annealing

Figure 6.7 illustrates the SAXS intensity profiles for the samples annealed for different periods at a S_{II} temperature of 215°C. The second-order scattering peak shifted to a smaller angle, simultaneously becoming broad with an increase in the annealing period, and was overlapped with the strong scattering around the central beam. Although it is obvious that lamellar thickening takes place, the accurate lamellar sizes could not be determined from the SAXS measurement. Therefore it is speculated upon the lamellar size from T_i by using the equation (1) as follows.

Figure 6.8 shows the DSC endotherms for the isotropization of the S_{II} samples of PB-14-II annealed at 215°C for the time periods indicated. To obtain the DSC endotherms with a certain baseline, the sample was first cooled rapidly from 215°C to 200°C, and then heated to the isotropization at a rate of 10°C min^{-1}. The shape and temperature of the endothermic peak significantly depended on the annealing time. The sample annealed for 1 min showed a single peak at 228°C. On increasing the annealing time, the endothermic peak position shifted to a higher temperature, and a small peak appeared at a lower temperature although it disappeared after 60 min. The main peak becomes broadened and separated into two peaks after 240 min. After annealing for 1440 min (24 hours), a single broad peak appeared at 257°C. Since all the annealed samples exhibited the same cooling and heating DSC thermograms as in Figure 6.1 once they experienced the isotropic melt, the shift of T_i by annealing is attributed to the lamellar thickening, but not to polymerization or

decomposition. In Figure 6.9, the lamellar spacings calculated from T_i by using the equation (1) are plotted (shown in circles) against the annealing time. The lamellar spacing increases from 330 Å to 2000 Å. Simultaneously, the isotropization enthalpy increases from 4.9 to 6.0 kcal mol^{-1} as shown by rectangles in Figure 6.9, reflecting the increase of liquid crystallinity. Thus the degree of liquid crystallinity increases with the lamellar thickening, which corresponds to a decrease of the probability of the folding sites. The folding sites may not be accommodated into the S_H structure, since the mesogens in the S_H phase should adopt a monoclinic layer packing.

Chain folding in the S_H phase may arise from a kinetic factor as generally discussed for the crystallization of conventional polymers. In the S_H phase, a rapid exchange between *trans* and *gauche* conformations of the alkyl spacer takes place and the two phenyl rings in the mesogenic moiety rotate around the central bond within a limited angle according to the analysis of solid state ^{13}C NMR spectra,[14] suggesting that the polymer chain is mobile in the S_H phase. Lamellar thickening in the S_H state may result from the conformational change from a folded to an extended form that is more suitable for the monoclinic packing of mesogens.

6.4. Chain Folded Lamellar Structure in the S_H Phase of Even-Membered PB-*n* Polyesters with *n* of 10 ~ 18

In this section, the investigation of the morphology of the S_H phase is extended for five PB-*n* polyesters, namely, PB-10, PB-12, PB-14, PB-16 and PB-18, forming isotropic, S_H, and crystalline phases in the order of decreasing temperature. The thermodynamic data as well as the inherent viscosities are listed in the Table 6.1. The procedure for the SAXS measurements of the S_H

phase is the same as that for PB-14 described in Section 6.3.2. The SAXS pattern of all the specimens include clear two reflection maxima with spacings attributed to the second and third order reflections, and the first order reflection significantly overlapped with the intense diffuse scattering from the central beam. The well-developed reflection profile thus shows that a stacked lamellar structure in the S_H phase of these PB-*n* polyesters. For PB-14, the long spacing was attributed to the stacked lamellar structure with chain folding (see previous sections). Hence it is reasonable to assume that the other PB-*n* polyesters with slightly shorter or longer methylene spacers could accommodate chain foldings and form the stacked lamellar structure with a lamellar spacing, L.

The lamellar sizes (L) of the S_H phase for PB-*n* polyesters were collected at various liquid crystal temperatures as shown in Figure 6.10. The lamellar size increases continuously with an increase in the liquid crystallization temperature over all the PB-*n* polyesters.

The isotropization temperatures of the lamellar S_H phase are presented in Figure 6.11 as a function of reciprocal lamellar size ($1/L$) determined SAXS measurements. The data are consistent with a strait line showing that the relationship described by the Thomson-Gibbs equation (eq. 1) and give the equilibrium isotropization temperatures, T_i° and the chain folding surface free energy, σ_e listed in Table 6.2. The values of σ_e for all PB-*n* polyesters are comparable to that in the polyethylene lamellar crystal, suggesting that the polymer chain folds at its methylene spacer moiety.

Chain folding in the S_H phase may arise from a kinetic factor as generally discussed for the crystallization of conventional polymers, where the lamellar thickness depends on the supercooling, $\Delta T = T_m^\circ - T_C$, rather than the crystallization temperature, T_C.[17] In Figure 6.12, the lamellar sizes are plotted against the supercooling, $\Delta T = T_i^\circ - T_{LC}$ (T_i°: the equilibrium isotropization

temperature; T_{LC}: the liquid crystallization temperature). The PB-*n* polyester with smaller *n*, in other words, the stiffer polymer chain shows the larger lamellar size at the same supercooling.

To quantitatively study the liquid crystallization kinetics, the exotherm peak time in the isothermal DSC curve (shown in Figure 6.13 for PB-14 measured with a Perkin-Elmer Pyris 1 DSC) for the corresponding liquid crystallization to represent the measure of the transition rate, t_p. The reason of for this choice is due to the fast kinetics for the liquid crystallization, and only the peak times can be precisely determined during the experimental equilibration. Therefore, one only may plot relationship between $(t_p)^{-1}$ and supercooling (ΔT) as illustrated in Figure 6.14. Note that $(t_p)^{-1}$ is proportional to the transition rate. The transition kinetics in the five PB-*n* polyesters shows an identical relationship polyesters. The difference in the lamellar sizes in the PB-*n* polyesters hence should merely be attributed to the difference in the chain stiffness rather than the kinetic factor.

The lamellar thickening upon annealing the S_{II} liquid crystal of PB-*n* polyesters was followed with the same procedure applied for PB-14 in Section 6.3. The annealing temperatures were standardized in supercooling, ΔT. The annealing the PB-*n* polyesters at a S_{II} temperature increased the isotropization enthalpy of the S_{II} liquid crystal. The increment in the isotropization temperature, showing thickening of the lamella, was observed for PB-10, PB-12 as well as PB-14 (see Figures 6.8, 6.15(a) and (b), 6.16 and 6.17), but not significant for PB-16 and PB-18 in the experimental time scale (see Figure 6.15(c) and (d), 6.16 and 6.17). This result suggests that the chain stiffness affects the thickening rate of lamella.

6.5. Concluding Remarks

The LC state morphology was studied for the main-chain LC polyester, PB-*n*, which forms the S_H phase. The well-defined lamellar structure was detected in the S_H phase from SAXS and electron microscopic measurements. The lamellar spacing increased with an increase in the liquid crystallization temperature, and the isotropization temperature of the S_H phase depended on the lamellar size as described with a variant of the Thomson-Gibbs equation. The top and bottom surface free energy of the lamellae corresponds to that of 87 erg cm^{-2} elucidated for polyethylene lamellar crystal.

By annealing PB-14 at a S_H temperature of 215°C, the isotropization temperature of the S_H phase increased from 228°C to 257°C. According to the Thomson-Gibbs equation, the increase in T_i corresponds to an increase in the lamellar size from 300 Å to 2000 Å. The isotropization enthalpy of the S_H phase also increased from 4.9 kcal mol^{-1} to 6.0 kcal mol^{-1}. Transformation from isotropic melt to the S_H mesophase thus takes place imperfectly in a finite period due to chain folding raised from a kinetic factor. Furthermore, the lamellar thickening may be followed by an alteration in the polymer chain conformation from a folded to an extended form that is suitable for the S_H liquid crystal structure. The whole feature of the liquid crystallization of the S_H phase is thus similar to that of the crystallization observed for conventional polymers, but different from that of the liquid crystallization of the S_A phase.[6.7] This may be due to the highly ordered structure of the S_H phase so that the folding sites are not compatible with the ordered S_H structure and form the boundary of lamellae.

The same investigation procedure was applied for homologous PB-*n* polyesters, namely PB-10, PB-12, PB-16 and PB-18. The obtained results are identical with that for PB-14, but the lamellar size and the lamella-thickening

rate depends on the chain stiffness. PB-n with the smaller n formed the thicker lamella and showed the faster lamella thickening rate under the identical ΔT and liquid crystallization rate. It suggests that the lamellar size and its thickening behavior are influenced mainly by the stiffness of the polymer chain.

References

(1) Watanabe, J.; Hayashi, M.; Nakata, Y.; Niori, T.; Tokita, M. *Prog. Polym. Sci.* **1997**, *22*, 1053.

(2) de Gennes, P. G. In *Polymer Liquid Crystals*; Cifferri, A.; Krigbaum, W. R.; Mayer, R. B.. Eds.; Academic Press: New York, 1982; p124.

(3) Williams, D. R. M.; Warner, M. *J. Phys. Fr.* **1990**, *51*, 317.

(4) Li, M. H.; Brulet, A.; Davidson, P.; Keller, P.; Cotton, J. P. *Phys. Rev. Lett.* **1993**, *70*, 2293.

(5) Li, M. H.; Brulet, A.; Cotton, J. P.; Davidson, P.; Strazielle, C.; Keller, P. *J. Phys. II (France)* **1994**, *4*, 1843.

(6) Tokita, M.; Takahashi, T.; Hayashi, M.; Inomata, K.; Watanabe, J. *Macromolecules* **1996**, *29*, 1345.

(7) Tokita, M; Osada, K.; Watanabe, J. Liq. Cryst. **1997**, *23*, 453.

(8) Krigbaum, W. R.; Watanabe, J. *Polymer* **1983**, *24*, 1299.

(9) Tokita, M.; Osada, K. Kawauchi, S.; Watanabe, J. *Polym. J.* **1998**, *30*, 687.

(10) Krigbaum, W. R.; Watanabe, J.; Ishikawa, T. *Macromolecules* **1983**, *16*, 1271.

(11) Watanabe, J.; Krigbaum, W.R. *Macromolecules* **1984**, 17, 2288.

(12) Maeda, Y.; Mabuchi, T.; Watanabe, J. *Thermochim. Acta.* **1995**, *266*, 189.

(13) Huang, H. W.; Horie, K.; Yamashita, T.; Machida, S.; Sone, M.; Tokita, M.; Watanabe, J.; Maeda, Y. *Macromolecules* **1996**, *29*, 3485.

(14) Tokita, M.; Sone, M.; Kurosu, H.; Ando, I.; Watanabe, J. *J. Mol. Struct.* **1998**, *446*, 215.

(15) Wunderlich, B., *Macromolecular Physics*; Academic Press: New York, **1980**.

(16) Lu, L.; Alamo, R. G.; Mandelkern, L. *Macromolecules* **1994**, *27*, 6571.

(17) Barham, P. J.; Keller, A, *J. Polym. Sci. Polym. Phys. Ed.* **1989**, *27*, 1029.

Table 6.1. Characterization of PB-*n* Polyesters

sample	η_{inh}	calorimetric data							
		heating process			cooling process			transition enthalpy[a]	
		T_1	T_2	T_i	T_1	T_2	T_i	$\Delta H_1 + \Delta H_2$	ΔH_i
	(dL g^{-1})	(°C)			(°C)			(kcal mol^{-1})	
PB-10	0.97	207		260	190		242	2.6	5.1
PB-12	0.85	196		239	183		220	3.1	5.1
PB-14-I	0.76	181	191	226	173	178	210	4.9	5.2
PB-14-II	1.17	180	191	228	173	178	210	4.9	5.1
PB-16	0.73	175	185	215	167	175	197	5.0	5.6
PB-18	0.69	171	180	205	162	169	188	6.4	6.0

[a] Based on cooling DSC data.

Table 6.2. Parameters of the Lamellar Smectic H Liquid Crystal of PB-*n* Polyesters

Sample	T_i° (°C)	σ_e (erg cm^{-2})
PB-10	289	93.8
PB-12	274	95.2
PB-14-II	263	72.4
PB-16	250	81.4
PB-18	243	72.2
Polyethylene[15]		87.4

Figure Captions

Figure 6.1. Heating and cooling DSC thermograms of PB-14-I measured at a scanning rate of 10°C min^{-1}.

Figure 6.2. Temperature dependence of the d spacings of the inner and outer reflections observed for PB-14-I.

Figure 6.3. (a) Small-angle X-ray photograph and (b) the corresponding intensity profile recorded for the S_{II} phase of PB-14-I at 207°C. The sample was quenched from the isotropic liquid state of 250°C to the S_{II} phase of 207°C. The arrows indicate the first, second and third reflections.

Figure 6.4. TEM photograph observed for the bulk PB-14-I specimen prepared by quenching the S_{II} phase of 207°C.

Figure 6.5. Dependence of the lamellar spacing on the liquid crystallization temperature observed for the S_{II} phases of PB-14-I (circle) and PB-14-II (square). The S_{II} sample was prepared by quenching from the isotropic liquid to the indicated temperature and annealed for 1 hour. The lamellar spacings were determined from the second order reflection of the SAXS measurements.

Figure 6.6. Isotropization temperatures for the S_{II} phase of PB-14-I as a function of reciprocal lamellar spacing.

Figure 6.7. SAXS intensity profiles recorded for the S_H phase of PB-14-II annealed at 215°C for the different time periods given in the figure. The arrows indicate the second order reflection.

Figure 6.8. DSC endotherms obtained on isotropization for the S_H phase of PB-14-II at a scanning rate of 10°C min^{-1} after annealing at 215°C for various times indicated in the figure.

Figure 6.9. Annealing time dependence of the lamellar size (circle) and isotropization enthalpy (square) for the S_H phases of PB-14-II annealed at 215°C. Here, the lamellar size was estimated from the isotropization temperature by using the equation (1).

Figure 6.10. Dependence of the lamellar spacing on the liquid crystallization temperature observed for the S_H phases of PB-10 (open circle), PB-12 (closed circle), PB-14 (triangle), PB-16 (closed triangle) and PB-18 (square). The S_H sample was prepared by quenching from the isotropic liquid to the indicated temperature and annealed for 1 hour. The lamellar spacings were determined from the second order reflection of the SAXS measurements.

Figure 6.11. Isotropization temperatures for the S_H phase of PB-10 (open circle), PB-12 (closed circle), PB-14 (triangle), PB-16 (closed triangle) and PB-18 (square) as a function of reciprocal lamellar spacing.

Figure 6.12. Dependence of the lamellar spacing on the supercooling, ΔT observed for the S_H phases of PB-10 (open circle), PB-12 (closed circle), PB-14 (triangle), PB-16 (closed triangle) and PB-18 (square). The data are identical with that in Figure 6.10.

Figure 6.13. Isothermal liquid crystallization curves for PB-14-II at the temperature indicated in the figure.

Figure 6.14. Relationship between $(t_p)^{-1}$ and ΔT for PB-12 (closed circle), PB-14 (triangle), PB-16 (closed triangle) and PB-18 (square).

Figure 6.15. DSC endotherms obtained on isotropization for the S_H phase of (a) PB-10, (b) PB-12, (c) PB-16 and (d) PB-18 at a scanning rate of 10°C min^{-1} after annealing at the temperature for various times indicated in the figure.

Figure 6.16. Annealing time dependence of the lamellar size for the S_H phases of PB-10 annealed at 240°C (open circle), PB-12 annealed at 220°C (closed circle), PB-14 annealed at 215°C (open triangle), PB-16 annealed at 205°C (closed triangle) and PB-18 annealed at 197°C(square). Here, the lamellar size was estimated from the isotropization temperature by using the equation (1).

Figure 6.17. Annealing time dependence of the isotropization enthalpy for the S_H phases of PB-10 annealed at 240°C (open circle), PB-12 annealed at 220°C (closed circle), PB-14 annealed at 215°C (open triangle), PB-16 annealed at 205°C (closed triangle) and PB-18 annealed at 197°C(square).

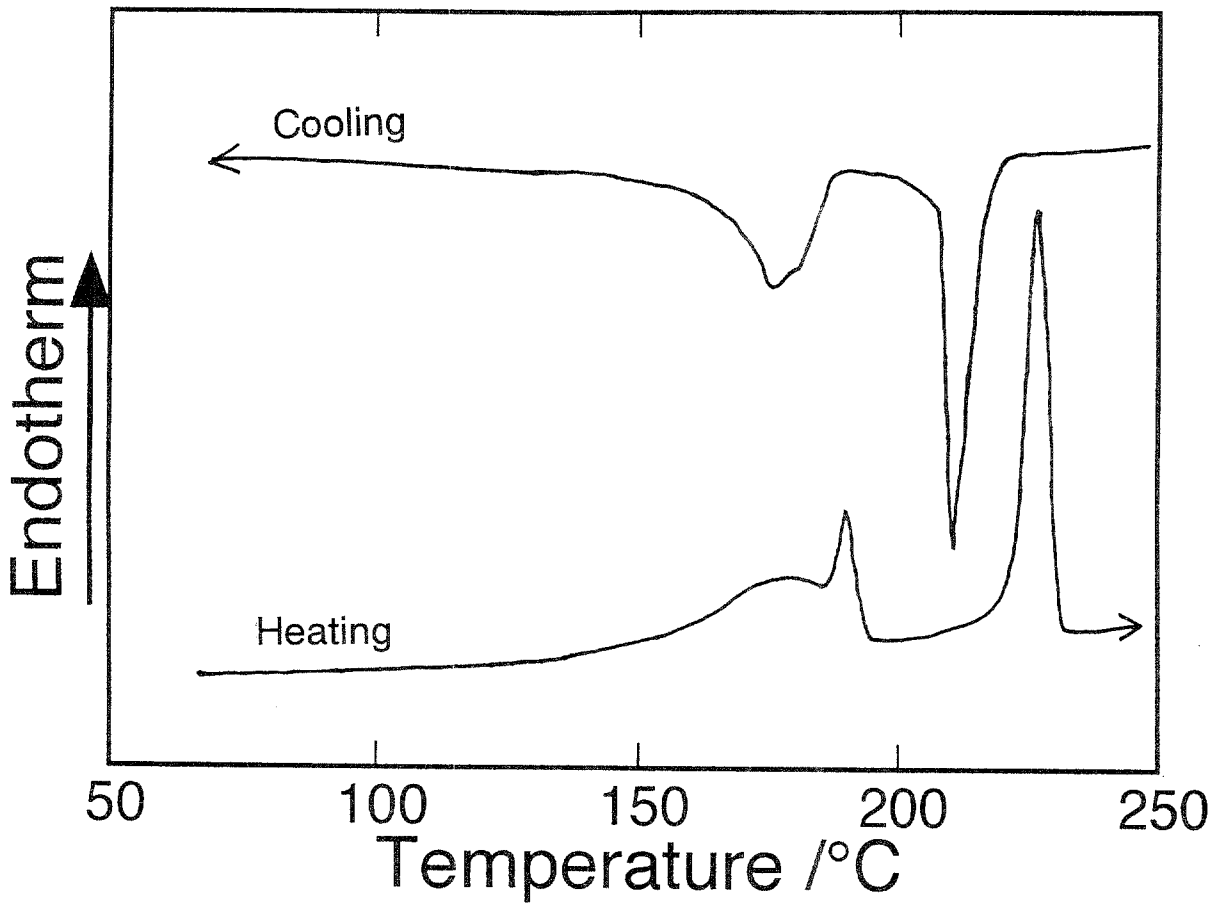

Figure 6.1. Heating and cooling DSC thermograms of PB-14-I measured at a scanning rate of 10°C min^{-1}.

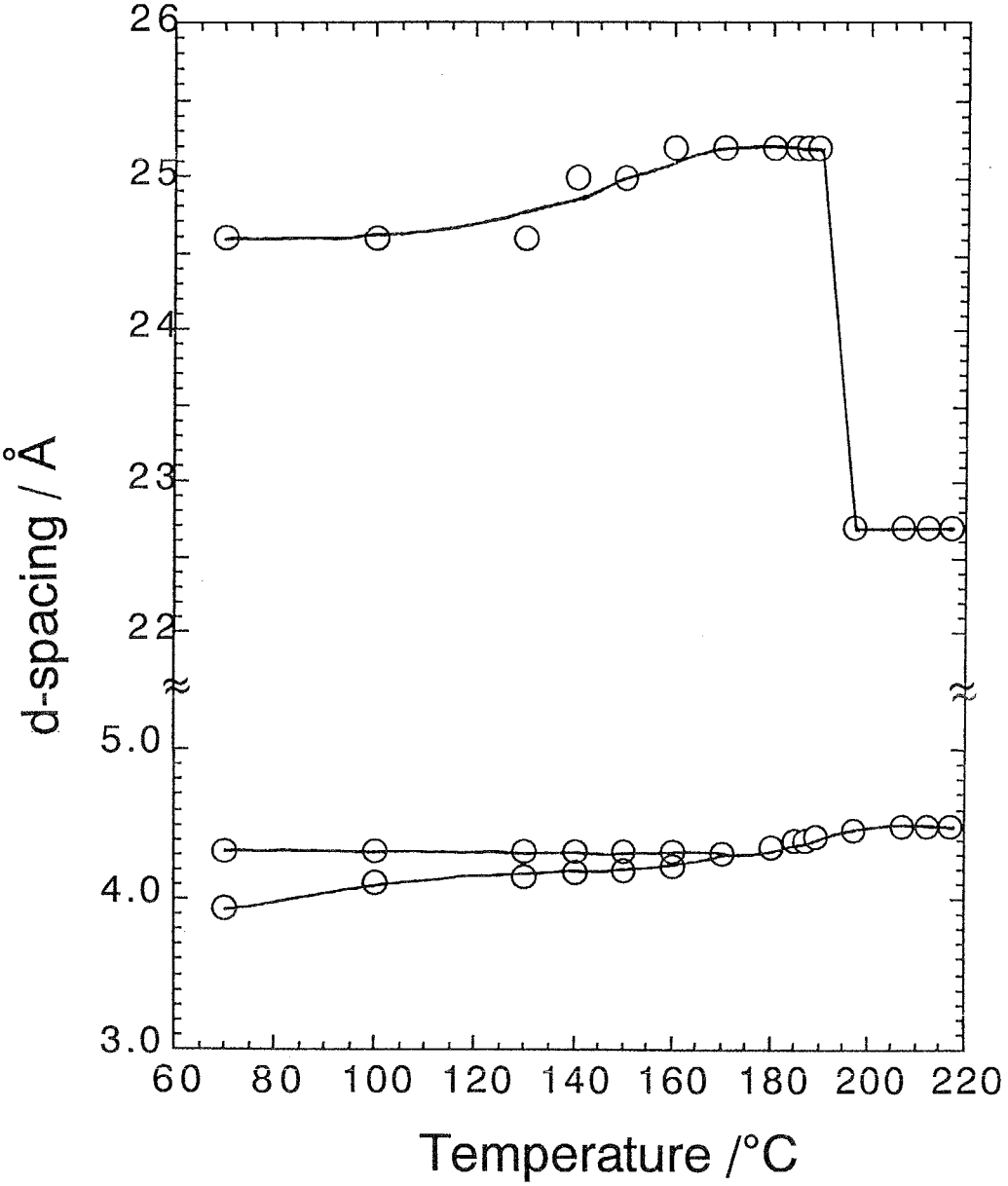

Figure 6.2. Temperature dependence of the d spacings of the inner and outer reflections observed for PB-14-I.

(a)

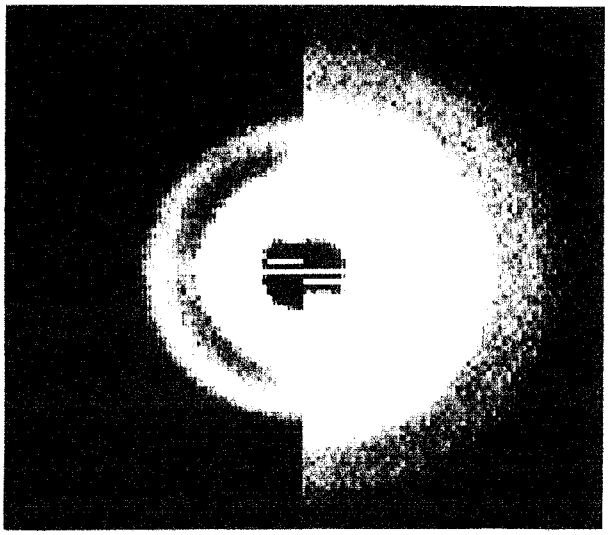

(b)

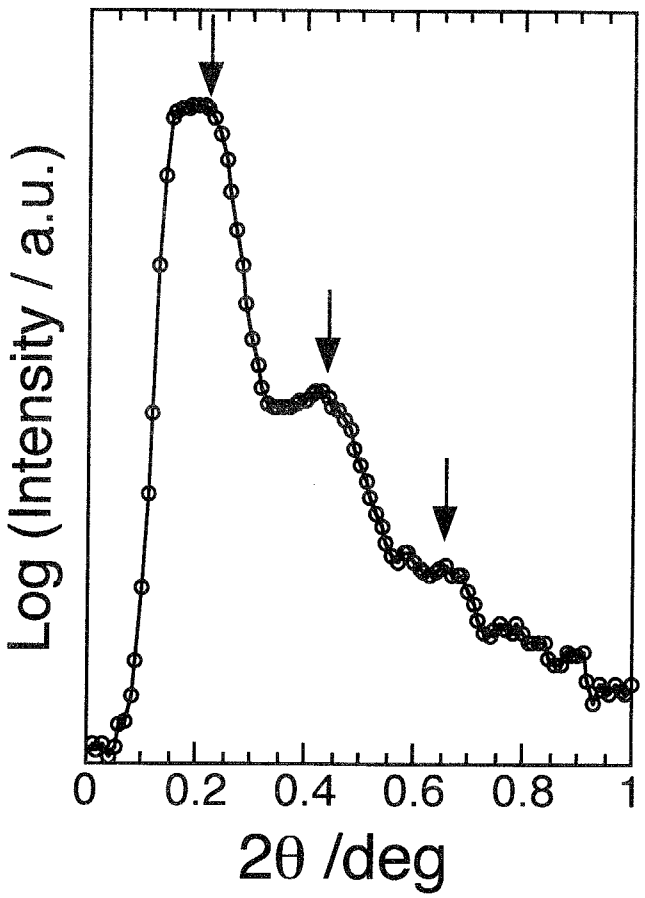

Figure 6.3. (a) Small-angle X-ray photograph and (b) the corresponding intensity profile recorded for the S_H phase of PB-14-I at 207°C. The sample was quenched from the isotropic liquid state of 250°C to the S_H phase of 207°C. The arrows indicate the first, second and third reflections.

Figure 6.4. TEM photograph observed for the bulk PB-14-I specimen prepared by quenching the S_H phase of 207°C.

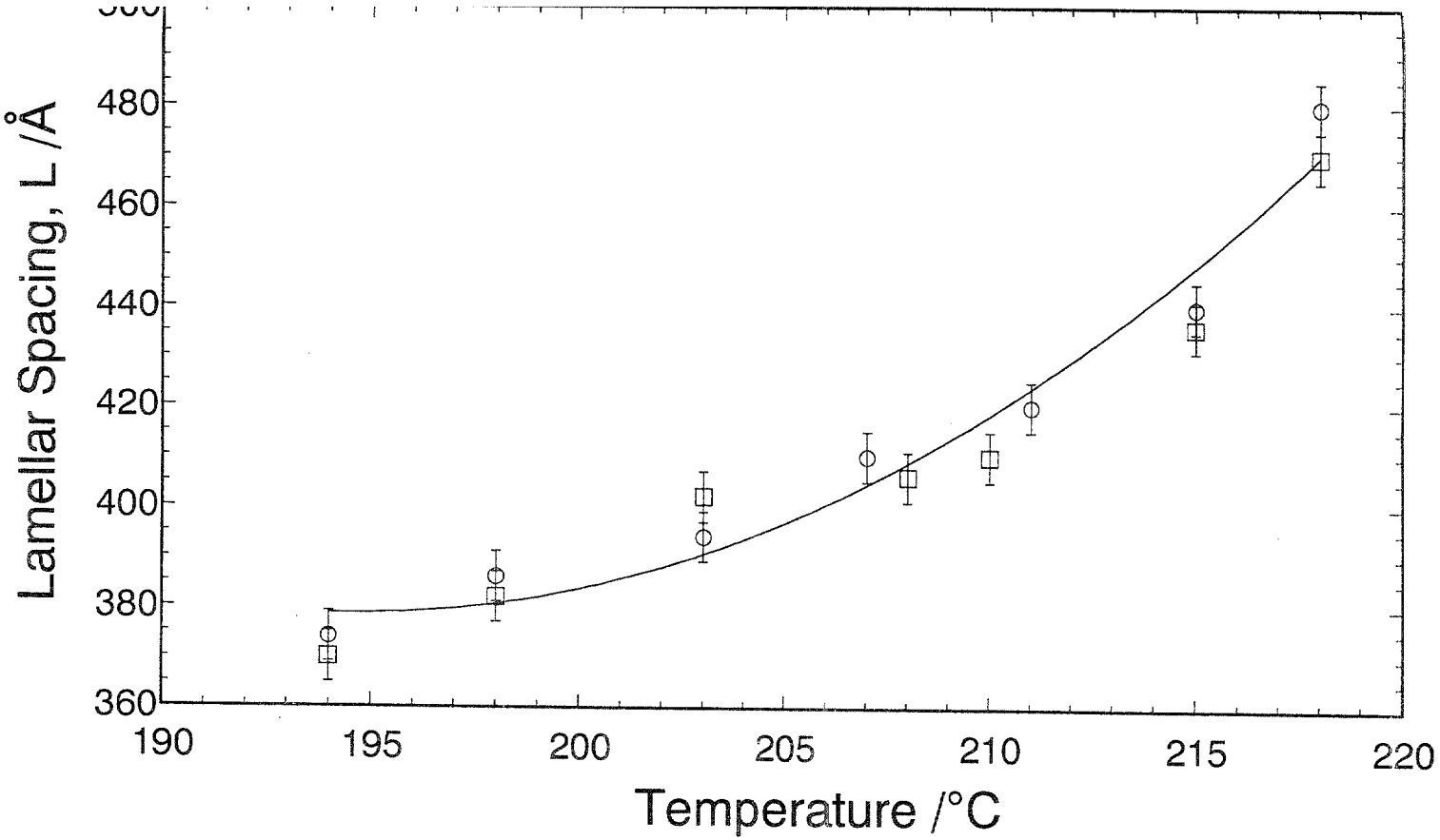

Figure 6.5. Dependence of the lamellar spacing on the liquid crystallization temperature observed for the S_H phases of PB-14-I (circle) and PB-14-II (square). The S_H sample was prepared by quenching from the isotropic liquid to the indicated temperature and annealed for 1 hour. The lamellar spacings were determined from the second order reflection of the SAXS measurements.

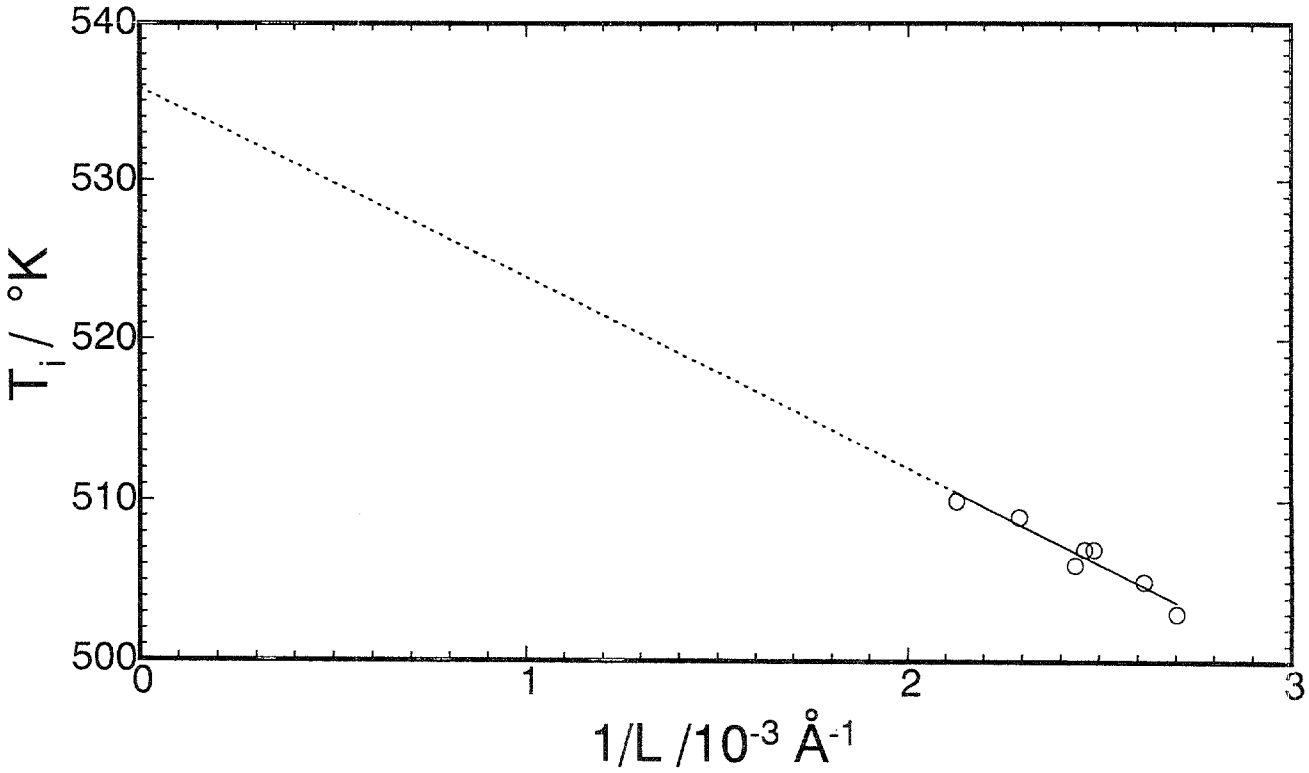

Figure 6.6. Isotropization temperatures for the S_H phase of PB-14-I as a function of reciprocal lamellar spacing.

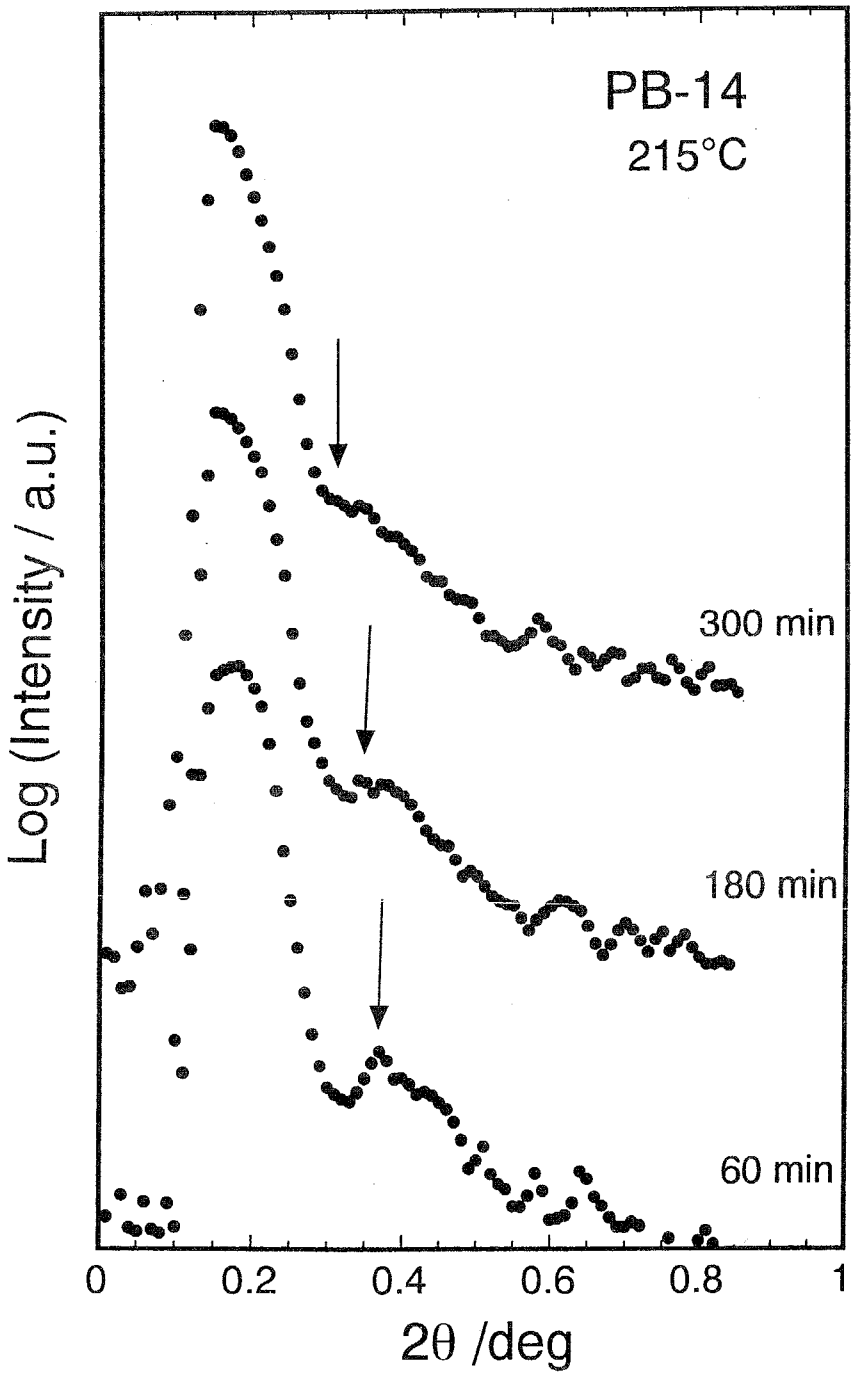

Figure 6.7. SAXS intensity profiles recorded for the S_H phase of PB-14-II annealed at 215°C for the different time periods given in the figure. The arrows indicate the second order reflection.

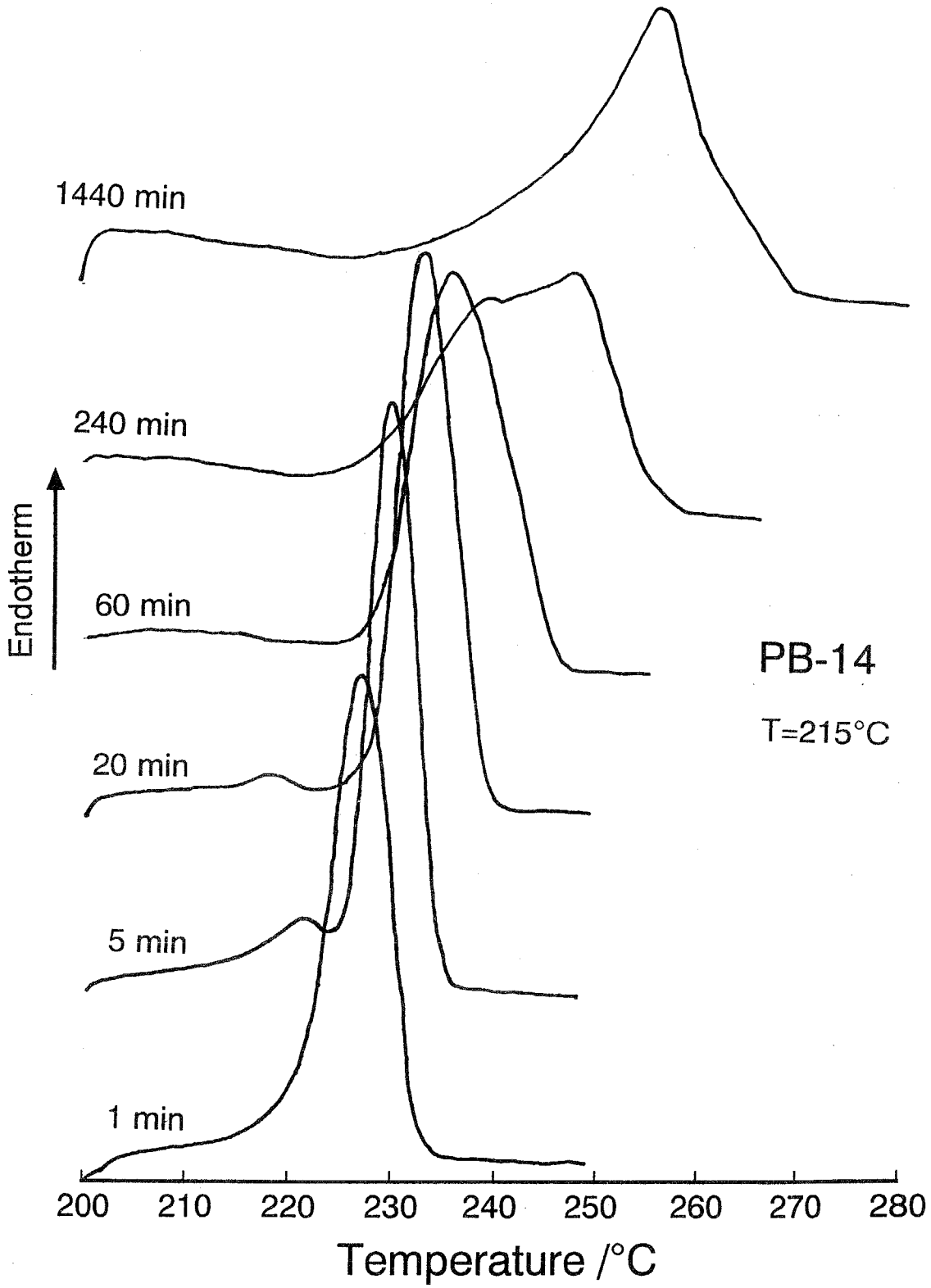

Figure 6.8. DSC endotherms obtained on isotropization for the S_H phase of PB-14-II at a scanning rate of 10°C min^{-1} after annealing at 215°C for various times indicated in the figure.

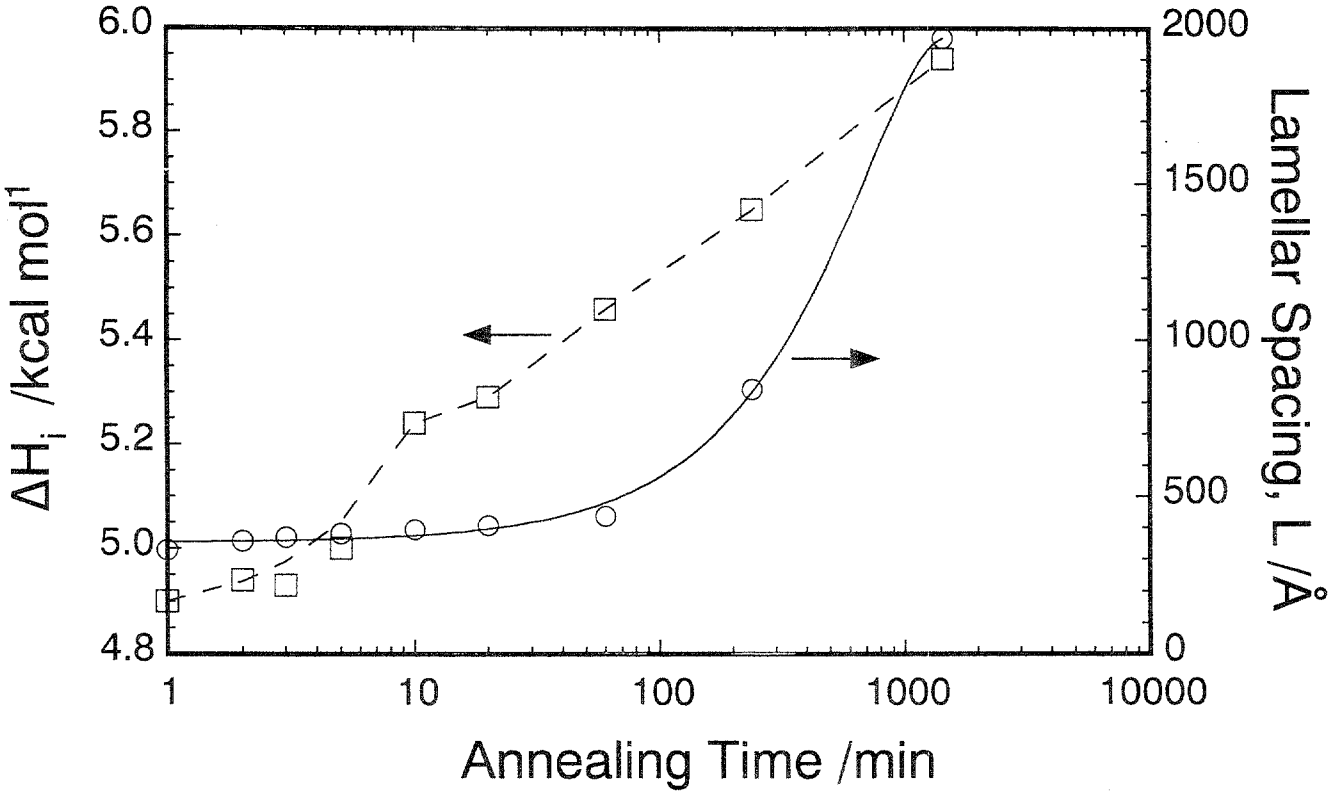

Figure 6.9. Annealing time dependence of the lamellar size (circle) and isotropization enthalpy (square) for the S_H phases of PB-14-II annealed at 215°C. Here, the lamellar size was estimated from the isotropization temperature by using the equation (1).

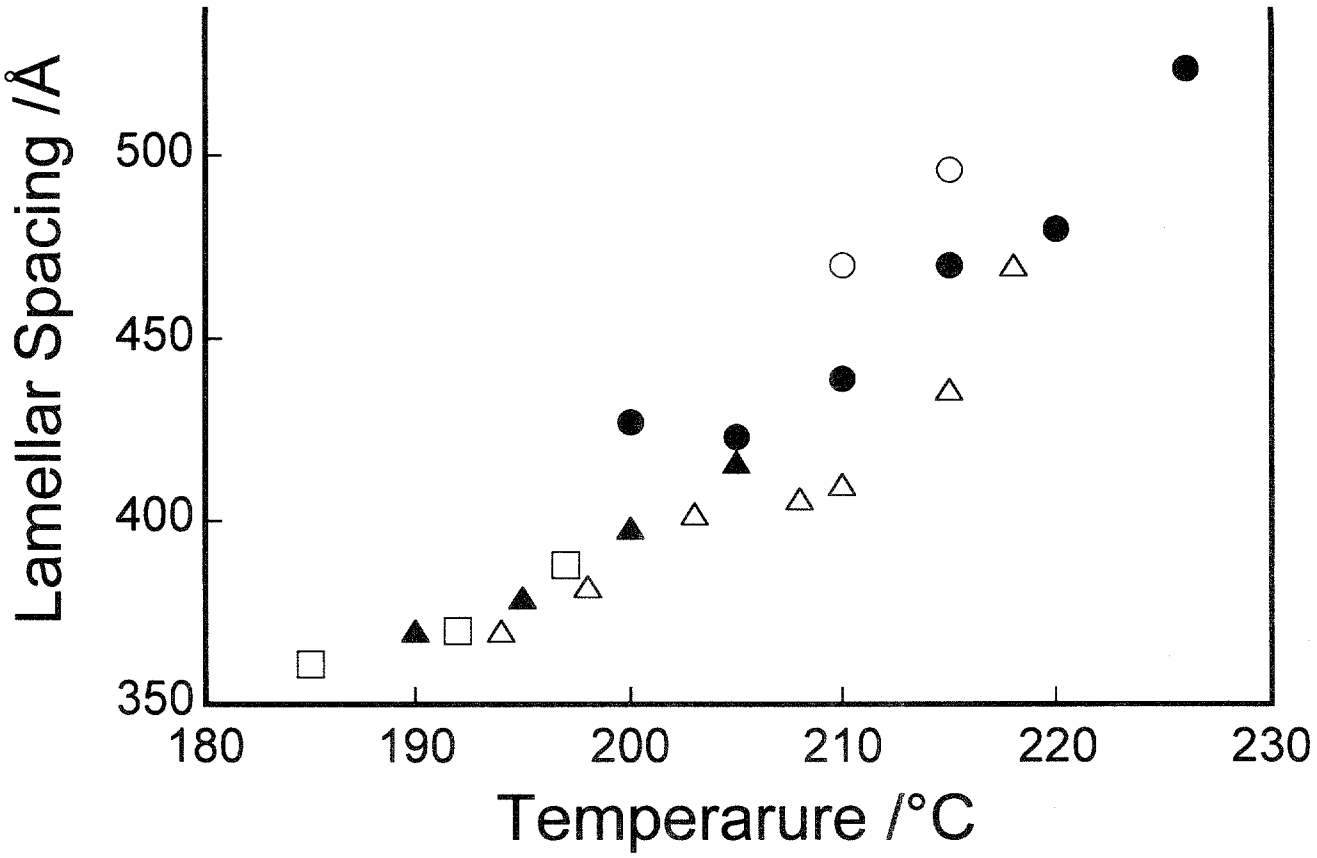

Figure 6.10. Dependence of the lamellar spacing on the liquid crystallization temperature observed for the S_H phases of PB-10 (open circle), PB-12 (closed circle), PB-14 (triangle), PB-16 (closed triangle) and PB-18 (square). The S_H sample was prepared by quenching from the isotropic liquid to the indicated temperature and annealed for 1 hour. The lamellar spacings were determined from the second order reflection of the SAXS measurements.

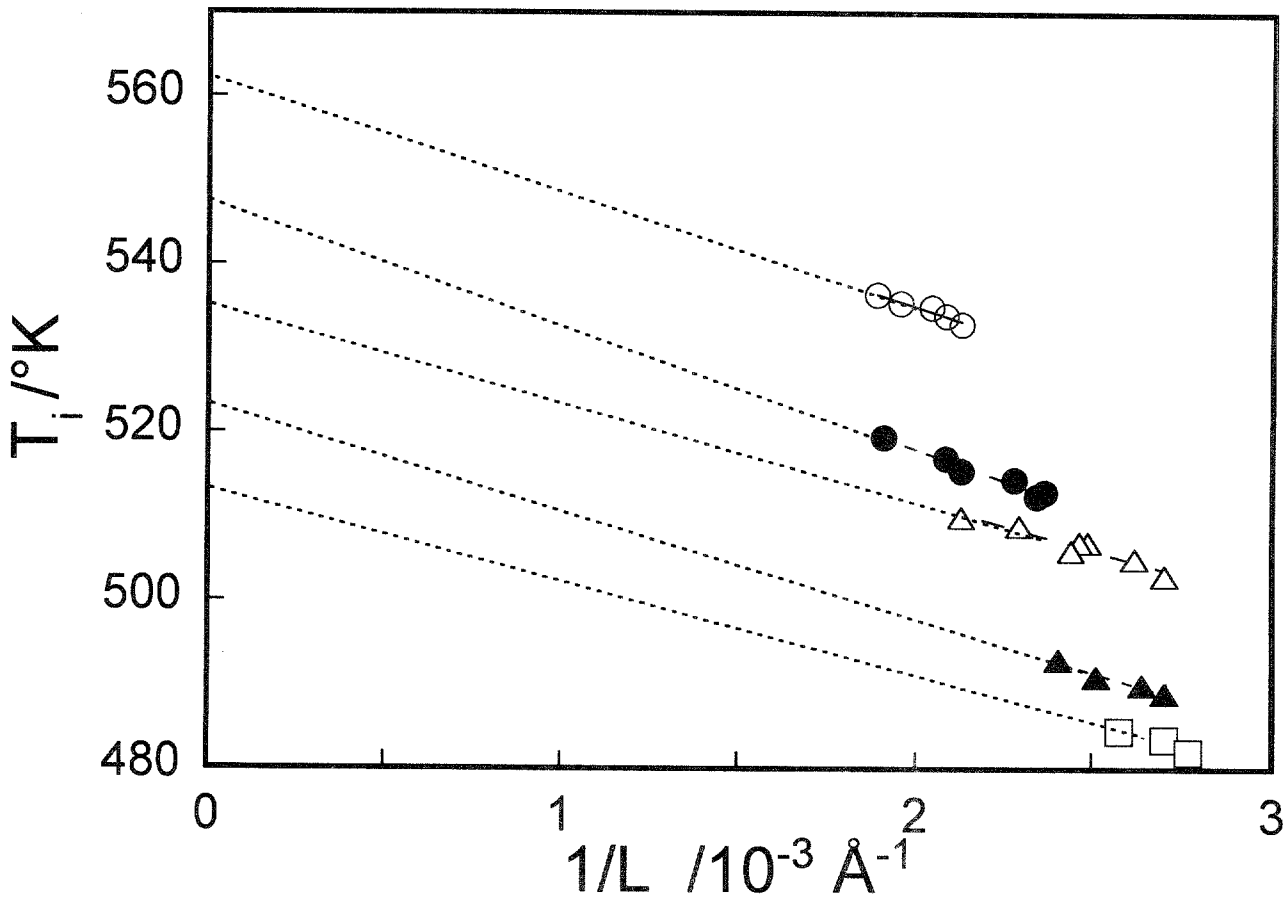

Figure 6.11. Isotropization temperatures for the S_H phase of PB-10 (open circle), PB-12 (closed circle), PB-14 (triangle), PB-16 (closed triangle) and PB-18 (square) as a function of reciprocal lamellar spacing.

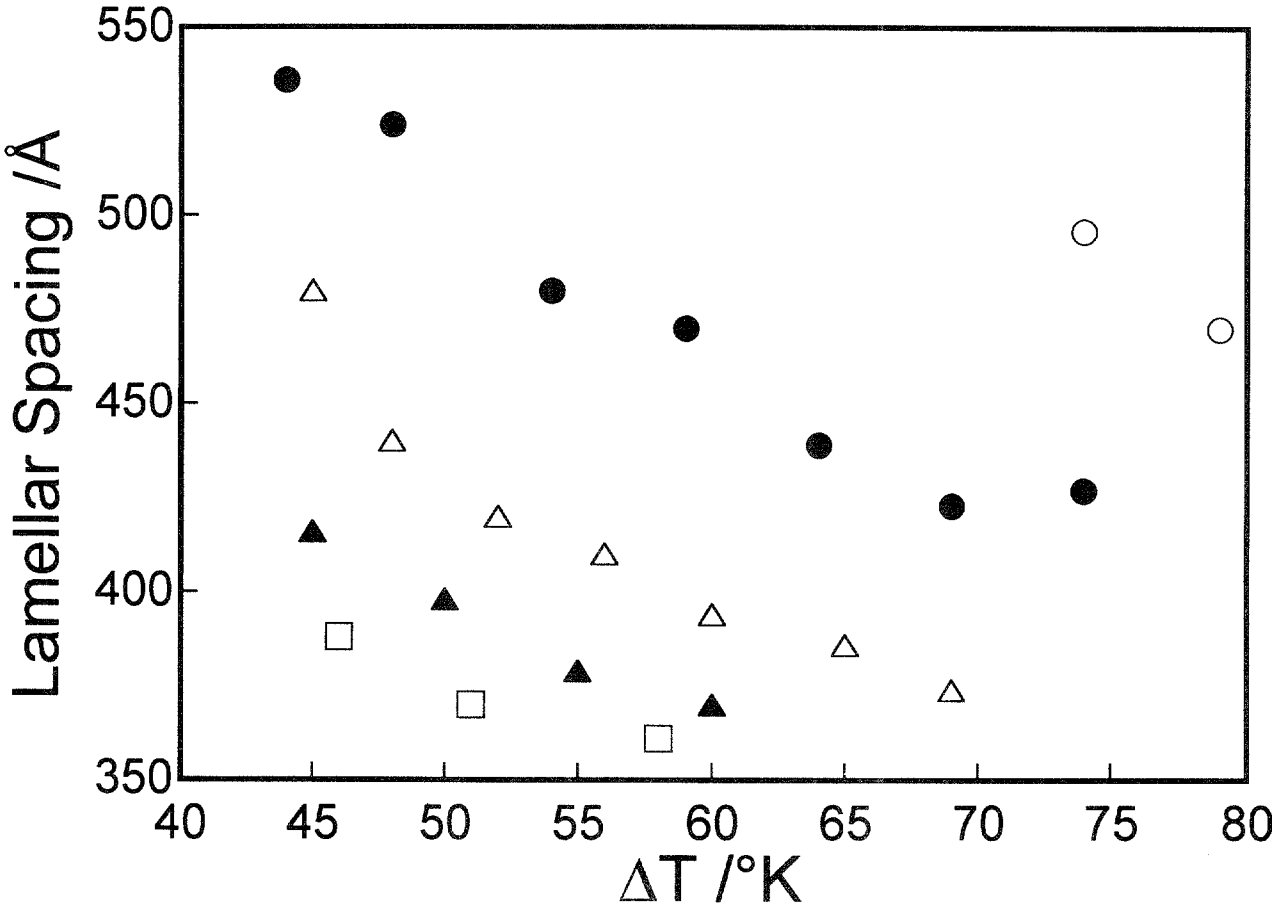

Figure 6.12. Dependence of the lamellar spacing on the supercooling, ΔT observed for the S_H phases of PB-10 (open circle), PB-12 (closed circle), PB-14 (triangle), PB-16 (closed triangle) and PB-18 (square). The data are identical with that in Figure 6.10.

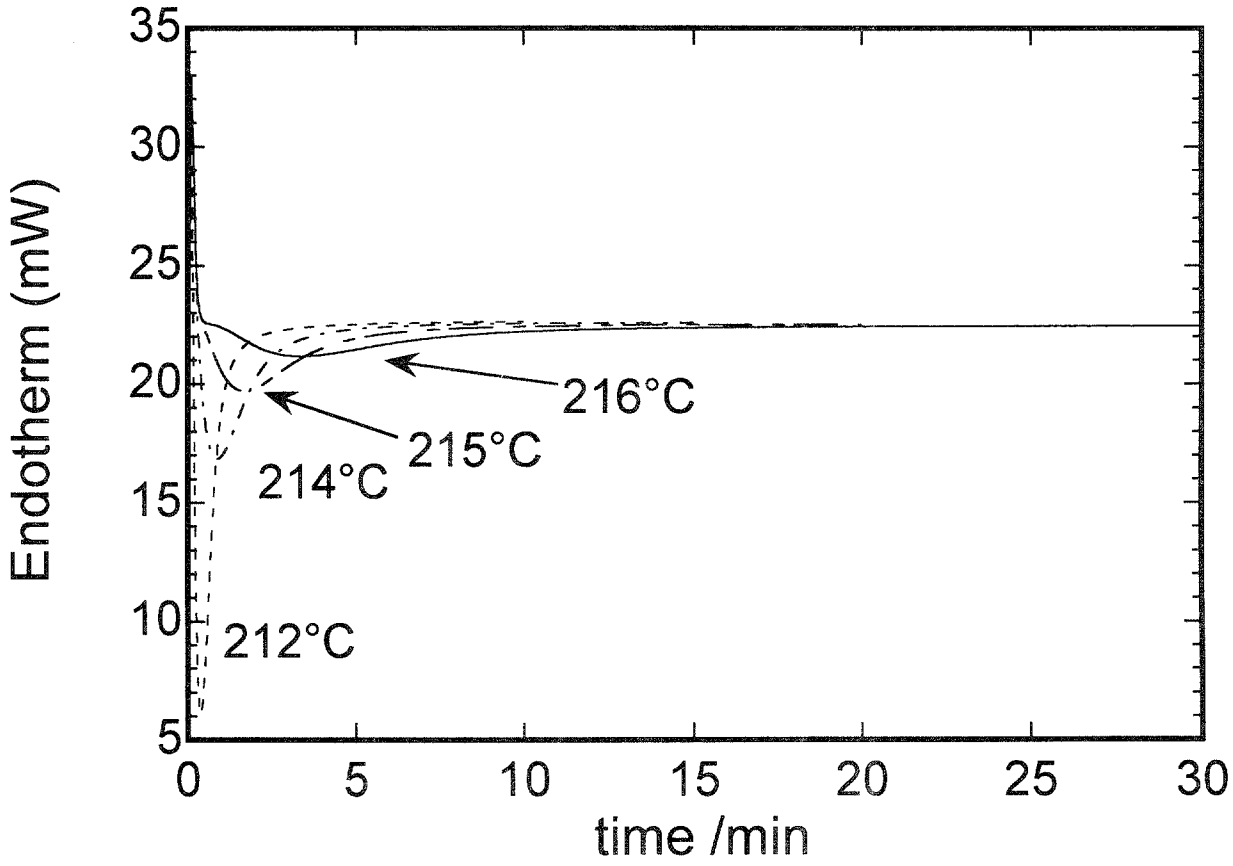

Figure 6.13. Isothermal liquid crystallization curves for PB-14-II at the temperature indicated in the figure.

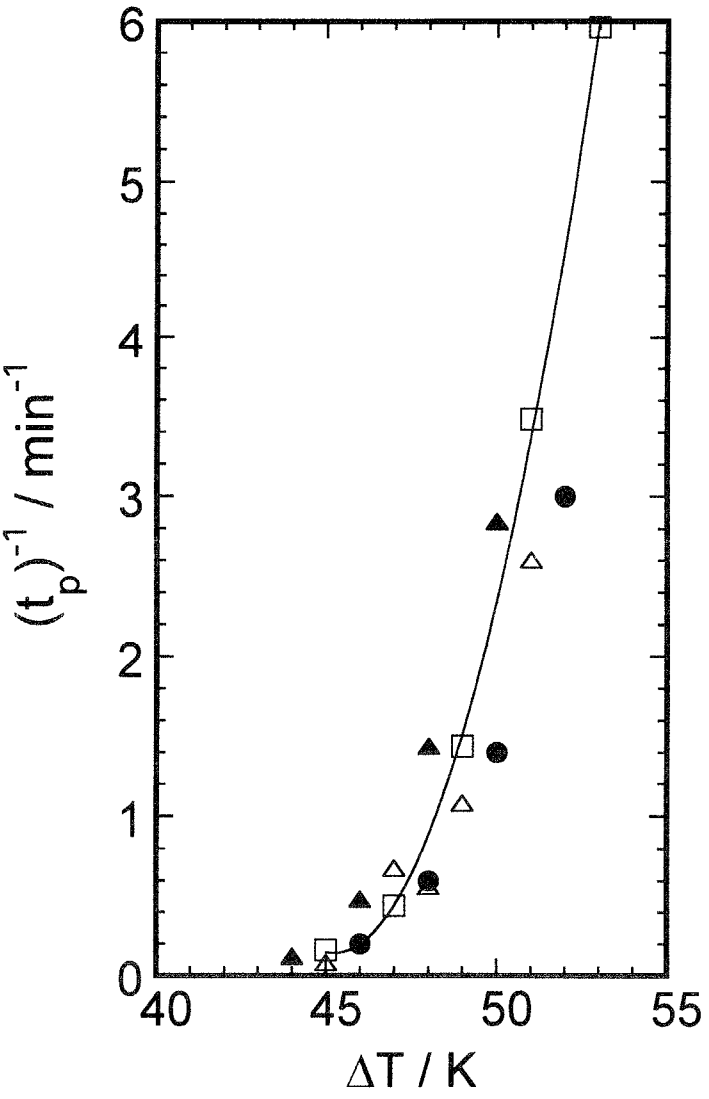

Figure 6.14. Relationship between $(t_p)^{-1}$ and ΔT for PB-12 (closed circle), PB-14 (triangle), PB-16 (closed triangle) and PB-18 (square).

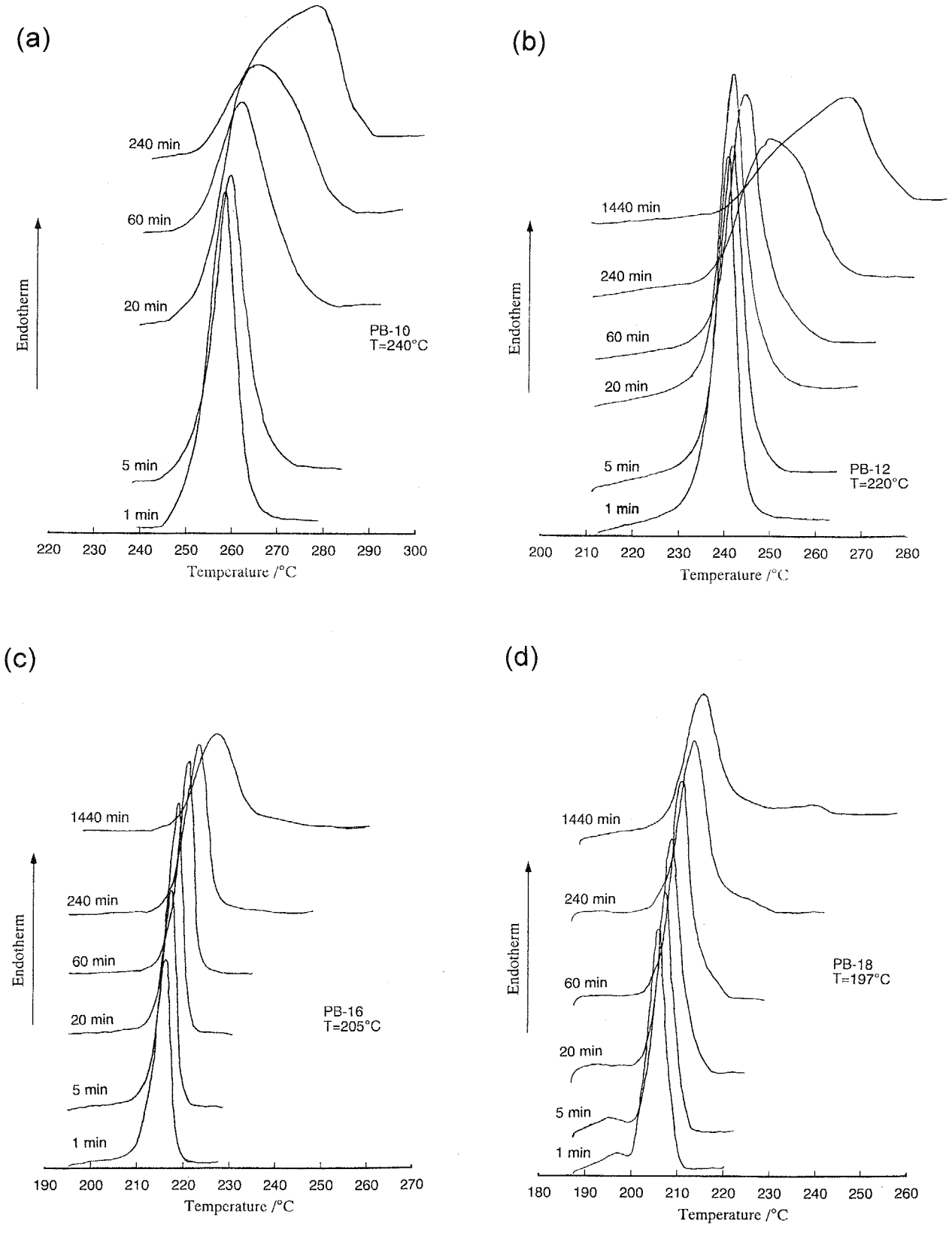

Figure 6.15. DSC endotherms obtained on isotropization for the S_H phase of (a) PB-10, (b) PB-12, (c) PB-16 and (d) PB-18 at a scanning rate of 10°C min^{-1} after annealing at the temperature for various times indicated in the figure.

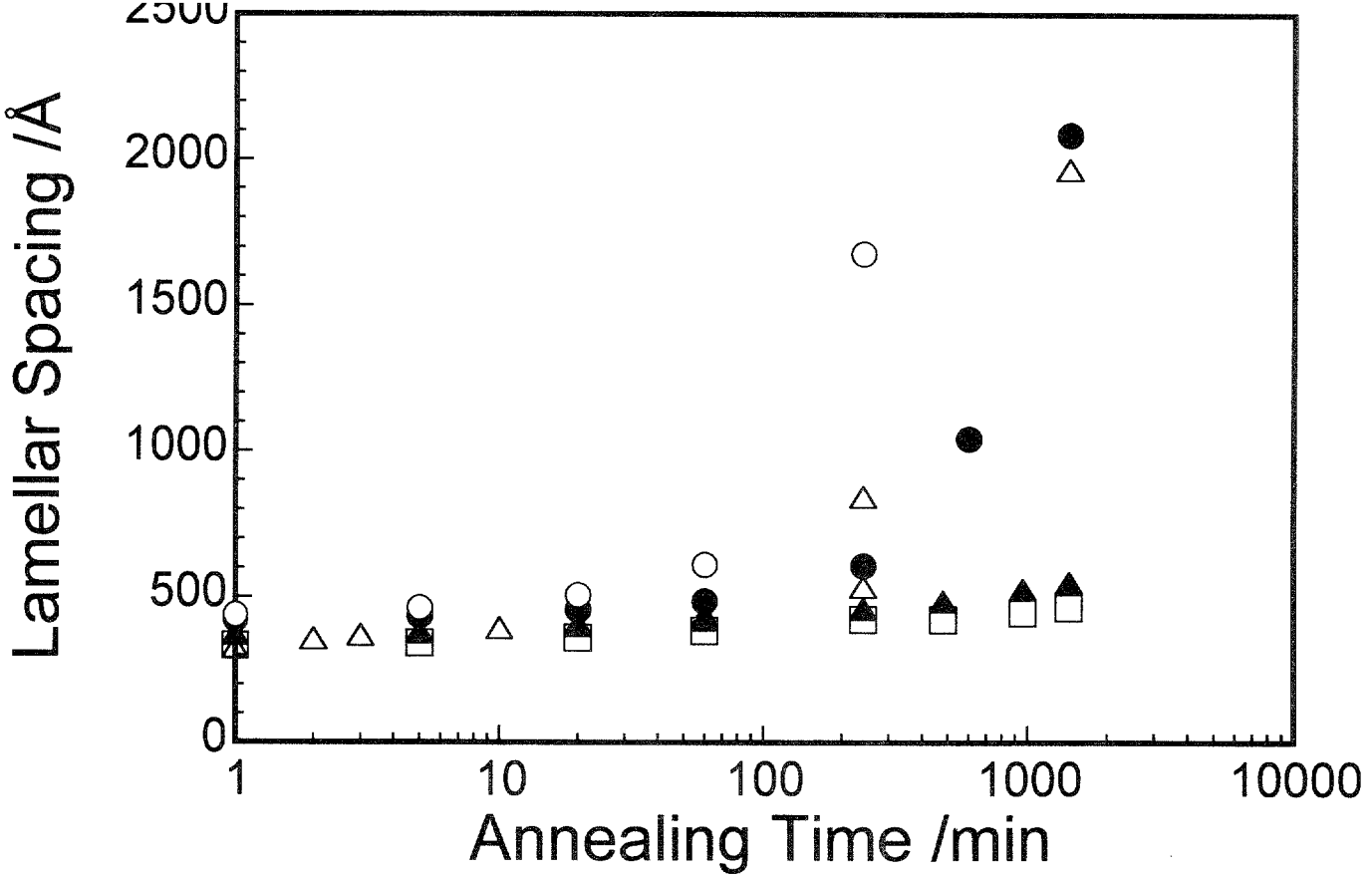

Figure 6.16. Annealing time dependence of the lamellar size for the S_H phases of PB-10 annealed at 240°C (open circle), PB-12 annealed at 220°C (closed circle), PB-14 annealed at 215°C (open triangle), PB-16 annealed at 205°C (closed triangle) and PB-18 annealed at 197°C(square). Here, the lamellar size was estimated from the isotropization temperature by using the equation (1).

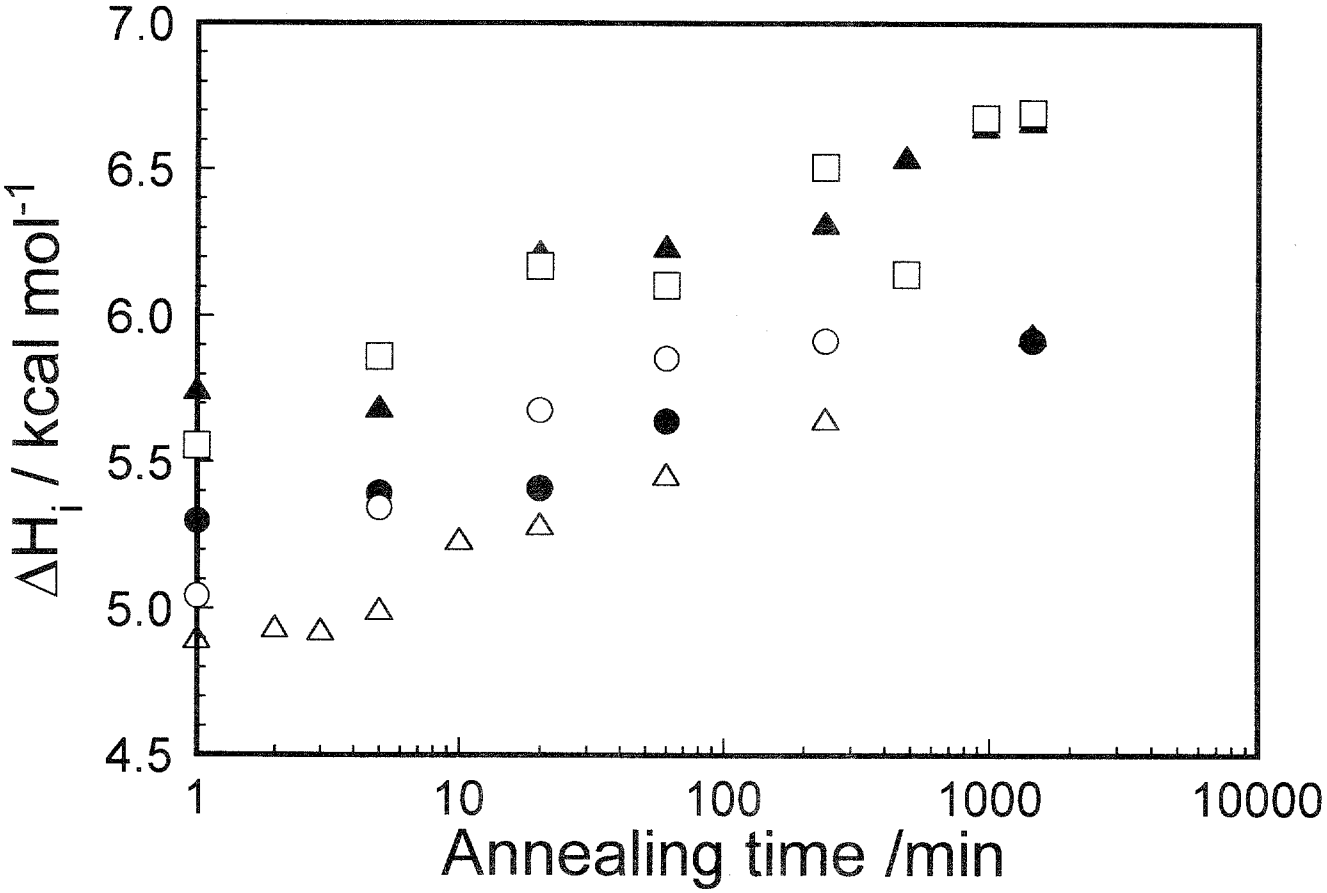

Figure 6.17. Annealing time dependence of the isotropization enthalpy for the S_H phases of PB-10 annealed at 240°C (open circle), PB-12 annealed at 220°C (closed circle), PB-14 annealed at 215°C (open triangle), PB-16 annealed at 205°C (closed triangle) and PB-18 annealed at 197°C(square).

Chapter 7

Kinetic Study on Phase Transitions in Smectic Liquid Crystal Polymers

ABSTRACT: The kinetics of the phase transitions in smectic liquid crystalline main-chain polyesters was investigated with the DSC method. The kinetic data were collected for the crystallization from S_A and S_{CA} phases and the form of S_A, S_{CA} and S_H phases from isotropic liquid. The data suggests that both processes are nucleation controlled. The growth geometry deduced with Avrami approximation. The formation of all the smectic phases from isotropic liquid shows two-dimensional growth geometry. The crystallization from the S_A and S_{CA} phases shows three-dimensional growth geometry. The melting behavior of the samples crystallized from the extended-chain S_H liquid crystal was compared with that of the sample crystallized from the folded-chain LC. The result suggests that the free surface energy of the interface between the liquid crystal and the crystal is fairly low and the crystallization takes place completely.

7.1. Introduction

Liquid crystalline materials form isotropic liquid, liquid crystal and crystalline phases in the order of decreasing in temperature, thus the crystallization takes place from the preceding liquid crystal. This situation is completely different from that encountered in the conventional materials in which the crystallization occurs from the isotropic liquid. There is no significant correlation in the arrangement of molecules in the isotropic liquid. On the other hand, liquid crystals have a long-range orientational order, further smectic liquid crystals have an additional one-dimensional positional order. It can be thus envisage that the crystallization to achieve full three-dimensional order takes place more easily and steadily from the liquid crystal than from isotropic liquid. It is also expected that the crystallization kinetics depend on the molecular arrangement order in the preceding phase, i.e., isotropic liquid or liquid crystals.

Crystallization from liquid crystals is more interesting from the viewpoint of polymer crystallization. Conventional polymers that have been used in the study on polymer liquid crystallization crystallize from isotropic liquid, where a polymer chain is characterized by random, haphazard arrangements of the polymer chain units. Moreover the polymer chains intertwine with each other. At the crystallization, these chains have to separate from each other and alter their coiled configuration to extended one. On the other hand, liquid crystal field forces a polymer chain to takes up an extended configuration without intertwining at least in part of its entire length. Crystallization of extended chain liquid crystal can realize according to the result of Chapter 6 in this thesis.

The isothermal transition kinetics of the liquid crystal phase from the isotropic melt is also interesting if the liquid crystallization behavior can be connected with the liquid crystalline structure.

This chapter shows the experimental results on the crystallization and

liquid crystallization kinetics investigated by DSC methods.

7.2. Experimental

A Perkin-Elmer Pyris 1 DSC was used to analyze the overall transformation kinetics of the thermotropic main-chain liquid crystalline polymers (BB-5, BB-6, and PB-14) as well as the non-liquid crystalline polymers of BB-10 with the following standard procedure. In order to eliminate any thermal history of the material, the samples were melted at the temperature 10°C above the isotropization temperature for 5 min before the measurement. After holding the samples in preceding phase for 10 min, the samples (about 15 mg) were rapidly cooled (at a rate of 50°C min^{-1}) to the temperature at which the transformation (liquid crystallization or crystallization) takes place and maintained at that temperature until the exothermal were not detected. The heat evolved during the isothermal condition was recorded as a function of time at different transformation temperature.

The isothermal transformation kinetics of a material was analyzed by evaluating its degree of conversion (X_t) as a function of time, at a constant temperature of T_c. X_t is defined as

$$X_t = \int_0^t (dH/dt)dt \Big/ \int_0^t (dH/dt)dt \tag{1}$$

where *dH/dt* is the rate of heat evolution. Assuming that the phase transformations of a polymer are nucleation controlled, the overall kinetics is analyzed with the Avrami equation

$$\log[-\ln(1 - X_t)] = n \log t + \log K_n \tag{2}$$

where n and K_n can be used to interpret qualitatively the nucleation mechanism

and morphology and overall transformation rate of the polymer, respectively.

To quantitatively study the transition kinetics, the peak time t_p is taken to represent the measure of the transition rate. The reason for this choice is due to the fast kinetics for some of the polymers, and only the peak time can be precisely determined during the experimental equilibration. Note that $(t_p)^{-1}$ is proportional to the transition rate.

7.3. Results and Discussion

7.3.1. Crystallization from S_A (BB-6) and S_{CA} (BB-5) Phases

The crystallization kinetics of BB-6 from the S_A phase was quantitatively analyzed from data obtained in the temperature interval from 157 to 180°C. At higher temperatures the rates were too slow to be measured by DSC in a reasonable time period, and at lower temperatures the process was so rapid as to preclude accurate measurements. Typical experimental curves and the corresponding Avrami plots are shown in Figures 7.1 and 7.2, respectively. The Avrami plot shows different linear relations with different slopes in the initial and following parts. The Avrami exponent, n obtained from the slope in the initial parts defines the mode of nucleation and growth. Assuming that thermal nucleation takes place, values of n are 2, 3, or 4 for one-, two-, or three-dimensional growth geometry, respectively. The Avrami exponents for various crystallization temperatures are listed in Table 7.1. The value of n for the lower temperature is larger than 4, which is not explainable with Avrami approximation, but it converges to around 4 with increment in the crystallization temperature. Considering the experimental error, the Avrami exponent obtained here may be 4, suggesting that the crystallization is homogeneous nucleation and one-dimensional growth.

Annealing the preceding S_A phase affects on the crystallization kinetics.

Isothermal DSC measurements performed after annealing the S_A phase at 220°C for 3 hours. The crystallization rate is slower and the Avrami exponent is lower than that for non-annealed sample. On the other hand, crystallization from the fibrous S_A phase takes place much more quickly at the lower temperature but is not observed at the higher temperature (Figure 7.3). The fibrous S_A phase shows an exothermal peak associated with crystallization at higher temperature than the bulk one on the cooling DSC scan (Figure 7.4). Optical microscopy observation shows that annealing a liquid crystal grows the size of its defects (for example, focal conic in smectic LC) particular in origomers as well as in low molecular weight materials. An fibrous sample can be assumed to be monodomain. Thus it can be said that size of defects in the liquid crystal affects on the crystallization kinetics.

Similar results were obtained for the crystallization from S_{CA} phase of BB-5. The Avrami exponent of 4 for the crystallization from these smectic phases is comparable with that observed for crystallization from isotropic liquid in BB-10 (n = 3.5), but slightly larger than that in BB-12 (n = 2.8). To argue this point would be far away from the aim of this thesis.

7.3.2. Crystallization from the Extended Chain S_H Phase

The most interesting point in crystallization from main-chain polymeric liquid crystals is that polymer chains crystallize with more extended configuration. Moreover it emerges from the work of this thesis that the extended chain liquid crystal can be prepared by annealing the S_H phase of PB-n polyester. However, unfortunately the crystallization kinetics for the PB-n polyesters with any thermal prehistory cannot be observed with the isothermal DSC method. Thereby the crystallization behavior was examined with heating DSC curves measured after an isothermal crystallization. The extended chain S_H liquid crystal was prepared by annealing the sample at a smectic temperature

of 215°C during 1 day. The DSC heating curves for the samples crystallized from a folded chain LC and an extended chain LC are shown in Figure 7.5 and the corresponding thermodynamic data are collected in Table 7.2. The transition temperatures and enthalpy show no significant difference between the samples crystallized from a folded chain LC and from the extended chain LC at different temperatures during one day, while that is significant in the isotropization of a folded chain LC and the extended chain LC (cf. Chapter 6). This suggests that the free surface energy between the S_{II} and the crystal is too low to cause a difference in the melting point of the crystal (cf. eq. (1)) and that the crystallinity does not vary in the samples crystallized from the S_{II} LC. The formation of the S_{II} LC takes place in part but with a high conversion (more than 80 %). The crystallization from the S_{II} LC may occurs close to equilibrium and completely, while a certain amount of isotropic liquid glass may exist in the solid.

7.3.3. Kinetics of Liquid Crystallization

Though the arrangement of molecules in S_A, S_{CA} and S_{II} phases are remarkably different, the Avrami exponents for the form of all the smectic phases from isotropic liquid are around 3, indicating two-dimensional growth process. The transition rate show negative dependence on the liquid crystallization temperature (Table 7.1), indicating that the liquid crystallization is nucleation controlled as in the crystallization.

7.4. Concluding Remarks

The kinetics of the phase transitions in smectic liquid crystalline main-chain polyesters was investigated with the DSC method. The kinetic data were collected for the crystallization from S_A and S_{CA} phases and the form of S_A, S_{CA} and S_H phases from isotropic liquid. The data suggests that both processes are nucleation controlled. The growth geometry deduced with Avrami approximation. The formation of all the smectic phases from isotropic liquid shows two-dimensional growth geometry though the molecular arrangements in these smectic phases are remarkably different. The crystallization from the S_A and S_{CA} phases shows three-dimensional growth geometry. The Avrami exponents for kinetics of other LC polymers as well as BB-*n* and PB-*n* polyesters are summarized in Table 7.3.

The melting behavior of the PB-14 crystal crystallized from the extended-chain S_H liquid crystal is independent on the crystallization temperature and shows no significant difference with that crystallized from a folded chain LC. It suggests that the free surface energy of the interface between the liquid crystal and the crystal is fairly low and the crystallization takes place completely.

References

(1) Wunderlich, B. *Macromolecular Physics*, Academic Press: New York, 1980.

(2) Ciora, R. J.; Magill, J. H. *Macrmolecules* **1990**, *23*, 2350.

(3) Gomez, M. A.; Marco, C.; Fatou, J. H. Bowmer, T. N.; Haddon, R. C.; Chichester-Hicks, S. V. *Macromolecules* **1991**, *24*, 3276.

(4) Pracella, M.; Frosini, V.; Galli, G.; Chiellini, E. *Mol. Cryst. Liq. Cryst.* **1984**, *113*, 201.

(5) Yoo, Y. D.; Kim. S. C. *Polym. J.* **1988**, *20*, 1117.

(6) Bhattacharya, S. K.; Misra, A.; Stein, R. S.; Lentz, R. W.; Hahn, P. E. *Polym. Bull.* **1986**, *16*, 465.

(7) Laus, M.; Ferruti, P.; Caretti, D.; Angeloni, A. S.; Galli, G.; Chiellini, E. *Thermochim. Acta* **1990**, *162*, 179.

(8) Cheng, S. Z. D. *Macromolecules* **1988**, *21*, 2475.

(9) Cheng, S. Z. D.; Wunderlich, B. *Macromolecules* **1988**, *21*, 3327.

(10) Jonsson, H.; Wallgren, E.; Hult, A.; Gedde, U. W. *Macromolecules* **1990**, *23*, 1041

(11) Warner, S. B.; Jaffe, M. *J. Cryst. Growth* **1980**, *48*, 184.

(12) Grebowics, J.; Wunderlich, B. *J. Polym. Sci. Polym. Phys. Ed.* **1983**, *21*, 141.

(13) Cheng, S. Z. D.; Janimak, J. J.; Lipinski, T. M.; Sridhar, K.; Huang X. Y.; Harris, F. W. *Polymer* **1990**, *31*, 1122.

(14) Liu, X.; Hu, S.; Shi, L.; Xu, M.; Duan, X. *Polymer* **1989**, *30*, 273.

(15) Cheng, S. Z. D.; Zhang, A.; Johnson, R. L.; Wu, Z.; Wu, H. H. *Macromolecules* **1990**, *23*, 1196.

(16) Cheng, S. Z. D.; Johnson, R. L.; Wu, Z.; Wu, H. H. *Macromolecules* **1991**, *24*, 150.

(17) Campoy, I.; Marco, C.; Gomez, M. A.; Fatou, J. G. *Macromolecules* **1992**, *25*, 4392.

Table 7.1. Kinetics Parameters for Phase Transitions of BB-*n* and PB-*n* Polyesters

sample	transition	temperature (°C)	Avrami exp *n*	$(t_p)^{-1}$ (min^{-1})
BB-5	Iso - S_{CA}	206		4.61×10^{-1}
		208	2.55	1.91×10^{-1}
	S_{CA} - Cryst	95	3.59	7.32×10^{-1}
		100	2.46	3.53×10^{-1}
		105	4.59	1.39×10^{-1}
		110	4.98	5.61×10^{-2}
		115		2.31×10^{-2}
	S_{CA} - Cryst	100	1.90	3.16×10^{-1}
	(After annealing	110	2.85	5.43×10^{-2}
	at 190°C for 3 hours)			
BB-6	Iso - S_A	231		7.65×10^{-1}
		232		3.97×10^{-1}
		233	3.13	2.33×10^{-1}
		234		1.34×10^{-1}
	S_A - Cryst	157		2.14
		160		1.13
		163		1.98
		165	5.25	2.93×10^{-1}
		167	4.31	1.86×10^{-1}
		170	4.64	1.30×10^{-1}
		172	4.26	1.21×10^{-1}
		174	4.31	9.87×10^{-2}
		176	4.24	8.52×10^{-2}
		178	4.86	7.50×10^{-2}
		180	3.91	6.94×10^{-2}
	S_A - Cryst	165	4.95	2.89×10^{-1}
	(after annealing	172	3.48	1.18×10^{-1}
	at 220°C for 3 hours)	178	2.95	8.39×10^{-2}
BB-10	Iso - Cryst	161	4.51	2.89×10^{-1}
		162	4.36	1.97×10^{-1}
		163	5.12	1.17×10^{-1}
		164	5.12	7.08×10^{-2}
BB-12	Iso - Cryst	150	2.88	2.03×10^{-1}
		152	2.70	9.12×10^{-2}
PB-14	Iso - S_H	212		2.61
		214	2.85	1.13
		215	2.91	5.94×10^{-1}
		216	3.01	2.99×10^{-1}

Table 7.2. Thermodynamic Data for the Melting of the PB-14 Crystals Crystallized from the Extended Chain S_H liquid Crystal

DSC Curves in Figure 7.5	T_1 (°C)	T_2 (°C)	ΔH_m (kJ mol^{-1})
(a)	178	189	4.60
(b)	178	193	5.14
(c)	177	193	5.21
(d)	177	194	5.07
(e)	179	193	5.00
(f)	178	193	5.05
(g)	177	192	5.17

Table 7.3. Avrami Exponents for Kinetics of Liquid Crystalline Polymers

transformation	sample	Avrami exp.	ref
isotropic — nematic	main-chain polyester	0.68~0.85	6
	poly(azomethines)	0.1~0.6	13
	polyphosphazenes	2	2
	polyester	1	14
isotropic — smectic	polyethers	2.5~3.0	10
nematic — crystal	copolyesters	0.24~0.73	8, 9
	copolyesters	2, 0.15~0.38	15, 16
	polyphosphazenes	2	2
	polyphosphazene	3, 4	3
	poly(azomethines)	2.4~3.8	13
	polyesters	2.7~4.2	7
	polyesters	2	11
	polyester	3 ~ 4	12
smectic — crystal	main-chain polyester	3 ~ 4	4
	main-chain polyester	2	4
nematic — crystal	main-chain polyester	2	5
smectic — crystal	main-chain polyester	2.89 ~ 3.22	5
	polyester	4	14
nematic — crystal	main-chain polyester	2, 3	17
isotropic — smectic A	BB-6	3.1	
isotropic — smectic CA	BB-5	2.6	
isotropic — smectic H	PB-14	2.9 ~ 3.1	
smectic A — crystal	BB-6	3.9 ~ 5.3	
smectic CA — crystal	BB-5	2.5 ~ 5.0	
isotropic – crystal	BB-10	4.5 ~5.1	
isotropic – crystal	BB-12	2.7 ~ 2.9	

Figure Captions

Figure 7.1. Experimental isothermal curves of BB-6 at three different temperatures: (a) 165, (b) 172 and (c) 178°C, crystallized from the S_A phase.

Figure 7.2. Avrami treatment of experimental isothermal curves shown in Figure 7.1.

Figure 7.3. DSC isothermal curve for crystallization of fibrous S_A specimen of BB-6 polyester at the temperature indicated in the figure.

Figure 7.4. Cooling DSC thermogram for the crystallization of (a) a bulk specimen (dotted line) and (b) a fibrous specimen (solid line) measured at a rate of 10°C min^{-1}.

Figure 7.5. Heating DSC thermogram for the melting of PB-14 crystals: (a) a crystal prepared by cooling the isotropic melt at a rate of 10°C min^{-1}; (b) crystal prepared by quenching the extended chain S_H LC; (c) - (g) crystals crystallized the extended chain S_H LC isothermally at the temperature indicated in the figure.

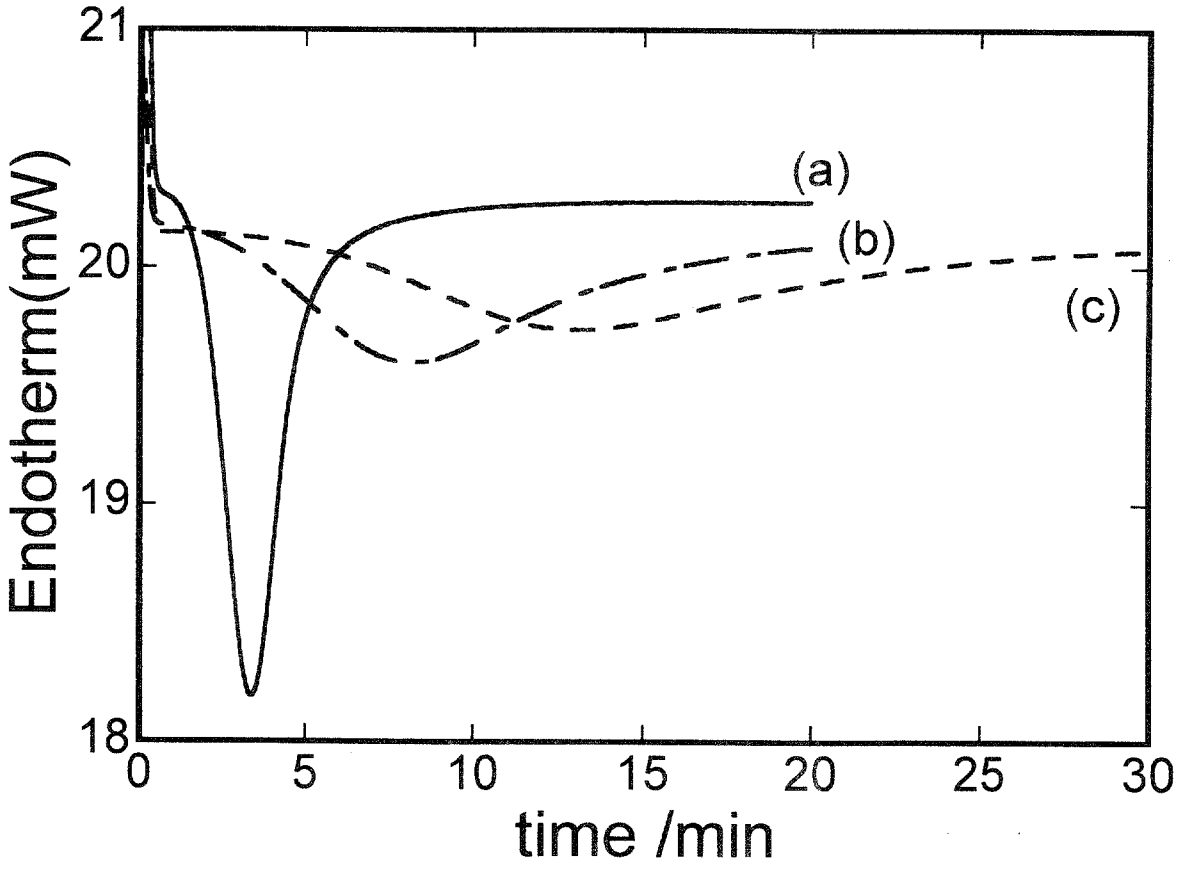

Figure 7.1. Experimental isothermal curves of BB-6 at three different temperatures: (a) 165, (b) 172 and (c) 178°C, crystallized from the S_A phase.

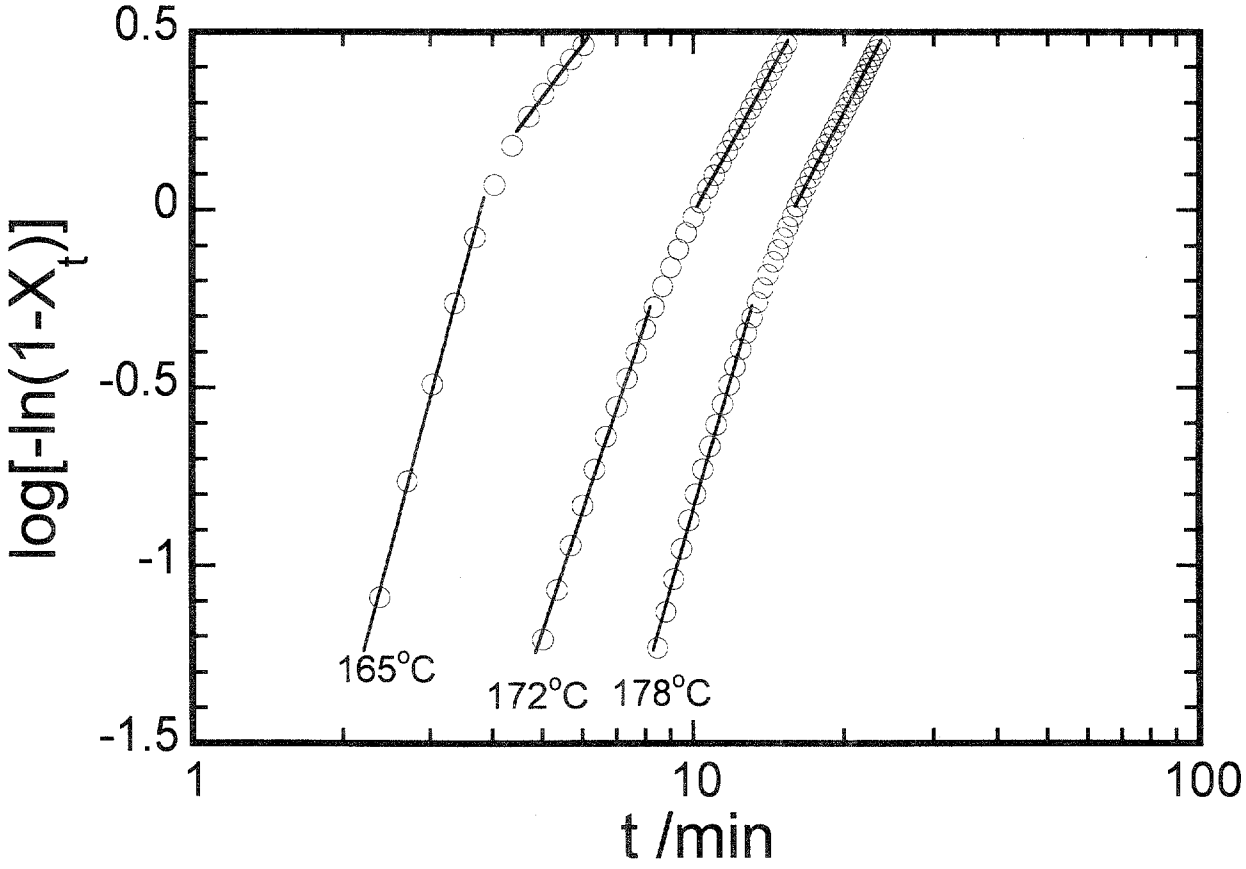

Figure 7.2. Avrami treatment of experimental isothermal curves shown in Figure 7.1.

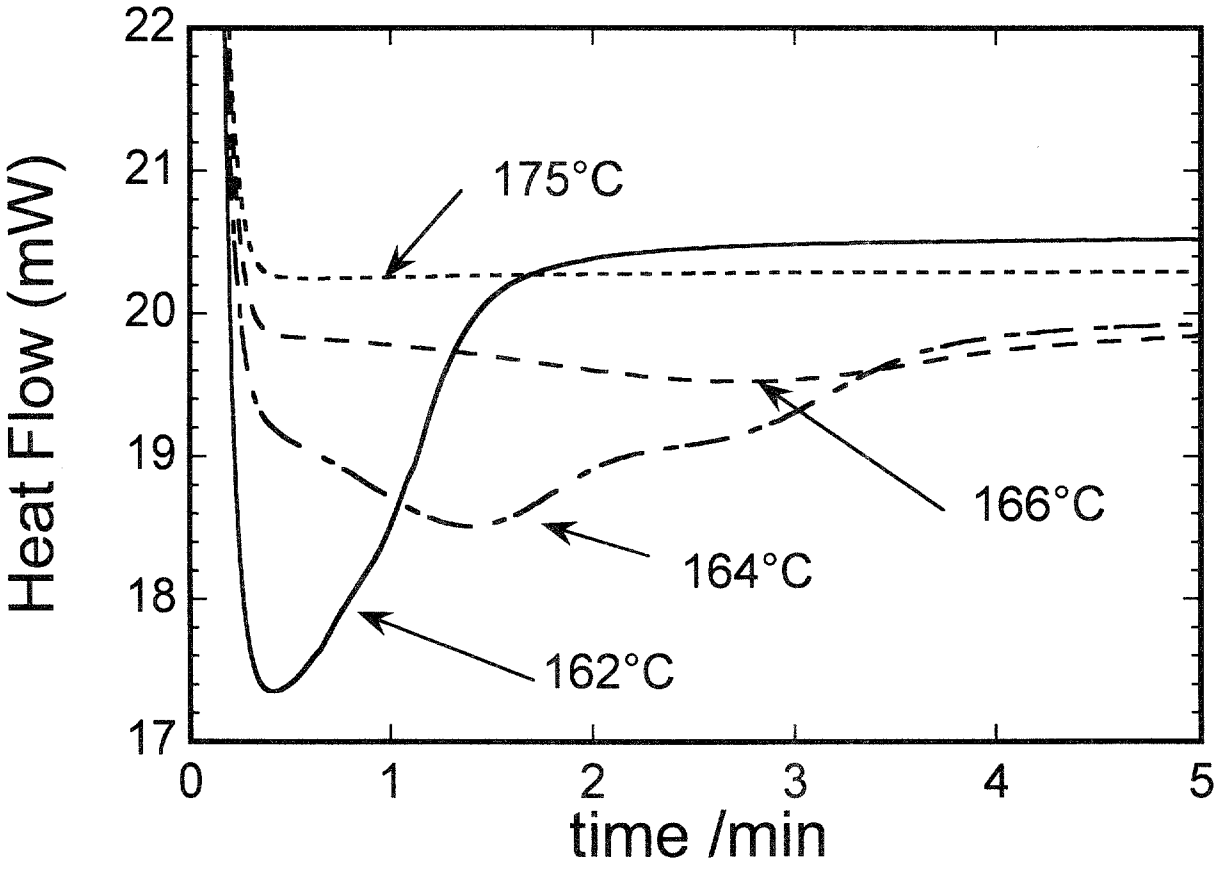

Figure 7.3. DSC isothermal curve for crystallization of fibrous S_A specimen of BB-6 polyester at the temperature indicated in the figure.

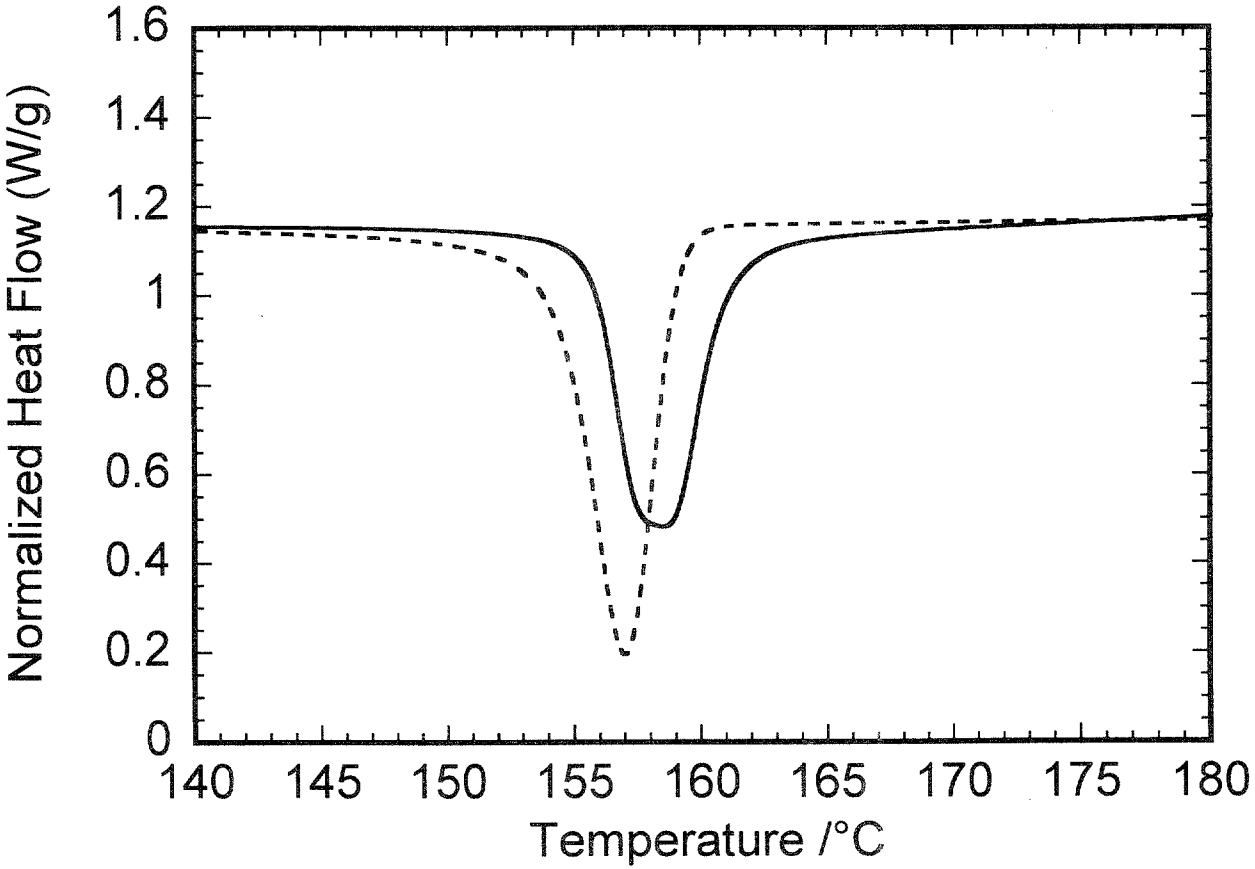

Figure 7.4. Cooling DSC thermogram for the crystallization of (a) a bulk specimen (dotted line) and (b) a fibrous specimen (solid line) measured at a rate of 10°C min^{-1}.

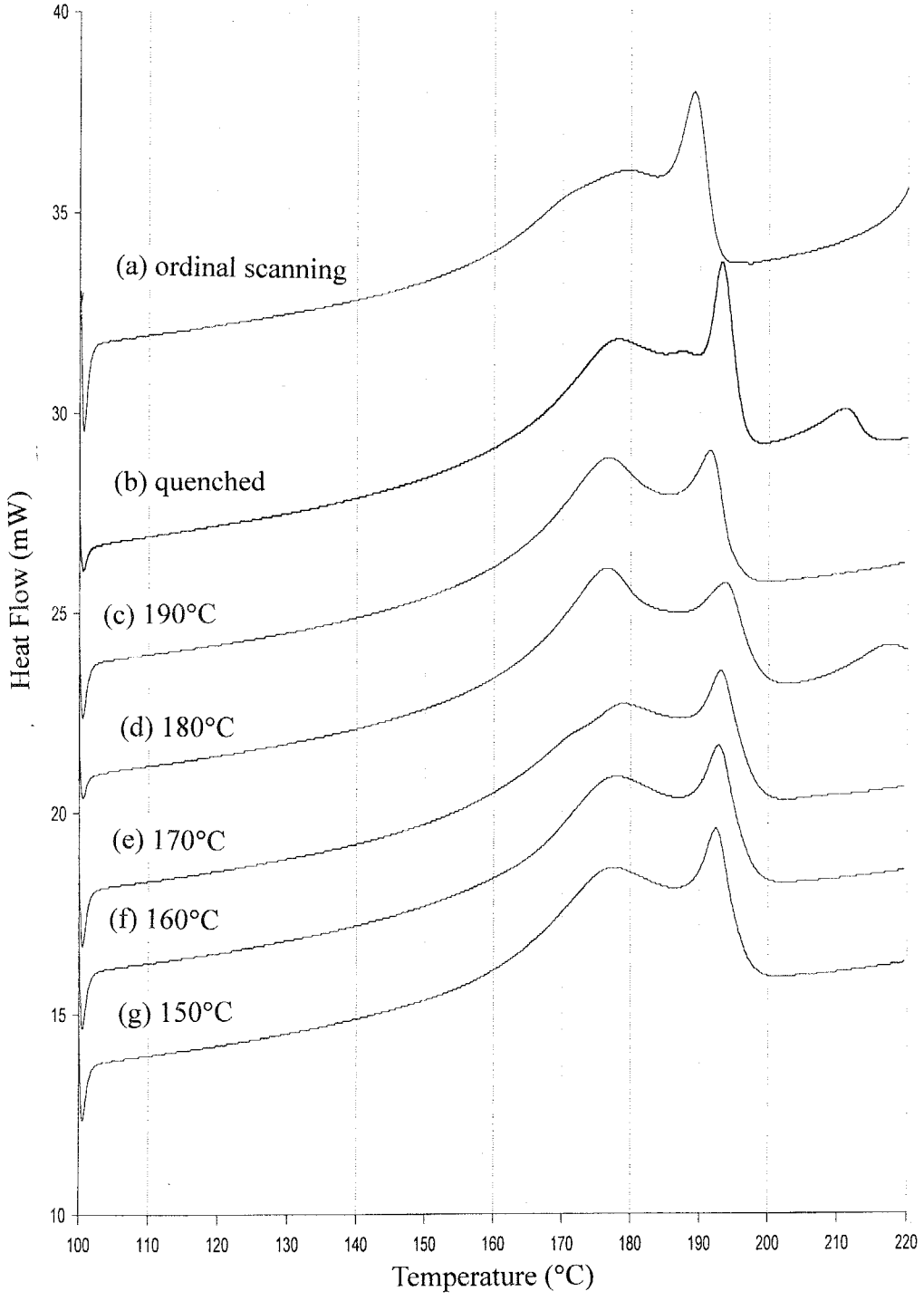

Figure 7.5. Heating DSC thermogram for the melting of PB-14 crystals: (a) a crystal prepared by cooling the isotropic melt at a rate of 10°C min^{-1}; (b) crystal prepared by quenching the extended chain S_H LC; (c) - (g) crystals crystallized the extended chain S_H LC isothermally at the temperature indicated in the figure.

Chapter 8
Conclusions

This thesis discusses the morphology of the smectic liquid crystal of two types of semiflexible main-chain polyesters with the biphenyl group as a common mesogen.

The smectic LC structures let us picture that the polymer takes up the extended configuration at least in a local space as discussed in Chapters 2 and 5. However, it was ambiguous if the polymer chains are extended along the entire length or not. This question arises from the following facts. The first is that polymer chains crystallize partially where they nevertheless include foldings but the configuration is unfavorable thermodynamically. The process in formation of liquid crystal from isotropic liquid is similar with that in crystallization in the respect that the polymer chains intertwining each other with random-coil configuration have to separate each other and alter their configuration to a rod-like one (cf. Chapter 1). The second is the polymeric smectic LC shows anomalous molecular orientation when flow deformation is applied. The

polymer chains align perpendicular to the flow direction (cf. Section 2.4). This anomalous flow orientation can be explained if chain folded lamellae are formed in the smectic phases and slip over each other.

Thus the same problems should be discussed for the polymer liquid crystals as for the polymer crystals. That is to say, (1) Are the polymer chains extended along the entire length? (2) Whether the chain folding is thermodynamically unstable as in the crystal or stable? (3) Whether the formation of the liquid crystal takes place completely or partly? And additionally, (4) whether crystallization from the liquid crystal takes place completely or partly? If it occurs partly, what compose the solid? Here the answer to the questions is given according to the preceding chapters.

Moreover, the problem can be treated with different degree of orders in molecular arrangement if different types of liquid crystal are examined. For that purpose, two types of main-chain polyester forming smectic phases, namely BB-*n* and PB-*n* are treated in this thesis. The smectic LC structures of BB-*n* and PB-*n* are characterized in Chapters 2 and 5, respectively mainly with using a wide-angle X-ray diffraction method, and with fluorescence and solid-state ^{13}C-NMR spectra. The even-membered BB-*n* and PB-*n* form S_A and S_H phases,

respectively.

Though the most stable polymer chain configuration is extended one, polymer chain folds and forms lamellar structure in the smectic LC fields. Origin of the chain folding may be attributable to kinetic reason on the liquid crystal formation from isotropic liquid because the conversion rate shows negative temperature dependence suggests that the liquid crystallization is a nucleation-controlled process (cf. Chapter 7). However the stability of the chain folding is completely different in these smectic phases. For the BB-*n* polyesters, the lamellar size is increased by annealing the crystal. In contrast, it is not altered by annealing the S_A phase. The lamellar spacing increases with a decrease in crystallization temperature. This trend is perfectly explainable if the chain folding exist at a thermodynamic equilibrium as an entropy effect in the S_A phase as expected in the theoretical discussions (cf. Chapter 3). Thus the chain folding in the S_A LC field is assumed to stabilized by an entropy effect. To the contrary, the lamella thickens under annealing the S_H phase of PB-*n* and finally the isotropization behavior indicates that the chain conformation alters to an extended one (cf. Chapter 5). It suggests that the chain folding in the S_H phase is metastable as in the polymer crystals. The molecular packing order,

especially lateral packing order may affect on the stability of chain folding.

It was found that the liquid crystallization of BB-*n* polyesters, i.e. S_A an S_{CA} phases, proceeds promptly and completely from the isotropic phase, though chains are folded in the smectic LC field. The disturbance in the packing of the mesogens cased by the chain folding can be allowed in the smectic phases with one-dimensional positional order. On the other hand, when the PB-*n* sample annealed at a S_H temperature, the isotropization temperature of the S_H phase increased and simultaneously the enthalpy change increased. The results shows that the S_H liquid crystallization takes place imperfectly in a finite period due to the chain folding. Thus the highly ordered structure of the S_H phase so that the folding sites are not accommodated in the ordered S_H structure. The experimental results suggest that the folding sites form the boundary of lamellae in both cases.

The crystallization of BB-*n* polyesters takes place partly even from the ordered smectic phases, while the liquid crystallization occurs completely. The solid state of the LCP is thus composed of crystal and smectic LC glass. The smectic LC glass shows a glass transition detected as an α-relaxation in a dynamic mechanical method and as a typical jump in the heat capacity by a DSC

method. The glass transition temperature is lower than the isotropic liquid glass temperature. On the other hand, the data suggests that the crystallization of PB-*n* polyesters occurs completely from the preceding S_H phase.

The results obtained in the works of this thesis depict the morphology of the BB-*n* and PB-*n* polymers both in the smectic phases and in solid state.

Smectic Phases (S_A and S_{CA}) of BB-*n* polyesters: The polymer chains are folded and form lamellae. The folding sites segregate and form the boundary of the lamella, but they are accommodated in the smectic structure and stabilized by an entropy effect. The liquid crystallization occurs completely so that isotropic liquid does not coexist.

Solid state of BB-*n* Polyesters: The morphology of the solid reflects that of the preceding smectic LC. The solid consists of lamella crystal and smectic LC glass.

Smectic Phases (S_H) of PB-*n* polyesters: The polymer chains are folded and form lamellae. The folding sites segregate and form the boundary of the lamella. They are not accommodated in the smectic structure and metastable in the LC state. The polymer chain alters its configuration from folded one to extended one in the S_H phase. The liquid crystallization occurs imperfectly due to the

chain folding so that isotropic liquid coexists. However the liquid crystallinity is fairly high (more than 80 %). The SAXS maxima observed for the S_H state is attributed to the contrast in the density between the LC and the coexisting isotropic liquid.

Solid state of PB-*n* Polyesters: The morphology of the solid reflects that of the preceding smectic LC. The solid consists of lamella crystal and isotropic liquid glass. The crystallization from the preceding S_H phase takes place completely and close to equilibrium.

Chain folding is usually discussed in polymer crystals. Lately, a transient liquid crystal like ordered structure is assumed for the induction period in the polymer crystallization process. Moreover, it has been reported that the polymer chain can be oriented by a magnetic field in the crystallization induction period.[1] The chain configuration alternation of polyethylene from folded one to extended one has been observed during pressure crystallization. The alternation occurs in a high-pressure crystalline phase with 'liquid crystal like disorder' hexagonal packing.[2] Thus the chain folding in the LC phase seems to be associated with that in the polymeric liquid crystalline polymer.

References

(1) Kimura, T.; Ito, E. *Polym. Prep. Jpn.* **1998**, *47*, 3837.

(2) Bassett, D. C.; Turner, B. *Phil. Mag.* **1974**, *29*, 925.

List of Publications

Chapter 2

(1) Smectic Liquid Crystals in Main-chain Polymers. J. Watanabe, M. Hayashi, Y. Nakata, and M. Tokita, *Prog. Polym. Sci.*, **22**,1053 - 1087(1997).

(2) Thermotropic Liquid Crystals of Main-Chain Polyesters Having a Mesogenic 4,4'-Bibenzoate Unit. 10 Distinct orientation of molecules in a thin SmCA film stretched from isotropic melt, providing evidence for the biaxiallity of the SmCA phase. M. Tokita, K. Osada and J. Watanabe, *Liq. Cryst.*, **24**, 477-450 (1998).

(3) Thermotropic Liquid Crystals of Main-Chain Polyesters Having a Mesogenic 4,4'-Bibenzoate Unit. 12. Unusual Orientation of Molecules in Fibers Drawn from Smectic Melt. M. Tokita, K. Osada and J. Watanabe, *Polym. J.*, **30**, 687-690(1998).

Chapter 3

(1) Thermotropic Liquid Crystals of Main-Chain Polyesters Having a Mesogenic 4,4'-Bibenzoate Unit. 7. Chain Folding in the Smectic Phase of BB-6. M. Tokita, T. Takahashi, M. Hayashi, K. Inomata, and J. Watanabe, *Macromolecules*, **29**, 1345-1348(1996).

(2) Thermotropic Liquid Crystals of Main-Chain Polyesters Having a Mesogenic 4,4'-Bibenzoate Unit. 9. Chain Folding in Solid Polyesters Crystallized from Smectic A. M. Tokita, K. Osada, and J. Watanabe, *Liq.Cryst.*, **23**, 453-456(1997).

(3) 主鎖型高分子のスメクチック液晶場における folding 構造、戸木田雅利、長田健介、土屋仁、渡辺順次、高分子論文集、**56**, 184-194(1999)

Chapter 4

(1) Thermotropic Liquid Crystals of Main-Chain Polyesters Having a Mesogenic 4,4'-Bibenzoate Unit. 11. Study on Smectic Liquid Crystalline Glass. M. Tokita, K. Osada and J. Watanabe, *Polym. J.*, **30**, 589-595(1998).

Chapter 5

(1) High Resolution ^{13}C NMR Studies for Crystalline and Liquid crystalline Phases of PB-18 Polyester Composed of 4,4'-Dihydroxybiphenyl and Octadecanedioic Acid. M. Tokita, M. Sone, H. Kurosu, I. Ando and J. Watanabe, *J. Mol. Struct.*, **446**, 215-221(1998).

(2) Fluorescens Study on Intermolecular Interactions between Mesogenic Biphenyl Moieties of a Thermotropic Liquid Crystalline Polyester (PB-10). H. W. Huang, K. Horie, T. Yamashita, S. Machida, M. Sone, M. Tokita, J. Watanabe, and Y Maeda, *Macromolecules,* **29**, 3485-3490(1996)

(3) Fluorescence study on intermolecular complex formation between mesogenic biphenyl moieties of main-chain thermotropic liquid crystalline polyesters with 8 - 18 methylene units. H. W. Huang, K. Horie, M. Tokita and J. Watanabe, *Polymer*, **40**, 3013-3023 (1999).

Chapter 6

(1) Chain-folded Lamellar Structure in the Smectic H phase of a Main-chain Polyester. M. Tokita, K. Osada, M. Yamada and J. Watanabe, *Macromolecules*, **31**, 8590-8594(1998).

Other publication not included in this thesis

(1)界面活性剤が形成する液晶の構造、戸木田雅利、宮田清蔵、化学と教育, **47**, 242-244(1999).

(2) Fluorescence study on intermolecular complex formation between mesogenic 4,4'-biphenyldicarboxylate moieties of thermotropic liquid crystalline polyesters with 5 and 6 methylene units. H. W. Huang, K. Horie, M. Tokita, and J. Watanabe, *Macromol. Chem. Phys.*, **199**, 1851-1858(1998).

(3) Polar Structure in Polypeptide Cholesteric Liquid Crystals Evidenced from Observation of Second-Harmonic Generation Due to the Helicoidal Cavity Effect. J. Watanabe, Y. Hirose, M. Tokita, T. Watanabe, and S. Miyata, *Macromoleucles*, **31**, 5937-5939(1998).

(4) Smectic characteristics of main-chain polyesters as elusidated from a variation of layer thickness with a carbon number of aliphatic spacer in a wide range 5 to 20. Y. Nakata, M.

Hayashi, M. Tokita and J. Watanabe, *High Perform. Polym.* **10**, 121-130(1998).

(5) Self-Assembly of Liquid-Crystalline Polyamide Complexes through thr Formation of Double Hydrogen Bonds between a 2,6-Bis(amino)pyridine Moiety and a Benzoic Acids, T. Kato, O. Ihata, M. Tokita and J. Watanabe, *Macromolecules*, **31**, 3551-3555(1998).

(6) Dielectric Behavior in Chiral Smectic Phases of Main-Chain Polyesters. K. Hiraoka, Y. Sugano, K. Monzen, Y. Uematsu, M. Tokita, and J. Watanabe, and T. Furukawa, *Mol. Cryst. Liq. Cryst.*, **299**, 229-234(1997)

(7) Thermotropic Liquid Crystals of Main-Chain Polyesters Having a Mesogenic 4,4'-Bibenzoate Unit. 6. Chiral Mesophase of Polyesters with a (S)-2-Methyl Butylene Spacer. J. Watanabe, M. Hayashi, A. Morita, and M. Tokita, *Macromolecules*, **28**, 8073-8079 (1995)

(8) Thermotropic Liquid Crystals of Main-Chain Polyesters Having a Mesogenic 4,4'-Bibenzoate Unit. 8. X-ray analyses of structural change on S_A to S_C transition. J. Watanabe, M. Hayashi, and M. Tokita *Reactive & Functional Polymers*, **30**, 191-196(1995).

Acknowledgements

Since the all persons to whom the author wishes to express his gratitude understand Japanese, he will write the acknowledgements in his native language of Japanese.

本論文の研究を遂行するにあたり、学部４年から７年余りにわたりご指導くださいました渡邊順次教授に深く感謝申し上げます。

謝辞として、渡辺研究室に入ってから私がこの論文をまとめあげるまでの思い出を述べておきたいと思います。研究室に入ったのは学部４年生のとき(1993 年)、卒論は「分枝メチル基を屈曲差に有する主鎖型高分子の液晶相転移と液晶構造」でした。午前中、研究室は、私と曽根正人博士(当時 D1)の二人きりであることが多く、そのときに曽根博士からさまざまなことを教わりました。修士課程に進学してから、卒論のテーマの一部は、「主鎖型高分子の強誘電液晶のダイナミクス」として東京理科大学理学部化学科古川猛夫教授と東京工芸大学工学部工業化学科平岡一幸先生との共同研究に発展していきました。その一方で、渡辺先生は私と顔を合わせると必ず「液晶相に chain folding があるのだ。小角 X 線散乱を測定しなさい。」とおっしゃっていました。はじめは液晶状態を凍結するために急冷した試料を測定し、散乱像はちっとも得られませんでした。思いつきで結晶化させた試料を測定したところ、第３章に述べたような散乱像が得られたのが、研究のスタートでした。M1 の秋から高橋敏行君（当時 B4）と一緒に研究を進め、渡辺先生、曽根博士、中田安一博士（当時博士課程）と頻繁にディスカッションした成果(第３章の前半の内容)を M2 の春に *Macromolecules* に投稿しました。平行して第５章の固体高分解能 NMR を曽根博士の指導のもとで行い、蛍光測定を東京大学大学院工学系研究科生命化学専攻堀江一之教授と黄　旭文博士(当時 D1)との共同研究として開始しました。

私が博士課程に進学したとき、新居輝樹博士(当時 D3)に加え、山田雅之博士(中濱精一研究室出身)、金子達雄博士(今井淑夫研究室出身)が D2 で、幸正　弘博士（大日精化㈱から社会人入学）が同期で在籍していました。このように多彩で優秀な先輩に恵まれ、今からすると夢のような日々を過ごしました。そして、第３章の後半、第４章の「液晶ガラス」、第７章の基礎的な研究を、研究室に入ってきた長田健介君（当時４年生）と協力して遂行し、それらの成果を多数の投稿論文にまとめあげました。東京大学大学院工学系研究科生命化学専攻加藤隆史助教授は、投稿論文に対して貴重な意見を下さり、さらに共同研究をとおして多くのことをご教示いただきました。渡辺先生に現職（東京農工大学大学院生物システム応用科学研究科助手）をお世話いただき、D2 の９月に博士課程を半分残して退学しました。

就職後は、宮田清蔵教授、渡辺敏行助教授のご理解とご支援のもと、浅井大恵秘書が宮田研究室の仕事をしっかりと支えてくださったおかげで、本研究を継続することができました。第６章、第７章は、土屋　仁君(当時 B4)の協力により、就職後にその内容を充実したものとしました。

本論文の製本は、株式会社博進企画印刷、浅井美博社長と社員の方々に協力いただきました。ここに厚く御礼申し上げます。

最後に、某大手繊維メーカーの就職内定を断って博士課程に進学し、またその博士課程も中退するという、親から見れば先の見えない選択を嘆きながらも支えてくれた母と、私の選択にはじめから賛成し、うろたえ嘆く母をなだめてくれた父に感謝します。

平成 11 年 5 月 6 日

戸木田　雅利